NATIONAL TECHNICAL UNIVERSITY OF ATHENS
SCHOOL OF CHEMICAL ENGINEERING
DEPARTMENT OF SYNTHESIS AND DEVELOPMENT OF INDUSTRIAL PROCESSES
BIOTECHNOLOGY LABORATORY

ISOLATION AND IDENTIFICATION OF METABOLITES FROM MARINE-DERIVED ACTINOBACTERIA

DOCTORAL THESIS

ENIKO RAB

ATHENS
DECEMBER 2018

ADVISORY COMMITTEE

Dimitrios Kekos (Supervisor)
Professor, School of Chemical Engineering, National Technical University of Athens

Vassilios Roussis
Professor, Department of Pharmacy, National and Kapodistrian University of Athens

Efstathia Ioannou
Assist. Professor, Department of Pharmacy, National and Kapodistrian University of Athens

EXAMINATION COMMITTEE

Dimitrios Kekos
Professor, School of Chemical Engineering, National Technical University of Athens

Vassilios Roussis
Professor, Department of Pharmacy, National and Kapodistrian University of Athens

Olga Tzakou
Professor, Department of Pharmacy, National and Kapodistrian University of Athens

Maria Couladis
Assoc. Professor, Department of Pharmacy, National and Kapodistrian University of Athens

Anastasia Detsi
Assoc. Professor, School of Chemical Engineering, National Technical University of Athens

Efstathia Ioannou
Assist. Professor, Department of Pharmacy, National and Kapodistrian University of Athens

Evangelos Topakas
Assist. Professor, School of Chemical Engineering, National Technical University of Athens

ABSTRACT

Intensive studies of mainly soil-derived bacteria and fungi have shown that microorganisms are a rich source of structurally unique and pharmaceutically important bioactive substances. Many secondary microbial metabolites show antibacterial, antifungal, antiviral, antitumor, antiprotozoal, hypocholesterolemic and other activities. They are commonly used in medicine, veterinary practice, agriculture and industry and they even serve as template for the synthesis of synthetic and semi-synthetic drugs.

The vast diversity of marine microorganisms represents a unique and virtually unexplored source of new bioactive molecules. Among the phyla of marine microorganisms, actinobacteria have shown to be the most prolific concerning the biosynthesis of novel bioactive metabolites. The members of this group are also common soil inhabitant with an unprecedented ability to produce clinically useful antibiotics. Since marine environmental conditions are extremely different from the terrestrial ones, it is expected that marine actinomycetes would produce different and in many cases structurally unprecedented bioactive compounds.

Within the framework of the present PhD thesis, a number of marine-derived bacterial strains deposited at the strain collection/microbank of the Section of Pharmacognosy and Chemistry of Natural Products, Department of Pharmacy, National and Kapodistrian University of Athens, were cultivated in small-scale liquid cultures and the obtained organic extracts were screened for their chemical profiles using high pressure liquid chromatography (HPLC). Among them, strain BI0048, isolated from the inner tissues of the red alga *Laurencia glandulifera*, exhibited an interesting chemical profile and was thus selected for further chemical investigation.

The algicolous endophytic strain, which was identified as *Streptomyces ambofaciens*, was cultured in large-scale in flasks containing a seawater-based liquid medium that were incubated at 37 °C for 8 days while shaking at 130 rpm in an orbit shaker. At the end of the fermentation period, Amberlite XAD-7HP resin was added to each flask to adsorb extracellular metabolites. The culture and resin were shaken overnight at low speed. The resin and cell mass were collected by filtration through cheesecloth and washed with deionized water to remove salts. Subsequently, the resin, cell mass and cheesecloth were extracted with acetone. Filtration of the extract and removal of the solvent under vacuum at 40 °C afforded a solid residue that was

subjected to a multi-step fractionation scheme using normal and reversed-phase vacuum column chromatography, gravity column chromatography and HPLC to allow for the isolation of a number of metabolites.

The structural characterization of the isolated metabolites was based on thorough analyses of their spectroscopic data, employing mainly nuclear magnetic resonance (NMR) spectroscopy and mass (MS) spectrometry, as well as infrared (IR) and ultraviolet-visible (UV-Vis) spectroscopy, and comparison of their spectroscopic and physical characteristics with those of relevant compounds previously reported in the literature.

In total, 23 metabolites were isolated and identified from the organic extract of the actinobacterial strain BI0048, including ten polyketides (**1**-**10**), four simple aromatic compounds (**11**-**14**), seven diketopiperazines (**15**-**21**), one nucleoside (**22**) and compound **23** bearing a methacrylate residue.

In particular, the isolated polyketides were identified as enterocin (**1**), also known as vulgamycin, 5-deoxy-enterocin (**2**), wailupemycin D (**3**), wailupemycin E (**4**), zoumbericin A (**5**), zoumbericin B (**6**), germicidin A (**7**), germicidin B (**8**), germicidin K (**9**) and germicidin L (**10**). Among them, 4 metabolites (**5**, **6**, **9** and **10**) are new natural products. All the isolated polyketides feature an α-pyrone moiety, which constitutes an essential pharmacophore in many naturally occurring and synthetic bioactive compounds. Natural products featuring a α-pyrone ring are often involved in defense processes, while frequently they possess antibacterial, antifungal, antiviral, cytotoxic, phytotoxic and neurotoxic properties. Furthermore, four simple aromatic compounds were isolated and identified as benzoic acid (**11**), hydrocinnamic acid (**12**), (*E*)-cinnamic acid (**13**) and tyrosol (**14**), also known as *p*-hydroxy-phenethyl alcohol. The isolated diketopiperazines were identified as *cis*-*cyclo*(L-Pro-L-Ala) (**15**), *cis*-*cyclo*(L-Pro-L-Val) (**16**), *cis*-*cyclo*(L-Pro-L-Leu) (**17**), *cis*-*cyclo*(L-Pro-L-Ile) (**18**), *cis*-*cyclo*(L-Pro-L-Phe) (**19**), *trans*-*cyclo*(L-Pro-L-Phe) (**20**) and *cis*-*cyclo*(L-Pro-L-Tyr) (**21**). Additionally, one nucleoside was isolated and identified as adenosine (**22**), as well as compound **23** bearing a rare methacrylate residue.

Compounds **1**–**10** were evaluated for their antibacterial activities against the epidemic methicillin-resistant strain EMRSA-15 and the multidrug-resistant effluxing strain SA1199B of *Staphylococcus aureus*, as well as the *Escherichia coli* strain NCTC-10418. Furthermore, the cytotoxic activities of **1**–**10** were tested against the MCF7 (breast adenocarcinoma) and A549 (lung carcinoma) human cancer cell lines. However,

metabolites **1**–**10** were proven inactive in both bioactivity assays.

ΠΕΡΙΛΗΨΗ

Συστηματικές μελέτες που έχουν εστιάσει κατά κύριο λόγο σε βακτήρια που προέρχονται από το έδαφος έχουν καταδείξει τους μικροοργανισμούς σαν μία από τις πλουσιότερες πηγές βιοδραστικών μεταβολιτών με ιδιαίτερα δομικά χαρακτηριστικά και σημαντική φαρμακολογική δράση. Πολλοί μεταβολίτες μικροβιακής προέλευσης έχουν επιδείξει σημαντικά επίπεδα δραστικότητας σε ένα ευρύ φάσμα βιολογικών δοκιμασιών, μεταξύ των οποίων είναι η αντιβακτηριακή, αντιμυκητιακή, αντιιική και αντικαρκινική δράση. Χρησιμοποιούνται ευρέως σαν θεραπευτικοί παράγοντες στην ιατρική, κτηνιατρική, σαν αγροχημικά και πολύ συχνά αποτελούν μόρια-οδηγούς για την σύνθεση ή ημισύνθεση ανάλογων χημικών μορίων.

Οι θαλάσσιας προέλευσης μικροοργανισμοί αντιπροσωπεύουν μια ιδιαίτερη και παράλληλα ελάχιστα μελετημένη πηγή βιοδραστικών μεταβολιτών. Μεταξύ των θαλάσσιας προέλευσης μικροοργανισμών, τα ακτινοβακτήρια εμφανίζονται ως τα πλέον παραγωγικά όσο αφορά την βιοσύνθεση βιοδραστικών μεταβολιτών με πρωτότυπες χημικές δομές. Στελέχη αυτής της ταξινομικής ομάδας συχνά απαντώνται και στο έδαφος και έχουν παρουσιάσει εξαιρετική ικανότητα παραγωγής κλινικά σημαντικών αντιβιοτικών ουσιών. Καθώς το θαλάσσιο περιβάλλον είναι σημαντικά διαφοροποιημένο από το χερσαίο είναι αναμενόμενο τα θαλάσσιας προέλευσης ακτινοβακτήρια να παράγουν βιοδραστικά μόρια με ιδιαίτερες χημικές δομές.

Στα πλαίσια της παρούσας Διδακτορικής Διατριβής, ένας αριθμός από βακτηριακά στελέχη θαλάσσιας προέλευσης, από την τράπεζα στελεχών του Τομέα Φαρμακογνωσίας και Χημείας Φυσικών Προϊόντων, του Τμήματος Φαρμακευτικής, του Εθνικού και Καποδιστριακού Πανεπιστημίου Αθηνών καλλιεργήθηκε σε μικρής κλίμακας υγρές καλλιέργειες και τα οργανικά εκχυλίσματα που προέκυψαν αξιολογήθηκαν ως προς το χημικό τους προφίλ με υγρή χρωματογραφία υψηλής πίεσης (HPLC). Μεταξύ αυτών, το στέλεχος BI0048, το οποίο είχε απομονωθεί ως ενδοφυτικό βακτήριο από το ροδοφύκος *Laurencia glandulifera*, εμφάνισε το πλέον ενδιαφέρον χημικό προφίλ και επιλέχθηκε για περαιτέρω μελέτη.

Το ενδοφυτικό αυτό στέλεχος, το οποίο ταυτοποιήθηκε ως *Streptomyces ambofaciens*, καλλιεργήθηκε σε μεγάλη κλίμακα σε κωνικές φιάλες με θρεπτικό μέσο βασισμένο σε θαλασσινό νερό. Οι καλλιέργειες επωάσθηκαν στους 37 °C για 8 ημέρες με τις κωνικές φιάλες σε σταθερή ανάδευση 130 rpm επί κινούμενης τράπεζας. Μετά το

πέρας της καλλιέργειας, προστέθηκε σε κάθε κωνική φιάλη ρητίνη Amberlite XAD-7HP ώστε να προσροφήσει τους εξωκυτταρικούς μεταβολίτες και ακολούθως το θρεπτικό μέσο και η ρητίνη παρέμειναν υπό ανακίνηση σε χαμηλή ταχύτητα για 12 ώρες. Η ρητίνη και τα κύτταρα διηθήθηκαν από ηθμό πολλαπλών στρωμάτων γάζας και το ίζημα εκπλύθηκε με απιονισμένο νερό για την απομάκρυνση των αλάτων. Στην συνέχεια, η ρητίνη και η κυτταρική βιομάζα εκχυλίσθηκαν εξαντλητικά με ακετόνη. Η διήθηση του εκχυλίσματος και στην συνέχεια η εξάτμιση των διαλυτών υπό κενό σε θερμοκρασία μικρότερη των 40 °C απέδωσε στερεό υπόλειμμα το οποίο υποβλήθηκε σε πολλαπλούς χρωματογραφικούς διαχωρισμούς με κανονικής και αντίστροφης φάσης χρωματογραφία με υποβοήθηση κενού, χρωματογραφία στήλης βαρύτητας και HPLC που οδήγησαν στην απομόνωση ενός σημαντικού αριθμού μεταβολιτών σε καθαρή μορφή.

Ο δομικός χαρακτηρισμός των απομονωμένων μεταβολιτών βασίσθηκε στην ανάλυση των φασματοσκοπικών τους δεδομένων που ελήφθησαν από Φασματοσκοπία Πυρηνικού Μαγνητικού Συντονισμού (NMR), Φασματομετρία Μάζας (MS), Φασματοσκοπία Υπερύθρου (IR) και Φασματοσκοπία Υπεριώδους-Ορατού (UV-Vis) και την σύγκριση τους με αντίστοιχα δεδομένα δημοσιευμένων μεταβολιτών που παρουσίαζαν δομικές ομοιότητες.

Συνολικά από το οργανικό εκχύλισμα του ακτινοβακτηριακού στελέχους BI0048 απομονώθηκαν 23 μεταβολίτες, μεταξύ των οποίων 10 πολυκετίδια (**1**-**10**), τέσσερεις απλοί αρωματικοί μεταβολίτες (**11**-**14**), επτά δικετοπιπεραζίνες (**15**-**21**), ένας νουκλεοσίδης (**22**) και ένας μεταβολίτης (**23**) με μεθακρυλική ομάδα.

Συγκεκριμένα, τα πολυκετίδια που απομονώθηκαν ταυτοποιήθηκαν ως η εντεροσίνη (**1**), η οποία επίσης έχει αναφερθεί και ως βουλγαμυκίνη, η 5-δεοξυ-εντεροσίνη (**2**), η γαϊλουπεμικίνη D (**3**), η γαϊλουπεμικίνη E (**4**), η ζουμπερικίνη A (**5**), η ζουμπερικίνη B (**6**), η γερμισιδίνη A (**7**), η γερμισιδίνη B (**8**), η γερμισιδίνη K (**9**) και η γερμισιδίνη L (**10**). Εξ αυτών, τέσσερεις μεταβολίτες είναι νέα φυσικά προϊόντα (**5**, **6**, **9** και **10**). Όλα τα πολυκετίδια που απομονώθηκαν έχουν στον σκελετό τους α-πυρανικό δακτύλιο που αποτελεί σημαντικό στοιχείο του φαρμακοφόρου τμήματος πολλών φυσικών και συνθετικών βιοδραστικών μορίων. Φυσικά προϊόντα που διαθέτουν α-πυρανικό δακτύλιο συχνά διαδραματίζουν ρόλους χημικής προστασίας για τους οργανισμούς που τους παράγουν, όπως επίσης πολύ συχνά εμφανίζουν αντιβακτηριακές, αντιμυκητιακές, αντιικές, κυτταροτοξικές, φυτοτοξικές και νευροτοξικές ιδιότητες. Οι αρωματικοί μεταβολίτες που απομονώθηκαν

ταυτοποιήθηκαν ως το βενζοϊκό οξύ (**11**), το υδροκινναμικό οξύ (**12**), το (*E*)-κινναμικό οξύ (**13**) και η τυροσόλη (**14**), η οποία επίσης ονομάζεται *p*-υδροξυ-φαινυλο-αιθανόλη. Οι δικετοπιπεραζίνες που απομονώθηκαν ταυτοποιήθηκαν ως η *cis*-*cyclo*(L-Pro-L-Ala) (**15**), η *cis*-*cyclo*(L-Pro-L-Val) (**16**), η *cis*-*cyclo*(L-Pro-L-Leu) (**17**), η *cis*-*cyclo*(L-Pro-L-Ile) (**18**), η *cis*-*cyclo*(L-Pro-L-Phe) (**19**), η *trans*-*cyclo*(L-Pro-L-Phe) (**20**) και η *cis*-*cyclo*(L-Pro-L-Tyr) (**21**). Επιπλέον, ο νουκλεοσίδης που απομονώθηκε ταυτοποιήθηκε ως η αδενοσίνη (**22**), ενώ ο μεταβολίτης **23** περιείχε μία μεθακρυλική ομάδα.

Οι μεταβολίτες **1**–**10** αξιολογήθηκαν ως προς την αντιβακτηριακή τους δράση έναντι του επιδημικού, ανθεκτικού στην μεθυκιλλίνη, στελέχους EMRSA-15 και του πολυανθεκτικού στελέχους SA1199B του *Staphylococcus aureus*, καθώς επίσης και έναντι του στελέχους NCTC-10418 της *Escherichia coli*. Επίσης, η κυτταροτοξική δράση των μεταβολιτών **1**–**10** αξιολογήθηκε έναντι των ανθρώπινων καρκινικών κυτταρικών σειρών MCF7 (αδενοκαρκίνωμα στήθους) και A549 (καρκίνωμα πνεύμονα). Παρ' όλα αυτά, οι μεταβολίτες **1**–**10** δεν επέδειξαν αξιοσημείωτη δραστικότητα σε καμία από τις δύο βιοδοκιμές.

ACKNOWLEDGEMENTS

There are many people that have really been very important for various reasons in the implementation of this PhD thesis and I wish to express my gratitude for that.

First of all, I would like to thank my supervisor Professor Dimitris Kekos for his constant support and advice during the long period of implementation of this study. I am also really grateful to him for his efforts to provide financial support to me through a PhD fellowship from the Special Account for Research Grants of the National Technical University of Athens.

I wish to thank Professor Vassilios Roussis and Assistant Professor Efstathia Ioannou for their supervision and advice throughout my studies, for providing space in their labs for the majority of the period of my studies, as well as consumables and access to the necessary instrumentation and financial assistance through a research project.

I would like to express my deepest gratitude to Assistant Professor Efstathia Ioannou not only for her constant supervision and advice, but more importantly for the valuable assistance with the isolation and structure elucidation of the metabolites and the preparation of the written text of my PhD thesis.

I wish to express my sincere thanks to all members of my Advisory Committee for being always ready to assist with any problems emerging during the period of my studies, as well as the members of the Examination Committee for reading the written text and evaluating the work done during my studies.

The assistance of Dr Dimitrios Kletsas and Dr. Eleni Mavrogonatou at the Institute of Biosciences and Applications, NCSR “Demokritos” with the evaluation of the cytotoxic activity of a number of the isolated metabolites is highly appreciated. Furthermore, the assistance of Ms. Eirini Nikolakopoulou at the laboratory at NKUA with the evaluation of the antibacterial activity of a number of the isolated metabolites is kindly acknowledged.

I am grateful to PhD student Maria Harizani for her friendship and the continuous help with technical issues in the lab, as well as all the postdoctoral fellows, students and technicians at the NKUA and NTUA labs for their friendship, as well as for providing a friendly and inspiring environment for me all these years.

My sincere thanks also go to my friends from the labs: Makis Ladoukakis,

Leonidas Matsakas, Thomas Paschos, Maria Savvidou, Natasa Petraki and Takis Perdikaris, for all their support and friendship.

I would like to express my appreciation to those people who helped me find a position for my postgraduate studies and followed my studies with interest and care during all these years: Vassilios Roussis, Anastasia Detsi, George N. Scarakis, Fragiskos Kolisis.

I would like to express my gratitude to Petros Katapodis for introducing me to research in Greece.

I would like to thank my very good friend Andreas Kourinakis for his suggestion to participate in PhD studies and for his constant support.

Last but not the least, I would like to thank my family: my parents and my brother for supporting me spiritually throughout my PhD studies and my life in general.

TABLE OF CONTENTS

ABBREVIATIONS

1D-NMR	one-dimensional nuclear magnetic resonance spectroscopy
2D-NMR	two-dimensional nuclear magnetic resonance spectroscopy
^{1}H NMR	proton nuclear magnetic resonance, 1D-NMR experiment with respect to ^{1}H nuclei
^{13}C NMR	carbon nuclear magnetic resonance, 1D-NMR experiment with respect to ^{13}C nuclei that is proton decoupled to remove the signal splitting
br	broad (NMR)
$CDCl_3$	deuterated chloroform
CD_3OD	deuterated methanol
$(CD_3)_2SO$	deuterated dimethyl sulfoxide
CH_2Cl_2	dichloromethane
cHex	cyclohexane
CIMS	chemical ionization mass spectrometry
COSY	correlation spectroscopy, 2D-NMR homonuclear (^{1}H-^{1}H) experiment which is used to identify spins which are coupled to each other, i.e. to establish correlations of proton nuclei which are adjacent
d	doublet (NMR)
DMSO	dimethyl sulfoxide
EIMS	electron impact mass spectrometry
EtOAc	ethyl acetate
HMBC	heteronuclear multiple-bond correlation spectroscopy, 2D-NMR heteronuclear (^{1}H-^{13}C) experiment which is used to detect correlations between proton and carbon nuclei over ranges of 2-4 bonds
HPLC	high performance liquid chromatography
HRESIMS	high resolution electrospray ionization mass spectrometry
HSQC	heteronuclear single-quantum correlation spectroscopy, 2D-NMR heteronuclear (^{1}H-^{13}C) experiment which is used to detect correlations between proton and carbon nuclei which are separated by one bond
IR	infrared spectroscopy
J	coupling constant (in Hz) (NMR)
m	multiplet (NMR)
Me_2CO	acetone
MeCN	acetonitrile
MeOH	methanol
MS	mass spectrometry
m/z	mass-to-charge ratio (MS)
NMR	nuclear magnetic resonance spectroscopy
RI	refractive index
q	quartet (NMR)
s	singlet (NMR)
t	triplet (NMR)
TLC	thin layer chromatography
UV-Vis	ultraviolet-visible spectroscopy
δ	scale for reporting the chemical shift of a nucleus (in ppm) in relation to TMS (tetramethylsilane) at δ = 0 ppm (NMR)

1. INTRODUCTION

1.1. Natural products

Chemical compounds that are produced by living organisms stemming from their secondary metabolism pathways and have a specific ecological role in nature (eg chemical defense, chemical communication) are considered as natural products. The secondary metabolites are usually present in small amount in the organisms and in many cases are characteristic of specific organisms or groups of organisms. Natural products since the ancient years are regarded as important molecules due to their wide range of biological activities. Traditionally, higher plants have been considered as the most prolific sources of drugs from the nature and the use of medicinal plants is well documented throughout human history.

1.2. Microbial natural products

Until the beginning of the 20th century, knowledge about bacteria, fungi and viruses was virtually non-existing. Although the antibiotic properties of some microorganisms were described in the late 1800s and early 1900s (Bugni and Ireland, 2004), it was much later, when penicillin was discovered in 1929 by Sir Alexander Fleming, that the potential of microorganisms was recognized. Since then, intensive studies on mainly soil-derived bacteria and fungi have shown that microorganisms can be rich sources of structurally unique pharmaceutically important bioactive substances (Fenical, 1993). They are produced at the end of the exponential growth phase and during the stationary phase and their biosynthesis greatly depends on the growth conditions. Their maximum production is usually observed when growth is limited by the exhaustion of one essential nutrient, such as carbon or nitrogen (Barrios-González & Mejýa, 2008; Sanchez & Demain, 2002).

Biosynthesis of secondary metabolites in microorganisms is catalyzed by a number of enzymes, usually encoded by genes. These genes occur adjacent to one another in clusters. The gene cluster contains all the necessary genes for the synthesis of a particular secondary metabolite. This includes the genes that encode the biosynthetic enzymes, regulatory proteins, genes for resistance to the toxic action of secondary metabolites and genes for secretion of the metabolites. The size of the gene cluster responsible for the synthesis of any particular secondary metabolite is usually between

10-100 kb (Adegboye & Babalola, 2013).

Many microbial secondary metabolites show, among others, antibacterial, antifungal, antiviral, antitumor, antiprotozoal and hypocholesterolemic activities. Secondary metabolites usually comprise various chemical entities, such as polyketide backbones, amino acid derivatives and carbohydrates. They are commonly used in medicine, veterinary practice, agriculture and various other industrial sectors. They frequently serve as lead molecules for the synthesis of synthetic and semi-synthetic drugs (Adegboye & Babalola, 2013).

Approximately 200,000-250,000 metabolites have been reported to possess some type of bioactivity and more than 22,000 of them have been produced by microorganisms (Bérdy, 2005; Demain & Sanchez, 2009). Among the approx. 22,000 microbial metabolites, about 17% (3,800) are metabolites of unicellular bacteria (especially *Bacillus* spp. and *Pseudomonas* spp.), 45% (10,100) are products of actinobacteria and about 38% (8,600) are of fungal origin (Bérdy, 2005; Demain & Sanchez, 2009). Among filamentous actinomycetes, about 75% (7,600) of the metabolites have been produced by species of the genus *Streptomyces* (Bérdy, 2005; Lam, 2007; Solecka et al., 2012).

1.3. Actinobacteria

The phylum *Actinobacteria* – in terms of number and variety of identified species – represents one of the largest taxonomic units among the 18 major lineages recognized within the *Bacteria* domain (Barka et al., 2016; Stackebrandt et al., 1997a). It comprises Gram-positive bacteria that are characterized by the high G+C content (>50 mol %) in their DNA (Stackebrandt & Goebel, 1994), even though there are exceptions that break this rule, such as freshwater actinobacteria that have low G+C content (Ghai et al., 2011).

Actinobacteria are widely distributed in both terrestrial and aquatic ecosystems and they have been found in all ecological niches, such as soil, compost, sludge, water (marine and fresh), the atmosphere, marshy places and extreme environments (Barka et al., 2016; Dhevendaran & Annie, 1999).

Actinobacteria may be inhabitants of soil or aquatic environments (e.g., *Streptomyces*, *Micromonospora*, *Rhodococcus*, and *Salinispora* species), plant symbionts (e.g., *Frankia* spp.), plant or animal pathogens (e.g., *Corynebacterium*, *Mycobacterium*, or *Nocardia* species), or gastrointestinal commensals (e.g.,

Bifidobacterium spp.) (Barka et al., 2016).

1.3.1. Morphology

Actinobacteria are a group of slow-growing prokaryotic organisms belonging to the subdivision of the Gram-positive bacteria and comprise a heterogeneous group of branching unicellular microorganisms. They produce branching mycelium which may be either substrate mycelium or aerial mycelium. The aerial mycelium is important as it is the part of the organism that produces spores. Their branching and manner of sporulation have suggested their relationship to the fungi in the past (Waksman, 1961), as is reflected in the name of the medically important genus *Actinomyces*, derived from the Greek words *aktino* which means ray and *mykes* which means mushroom/fungus.

Actinobacteria, when growing on solid agar, develop branching network of hyphae (vegetative mycelium) which grows both on the surface of the substratum and into it forming substrate mycelium (Fig. 1). Septa usually divide the hyphae into long cells containing several nucleoids. Many actinobacteria also have an aerial mycelium that extends above the substratum and usually on the ends of the filaments form asexual, thin walled spores called conidia or conidiospores (Fig. 2) (Li et al., 2016).

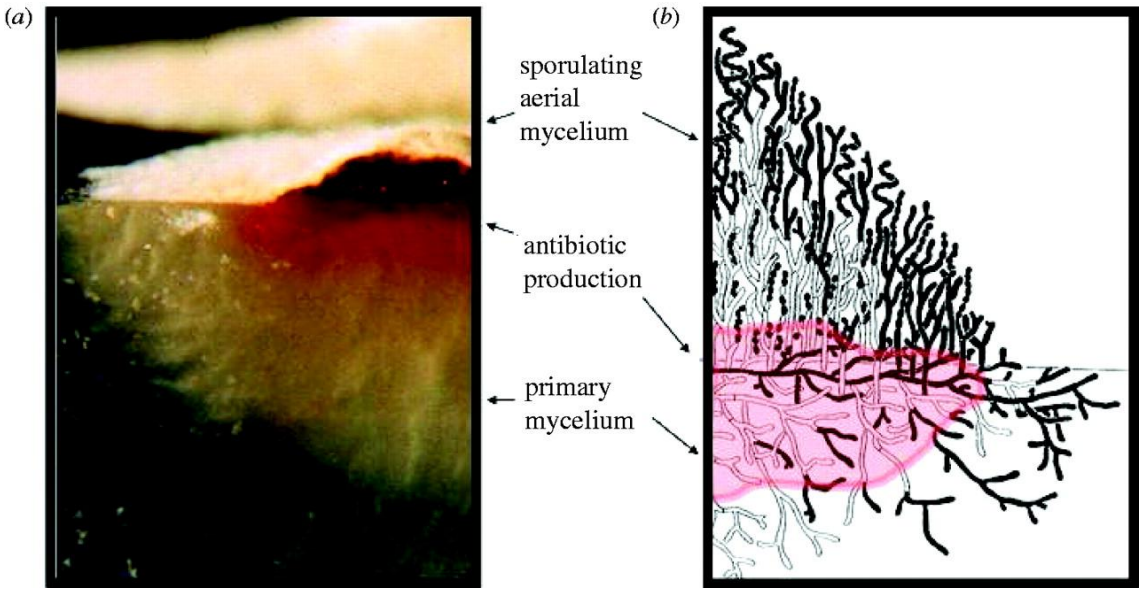

Figure 1. Vertical sections through a *Streptomyces* colony: (a) Photograph of colony growing on agar, (b) Diagram indicating how antibiotic production by the aging cells in the lower part of the colony can protect the nutrients released from dead cells (white) which also attract other scavengers which may be killed by antibiotics so aerial growth and sporulation can be supported; living cells are shown as black (Chater, 2006).

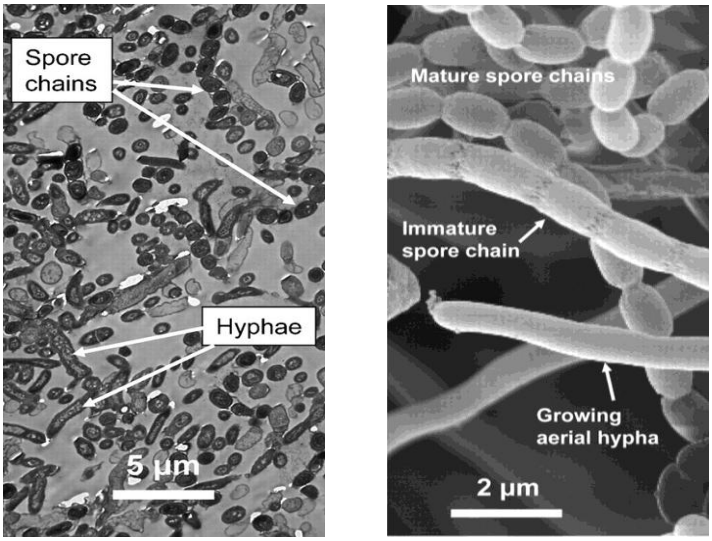

Figure 2. Electron microscopy images of 6-day old colonies of *Streptomyces coelicolor* A3(2): Transmission electron micrograph of wild-type (M145) aerial mycelium showing frequent dark spore chains and the aerial hyphae which are never bundled in a matrix (left) and Scanning electron micrograph of wild-type (M145) aerial mycelium showing stages in the development of spore chains (Fowler-Goldsworthy et al., 2011).

Actinobacteria are transitional forms between bacteria and fungi, sometimes called filamentous bacteria. Like bacteria, they possess cell walls containing muramic acid. They also have prokaryotic nuclei and are susceptible to antibiotics. In the composition of cell wall they do not have chitin and cellulose that are commonly found in the cell wall of fungi, but like fungi they form filaments called hyphae, similar to the hyphal forms of fungi, although the diameter of the filaments is much smaller than that of the fungi (Ananthanarayan & Paniker, 2005).

Actinobacteria exhibit a wide range of morphologies, from coccoid (e.g., *Micrococcus* spp. from the order *Actinomycetales*) or rod-coccoid (e.g., *Arthrobacter* spp. from the order *Actinomycetales*) to fragmenting hyphal forms (e.g., *Nocardia* spp. from the order *Actinomycetales*) or permanent and highly differentiated branched mycelium (e.g., *Streptomyces* spp. from the order *Actinomycetales*) (Atlas, 1997).

1.3.2. Ecology and physiology

Many actinobacteria are harmless to animals and higher plants, some are dreadful pathogens, such as species of the genera *Mycobacterium* (causing tuberculosis-Mycobacterium tuberculosis, leprosy -Mycobacterium leprae), *Nocardia* (causing pulmonary nocardiosis or systemic nocardiosis), *Tropheryma* (causing Whipple's disease), and *Corynebacterium* (causing diphtheria), while many others have been

proven rich sources of antibiotics.

Most of the actinobacteria (the streptomycetes in particular) are saprophytic, soil-dwelling organisms that spend the majority of their life cycles as semidormant spores, especially under nutrient-limited conditions (Barka et al., 2016).

The characteristic odor of soil was first investigated by Berthelot and Andre in 1891 (Berthelot and Andre, 1891) and was found to be due to the presence of two compounds. In 1965 the structure of one of the two responsible compounds, geosmin, was elucidated by Gerber (Gerber, 1979), while the second molecule was later identified as 2-methyl-isoborneol. These compounds are mostly produced by bacteria belonging to the genus *Streptomyces*. The presence of *Streptomyces* gives the earthy taste and odor to the potable water (Chavan et al., 2013).

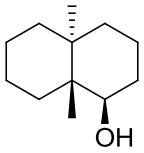

geosmin

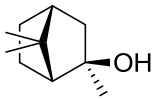

2-methyl-isoborneol

A large number of actinobacterial species have been found in the soil. Their role as soil microbes is the degradation, acting also as biocontrol agents. As degradation agents they play a role in humus formation since they degrade soil organic materials into humus. Some actinobacteria secrete a range of enzymes that can completely degrade all components of lignocellulose, as well as many other naturally occurring polymers in the soil, such as pectin, keratin, chitin and fungal cell wall materials (Chavan et al., 2013). Furthermore, actinobacteria are important organisms in the mediation of plant litter decay. With their ability to secrete the appropriate enzymes, they are effective on tough raw plant tissues softening them for other microbes. As biocontrol agents (Table 1), these microorganisms can protect plant roots from plant pathogens and promote the plant growth (El-Tarabily & Sivasithamparam, 2006). There is currently significant interest in the isolation of actinobacteria with ability to act as biocontrol agents so that they can replace chemicals in the control of plant pathogens.

Table 1. Examples of actinobacteria acting as biocontrol agents against plant pathogenic fungi (El-Tarabily & Sivasithamparam, 2006).

Species	**Pathogen**	**Host plant**
Streptomyces netropis	*Verticillium* sp.	Cotton
Actinomadura sp.	*Phytophthora cinnamomi*	Snapdragon
Micromonospora carbonacea	*Phytophthora cinnamomi*	Banksia
Micromonospora globosa	*Fusarium udum*	Cotton
Actinoplanes missouriensis	*Phytophthora megasperma*	Soy Bean

Actinobacteria exhibit a range of life cycles which are unique and the most complex among the prokaryotes (Fig. 3). They reproduce either by spore formation or hyphae fragmentation (Waksmann, 1961). Under favorable nutrient conditions, a germ tube emerges from a germinating spore, grows from its tip (tip extension), and forms branches that grow along the surface of its food source. This type of growth produces an intertwined network of long multinucleate filaments (hyphae) collectively called substrate mycelia. These vegetative mycelia of branched hyphae form a colony. A few days later, new genes are activated that cause the hyphae to grow upward, rising above the surface to form aerial mycelia. When aerial hyphae stop growing, a developmental program is triggered that leads to the synthesis of antibiotics and production of prespores which are further matured to single spores. A single spore can eventually germinate and grow out into new mycelium when encountering favorable conditions (Flärdh et al., 1999).

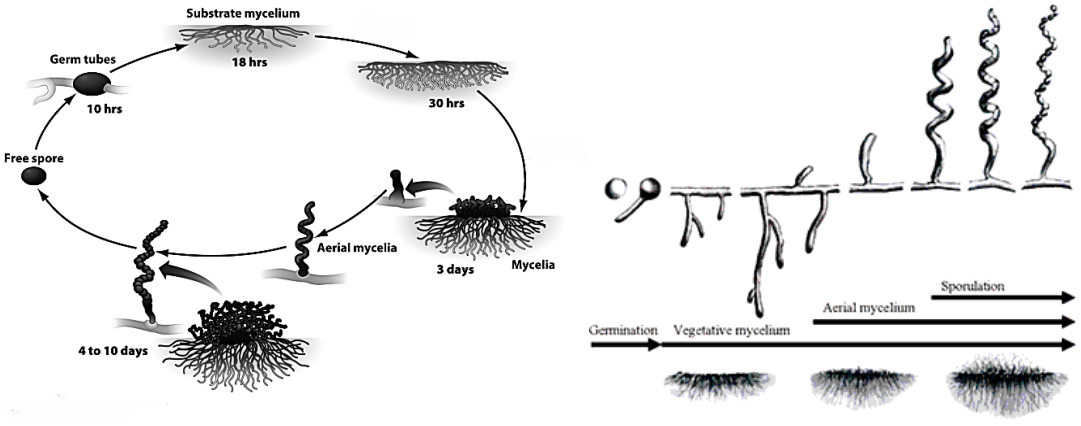

Figure 3. The developmental life cycle of *Streptomyces coelicolor* (Miyadoh et al., 1997).

1.3.3. Taxonomy

The phylum *Actinobacteria* represents one of the largest taxonomic units among the 18 major lineages recognized within the domain *Bacteria* (Stackebrandt et al.,

1997a), presently including six classes (*Actinobacteria*, *Acidimicrobiia*, *Coriobacteriia*, *Nitriliruptoria*, *Rubrobacteria*, and *Thermoleophilia*) (Barka et al., 2016). Among them, the class *Actinobacteria* contains 16 orders, including the order *Actinomycetales*.

The taxonomic characterization of the strains can be implemented by different approaches (Miyadoh et al., 1997), including the classical approach, using morphological, physiological, and biochemical characters (the classical approach has been frequently employed in the taxonomy of streptomycetes), the chemotaxonomical approach, using chemical characters as markers and the molecular approach, e.g. using 16S rDNA sequences (Fig. 4).

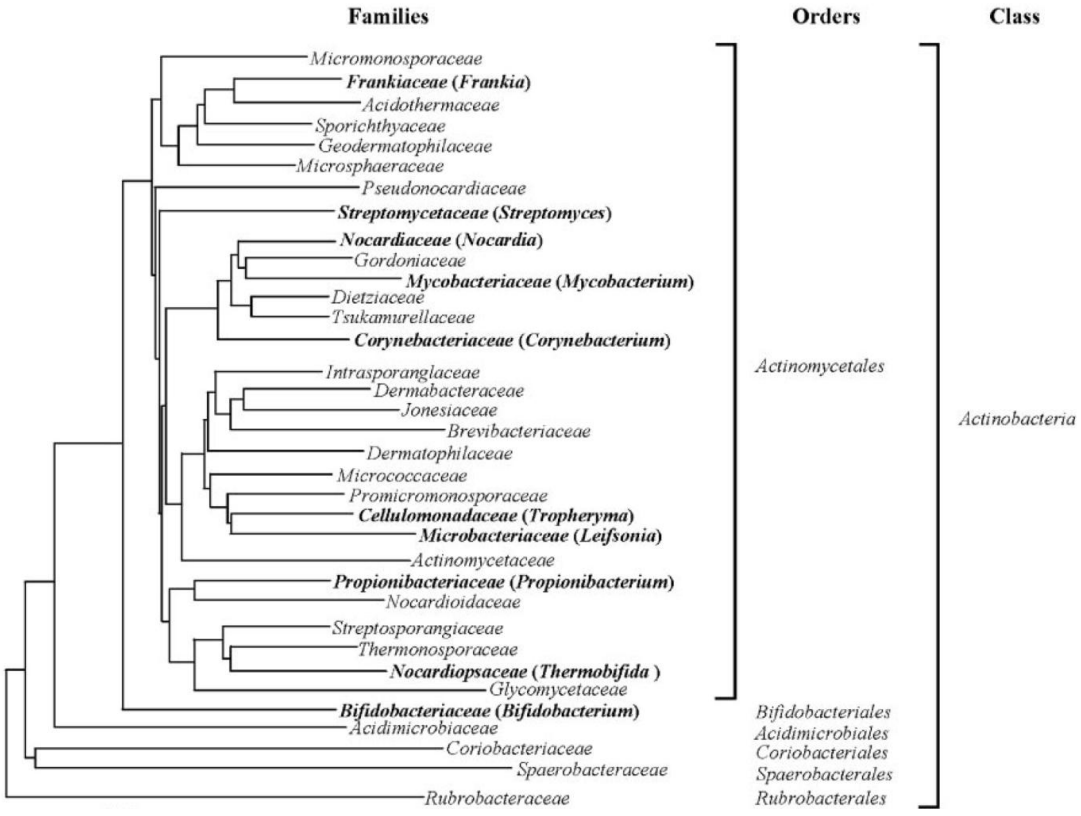

Figure 4. Phylogenetic tree of *Actinobacteria* based on 1,500 nucleotides of 16S rRNA (Ventura et al., 2007).

A classification of actinobacteria to various sections according to their characteristics (Chavan et al., 2013) is shown in Table 2.

Table 2. Classification of actinobacteria to various sections according to their characteristics (Chavan et al., 2013).

Section	Characteristics
Nocardioform actinomycetes	Aerobic, may be acid-alcohol fast; occur as rods, cocci and branched filaments or form substrate and aerial mycelium that fragment; wall chemotype IV; contain mycolic acids.
Actinomycetes with multilocular sporangia	Aerobic to facultatively anaerobic; mycelium divides in all planes, no aerial hyphae, wall chemotype III.
Actinoplanetes	Aerobic sporoactinomycetes, nonmotile, spores may be enclosed within vesicles; no aerial mycelium; wall chemotype II; whole-organism hydrolysates contain arabinose and xylose.
Streptomycetes and related genera	Aerobic sporoactinomycetes; form an extensively branched substrate and aerial mycelium.
Thermomonospora and related genera	Aerobic spordactinomycetes; form an extensively branched substrate and aerial mycelium both of which may carry single of chains of spores; spores either motile or non-motile; wall chemotype III.
Thermoactinomycetes	The stable filaments produce aerial growth; single spores (endospores) are formed on both aerial and vegetative filaments; all species are thermophilic; the cell wall contains meso-DAP but no characteristic amino acids or sugars.
Other genera	They all produce aerial growth bearing chains of spores.

1.3.4. Production of antibiotics

Actinobacteria are widely known for their ability to produce antibiotics. Among them, streptomycetes are the predominant. Streptomycetes undergo a program of colonial morphogenesis that is coordinated with the excretion of bioactive compounds that are often colored: blue, red, orange, brown, green, or grey, depending on their distinctive products (Fig. 5).

The most extensively studied *Streptomyces* species regarding the control of antibiotic production is *Streptomyces coelicolor* (Barka et al., 2016), which produces different antibiotics, some of which are pigmented. The genome of the genetically well-known strain *S. coelicolor* A3(2), being unusually large for bacteria, has 8.66 million base pairs (Mbp) of DNA (in contrast to the genome of *Escherichia coli* K-12 which comprises 4.6 Mbp) and includes more than 20 gene clusters that encode enzymes involved in the formation of secondary metabolites (Bentley et al., 2002).

Figure 5. Typical colonial morphologies of *Streptomyces*. Colonies often excrete colored pigments, providing a visual recording of secondary metabolites biosynthesis (Miyadoh et al., 1997).

Strain *S. coelicolor* A3(2) produces the pH indicator (red/blue) antibiotic actinorhodin, but not all the "blue pigments" produced by this strain are actinorhodin (Bystrykh et al., 1996). The blue color (Fig. 6) gives the species its name, i.e., coelicolor means heavenly color or sky-colored from the Latin words coelus (sky) and color (color).

The genus *Streptomyces* was created in 1943 to separate certain aerial mycelium producing actinobacteria from the rest of the order *Actinomycetales*. Streptomycin, discovered in October of the same year, was first isolated from *Streptomyces griseus* by Albert Schatz, a graduate student in the laboratory of Selman Abraham Waksman at Rutgers University (Singh et al., 2014). Streptomycin was the first antibiotic that could be used to cure the disease tuberculosis and accrued its first patients in January 1947 (Sakula, 1988). Subsequently, Waksman and his group discovered several antibiotics, of which streptomycin and neomycin found extensive application in the treatment of numerous infectious diseases. The discovery of antimicrobial agents from actinobacteria led to a breakthrough in the world of medicine, due to their tremendous contribution in saving human lives from infectious diseases.

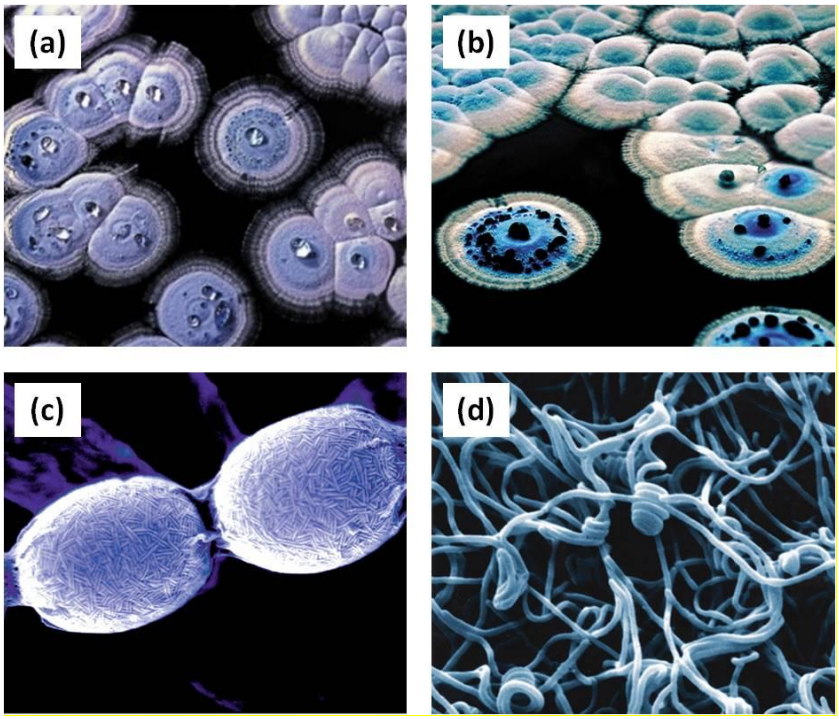

Figure 6. (a) *Streptomyces coelicolor* colonies grow blue and the droplets on the colonies are accumulations of some of its many secondary metabolites. (b) A panoramic view of *S. coelicolor* colonial morphology. Both peripheral and aerial mycelia develop from the central mass of the colony. Metabolites, including the blue antibiotic actinorhodin, are excreted into the medium and into aqueous droplets on the hydrophobic surface of the colony. (c) False-colored scanning electron micrograph of wild-type *S. coelicolor* spores grown on agar medium. (d) Scanning electron micrograph showing aerial hyphae in the form of coils on the surface of a colony of *S coelicolor*.

1.4. Bioactive natural products from actinobacteria

Among the various microorganisms, actinobacteria have gained special attention due to their ability to produce bioactive secondary metabolites and enzymes that find applications in the medicinal and agricultural sectors.

To date, more than 140 actinobacterial genera have been described. A few of these (*Streptomyces*, *Saccharopolyspora*, *Amycolatopsis*, *Micromonospora* and *Actinoplanes*) are responsible for the majority of known pharmaceutically important compounds (Bull & Stach, 2007; Pimentel-Elardo et al., 2010). However, many other actinobacterial genera also produce bioactive metabolites (Table 3).

Table 3. Number of strains producing bioactive metabolites per actinobacterial genus (Bérdy, 2005; Raja & Prabakarana, 2011).

Genus	**No. of strains**	**Genus**	**No. of strains**
Streptomycetaceae		**Thermomonosporaceae**	
Streptomyces	~8000	*Actinomadura*	345
Streptoverlicillium	258	*Saccharothrix*	68
Kitasatosporia	37	*Microbispora*	54
Chainia	30	*Actinosynnema*	51
Microellobosporia	11	*Nocardiopsis*	41
Nocardioides	9	*Microtetraspora / Nonomuria*	26 / 21
Micromonosporaceae (Actinoplanetes)		*Thermomonospora*	19
Micromonospora	740	*Micropolyspora / Faenia*	13 / 3
Actinoplanes	248	*Thermoactinomyces*	14
Dactylosporangium	58	*Thermopolyspora*	1
Ampullariella	9	*Thermoactinopolyspora*	1
Glycomyces	2	**Mycobacteriaceae (Actinobacteria)**	
Catenuloplanes	3	*Nocardia*	357
Catellatospora	1	*Mycobacterium*	57
Pseudonocardiaceae		*Arthrobacter*	25
Saccharopolyspora	131	*Brevibacterium*	17
Amycolatopsis / Nocardia	120 / 357	*Proactinomyces*	14
Kibdellosporangium	34	*Rhodococcus*	13
Pseudonocardia	27	**Other (unclassified) species**	
Amycolata	12	*Actinosporangium*	30
Saccharomonospora	2	*Microellobosporia*	11
Actinopolyspora	1	*Frankia*	7
Streptosporangiaceae (Maduromycetes)		*Westerdykella*	6
Streptosporangium	79	*Kitasatoa*	5
Streptoalloteichus	48	*Synnenomyces*	4
Spirillospora	11	*Sebekia*	3

The secondary metabolites produced by actinobacteria reveal multifarious biological activities, such as antibacterial, antifungal, antiviral, anticancer, antiprotozoal, anticholesterol, anti-ageing, immunostimulatory and immunosuppressive (Table 4) (Barka et al., 2016; Bhat et al., 2013).

Table 4. Examples of bioactive metabolites produced by actinobacteria and their biological activity (Adegboye & Babaola, 2013; Barka et al., 2016; Solecka et al., 2012).

Species	**Bioactive metabolite(s)**
Antibacterial activity	
Streptomyces griseus	Streptomycin
Streptomyces clavuligerus	Clavulanic acid, Cephamycin C, Penicillin N
Streptomyces fimbriatus	Cephamycins A and B
Streptomyces cattleya.	Yhienamycin
Streptomyces aureofaciens	Chlortetracycline
Streptomyces rimosus	Tetracycline, Oxytetracycline
Micromonospora purpurea	Gentamycin
Streptomyces kanamyceticus	Kanamycin
Streptomyces tenebrarius	Apramycin
Streptomyces fradiae	Neomycin, Tylosin
Amycolatopsis orientalis	Vancomycin
Actinoplanes teichomyceticus	Teicoplanin
Saccharopolyspora erythraea	Erythromycin
Streptomyces ambofaciens	Spiramycin
Streptomyces noursei	Nystatin
Streptomyces avermitilis	Avermectin, Filipin
Streptomyces griseus	Etamycin
Streptomyces virginiae	Virginiamycin M1, Virginiamycin S
Streptomyces pristinaespiralis	Pristinamycin
Streptomyces roseosporus	Daptomycin
Streptomyces platensis	Platencin
Amycolatopsis fastidiosa	Nocathiacins, Thiazomycins
Amycolatopsis sp. ML1-hF4	Pargamycin A
Antifungal activity	
Streptomyces nodosus	Amphotericin B
Streptomyces cacaoi var. *asoensis*	Polyoxins
Streptomyces tendae	Nikkomycins
Streptomyces libani	Oligomycins
Streptomyces hygroscopicus	Rapamycin
Antiviral activity	
Streptomyces lyososuperficus nov. sp.	Tunicamycin
Streptomyces griseoflavus subsp. *thuringiensis*	Streptovirudin
Corynebacterium rathayi	Corynetoxins
Anticancer activity	
Streptomyces antibioticus	Actinomycin D
Streptomyces peuceticus.	Daunorubicin (Daunomycin), Doxorubicin (Adriamycin), Epirubicin
Streptomyces verticillus	Bleomycin
Streptomyces caesptitosus	Mitomycins
Streptomyces achromogenes	Streptozotocin
Micromonospora echinospora	Calicheamicins

Species	Bioactive metabolite(s)
Antiparasitic activity	
Streptomyces hygroscopicus subsp. *aureolacrimosus*	Milbemycins
Streptomyces avermitilis	Avermectins
Streptomyces nanchangensis	Nanchangmycin, Meilingmycin
Streptomyces fulvissimus	Valinomycin
Streptomyces sp.	Staurosporine
Streptomyces sp. K05-0178	Sinefungin VA, Dehydrosinefungin V
Insecticidal activity	
Saccharopolyspora spinosa	Spinosyns A and D
Immunosuppressive activity	
Streptomyces hygroscopicus	Rapamycin (Sirolimus)
Streptomyces tsukubaensis	Fujimycin (Tacrolimus, FK-506)
Immunostimulatory activity	
Nocardia rubra	Rubrattin
Streptomyces olivoreticuli	Bestatin

The major classes of antibiotics produced by actinobacteria include (Adegboye & Babaola, 2013):

- β-lactams

They are bacteriocidal in nature and exhibit a broader spectrum of antibiotic activities, being active against both Gram-positive and Gram-negative bacteria. The mechanism of action of β-lactams is through the synthesis' inhibition of the peptidoglycan layer in the bacterial cell wall (Anderson et al., 2012).

- aminoglycosides

They are classified into two groups according to the structure of the aglycone. The mechanism of action of aminoglycosides is expressed by inhibiting the polypeptide chain elongation phase resulting in protein synthesis inhibition. Streptomycin was the first aminoglycoside antibiotic identified (Vakulenko & Mobashery, 2003).

- glycopeptides

They are a class of antibiotics composed of glycosylated cyclic or polycyclic non-ribosomal peptides and are characterized by the presence of a unique long aliphatic chain attached to a sugar moiety. The mechanism of action of glycopeptides is expressed by inhibiting the maturation of the peptidoglycan layer in bacterial cell wall biosynthesis at the transglycosylation and transpeptidation steps (Jeya et al., 2011).

- anthracyclines

Their chemical diversity is based on the structural differences in the aglycone part and on the wide array of attached sugar residues. These compounds are used in the

clinical treatment of various cancer types, such as acute myeloid leukemia, lymphomas, and diverse solid tumors including breast, small cell lung, cervical, head, and neck cancer (Abdelfattah.et al., 2008). Anthracyclines have three mechanisms of action: (a) inhibition of DNA and RNA synthesis by intercalating between base pairs of the DNA/RNA strand, (b) inhibition of topoisomerase II enzyme (an enzyme that unzips the DNA for replication), (c) creation of iron-mediated free-oxygen radicals that damage the DNA, proteins and cell membranes (Muindi et al., 1984).

- macrolides

They are composed of a large macrocyclic lactone ring on which one or more deoxy sugars are attached. The mechanism of action of macrolides is through the inhibition of bacterial protein biosynthesis (Zuckerman, 2004).

- tetracyclines

They are derivatives of polycyclic naphthacene carboxamide. They exhibit activity against a wide range of microorganisms, including Gram-positive and Gram-negative bacteria, chlamydiae, mycoplasmas, rickettsiae, and protozoan parasites. The mechanism of action of tetracyclines was found to be through the inhibition of bacterial protein biosynthesis (Nelson & Levy, 2011).

- polyenes

They are antifungal agents with 3 to 8 conjugated double bonds in the macrolactone ring. Polyenes have a broad spectrum of action and are useful in treating fungal infections, such as candidosis, cryptococcosis, histoplasmosis, blastomycosis, paracoccidioidomycosis, coccidioidomycosis, aspergillosis, extracutaneous sporotrichosis, mucormycosis, hyalohyphomycosis and phaeohyphomycosis. The mechanism of action of polyenes is expressed by binding to ergosterol, the primary sterol in the fungal cell membrane (Paquet & Carreira, 2006).

- streptogramins

They consist of at least two structurally unrelated compounds, group A or M (macrolactones) and group B or S (cyclic hexadepsipeptides). These antibiotics act at the level of inhibition of translation through binding to the bacterial ribosome and inhibit protein synthesis at the elongation step. The two groups act synergistically and their combined action is irreversible (Bonfiglio & Furneri, 2001).

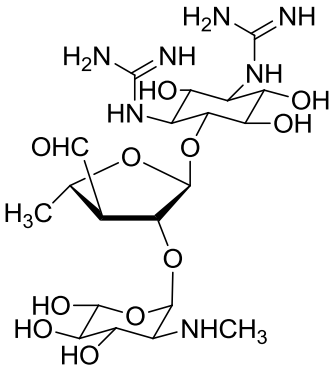

streptomycin A

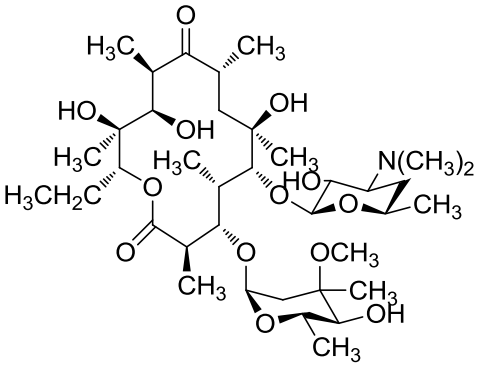

erythromycin

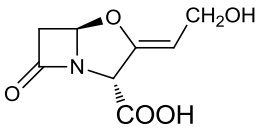

clavulanic acid

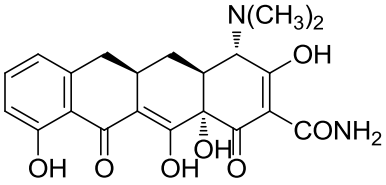

6-deoxy-6-demethyltetracycline

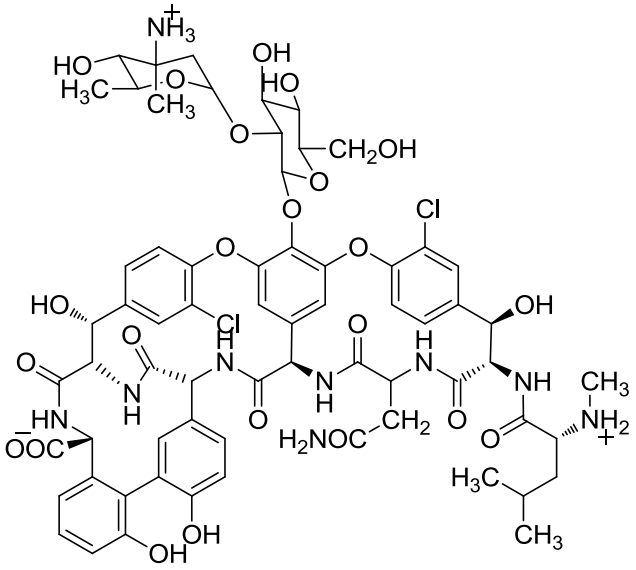

vancomycin

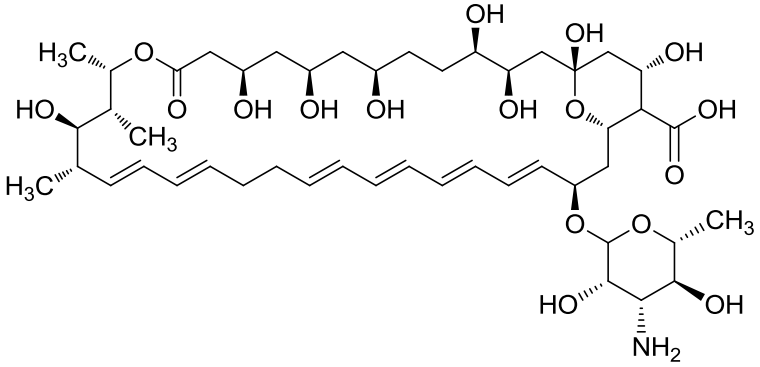

nystatin A_1

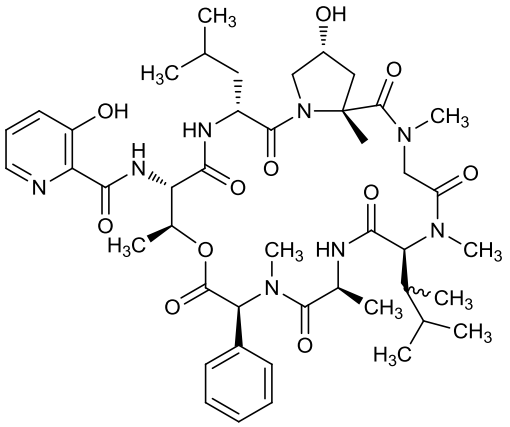

etamycin

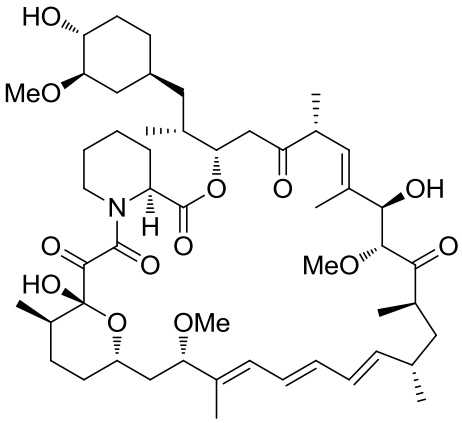

rapamycin

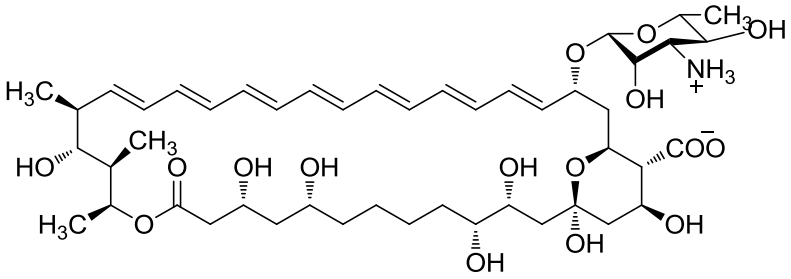

amphotericin B

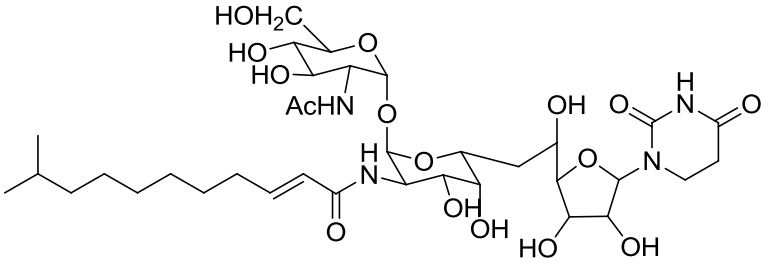

streptovirudin A1

A number of compounds with antibiotic activity produced by *Streptomyces* have proven dangerous for use in humans as antibiotics, but due to their toxicity towards cells (specifically dividing cells) they have been reconsidered as chemotherapeutic drugs (Birnbaum et al., 1985).

Additionally, actinobacteria produce secondary metabolites that act as enzyme inhibitors, immunosuppressors, phytotoxins and pesticides (Bérdy, 1995). The indolocarbazole alkaloid staurosporine has antiparasitic activity, besides being a well known inducer of apoptosis in a wide range of cell lines (Andréo et al., 2012). Avermectin B1 (Abamectin) is a widely used insecticide and anthelminthic agent, containing more than 80% of avermectin B1a and less than 20% of avermectin B1b (Deng and Bai, 2006). The glycosylated polyketides spinosyns possess high insecticidal activity and are used as biocontrol agents in commercial products for the management of insect pests. They exhibit their activity through a novel mechanism of action that

involves disruption of the binding sites on nicotinic acetylcholine receptors of the insect nervous system (Tietze et al., 2013).

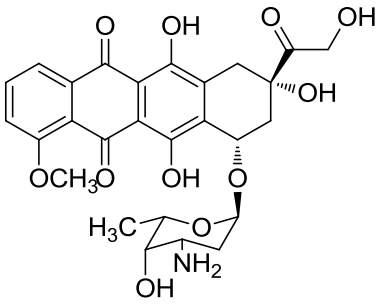

doxorubicin

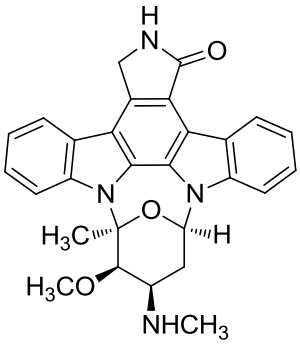

staurosporine

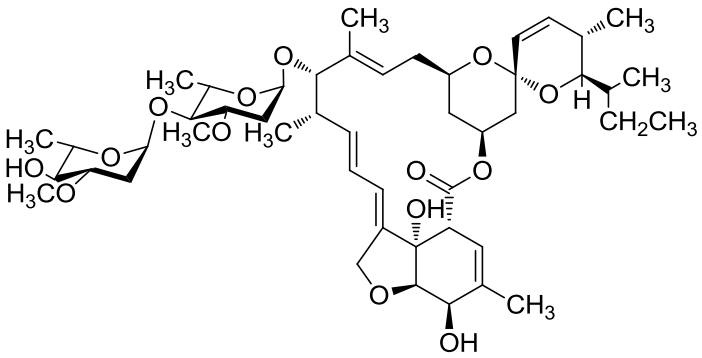

avermectin B1a

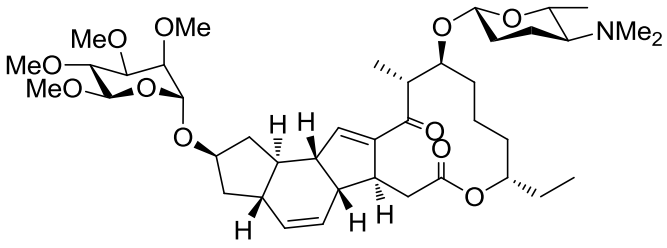

spinosyn A

1.5. Marine-derived *Streptomyces* strains as a source of bioactive natural products

Among actinobacteria, the genus *Streptomyces* is the richest source of antibiotics, as well as other industrially-important compounds. About 70% of all known antibiotics are obtained from actinobacteria and the majority of those (~80%) are derived from *Streptomyces* strains (Chavan et al., 2013).

The marine environmental conditions are extremely different from terrestrial ones and it is thought that marine actinobacteria have different characteristics from those of terrestrial counterparts, therefore probably producing different types of secondary metabolites. Over the past two decades, information on the diversity of

actinobacteria in marine habitats has grown considerably, while the interest in their ability to produce secondary metabolites has continued quite strongly (Stackebrandt et al., 1997b).

The marine environment contains a wide range of distinct *Streptomyces* that are not present in the terrestrial environment (Dharmaraj, 2010). Indeed, marine *Streptomyces* occur in different biological sources, such as fish, molluscs, sponges, seaweeds and mangroves, besides seawater and sediments.

Four butenolides, namely 4,10-dihydroxy-10-methyldodec-2-en-1,4-olide (**1**), two diastereoisomeric 4,11-dihydroxy-10-methyldodec-2-en-1,4-olides (**2** and **3**), and 4-hydroxy-10-methyl-11-oxododec-2-en-1,4-olide (**4**), were isolated from *Streptomyces* strains B 5632 and B 3497, both of which were isolated from marine sediments (Mukku et al., 2000).

N-Acetyl-γ-hydroxyvaline lactone (**5**), obtained from a streptomycete isolated from a marine sediment from Brazil, belongs to a class of compounds implicated in quorum sensing (Hernández et al., 2000).

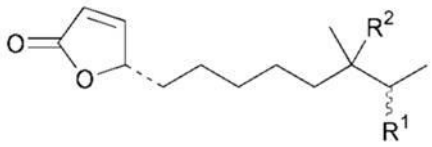

1 $R^1 = H; R^2 = OH$
2, 3 $R^1 = OH; R^2 = H$
4 $R^1 = O; R^2 = H$

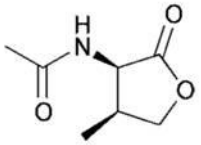

5

Culture of a *Streptomyces* sp. from a sediment sample from Oahu, Hawaii, yielded the antibacterial and antifungal metabolite bonactin (**6**) (Schumacher et al., 2003).

Parimycin (**7**), an 1,4-anthraquinone isolated from a streptomycete from a sediment sample from Laguna de Terminos, Gulf of Mexico, had moderate activity against *Bacillis subtilis*, *Streptomyces viridochromogenes*, *Staphylococcus aureus* and *Escherichia coli*, in addition to activity against a number of human tumour cell lines (Maskey et al., 2003).

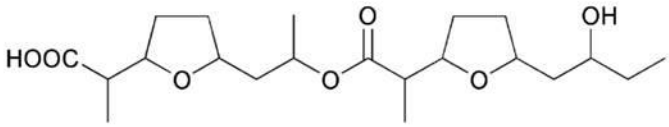

6

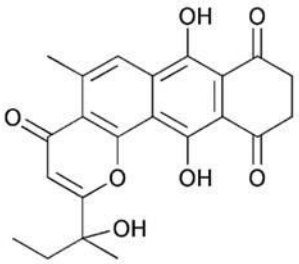

7

A *Streptomyces* sp. cultured from an unidentified Mexican marine invertebrate yielded the cytotoxic indoles **8-10** which had moderate activity against a panel of 14 tumour cell lines (Sánchez López et al., 2003).

The anthracycline komodoquinone A (**11**) and the aglycone komodoquinone B (**12**) were isolated from a culture of a *Streptomyces* sp. isolated from marine sediment off Komodo Island, Indonesia. Komodoquinone A (**11**) displayed dose-dependent neuritogenic activity against the neuroblastoma cell line Neuro 2A (Itoh et al., 2003).

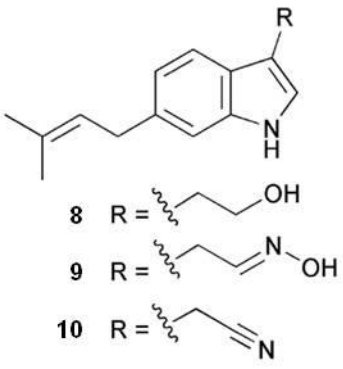

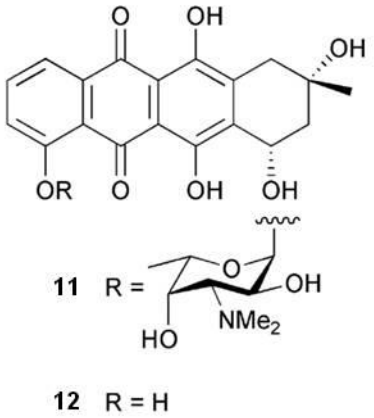

12 R = H

Gutingimycin (**13**), whose absolute configuration was determined by X-ray analysis, is a highly polar trioxacarcin derivative from a *Streptomyces* species isolated from sediment (Laguna de Terminos, Gulf of Mexico) (Maskey et al., 2002; Maskey et al., 2004a). The same *Streptomyces* species (Maskey et al., 2002) also yielded trioxacarcins D–F (**14-16**), in addition to the known trioxacarcins A–C (Tomita et al., 1981; Tamaoki et al., 1981; Shirahata et al., 1981). The structures and absolute configurations of the new trioxacarcins followed from the X-ray analysis of gutingimycin (**13**) and the known stereochemistry of L-trioxacarcins A and B (Shirahata et al., 1981). The trioxacarcins and gutingimycin exhibited strong antibacterial activity

against a range of test organisms. The antitumour activity of trioxacarcin D (**14**) was similar to that previously reported for trioxacarcins A–C (Tomita et al., 1981; Tamaoki et al., 1981; Shirahata et al., 1981), while trioxacarcin A and trioxacarcin D (**14**) were also potently antiplasmodial (Maskey et al., 2004b).

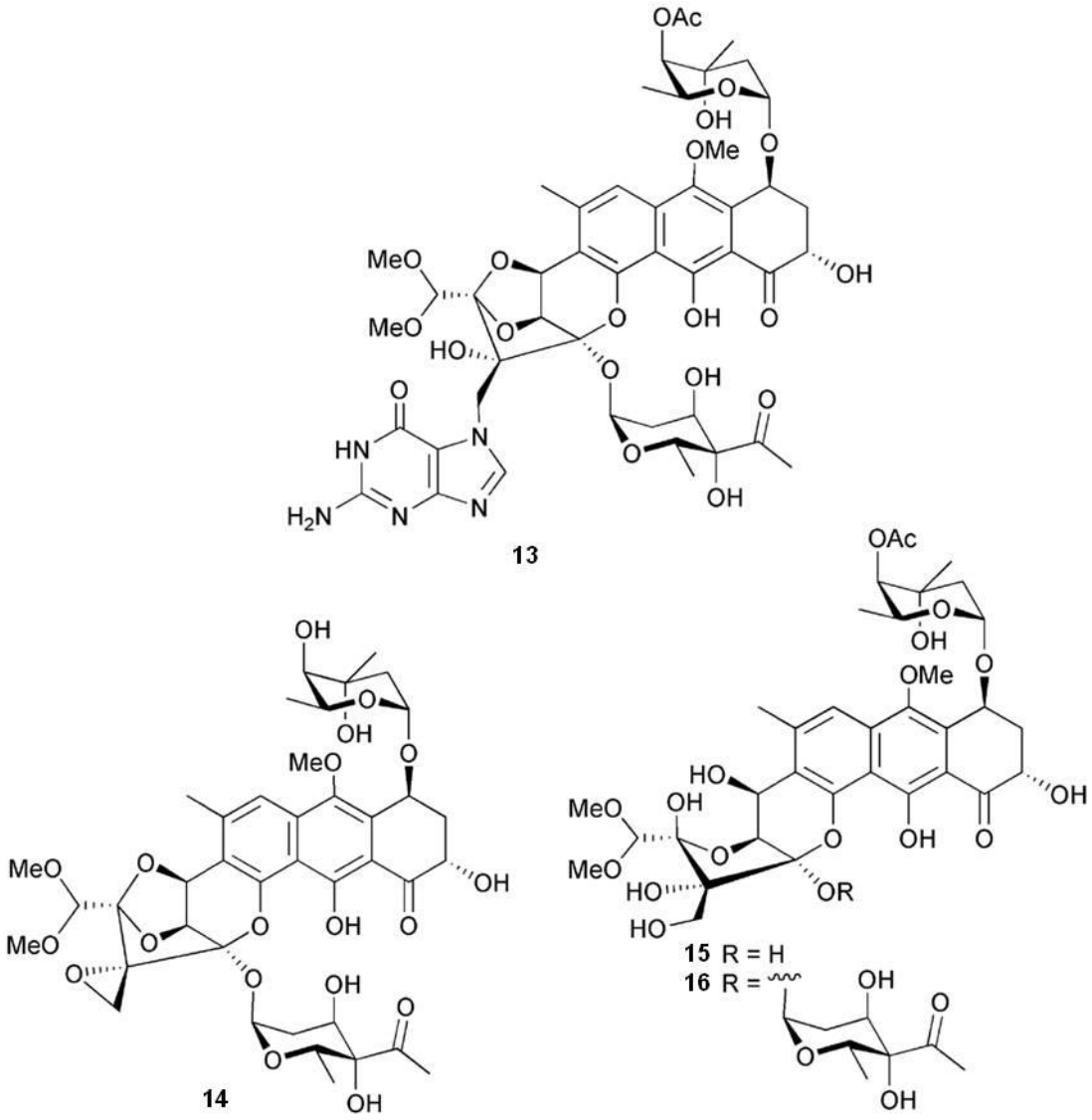

Streptomyces acrimycini, isolated from sediment (São Sebastião channel, Brazil), provided two dipeptide derivatives, namely 8-amino-[1,4]-diazonane-2,5-dione (**17**) and leucyl-4-hydroxyproline (Hernández et al., 2004).

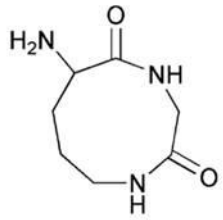

17

Streptomyces nodosus, isolated from marine sediment (Scripps Canyon, California), yielded the antibiotic lajollamycin (**18**) active against both drug-sensitive and drug-resistant Gram positive microorganisms and inhibited growth of the murine melanoma cell line B16-F10 (Manam et al., 2005).

The chlorine-containing manumycin derivatives, chinikomycins A (**19**) and B (**20**) were isolated from a *Streptomyces* species obtained from sediment (Jiaozhou Bay, China). Both **19** and **20** displayed antitumour activity against a number of human cancer cell lines (Li et al., 2005).

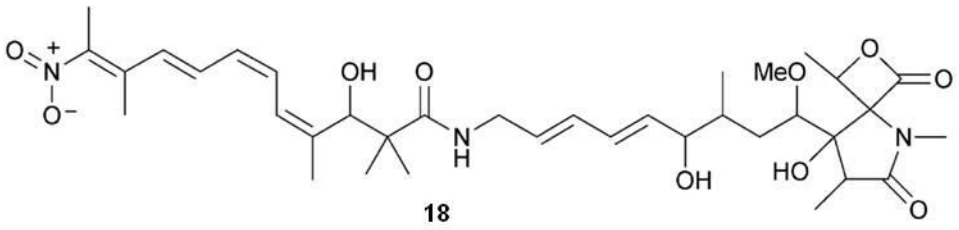

18

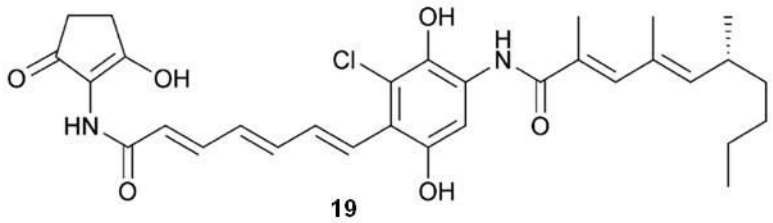

19

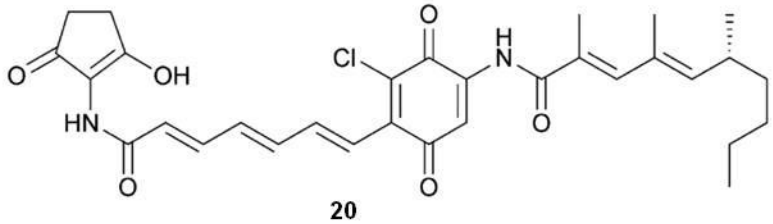

20

A *Streptomyces* species isolated from an unidentified sponge (Jaeju Island, Korea) was the source of the cyclic peptides dehydroxynocardamine (**21**) and desmethylenylnocardamine (**22**), weak inhibitors of the recombinant enzyme sortase B

(Lee et al., 2005).

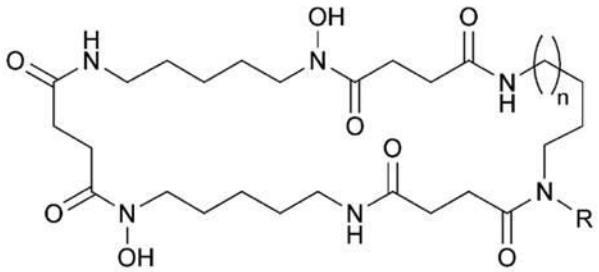

21 R = H, n = 2
22 R = OH, n = 1

The pyrrolosesquiterpenes glaciapyrroles A–C (**23-25**) were obtained from a *Streptomyces* species isolated from marine sediment (Alaska). Glaciapyrrole A (**23**) exhibited activity against HT-29 and B16-F10 cell lines (Macherla et al., 2005).

A resistomycin derivative, 1-hydroxy-1-norresistomycin (**26**), has been independently isolated from different cultures of sediment-derived *Streptomyces* species, one from Laguna de Terminos, Gulf of Mexico (Kock et al., 2005) and the other from *Streptomyces chibaensis* (Bay of Bengal, India) (Gorajana et al., 2005). Compound **26** was active against *E. coli*, *S. aureus* and *Streptomyces viridochromogenes* (Kock et al., 2005) and cytotoxic to HMO2 (gastric adenocarcinoma) and HePG2 (hepatic carcinoma) cell lines (Gorajana et al., 2005).

Feigrisolide C (**27**), isolated originally from *Streptomyces griseus* (Tang et al., 2000), was also isolated from a marine *Streptomyces* species (Sobolevskaya et al., 2004).

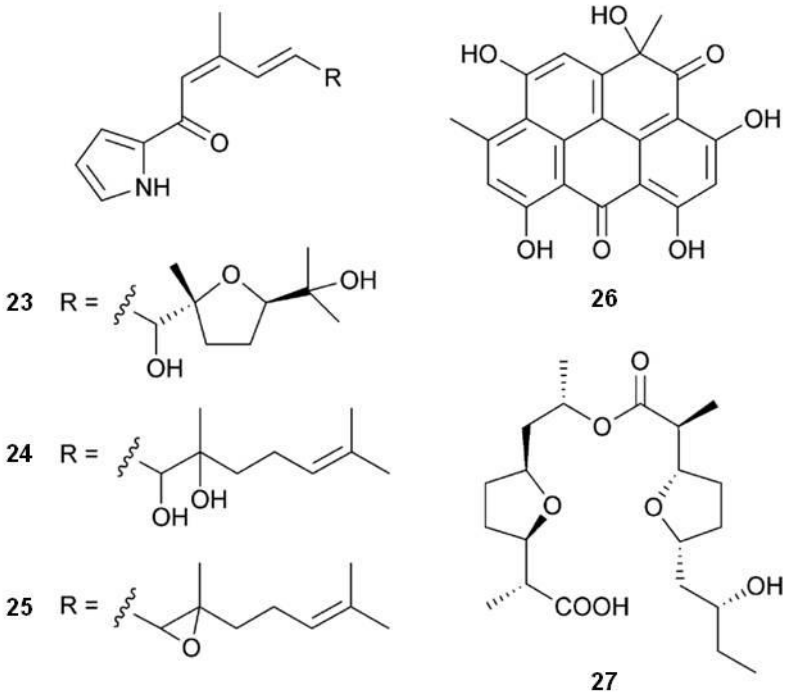

From a North Sea strain of *Streptomyces*, new methyl branched γ- and δ-lactones **28-33** were obtained along with two previously reported lactones (Mertens et al., 1960; McGhie et al., 1962) isolated for the first time from a natural source (Dickschat et al., 2005).

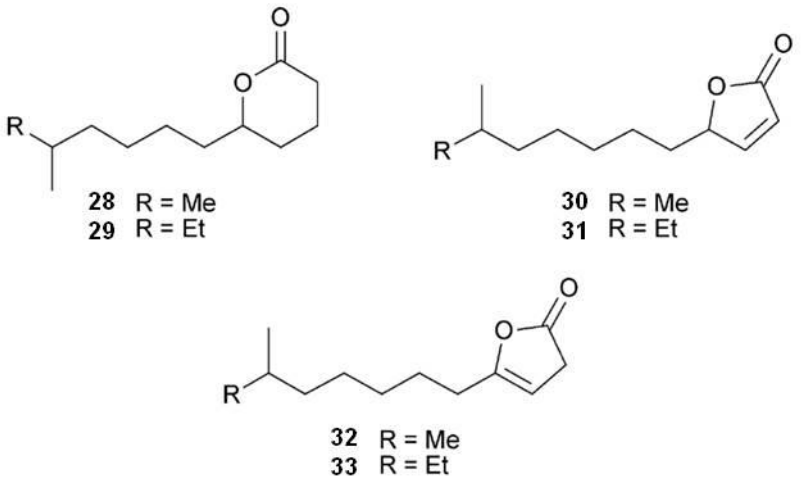

A *Streptomyces* species from marine driftwood (West Coast, New Zealand) gave four new cytotoxic anthracycline derivatives (7*S**,9*R**,10*R**)-pyrromycin (**34**), (7*R**,9*R**,10*R**)-pyrromycin (**35**), 1-hydroxyauramycin T (**36**) and 1-hydroxysulfurmycin T (**37**) (Han et al., 2005).

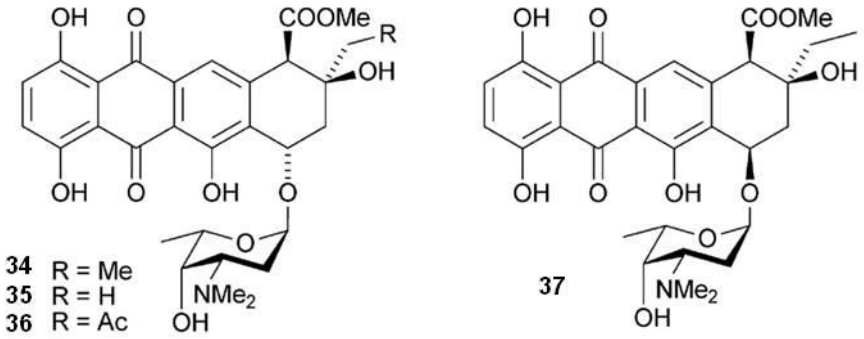

Four amides, daryamides A–C (**38-40**) and (2*E*,4*E*)-7-methylocta-2,4-dienoic acid amide (**41**), were isolated from culture of a *Streptomyces* sp. obtained from marine sediment (San Diego, California). Compounds **38–41** were weak to moderately cytotoxic to HCT-116 and weakly active against *Candida albicans* (Asolkar et al., 2006).

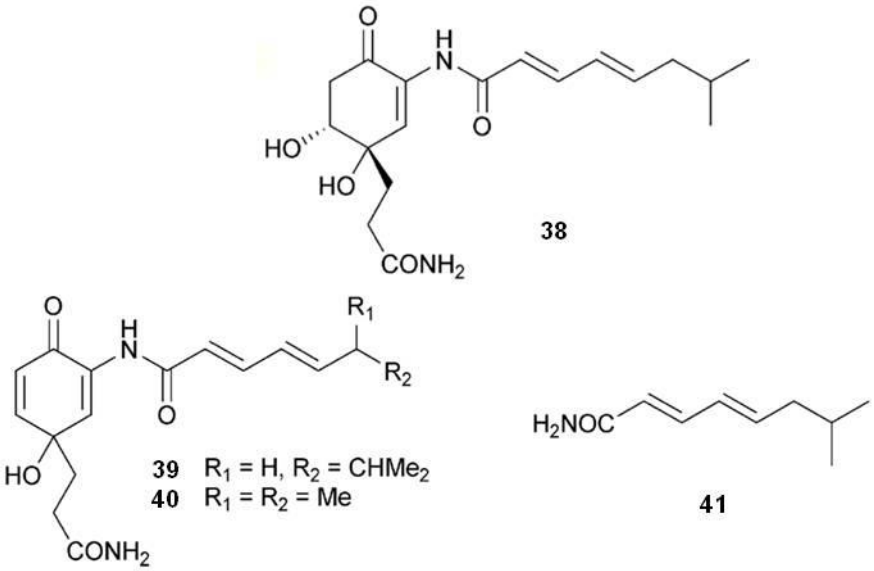

A staurosporine derivative (**42**) and a sesquiterpene (**43**) were isolated from the culture broth of a *Streptomyces* sp. derived from sediment (Jiaozhou Bay, China) together with the new alkaloid 5,7-dihydroxy-5,6,7,8-tetrahydro-1*H*-azocin-2-one (**44**) (Wu et al., 2006; Fotso et al., 2006). Compound **42** was selectively active against a number of solid tumour derived human tumour cell lines and weakly active against *Streptomyces viridochromogenes* (Wu et al., 2006).

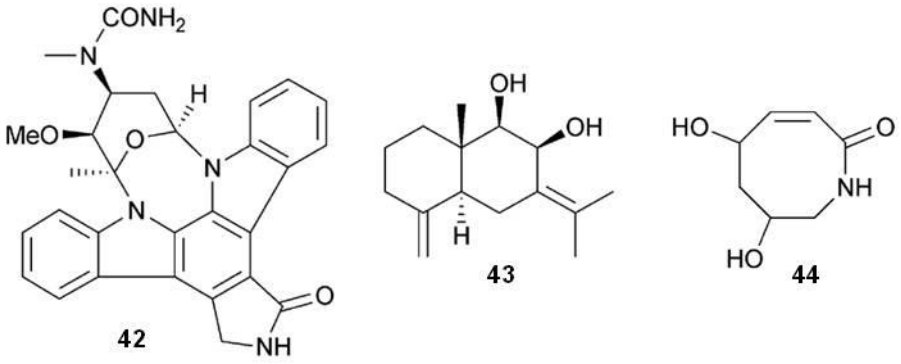

The pyrrolizidine alkaloids bohemamine B (**45**), bohemamine C (**46**) and 5-chlorobohemamine C (**47**) were isolated from culture of *Streptomyces* sp. from sediment off Guam (Bugni et al., 2006), while urauchimycin C (**48**) and urauchimycin D (**49**) were isolated from culture of a *Streptomyces* strain from sediment off Shetland Islands (Yao et al., 2006).

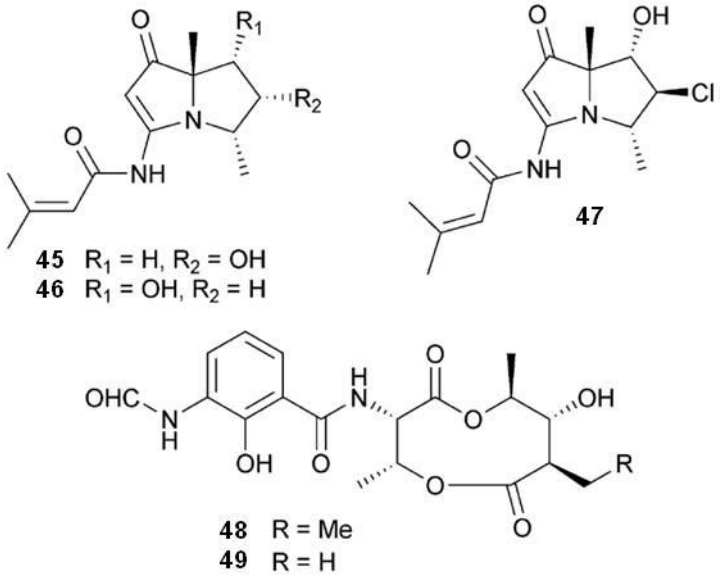

A deep-sea sediment (Ayu Trough, western Pacific Ocean) *Streptomyces* sp. yielded the cytotoxic streptokordin (**50**) (Jeong et al., 2006), while anthraquinones **51** and **52**, which displayed moderate activity against *Staphylococcus aureus* and *Streptomyces viridochromogenes*, came from culture of a *Streptomyces* strain separated from sediment (Laguna de Terminos, Gulf of Mexico) (Poumale et al., 2006).

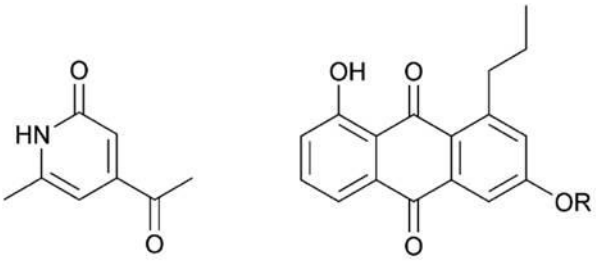

50

51 R = Me
52 R = H

The pentacyclic anthraquinone C-glycosides marmycins A (**53**) and B (**54**) were isolated from fermentation of a *Streptomyces* actinomycete (sediment, Cabo San Lucas, Mexico). Marmycin A (**53**) was potently cytotoxic against a panel of human tumour cell lines. Treatment of marmycin A (**53**) with dilute hydrochloric acid produced trace quantities of marmycin B (**54**), suggesting the possibility that marmycin B (**54**) arose by acidcatalysed chloride substitution of marmycin A (**53**) (Martin et al., 2007).

The cyclic hexadepsipeptides piperazimycins A–C (**55-57**), isolated from the fermentation broth of a *Streptomyces* sp. (sediment, Guam), contained rare amino acids and were all significantly cytotoxic (HCT-116). Piperazimycin A (**55**) was also potent in the 60-cell line panel of the National Cancer Institute, especially against solid tumour cell lines (Miller et al., 2007).

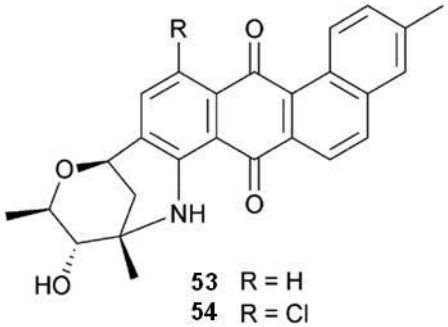

53 R = H
54 R = Cl

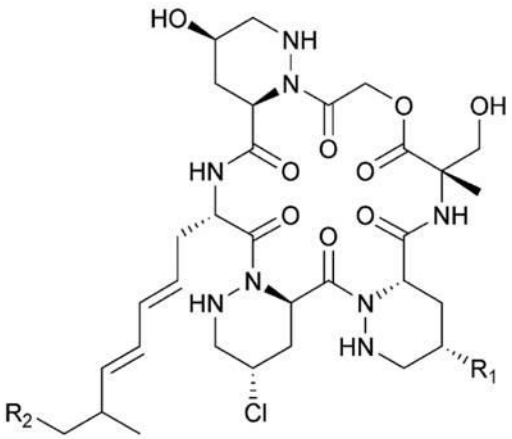

55 R_1 = OH, R_2 = H
56 R_1 = R_2 = H
57 R_1 = OH, R_2 = Me

Piericidins C7 (**58**) and C8 (**59**) were isolated from a culture of a marine *Streptomyces* sp. (unidentified ascidians, Iwayama Bay, Palau) and were selectively

cytotoxic to transformed rat glia cells and to Neuro-2a mouse neuroblastoma cells (Hayakawa et al., 2007).

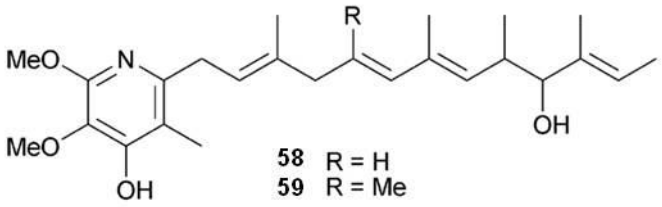

Marinopyrroles A (**60**) and B (**61**) are halogenated axially chiral bispyrroles obtained from culture of a *Streptomyces* sp. (sediment, La Jolla, California). Although they exist as a single atropisomer at room temperature they can be racemised at a higher temperature. Marinopyrroles A (**60**) and B (**61**) exhibited potent activity against MRSA and moderate activity against HCT-116 cancer cells (Hughes et al., 2008).

Cultivation of a *Streptomyces* species (saline mud, Tokushima, Japan) yielded two new terpenoids, a 5-dimethylallylindole- 3-carboxylic acid (**62**), and a quinone (**63**) which was weakly active against *B. subtilis* (Motohashi et al., 2008).

Essramycin (**64**) is a triazolopyrimidine antibiotic obtained from culture of a *Streptomyces* sp. (sediment, Paltium coast, Egypt) and was active against a range of Gram-positive and Gram-negative bacteria (El-Gendy et al., 2008).

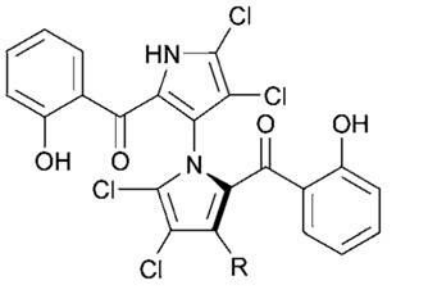

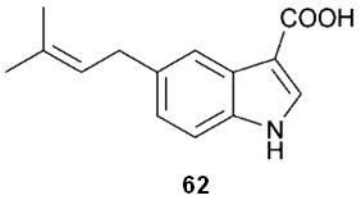

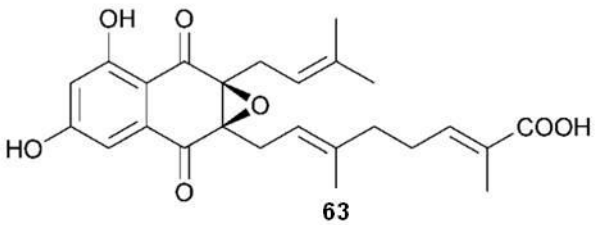

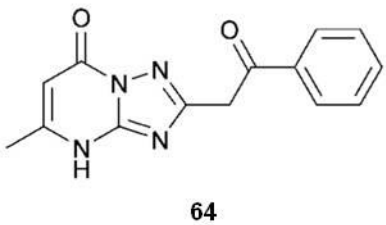

Culture of a *Streptomyces* sp. separated from the sponge *Halichondria panicea* (Baltic Sea, Germany) yielded the streptophenazines A–H (**65-72**), several of which showed weak to moderate activity against *B. subtilis* and *Staphylococcus lentus*. Addition of subinhibitory concentrations of antibiotics to the cultivation media affected the pattern of streptophenazine production depending on the antibiotic added (Mitova et al., 2008).

Cultivation of a *Streptomyces* strain associated with the ascidian *Aplidium lenticulum* (Great Barrier Reef) led to the isolation of cinnamoylphosphoramide (**73**), a weak inhibitor of acetylcholinesterase (Quitschau et al., 2008).

A *Streptomyces* sp. (sediment, Hawaii) yielded a polyether metabolite (**74**) with antiprotozoal activity against both chloroquine-susceptible and chloroquine-resistant clones of *Plasmodium falciparum*, but without cytotoxicity to normal (Vero) cells (Na et al., 2008).

Culture of a *Streptomyces* strain (sediment, Laguna de Terminos, Gulf of Mexico) has yielded two dodecanoic acid derivatives, a butenolide (**75**) and the respective acid (**76**) (Shaaban et al., 2008).

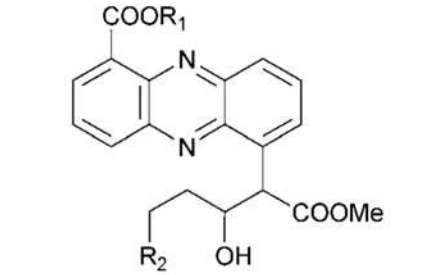

65 R_1 = Me, R_2 = CH_2CHMe_2
66 R_1 = Me, R_2 = $(CH_2)_3Me$
67 R_1 = H, R_2 = CH_2CHMe_2
68 R_1 = Me, R_2 = $CHMe_2$
69 R_1 = Me, R_2 = CH_2Me
70 R_1 = Me, R_2 = $CH_2CH_2CHMe_2$
71 R_1 = Me, R_2 = $CH_2CH(Me)CH_2Me$
72 R_1 = Me, R_2 = CH_2COHMe_2

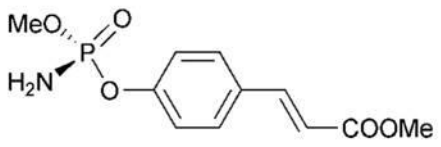

73

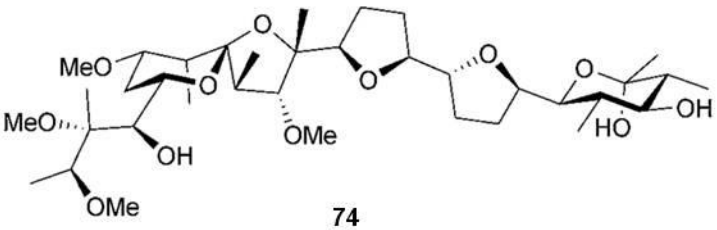

74

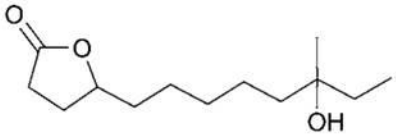

75

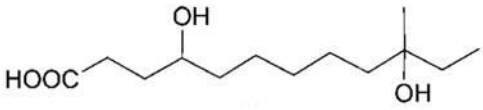

76

Phaechromycins F–H (**77-79**) are polyketides isolated from culture of a *Streptomyces* species (deep sea sediment, Western Pacific Ocean) with weak to modest

cytotoxicity against the HeLa cell line (Li et al., 2008).

Culture of a *Streptomyces*-related actinomycete (marine sediment, location not given) yielded the spiroaminals marineosins A (**80**) and B (**81**), selective inhibitors of HCT-116 cells. Marineosin A (**80**) was an order of magnitude more active than marineosin B (**81**) and displayed selective cytotoxicity against melanoma and leukaemia cell lines (Boonlarppradab et al., 2008).

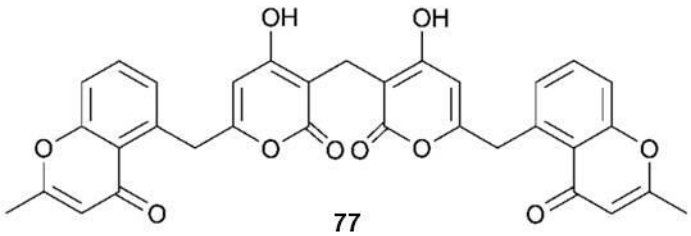

77

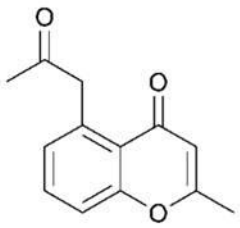

78

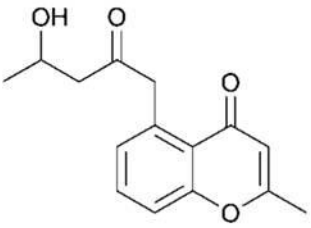

79

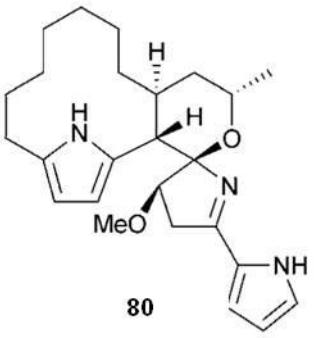

80

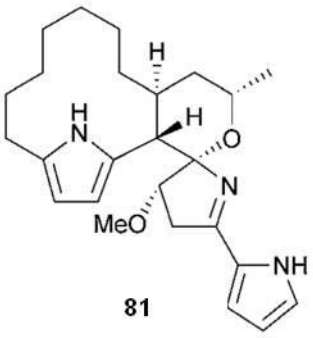

81

All of the indoxamycins A–F (**82-87**), unusual polyketides with six consecutive chiral centres isolated from *Streptomyces* sp. (sediment, Kochi Harbour, Japan), were moderately cytotoxic to HT-29 cells. Biosynthetic-feeding experiments indicated that indoxamycin A (**82**) was assembled from propionate units which initially formed a pentamethylindenofuran (Sato et al., 2009).

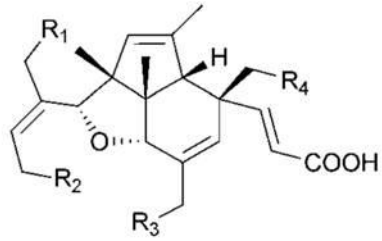

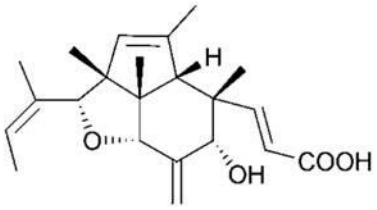

87

82 $R_1 = R_2 = R_3 = R_4 = H$
83 $R_1 = R_2 = R_3 = H$, $R_4 = OH$
84 $R_1 = R_2 = R_4 = H$, $R_3 = OH$
85 $R_1 = OH$, $R_2 = R_3 = R_4 = H$
86 $R_1 = R_3 = R_4 = H$, $R_2 = OH$

Ammosamides A (**88**) and B (**89**) are chlorinated tricyclic pyrroloquinoline alkaloids from *Streptomyces* sp. (sediment, Bahamas). Ammosamide A (**88**) contains an unusual thio-γ-lactam ring and gradually converted to ammosamide B (**89**) on exposure to air. Both **88** and **89** displayed potent cytotoxicity against a number of cancer cell lines. The target was identified as the motor protein, myosin (Hughes et al., 2009a; Hughes et al., 2009b).

Splenocins A–J (**90-99**) are nine-membered bis-lactones isolated from *Streptomyces* sp. (sediment, La Jolla, California) with potential for development for asthma treatment, due to suppression of cytokine production with minimal mammalian cell cytotoxicity (Strangman et al., 2009).

Culture of *Streptomyces* sp. (sediment, Atlantic Ocean) resulted in isolation of albidopyrone (**100**), a moderate inhibitor of protein-tyrosine phosphatase B (Hohmann et al., 2009).

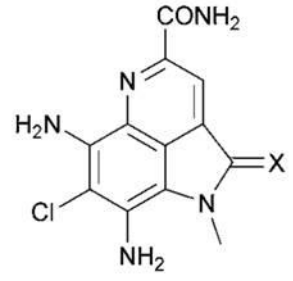

88 X = S
89 X = O

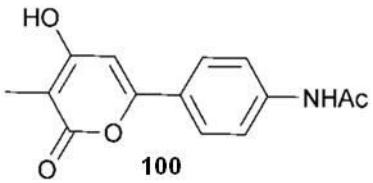

100

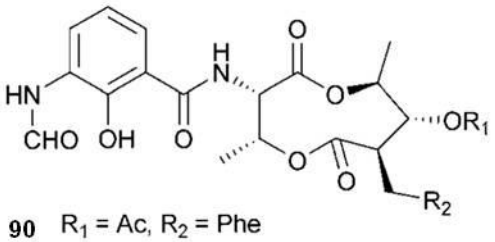

90 R_1 = Ac, R_2 = Phe
91 R_1 = *i*-propanoyl, R_2 = Phe
92 R_1 = *s*-butanoyl, R_2 = Phe
93 R_1 = benzoyl, R_2 = Me
94 R_1 = benzoyl, R_2 = $(CH_2)_2Me$
95 R_1 = benzoyl, R_2 = $(CH_2)_3Me$
96 R_1 = benzoyl, R_2 = $(CH_2)_4Me$
97 R_1 = benzoyl, R_2 = $CH(Me)(CH_2)_3Me$
98 R_1 = benzoyl, R_2 = Phe
99 R_1 = H, R_2 = Phe

Mansouramycins A–D (**101-104**) are isoquinolinequinones obtained from culture of *Streptomyces* sp. (mud, Jade Bay, German North Sea Coast). Mansouramycin A (**101**) was moderately active against *S. aureus*, *B. subtilis* and *E. coli* and a strong inhibitor of the microalgae *Chlorella vulgaris*, *C. sorokiniana* and *Scenedesmus subspicatus*. All isolated compounds exhibited high cytotoxicity when tested in a panel of 36 tumour cell lines, with several showing high selectivity (Hawas et al., 2009).

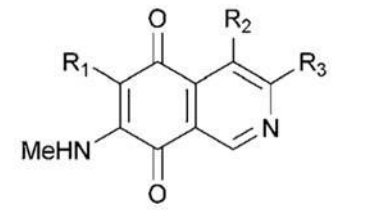

101 R_1 = H, R_2 = R_3 = Me
102 R_1 =Cl, R_2 = H, R_3 = Me
103 R_1 = R_2 = H, R_3 = COOMe

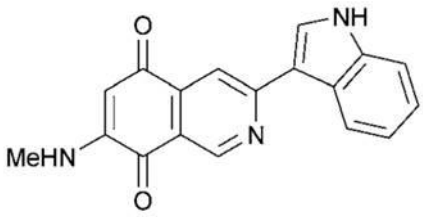

104

Fermentation of *Streptomyces* sp. (sediment, Madagascar) gave tartrolon D (**105**) which was strongly cytotoxic to A549, HT- 29 and MDA-MB-231 cells (Pérez et al., 2009), while culture of another *Streptomyces* sp. (sediment, Miyazaki Harbor, Japan) gave two trialkyl-substituted aromatic acids, lorneic acids A (**106**) and B (**107**). Both inhibited human platelet phosphodiesterase 5 (PDE5), but (**106**) was the stronger inhibitor (Iwata et al., 2009).

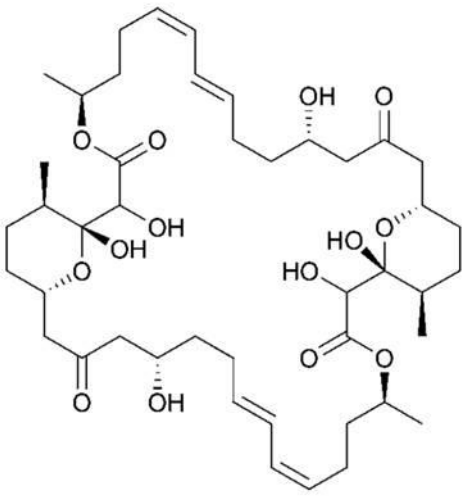

105

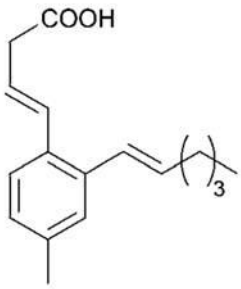

106

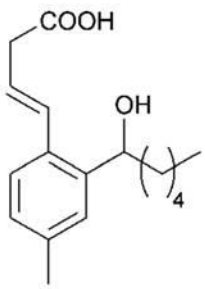

107

Naseseazines A (**108**) and B (**109**), diketopiperazines with a new dimeric

framework, were isolated from culture of *Streptomyces* sp. (sediment, Fiji) (Raju et al., 2009).

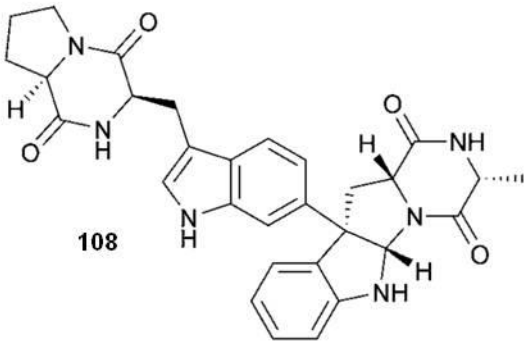

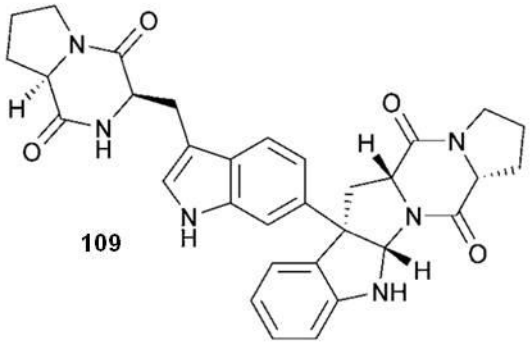

Tirandamycins C (**110**) and D (**111**) are dienoyl-tetramic acids isolated from fermentation of *Streptomyces* sp. (sediment, Salt Cay, Virgin Islands) along with the previously identified compounds tirandamycin A (Meyer, 1971) and B (Hagenmaier et al., 1976). This represented the first marine isolation of tirandamycins A and B. All metabolites displayed activity against vancomycin-resistant *Enterococcus faecalis* (VRE) with varying degrees of potency (Carlson et al., 2009).

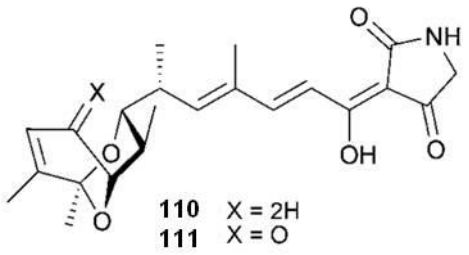

Culture of *Streptomyces* sp. (sand, Qingdao coast, China) yielded two new sesquiterpenes, 15-hydroxy-T-muurolol (**112**) and 11,15-dihydroxy-T-muurolol (**113**) (Ding et al., 2009). The absolute configurations of a number of sesquiterpenes isolated previously from the same strain and reported as amorphanes (Wu et al., 2007) have now been revised to those of the muurolane series, namely compounds **114-117**.

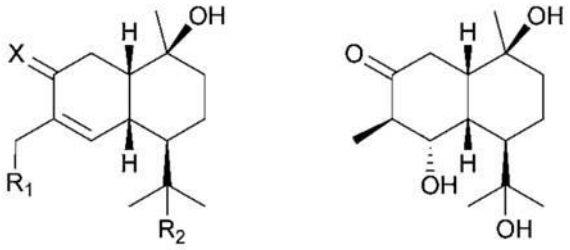

112 X = 2H, R_1 = OH, R_2 = H
113 X = 2H, R_1 = R_2 = OH
114 X = O, R_1 = R_2 = H
115 X = 2H, R_1 = H, R_2 = OH
116 X = O, R_1 = OH, R_2 = H

117

Optimization of culture conditions for a *Streptomyces* sp. (sediment, La Jolla, California) that previously yielded the halogenated bispyrroles marinopyrroles A and B (Hughes et al., 2008) has resulted in isolation of further members of the series, marinopyrrole C–F (**118-121**). All of the marinopyrroles were isolated as single *M*-configured *atropo*-enantiomers and thus were configurationally stable at room temperature, except for marinopyrrole F (**121**), which was isolated as a racemic mixture. Like marinopyrroles A and B, marinopyrrole C (**118**) exhibited potent activity against methicillin-resistant *Staphylococcus aureus* (MRSA) and moderate activity against HCT-116 cells (Hughes et al., 2010).

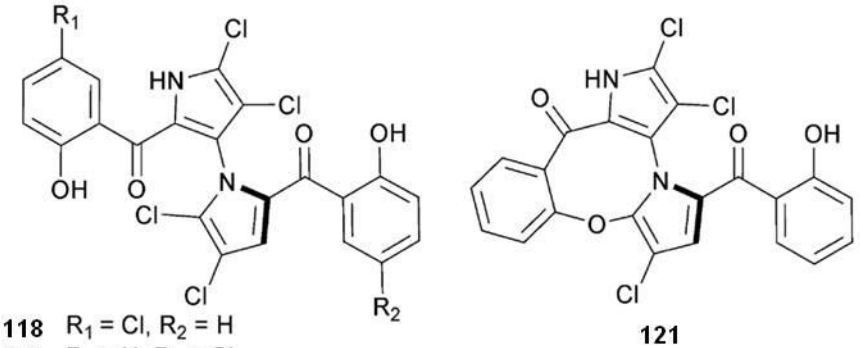

118 R_1 = Cl, R_2 = H
119 R_1 = H, R_2 = Cl
120 R_1 = H, R_2 = Br

121

Tumescenamides A (**122**) and B (**123**) are cyclic peptides from *Streptomyces tumescens* (sediment, Big Drop-off, Republic of Palau). Tumescenamide A (**122**) induced reporter gene expression under the control of the insulin-degrading enzyme (IDE) promoter, suggesting promise as a potential treatment for Alzheimer's disease (Motohashi et al., 2010a).

Screening of marine actinobacterial strains for the presence of hydroxy-3-methyl glutaryl CoA reductase (HMGR), a key enzyme in the mevalonate (MVA) pathway, identified a *Streptomyces* sp. (sponge *Cinachyra* sp., Nagura Bay, Ishigaki, Okinawa), the culture of which yielded three new phenazine-derived isoprenoids, JBIR-46–48 (**124-126**). Feeding experiments utilising [1-^{13}C]-acetate confirmed that the dimethylallyl moieties of these metabolites were indeed formed via the MVA pathway (Izumikawa et al., 2010a).

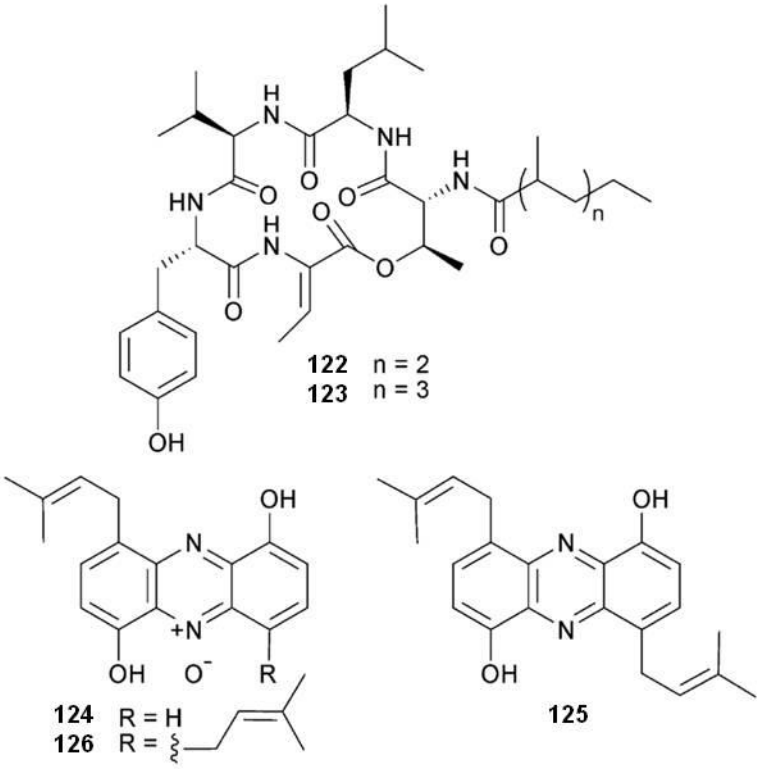

Three new species of *Streptomyces* (sponge *Haliclona* sp., Tateyama City, Chiba, Japan) have been studied. The first species yielded two chlorinated indole-containing tetrapeptides, JBIR-34 (**127**) and JBIR-35 (**128**), both with weak DPPH activity (Motohashi et al., 2010b). From the second species, a new teleocidin analogue, 2-oxoteleocidin A1 JBIR-31 (**129**) was weakly active against HeLa and human malignant pleural mesothelioma (MPM) ACC-MESO-1 cells (Izumikawa et al., 2010b), while the third species gave two new anthracyclines, tetracenoquinocin (**130**) and 5-iminoaranciamycin (**131**). Tetracenoquinocin (**130**) displayed modest cytotoxicity to the HeLa and HL- 60 cells. Feeding of [1,2-$^{13}C_2$]-acetate confirmed the polyketide origins of 5-iminoaranciamycin (**131**) and was used to assist in assignment of the ^{13}C NMR

spectra of the compounds (Motohasi et al., 2010c).

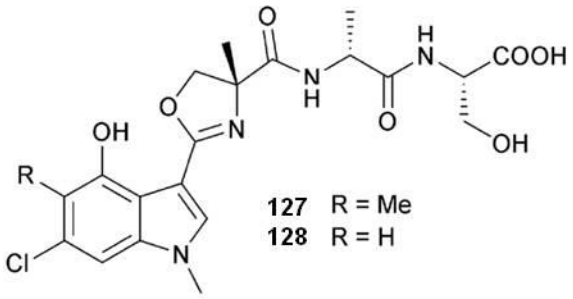

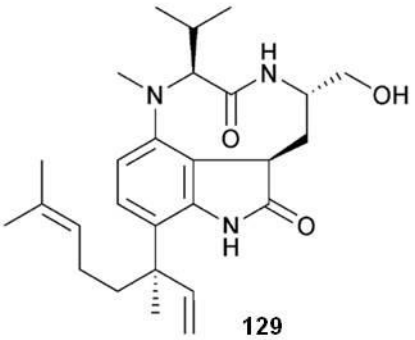

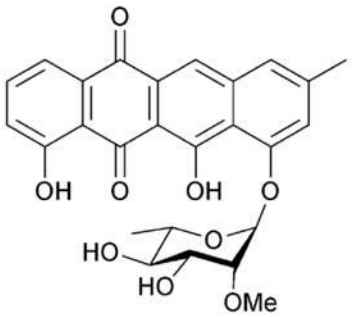

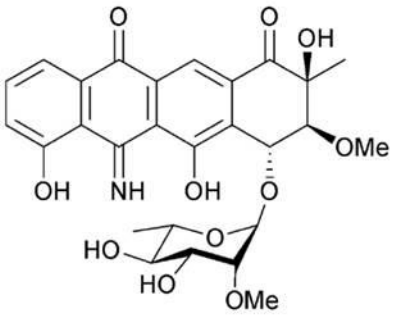

A salicylamide derivative, JBIR-58 (**132**), was isolated from a new *Streptomyces* sp. (Demospongiae sponge, Ishigaki City, Okinawa) and had moderate toxicity to HeLa cells (Ueda et al., 2010).

Mayamycin (**133**) is a benz[*a*]anthracene derivative from a *Streptomyces* sp. (sponge *Halichondria panicea*, Baltic Sea). Treatment of previous cultures of this strain with low doses of antibiotics induced production of streptophenazines A–H (Mitova et al., 2008), while variation of culture conditions induced production of mayamycin (**133**). Mayamycin (**133**) exhibited potent activity against several human cancer cell lines and inhibited growth of a number of bacteria including antibiotic-resistant strains (Schneemann et al., 2010).

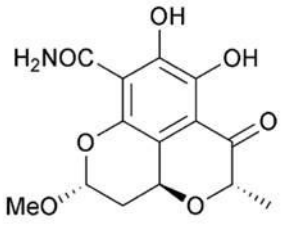

132

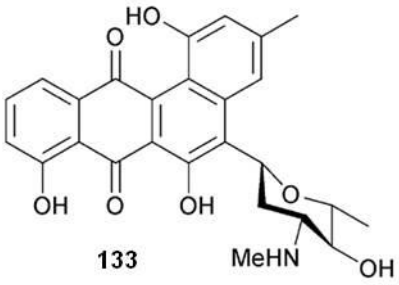

133

A Thai *Streptomyces* strain (sediment, Samut Sakhon province) gave the cyclic peptide rakicidin D (**134**), an inhibitor of murine carcinoma colon 26-L5 cell invasion (metastasis inhibitor) (Igarashi et al., 2010).

Cultivation of *Streptomyces* sp. (sediment, Heron Is., Australia) resulted in isolation of heronamides A–C (**135-137**). Heronamide C (**137**) had a pronounced, reversible and non-cytotoxic effect on mammalian cell morphology (Raju et al., 2010a).

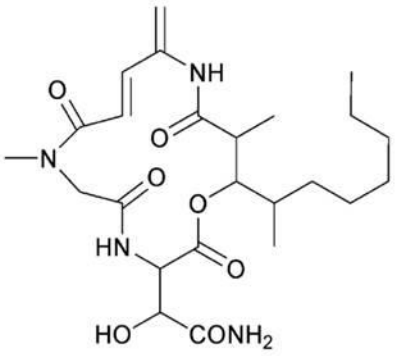

134

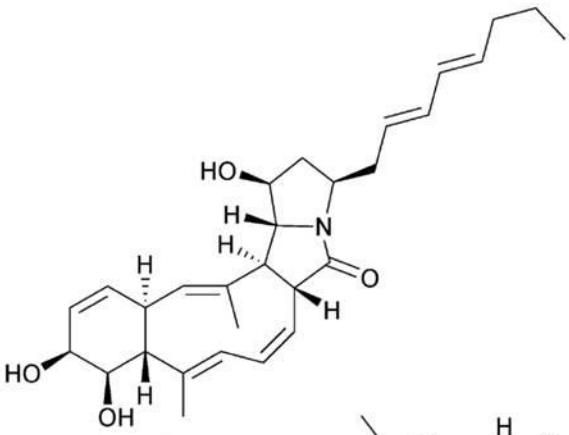

135

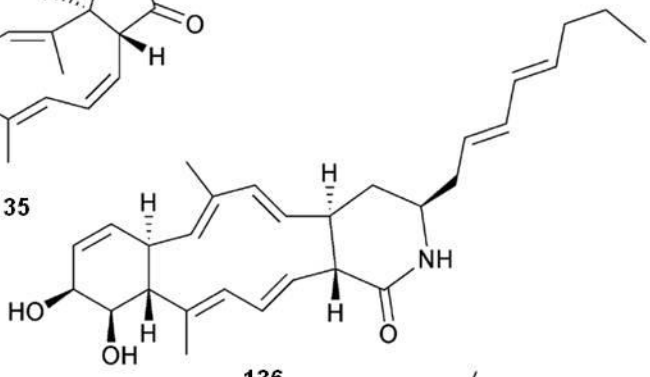

136

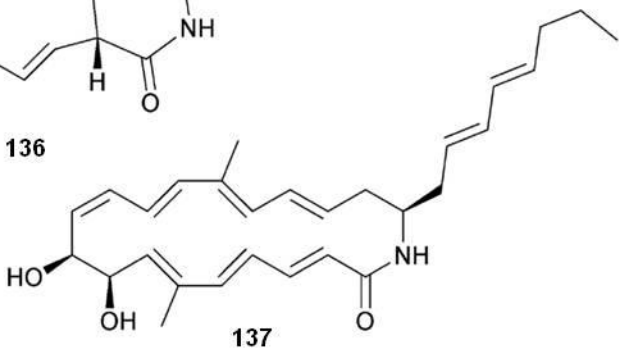

137

Heronapyrroles A–C (**138-140**), also from a *Streptomyces* sp. (beach sand, Heron Is., Australia), were active against Gram-positive bacteria (Raju et al., 2010b).

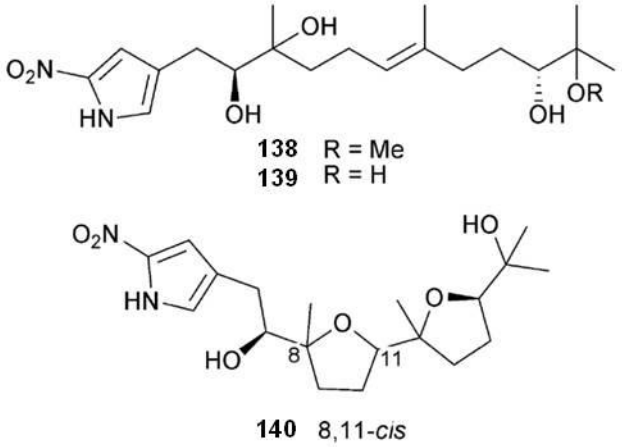

138 R = Me
139 R = H

140 8,11-*cis*

Of the four pyranones **141-144** isolated from *Streptomyces albus* (sediment, Punta Sagres, Portugal), compounds **141** and **144** exhibited strong cytotoxicity against three HTCLs, while **142** was sub-nanomolar active as an inhibitor of mitogenic signalling. The 9*R*,10*R* configuration was established for **142** (Schleissner et al., 2011).

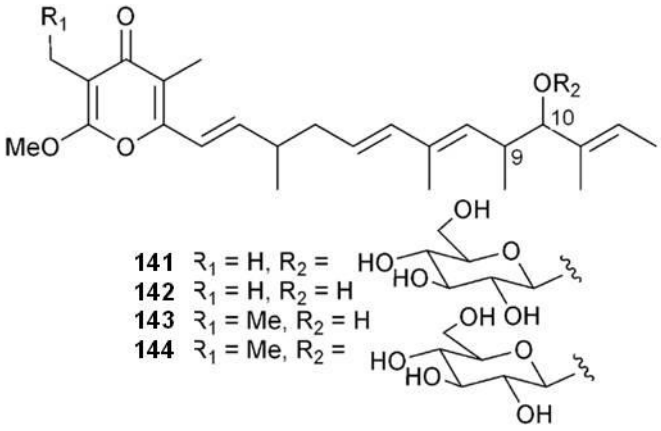

141 R_1 = H, R_2 =
142 R_1 = H, R_2 = H
143 R_1 = Me, R_2 = H
144 R_1 = Me, R_2 =

The antibiotics antimycins A19 (**145**) and A20 (**146**) were isolated from *Streptomyces antibioticus* (sediment, Guangdong province, South China Sea) and exhibited potent activity against *C. albicans* (Xu et al., 2011).

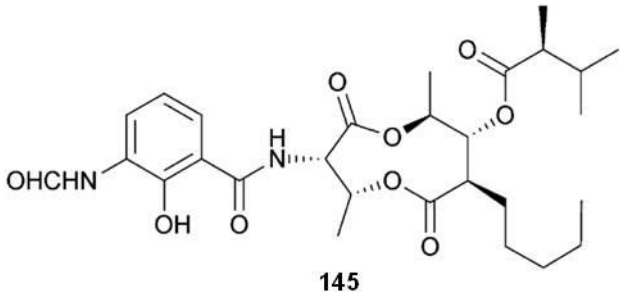

145

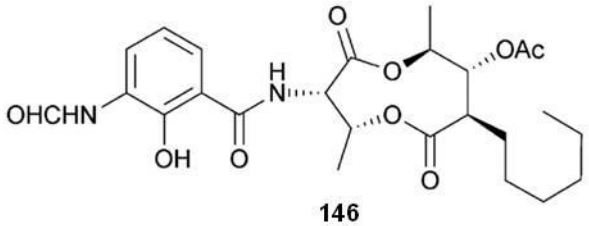

146

The tetromycins 1–4 (**147-150**) and the previously reported tetromycin B (Takeuchi et al., 1996) from *Streptomyces axinellae* (sponge *Axinella polypoides*, Banyuls-sur-Mer, France) were active against *Trypanosoma brucei* but only tetromycin 3 (**149**) was active against *Leishmania major*, while tetromycins 3 (**149**), 4 (**150**) and tetromycin B displayed time-dependent inhibition of cathepsin L-like proteases (Pimentel-Elardo et al., 2011). Tetromycin 4 (**150**) is isomeric with the known tetromycin C2 (Takeuchi et al., 1998) and this was the first report of tetromycin B as a marine metabolite.

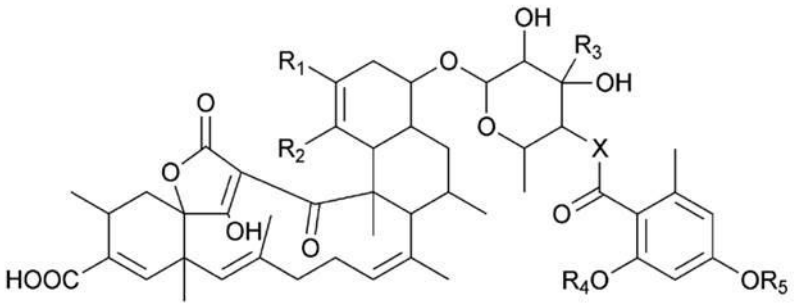

147 $R_1 = R_3 = R_5 = Me$, $R_2 = R_4 = H$, X = NH
148 $R_1 = R_4 = R_5 = Me$, $R_2 = R_3 = H$, X = O
149 $R_1 = R_3 = R_5 = H$, $R_2 = R_4 = Me$, X = O
150 $R_1 = R_4 = Me$, $R_2 = R_3 = R_5 = H$, X = O

A family of peptidic metabolites was obtained from two bacterial strains separated from mollusks. Nobilamides A–E (**151-155**) were obtained from one

Streptomyces strain (*Chicoreus nobilis*, Cebu, Philippines) and nobilamides A (**151**) and F–H (**156-158**) were isolated from another *Streptomyces* species (*Conus tribblei*, Cebu, Philippines). Related peptides A-3302-A and A-3302-B (Ogawa et al., 1977), previously obtained from terrestrial *B. subtilis*, were isolated for the first time from a marine source and the known synthetic peptide, *N*-acetyl-L-phenylalanyl-L-leucinamide (Gorlero et al., 2009) was obtained for the first time from a natural source. Nobilamide B (**152**) and A-3302-B were potent and long-acting antagonists of mouse and human transient receptor potential vanilloid-1 (TRPV1) channels (pain and inflammation mediators) (Lin et al., 2011).

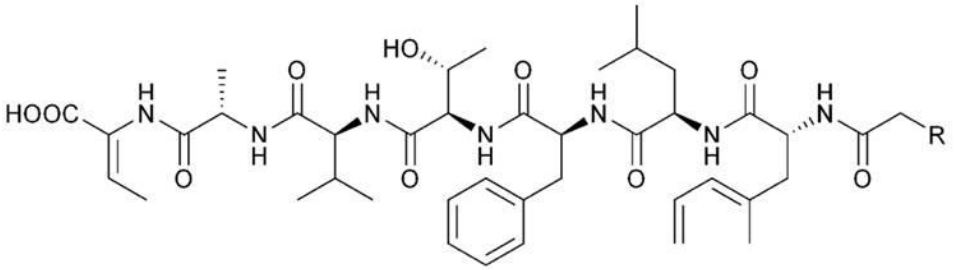

151 R = H
152 R = Me

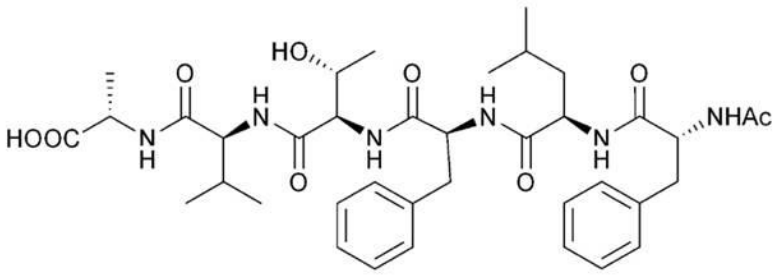

153

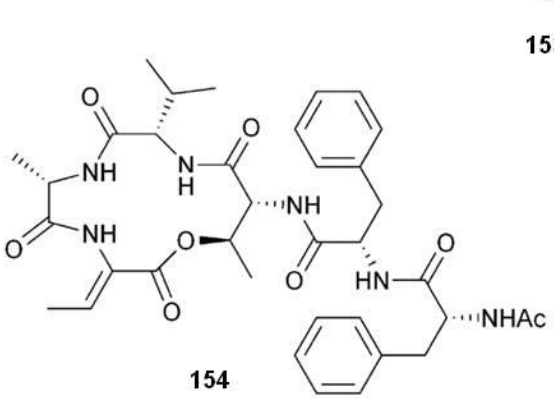

154

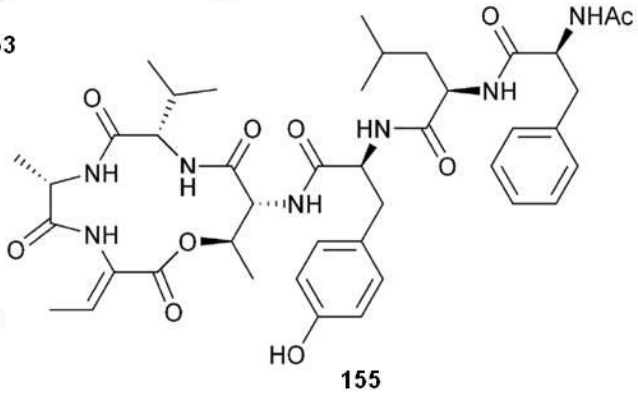

155

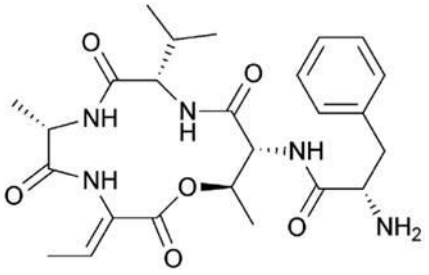

156

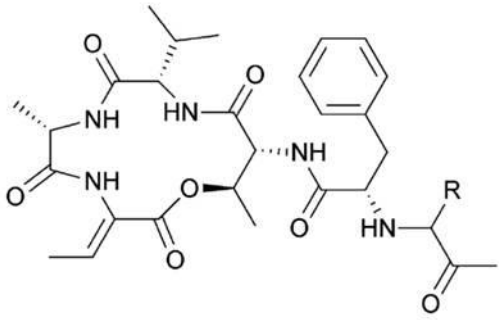

157 R = —Me
158 R = ····Me

Actinoramides A–C (**159-161**) are modified peptides composed of the unusual amino acids, 2-amino-4-ureidobutanoic acid and 4-amino-3-hydroxy-2-methyl-5-phenylpentanoic acid, that were isolated from a bacterium closely related to the genus *Streptomyces* (sediment, San Diego, California, USA) (Nam et al., 2011). Actinoramide A (**159**) was coincidentally isolated as pandanamide A from *Streptomyces* sp. (sediment, Padana Nahua, Papua New Guinea), along with pandanamide B (**162**) (Williams et al., 2011). Pandanamide B (**162**) was cytotoxic to Jurkat T lymphocyte cells, whilst chemical genomics analysis utilising *Saccharomyces cerevisiae* mutants implicated actinoramide A (pandanamide A) (**159**) as an inhibitor in the biosynthesis of sulfur-containing amino acids, or in some interaction with them (Williams et al., 2011).

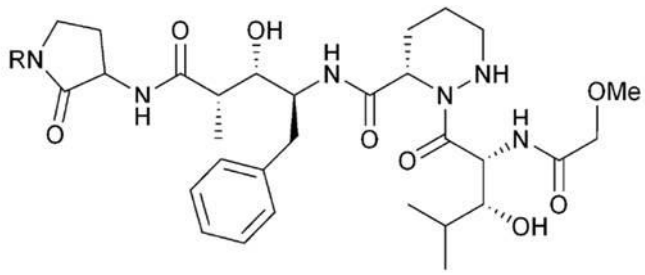

159 R = $CONH_2$
160 R = Ac

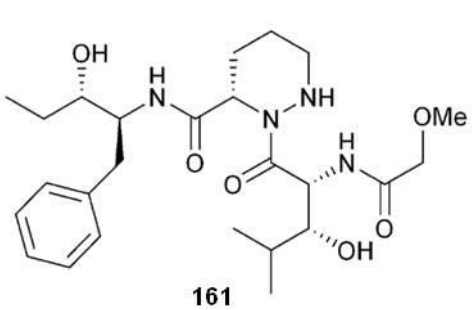

161

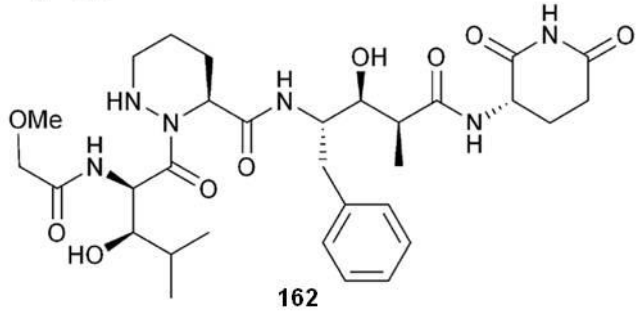

162

The siderophores streptobactin (**163**), dibenarthin (**164**) and tribenarthin were isolated from a *Streptomyces* sp. (brown alga *Analipus japonicus*, Charatsunai beach, Muroran, Japan) along with the known siderophore benarthin (Aoyagi et al., 1992). Streptobactin (**163**) and dibenarthin (**164**) possessed iron chelating activity comparable to that of deferoxamine mesylate (Matsuo et al., 2011).

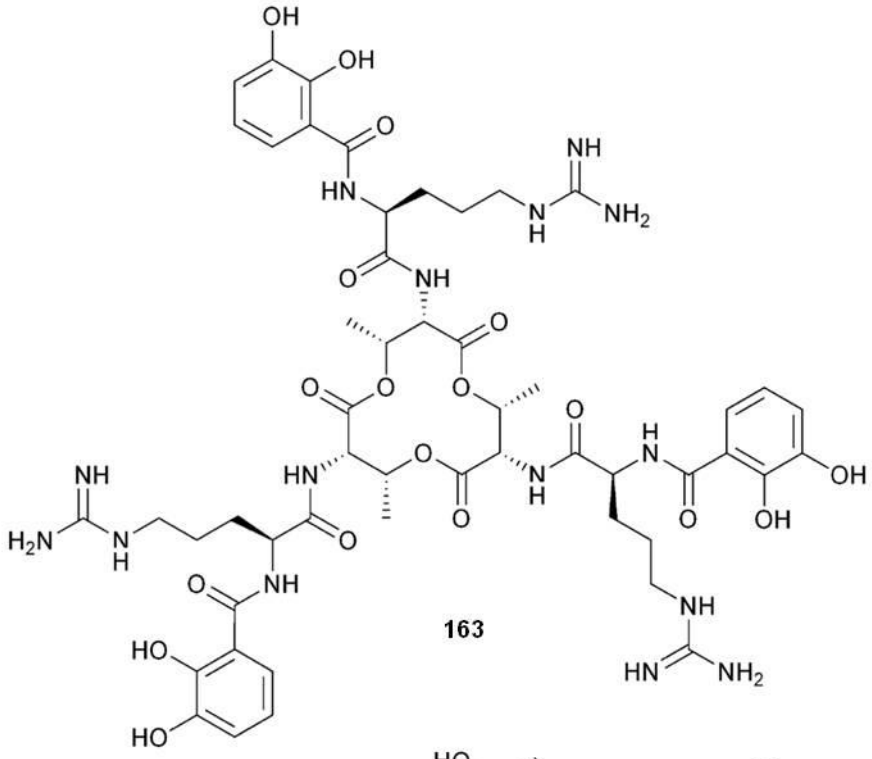

163

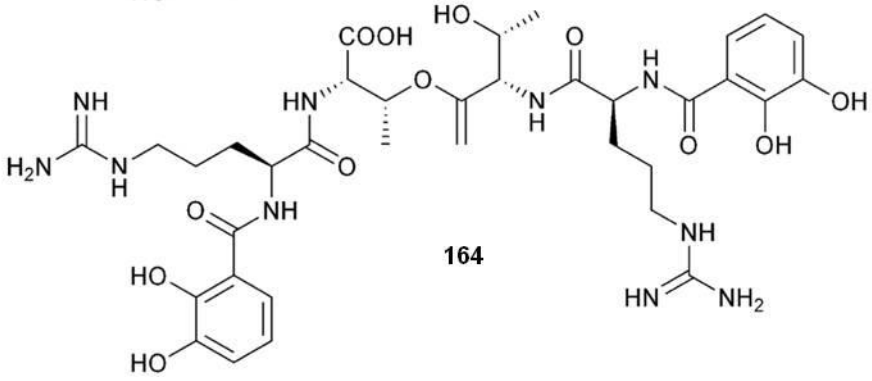

164

A *Streptomyces* strain (sediment, Nasese, Fiji) produced three depsipeptides, fijimycins A–C (**165-167**), which occurred as complex conformational mixtures and displayed significant activity against three methicillin-resistant *S. aureus* (MRSA) strains (Sun et al., 2011).

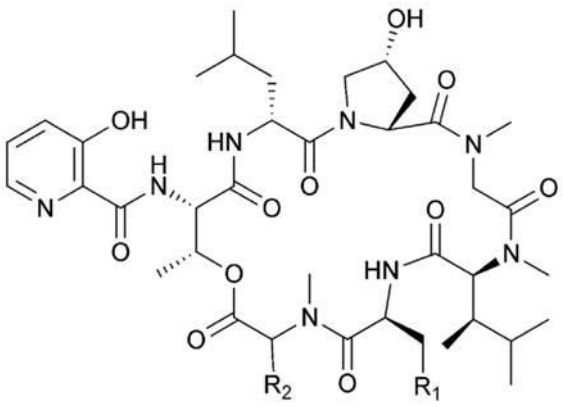

165 R_1 = H, R_2 = Phe
166 R_1 = H, R_2 = *i*Bu
167 R_1 = OH, R_2 = Phe

The polyketide ansalactam A (**168**), which contained a spiro γ-lactam moiety and an isobutyryl polyketide fragment, was isolated from a *Streptomyces* species (sediment, Oceanside, California, USA). Biosynthetic feeding experiments with stable isotopes indicated that an (*E*)-4-methyl-2-pentenoic acid-derived branched chain polyketide synthase extender unit was utilized for polyketide assembly (Wilson et al., 2011).

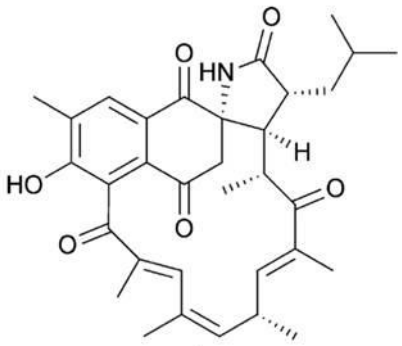

168

Benzoxacystol (**169**), a 1,4-benzoxazine-type metabolite obtained from *Streptomyces griseus* (deep sea sediment, Canary Basin), was an inhibitor of glycogen synthase kinase 3β, in addition to displaying weak antiproliferative activity against mouse fibroblast cells (Nachtigall et al., 2011).

Glucopiericidin C (**170**), obtained from a *Streptomyces* species (sediment, Laguna de Terminos, Gulf of Mexico), was active against the fungus *Mucor miehei*, in addition to exhibiting cytotoxicity towards a number of HTCLs (Shaaban et al., 2011).

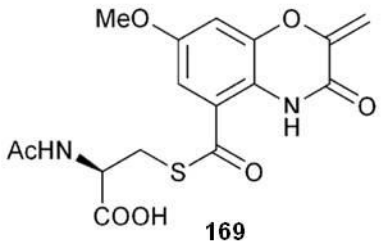

169

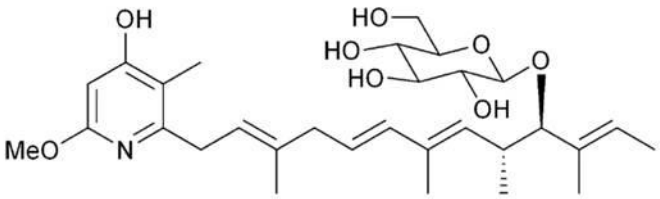

170

A *Streptomyces* sp. (sediment, Nelson, South Australia) yielded a new member of the reveromycin polyketide spiroketals, reveromycin E (**171**) (Fremlin et al., 2011), while pyridinopyrones A–C (**172-174**) were isolated from another *Streptomyces* sp. (sediment, La Jolla, California, USA) but with **173** and **174** obtained as an inseparable mixture. Incorporation of ^{13}C-labelled precursors indicated that the starter unit was nicotinic acid and that the polyene chain and pendant methyl groups are respectively acetate- and methionine-derived (Fukuda et al., 2011).

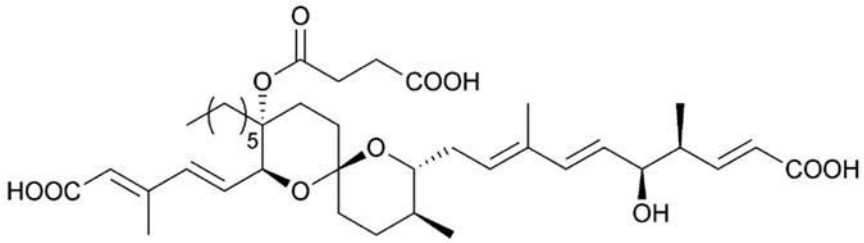

171

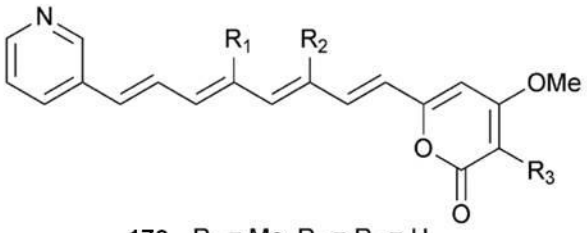

172 R_1 = Me, R_2 = R_3 = H
173 R_1 = R_3 = Me, R_2 = H
174 R_1 = H, R_2 = R_3 = Me

A new species of *Streptomyces* (unidentified sponge, Ishigaki City, Okinawa, Japan) yielded the pyrazinones, JBIR-56 (**175**) and JBIR-57 (**176**). JBIR-56 (**175**) was synthesized from 2,6-dichloropyrazine (Motohashi et al., 2011).

A *Streptomyces* sp. from the sponge *Craniella australiensis* (Sanya Bay, Hainan Province, China) led to streptomycindole (**177**), in addition to the known related synthetic product *N*-phenylacetyl-L-tryptophan (Suyama et al., 1965), isolated for the

first time as a natural product (Huang et al., 2011).

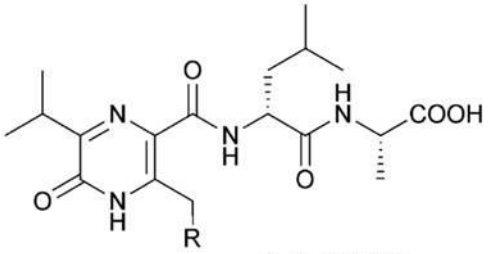

175 R = Me
176 R = H

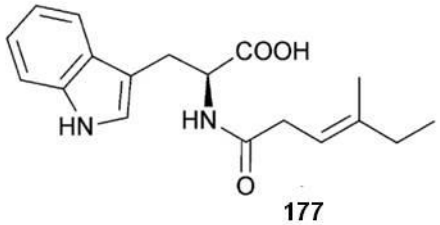

177

A further *Streptomyces* sp. (sediment, Bohai Bay, China) produced N_1-acetyl-N_7-phenylacetyl cadaverine (**178**), the diketopiperazine *cyclo*(2-hydroxy-Pro-*R*-Leu) (**179**) and the known synthetic intermediate *cyclo*(4-hydroxy-*S*-Pro-*S*-Trp) (De Boer et al., 2003). All three were moderately cytotoxic to the HL-60 cell line (Li et al., 2011).

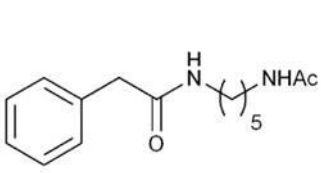

178

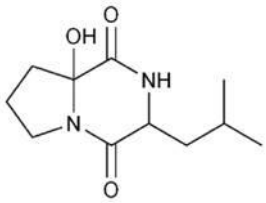

179

The anthramycin-type analogues usabamycin A–C (**180-182**) obtained from *Streptomyces* sp. (sediment, Usa Bay, Kochi Prefecture, Japan) were weakly inhibitory of HeLa cell growth and selective inhibitors of serotonin uptake (5-HT2B) (Sato et al., 2011).

Investigation of a *Streptomyces* sp. (sediment, Kiaochow Bay, Qingdao, China) afforded the anthracene derivative (**183**), cytotoxic to the A549 cell line (Zhang et al., 2011).

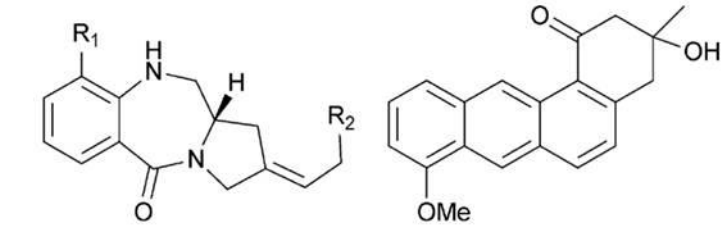

180 R_1 = OMe, R_2 = Me
181 R_1 = OMe, R_2 = H
182 R_1 = H, R_2 = Me

183

The marine environment has a vast biological diversity and it has been recognized as a valuable source of a large number of novel chemical entities. In the last 15 years, marine-derived *Streptomyces* strains have been proven to be an important reservoir for the isolation of bioactive metabolites.

1.6. Aim of the present study

In view of the immense and largely unexplored potential of marine microorganisms, the aim of the present PhD thesis was to perform a preliminary screening of a number of marine-derived bacterial strains deposited at the strain collection/microbank of the Section of Pharmacognosy and Chemistry of Natural Products, Department of Pharmacy, National and Kapodistrian University of Athens and to subsequently focus - according to their chemical profiles - on strain/s that could potentially produce interesting, from the chemical point of view, secondary metabolites.

Thus, the investigation was designed to start with the small-scale cultivation of a number of bacterial strains from the marine microbial strain collection and continue with the chemical profile analyses of the corresponding extracts so as the most promising, from the chemical point of view, strain could be selected for large-scale cultivation. The large-scale extract would via chromatographic separations lead to the isolation of secondary metabolites in pure form that could subsequently be structurally elucidated through extensive spectroscopic studies.

2. MATERIALS AND METHODS

2.1. General experimental procedures

Nuclear magnetic resonance (NMR) spectra were recorded on Bruker AC 200 and Bruker DRX 400 spectrometers. Chemical shifts are given on the δ (ppm) scale using the residual solvent signal for calibration, whereas coupling constants *J* are given in Hz. The 2D-NMR experiments (HSQC, HMBC, COSY) were performed using standard Bruker pulse sequences.

Low resolution electron impact mass spectra (EIMS) were measured on a Hewlett Packard 5973 mass spectrometer or a Thermo Electron Corporation DSQ mass spectrometer using a Direct-Exposure Probe. Low resolution chemical ionization mass spectra (CIMS) were measured on a Thermo Electron Corporation DSQ mass spectrometer using a Direct-Exposure Probe and methane as the CI reagent gas.

High resolution electrospray ionization mass spectra (HRESIMS) were measured on a Thermo Scientific LTQ Orbitrap Velos mass spectrometer.

IR spectra were obtained on a Bruker Tensor 27 spectrometer, while UV-Vis spectra were obtained on a Perkin Elmer Lambda 40 spectrophotometer.

High pressure liquid chromatography (HPLC) separations were conducted on a Waters 600 liquid chromatography pump with a Waters 410 refractive index detector, using a Kromasil 100 C_{18} (MZ-Analysentechnik GmbH, 5 μm, 250 mm × 8 mm i.d.) or a Nucleosil 100 C_{18} (Macherey-Nagel, 7 μm, 250 mm × 10 mm i.d.) column.

Evaporation of the solvents was performed under vacuum using a BÜCHI Rotavapor R-200 rotary evaporator at temperatures up to 40 °C.

2.2. Chemicals

Normal- or reversed-phase vacuum column chromatography separations were performed with Silica 60, 0.015-0.04 mm (Macherey-Nagel) or Kieselgel 60 RP-18, 40-63 μm (Merck), respectively.

Normal-phase gravity column chromatography separations were performed with Silica 60, 0.04-0.063 mm (Macherey-Nagel).

Solid phase extractions were performed using CHROMABOND C18 ec (Macherey-Nagel, adsorbent weight 500 mg) polypropylene columns.

Normal- or reversed-phase thin layer chromatography (TLC) separations were

performed using ALUGRAM SIL G/UV_{254} (Macherey-Nagel, thickness of layer 0.2 mm) or ALUGRAM RP-18 W/UV_{254} (Macherey-Nagel, thickness of layer 0.15 mm) aluminium sheets, respectively, and spots were detected under a UV lamp at 254 and 365 nm and after spraying with 15% H_2SO_4 in MeOH reagent and heating at 100 °C for 1-2 min.

All solvents used in extractions and chromatographic separations, with the exception of H_2O, were purchased from LAB-SCAN Analytical Sciences. Me_2CO was of A.R. grade, cHex, EtOAc, CH_2Cl_2 and MeOH were of A.R. grade that were distilled prior to use and MeCN was of HPLC grade. H_2O used in chromatographic separations was initially distilled and further purified through a reverse osmosis membrane and filtered through a deionization resin. All solvents prior to use in HPLC separations were filtered under vacuum and sonicated.

NMR spectra were measured in deuterated solvents [$CDCl_3$, CD_3OD, $(CD_3)_2SO$] without TMS as internal standard obtained from Deutero GmbH.

2.3. Isolation and identification of bacterial strain

The actinobacterial strain BI0048 (Fig. 7), provided from the strain collection/microbank available at the laboratory of Prof. V. Roussis and Assist. Prof. E. Ioannou at the Section of Pharmacognosy and Chemistry of Natural Products, Department of Pharmacy, National and Kapodistrian University of Athens, was isolated from the inner tissues of the red alga *Laurencia glandulifera*, collected in Zoumberi bay, south of Nea Makri, Attiki, Greece in November of 2009.

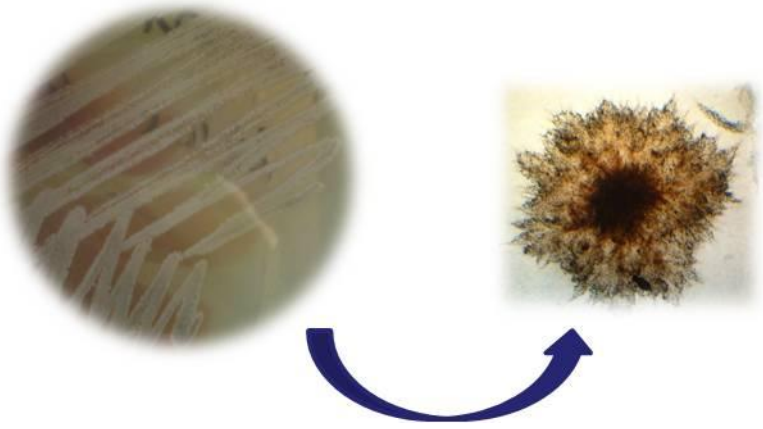

Figure 7. Strain BI0048 as observed with the naked eye (left) and under an optical microscope (right).

Strain BI0048 was identified as *Streptomyces ambofaciens* based on comparison of its 16S rRNA sequence with data from the Genbank database of the National Center for Biotechnology Information (NCBI) using BLAST (Basic Local Alignment Search Tool) (GenBank accession number EU593561).

2.4. Fermentation of bacterial strain and extraction

Strain BI0048 was streaked from a glycerol stock onto a freshly prepared agar plate containing A1Bfe+C medium (Table 5) (Bugni et al., 2006). When sufficient growth of the strain was observed, mycelia were picked from the plate and were inoculated into 250 mL flasks containing 100 mL of A1Bfe+C medium that were incubated at 37 °C for 4 days while shaking at 130 rpm in an orbit shaker. Subsequently, the starter cultures were inoculated into 2 or 3 L flasks containing 1 or 1.5 L of A1Bfe+C medium (10% v/v inoculum), respectively, to a total of 21 L of medium, that were incubated at 37 °C for 8 days while shaking at 130 rpm in an orbit shaker (Fig. 8).

Table 5. Composition and preparation of A1Bfe+C medium.

Ingredient	**Amount (g/L)**
Starch	10
Yeast extract	4
Peptone	2
$CaCO_3$	1
KBr	0.1
$Fe_2(SO_4)_3$ $5H_2O$	0.04
Agar *(only added for solid cultures)*	17

The ingredients are added to 1 L of filtered seawater and subsequently the medium is sterilized by autoclaving at 121 °C for 20 min prior to use.

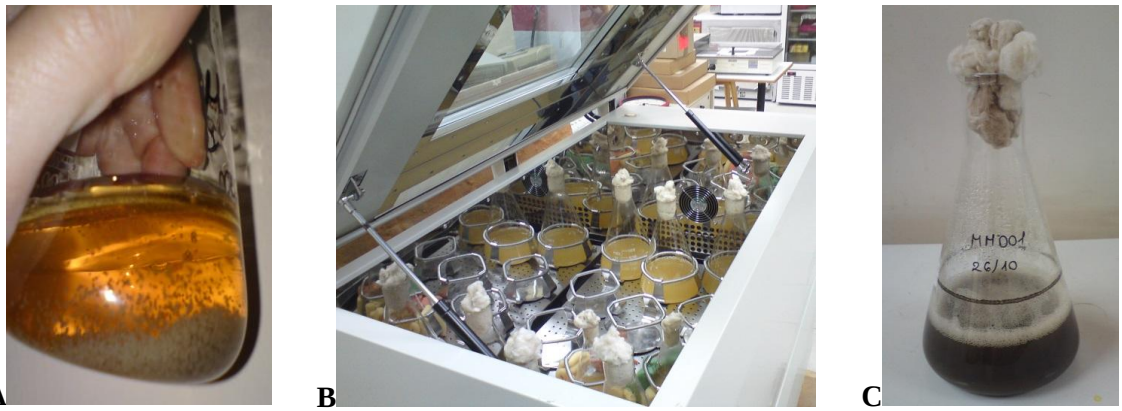

A **B** **C**

Figure 8. (A) Starter culture after 4 days of incubation, (B) Large-scale culture in orbital shaker, (C) Culture after 8 days of incubation.

At the end of the fermentation period, Amberlite XAD-7HP resin (20 g/L) was added to each flask to adsorb extracellular metabolites. The culture and resin were shaken overnight at low speed. The resin and cell mass were collected by filtration through cheesecloth and washed with deionized water to remove salts. The resin, cell mass and cheesecloth were then extracted for 2 h with Me_2CO (6 L). Filtration of the extract and removal of the solvent under vacuum at 40 ºC afforded a solid residue (12.5 g) that was subjected to chromatographic separations for the isolation of metabolites.

2.5. Chromatographic separations and isolation of metabolites

The crude actinobacterial extract was subjected to a series of chromatographic separations (Fig. 9-14), including normal- and reversed-phase vacuum column chromatography, normal-phase gravity column chromatography and reversed-phase HPLC, to allow for the isolation of a number of metabolites in pure form. After each chromatographic step, the fractions were analyzed by ^{1}H NMR spectroscopy.

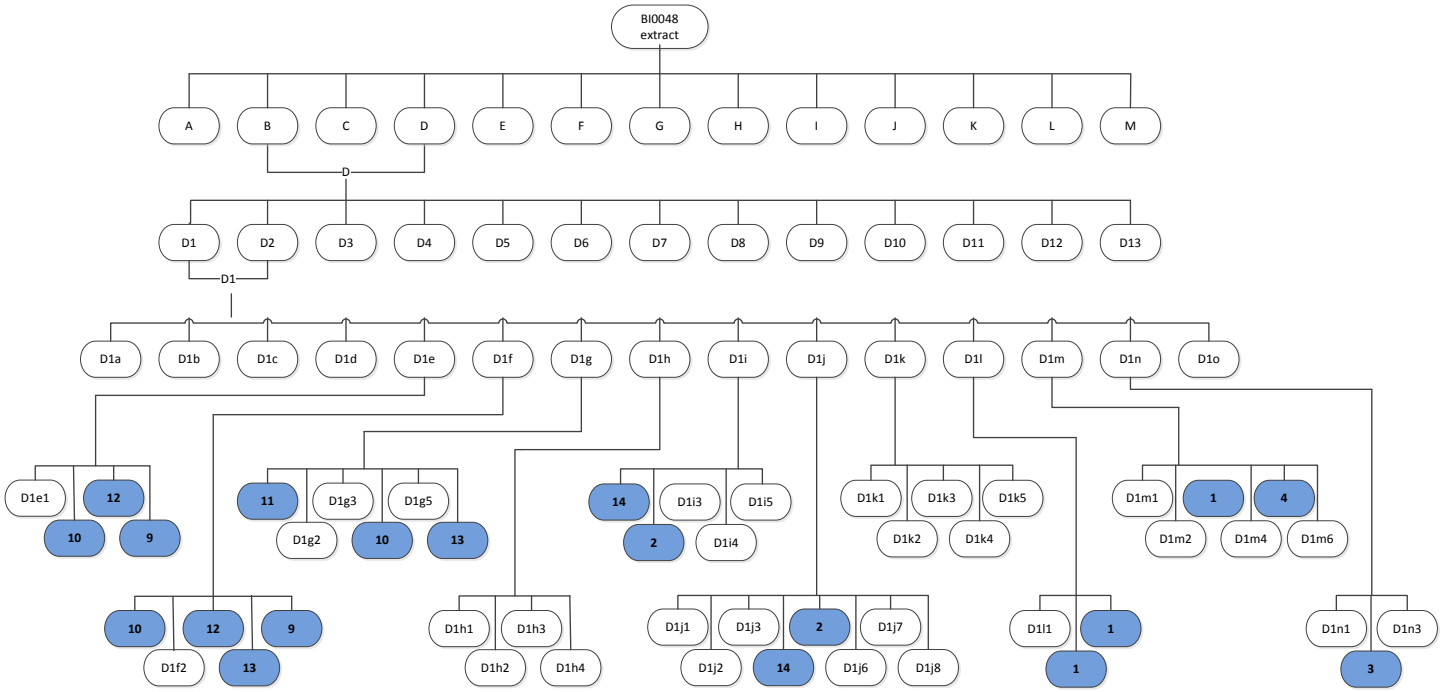

Figure 9. Fractionation scheme for the isolation of metabolites from the crude actinobacterial extract (part A).

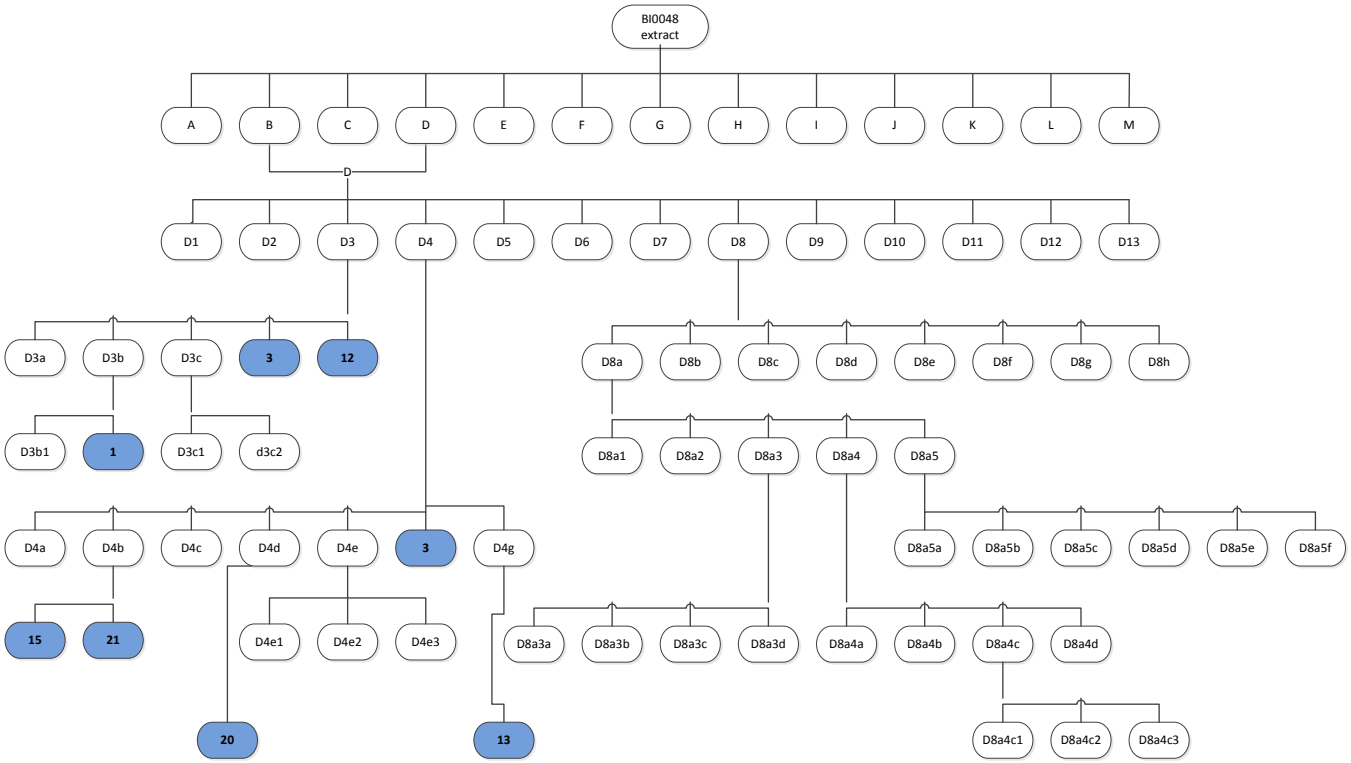

Figure 10. Fractionation scheme for the isolation of metabolites from the crude actinobacterial extract (part B).

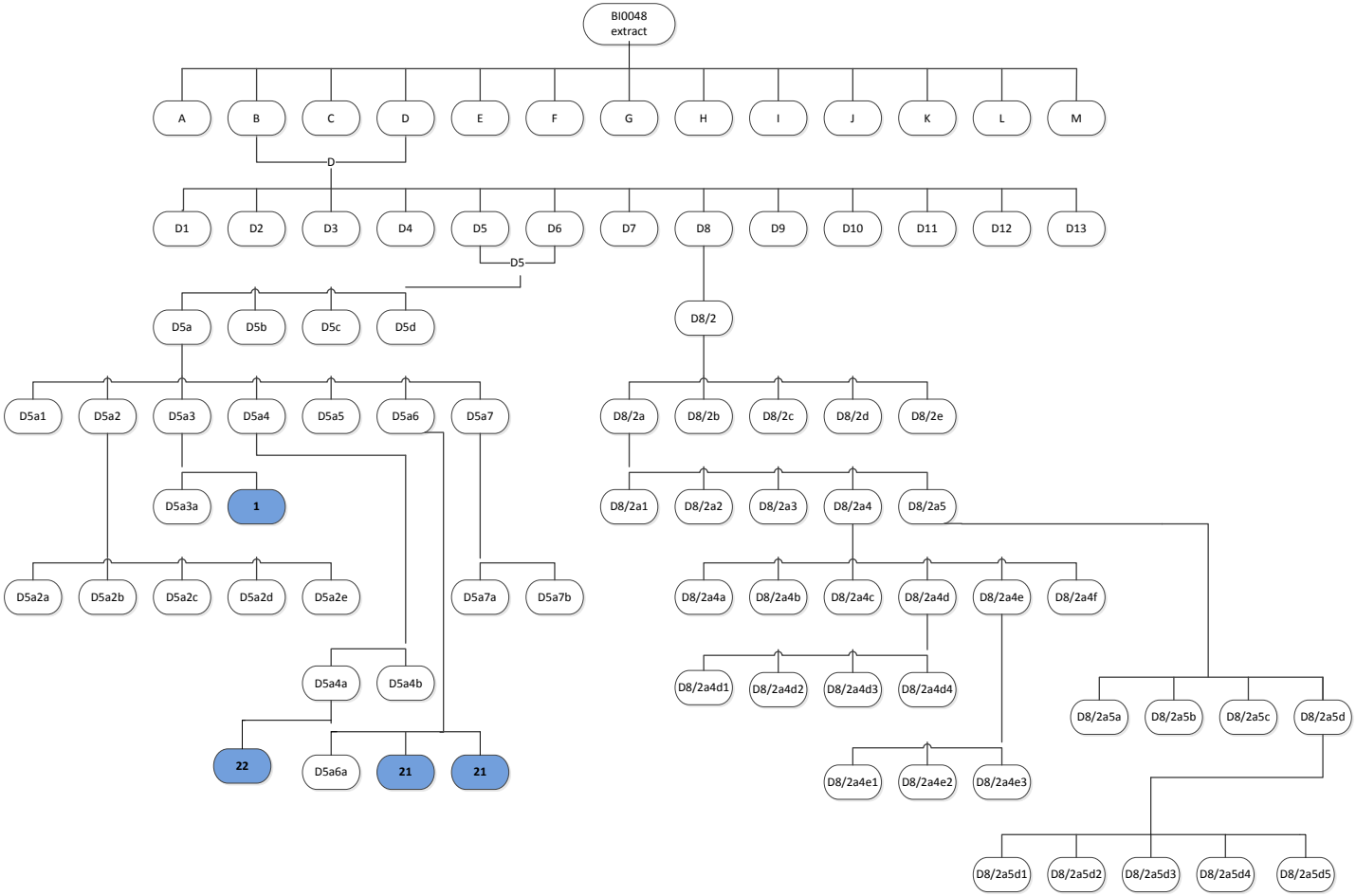

Figure 11. Fractionation scheme for the isolation of metabolites from the crude actinobacterial extract (part C).

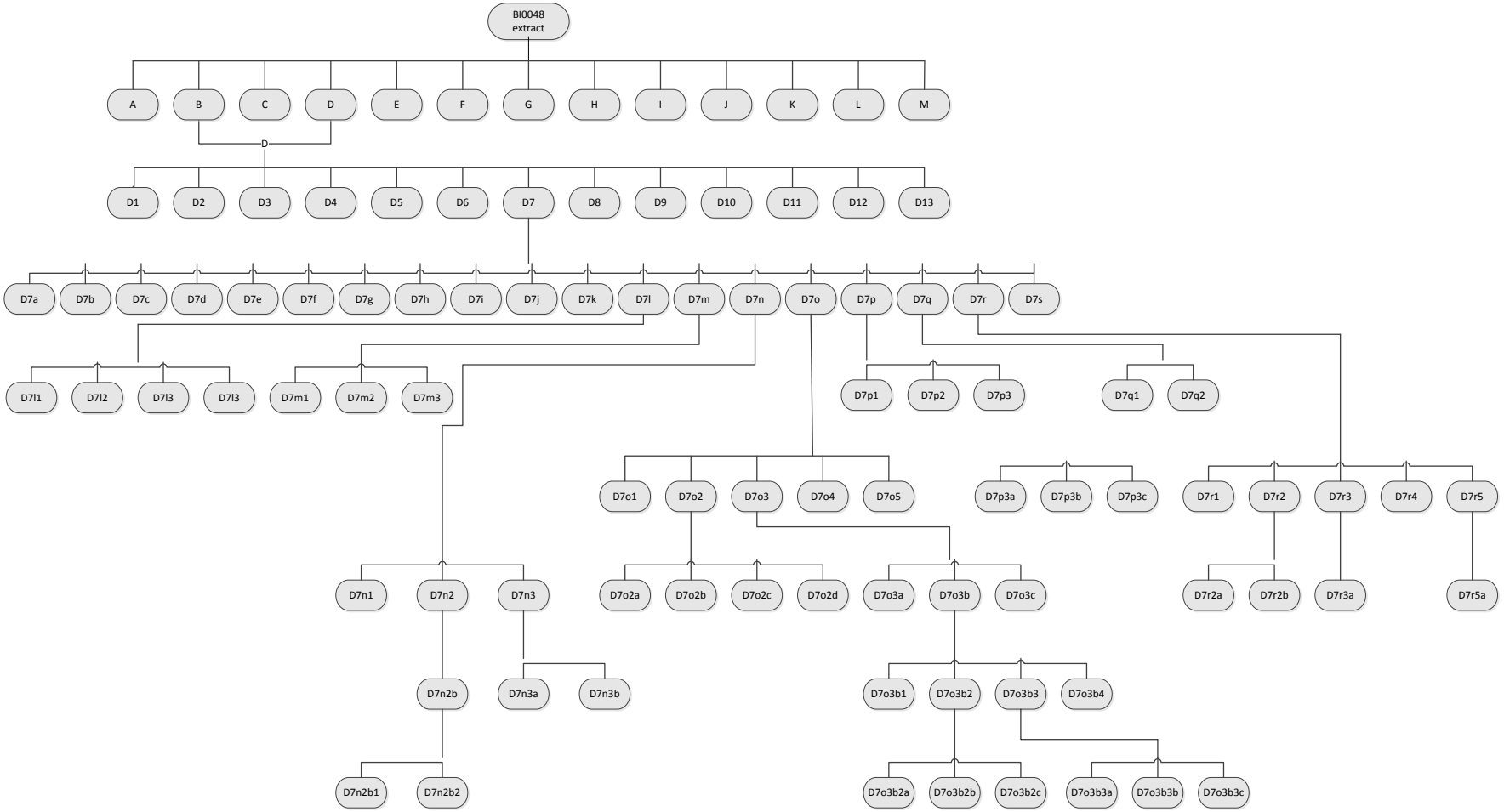

Figure 12. Fractionation scheme for the isolation of metabolites from the crude actinobacterial extract (part D).

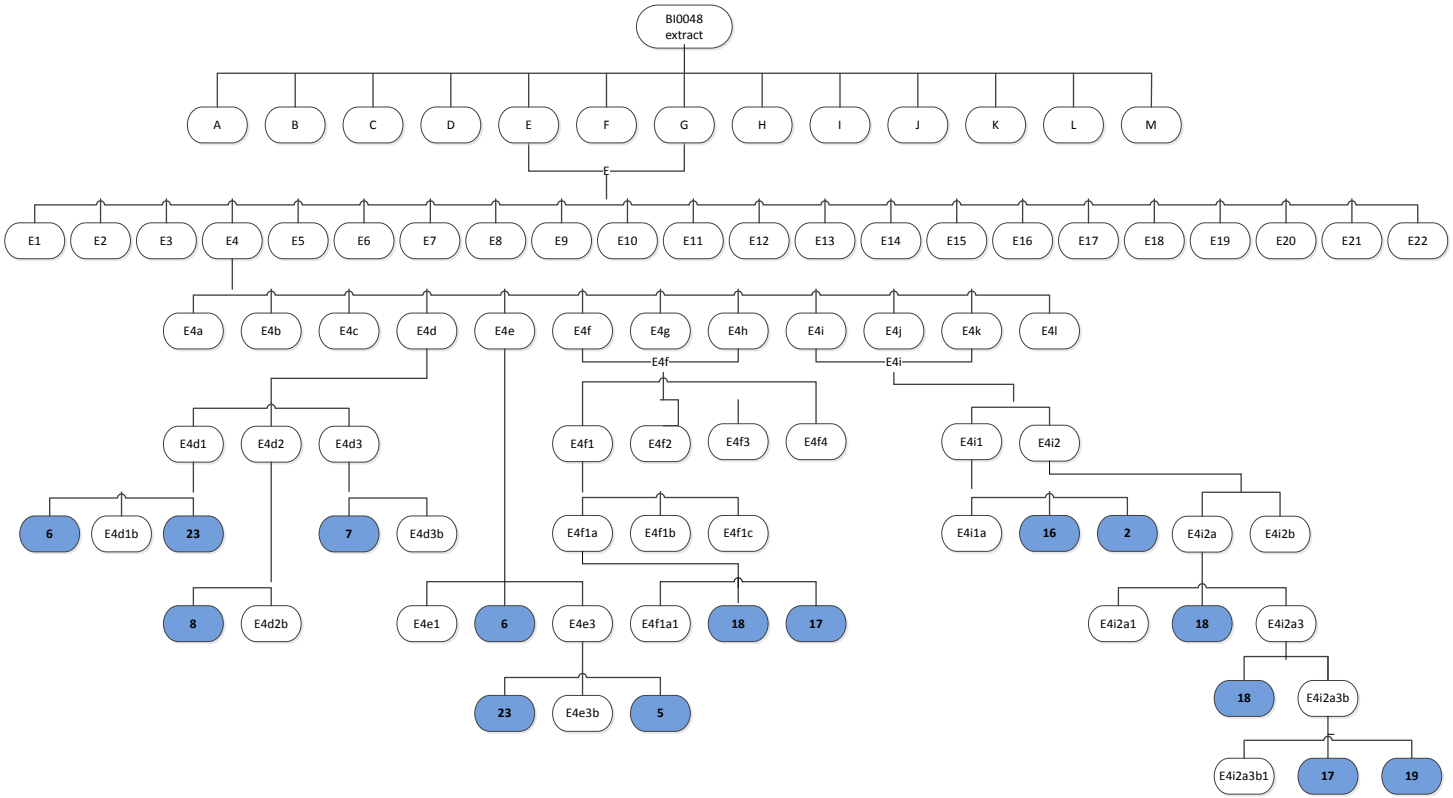

Figure 13. Fractionation scheme for the isolation of metabolites from the crude actinobacterial extract (part E).

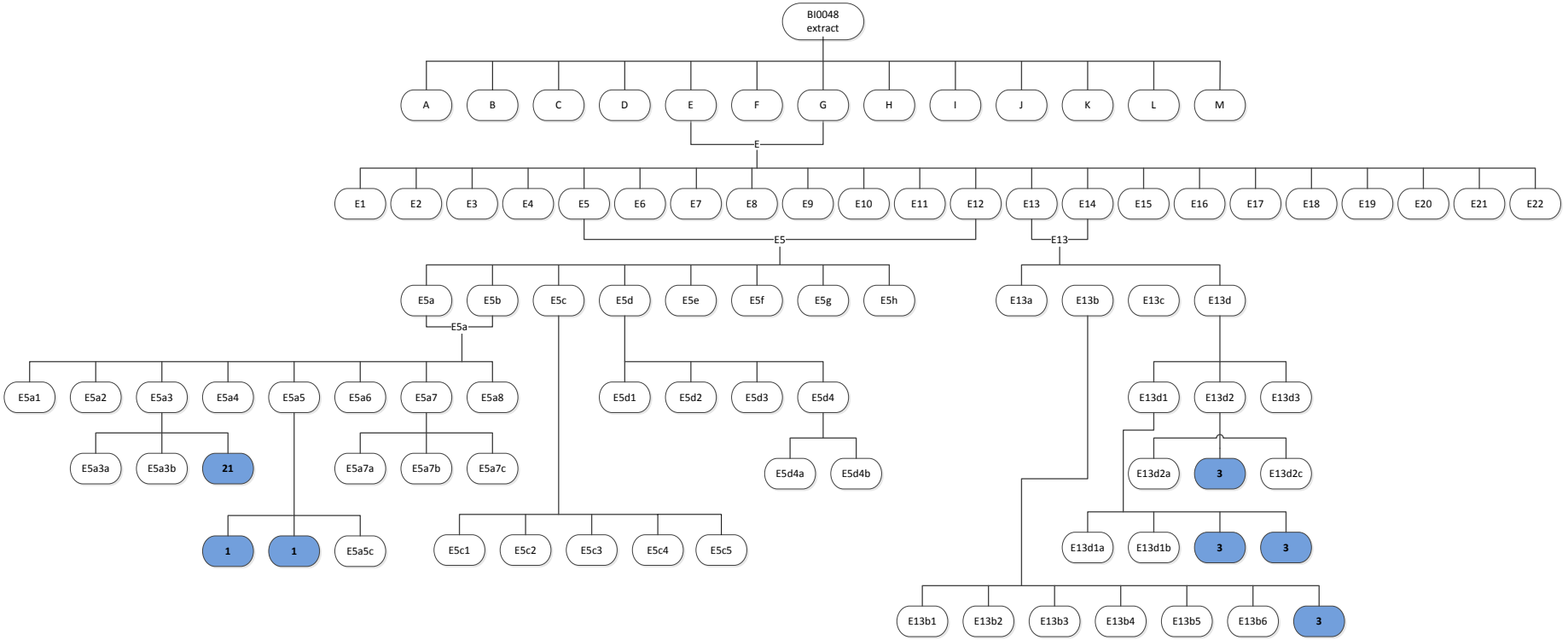

Figure 14. Fractionation scheme for the isolation of metabolites from the crude actinobacterial extract (part F).

Initially, the organic extract (12.5 g) was subjected to reversed-phase vacuum column chromatography, using H_2O with increasing amounts of MeOH, followed by MeOH with increasing amounts of CH_2Cl_2 as the mobile phase, to afford 28 fractions, which after an initial screening with TLC were combined into 13 fractions (Table 6).

Table 6. Experimental details for the separation of the crude actinobacterial extract.

Fraction	Mobile phase			Volume (mL)
	H_2O %	MeOH %	CH_2Cl_2 %	
A	100	-	-	400
B	100	-	-	250
	100	-	-	250
C	95	5	-	500
	90	10	-	500
	80	20	-	250
D	80	20	-	250
	70	30	-	250
	70	30	-	250
E	60	40	-	250
	60	40	-	250
	50	50	-	250
	50	50	-	250
F	40	60	-	250
	40	60	-	250
G	30	70	-	250
	30	70	-	250
H	20	80	-	250
	20	80	-	250
I	10	90	-	250
	10	90	-	250
J	-	100	-	500
K	-	50	50	300
	-	50	50	300
	-	-	100	250
L	-	-	100	500
M	-	30	70	1000

Fractions B, C and D, pooled together in one fraction thereafter designated as D (2.335 g), were further fractionated by normal-phase vacuum column chromatography, using EtOAc with increasing amounts of MeOH as the mobile phase, to afford 20 fractions, which after an initial screening with TLC were combined into 13 fractions (Table 7).

Table 7. Experimental details for the separation of fraction D.

Fraction	Mobile phase		Volume (mL)
	EtOAc %	MeOH %	
D1	100	-	450
D2	95	5	300
D3	90	10	300
D4	85	15	300
D5	80	20	300
D6	75	25	300
D7	70	30	300
D8	65	35	300
	60	40	300
D9	55	45	300
	50	50	300
	40	60	300
D10	30	70	300
D11	20	80	300
	10	90	300
D12	-	100	300
D13	-	100	150
	-	100	150
	-	100	150
	-	100	150

Fractions D1 and D2, pooled together in one fraction thereafter designated as D1 (93.0 mg), were further fractionated by normal-phase gravity column chromatography, using CH_2Cl_2 with increasing amounts of MeOH as the mobile phase, to afford 128 fractions of approx. 20 mL each, which after an initial screening with TLC were combined into 15 fractions (Table 8).

Table 8. Experimental details for the separation of fraction D1.

Fraction	Mobile phase		Volume (mL)
	CH_2Cl_2 %	MeOH %	
D1a	100	-	130
D1b	100	-	220
	99	1	120
D1c	99	1	180
	98	2	40
D1d	98	2	180
D1e	98	2	40
D1f	98	2	40
	97	3	50
D1g	97	3	110
D1h	97	3	90

D1i	97	3	50
	96	4	30
D1j	96	4	130
D1k	96	4	40
	94	6	30
D1l	94	6	90
D1m	94	6	180
	90	10	20
D1n	90	10	220
D1o	90	10	60
	80	20	200
	50	50	100

Fraction D1e (21.8 mg) was subjected to reversed-phase HPLC to yield four fractions (Table 9), among which fractions D1e2, D1e3 and D1e4 were identified as metabolites **10**, **12** and **9**, respectively.

Table 9. Experimental details for the separation of fraction D1e.

Chromatographic conditions	
Column	Kromasil 100 C_{18} (250 mm × 8 mm i.d.)
Mobile phase	MeOH/H_2O 60:40, 1.5 mL/min

Fraction	**Retention time (min)**	**Weight (mg)**
D1e1	10.0	0.8
D1e2	21.0	1.2
D1e3	24.5	6.4
D1e4	27.7	2.7

Fraction D1f (9.1 mg) was subjected to reversed-phase HPLC to yield five fractions (Table 10), among which fractions D1f1, D1f3, D1f4 and D1f5 were identified as metabolites **10**, **12**, **13** and **9**, respectively.

Table 10. Experimental details for the separation of fraction D1f.

Chromatographic conditions	
Column	Kromasil 100 C_{18} (250 mm × 8 mm i.d.)
Mobile phase	MeOH/H_2O 60:40, 1.5 mL/min

Fraction	**Retention time (min)**	**Weight (mg)**
D1f1	9.7	3.2
D1f2	10.7	0.9
D1f3	11.2	1.5
D1f4	18.0	1.0
D1f5	28.0	1.9

Fraction D1g (4.1 mg) was subjected to reversed-phase HPLC to yield six fractions (Table 11), among which fractions D1g1, D1g4 and D1g6 were identified as metabolites **11**, **10** and **13**, respectively.

Table 11. Experimental details for the separation of fraction D1g.

Chromatographic conditions	
Column	Kromasil 100 C_{18} (250 mm × 8 mm i.d.)
Mobile phase	MeOH/H_2O 60:40, 1.5 mL/min

Fraction	**Retention time (min)**	**Weight (mg)**
D1g1	10.2	0.7
D1g2	11.2	0.8
D1g3	19.2	0.2
D1g4	21.0	0.7
D1g5	21.5	0.5
D1g6	25.2	0.9

Fraction D1i (4.2 mg) was subjected to reversed-phase HPLC to yield five fractions (Table 12), among which fractions D1i1 and D1i2 were identified as metabolites **14** and **2**, respectively.

Table 12. Experimental details for the separation of fraction D1i.

Chromatographic conditions	
Column	Kromasil 100 C_{18} (250 mm × 8 mm i.d.)
Mobile phase	MeOH/H_2O 60:40, 1.5 mL/min

Fraction	**Retention time (min)**	**Weight (mg)**
D1i1	9.7	0.9
D1i2	10.6	0.6
D1i3	11.2	0.8
D1i4	11.7	0.2
D1i5	14.0	0.1

Fraction D1j (3.3 mg) was subjected to reversed-phase HPLC to yield eight fractions (Table 13), among which fractions D1j4 and D1j5 were identified as metabolites **14** and **2**, respectively.

Table 13. Experimental details for the separation of fraction D1j.

Chromatographic conditions	
Column	Kromasil 100 C_{18} (250 mm × 8 mm i.d.)
Mobile phase	MeOH/H_2O 60:40, 1.5 mL/min

Fraction	**Retention time (min)**	**Weight (mg)**
D1j1	6.7	0.1
D1j2	7.3	0.3
D1j3	8.3	0.1
D1j4	9.3	0.4
D1j5	10.8	1.0
D1j6	11.2	0.5
D1j7	11.8	0.3
D1j8	18.2	0.3

Fraction D1l (8.7 mg) was subjected to reversed-phase HPLC to yield three fractions (Table 14), among which both fractions D1l2 and D1l3 were identified as metabolite **1**.

Table 14. Experimental details for the separation of fraction D1l.

Chromatographic conditions	
Column	Nucleosil 100 C_{18} (250 mm × 10 mm i.d.)
Mobile phase	MeOH/H_2O 80:20, 1.5 mL/min

Fraction	**Retention time (min)**	**Weight (mg)**
D1l1	6.3	0.8
D1l2	9.0	2.5
D1l3	10.3	3.8

Fraction D1m (10.7 mg) was subjected to reversed-phase HPLC to yield six fractions (Table 15), among which fractions D1m3 and D1m5 were identified as metabolites **1** and **4**, respectively.

Table 15. Experimental details for the separation of fraction D1m.

Chromatographic conditions	
Column	Kromasil 100 C_{18} (250 mm × 8 mm i.d.)
Mobile phase	MeOH/H_2O 60:40, 1.5 mL/min

Fraction	**Retention time (min)**	**Weight (mg)**
D1m1	6.7	1.0
D1m2	7.7	0.6
D1m3	9.3	1.4
D1m4	9.8	1.4
D1m5	14.6	1.3

D1m6	20.5	1.1

Fraction D1n (11.5 mg) was subjected to reversed-phase HPLC to yield three fractions (Table 16), among which fraction D1n2 was identified as metabolite **3**.

Table 16. Experimental details for the separation of fraction D1n.

Chromatographic conditions	
Column	Kromasil 100 C_{18} (250 mm × 8 mm i.d.)
Mobile phase	MeOH/H_2O 60:40, 1.5 mL/min

Fraction	**Retention time (min)**	**Weight (mg)**
D1n1	6.5-9.7	1.7
D1n2	23.5	3.2
D1n3	28.7	0.5

Fraction D3 (64.7 mg) was subjected to reversed-phase HPLC to yield five fractions (Table 17), among which fractions D3d and D3e were identified as metabolites **3** and **12**, respectively.

Table 17. Experimental details for the separation of fraction D3.

Chromatographic conditions	
Column	Kromasil 100 C_{18} (250 mm × 8 mm i.d.)
Mobile phase	MeOH/H_2O 60:40, 1.5 mL/min

Fraction	**Retention time (min)**	**Weight (mg)**
D3a	7.7	2.8
D3b	9.1	7.4
D3c	9.9	4.3
D3d	24.0	13.9
D3e	25.0	5.2

Fraction D3b (7.4 mg) was subjected to reversed-phase HPLC to yield two fractions (Table 18), among which fraction D3b2 was identified as metabolite **1**.

Table 18. Experimental details for the separation of fraction D3b.

Chromatographic conditions	
Column	Kromasil 100 C_{18} (250 mm × 8 mm i.d.)
Mobile phase	MeOH/H_2O 50:50, 1.5 mL/min

Fraction	**Retention time (min)**	**Weight (mg)**
D3b1	10.8	0.7
D3b2	11.4	5.9

Fraction D4 (91.2 mg) was subjected to reversed-phase HPLC to yield seven fractions (Table 19), among which fraction D4f was identified as metabolite **3**.

Table 19. Experimental details for the separation of fraction D4.

Chromatographic conditions	
Column	Kromasil 100 C_{18} (250 mm × 8 mm i.d.)
Mobile phase	MeOH/H_2O 60:40, 1.5 mL/min

Fraction	**Retention time (min)**	**Weight (mg)**
D4a	6.0-8.5	8.7
D4b	8.5	44.3
D4c	9.0-12.0	18.9
D4d	12.2	3.3
D4e	18.2	1.3
D4f	24.7	3.7
D4g	26.5	2.6

Fraction D4b (44.3 mg) was subjected to reversed-phase HPLC to yield two fractions (Table 20), among which fractions D4b1 and D4b2 were identified as metabolites **15** and **21**, respectively.

Table 20. Experimental details for the separation of fraction D4b.

Chromatographic conditions	
Column	Kromasil 100 C_{18} (250 mm × 8 mm i.d.)
Mobile phase	MeCN/H_2O 30:70, 1.5 mL/min

Fraction	**Retention time (min)**	**Weight (mg)**
D4b1	7.5	1.5
D4b2	8.3	31.0

Fraction D4d (3.3 mg) was subjected to reversed-phase HPLC to yield one fraction (Table 21), which was identified as metabolite **20**.

Table 21. Experimental details for the separation of fraction D4d.

Chromatographic conditions	
Column	Kromasil 100 C_{18} (250 mm × 8 mm i.d.)
Mobile phase	MeOH/H_2O 50:50, 1.5 mL/min

Fraction	**Retention time (min)**	**Weight (mg)**
D4d1	2.7	16.8

Fraction D4g (2.6 mg) was subjected to reversed-phase HPLC to yield one

fraction (Table 22), which was identified as metabolite **13**.

Table 22. Experimental details for the separation of fraction D4g.

Chromatographic conditions	
Column	Kromasil 100 C_{18} (250 mm × 8 mm i.d.)
Mobile phase	MeOH/H_2O 60:40, 1.5 mL/min

Fraction	**Retention time (min)**	**Weight (mg)**
D4g1	1.5	24.5

Fractions D5 and D6, pooled together in one fraction thereafter designated as D5 (120.0 mg), were further fractionated by reversed-phase vacuum column chromatography, using H_2O with increasing amounts of MeOH as the mobile phase, to afford four fractions (Table 23).

Table 23. Experimental details for the separation of fraction D5.

Fraction	**Mobile phase**		**Volume (mL)**
	H_2O %	**MeOH %**	
D5a	50	50	20
D5b	40	60	20
D5c	30	70	20
D5d	-	100	20

Fraction D5a (109.1 mg) was subjected to reversed-phase HPLC to yield seven fractions (Table 24).

Table 24. Experimental details for the separation of fraction D5a.

Chromatographic conditions	
Column	Kromasil 100 C_{18} (250 mm × 8 mm i.d.)
Mobile phase	MeOH/H_2O 50:50, 1.5 mL/min

Fraction	**Retention time (min)**	**Weight (mg)**
D5a1	6.8	9.9
D5a2	7.2	25.2
D5a3	7.6	9.2
D5a4	8.2	12.2
D5a5	8.6-9.1	5.7
D5a6	9.8	7.5
D5a7	11.7	5.6

Fraction D5a3 (9.2 mg) was subjected to reversed-phase HPLC to yield two fractions (Table 25), among which fraction D5a3b was identified as metabolite **1**.

Table 25. Experimental details for the separation of fraction D5a3.

Chromatographic conditions	
Column	Kromasil 100 C_{18} (250 mm × 8 mm i.d.)
Mobile phase	MeCN/H_2O 40:60, 1.5 mL/min

Fraction	Retention time (min)	Weight (mg)
D5a3a	5.9	1.7
D5a3b	6.2	4.3

Fraction D5a4 (12.2 mg) was subjected to reversed-phase HPLC to yield two fractions (Table 26).

Table 26. Experimental details for the separation of fraction D5a4.

Chromatographic conditions	
Column	Kromasil 100 C_{18} (250 mm × 8 mm i.d.)
Mobile phase	MeCN/H_2O 40:60, 1.5 mL/min

Fraction	Retention time (min)	Weight (mg)
D5a4a	6.3	4.1
D5a4b	6.8	3.3

Fraction D5a4a (4.1 mg) was subjected to reversed-phase HPLC to yield one fraction (Table 27), which was identified as metabolite **22**.

Table 27. Experimental details for the separation of fraction D5a4a.

Chromatographic conditions	
Column	Kromasil 100 C_{18} (250 mm × 8 mm i.d.)
Mobile phase	MeCN/H_2O 40:60, 1.5 mL/min

Fraction	Retention time (min)	Weight (mg)
D5a4a1	6.6	1.1

Fraction D5a6 (7.5 mg) was subjected to reversed-phase HPLC to yield three fractions (Table 28), among which both fractions D5a6b and D5a6c were identified as metabolite **21**.

Table 28. Experimental details for the separation of fraction D5a6.

Chromatographic conditions	
Column	Kromasil 100 C_{18} (250 mm × 8 mm i.d.)
Mobile phase	MeCN/H_2O 40:60, 1.5 mL/min

Fraction	Retention time (min)	Weight (mg)
D5a6a	7.0	3.6
D5a6b	7.4	0.5
D5a6c	7.9	0.9

Fraction D7 (405.0 mg) was further fractionated by normal-phase gravity column chromatography, using CH_2Cl_2 with increasing amounts of MeOH as the mobile phase, to afford 186 fractions of approx. 25 mL each, which after an initial screening with TLC were combined into 19 fractions (Table 29).

Table 29. Experimental details for the separation of fraction D7.

Fraction	Mobile phase		Volume (mL)
	CH_2Cl_2%	MeOH %	
D7a	95	5	260
D7b	95	5	160
D7c	95	5	160
D7d	95	5	90
D7e	95	5	130
	93	7	70
D7f	93	7	330
D7g	90	10	400
D7h	85	15	320
D7i	85	15	180
D7j	85	15	140
D7k	85	15	60
	80	20	50
D7l	80	20	160
D7m	80	20	160
D7n	80	20	30
	75	25	300
D7o	75	25	100
	65	35	400
D7p	60	40	280
D7q	60	40	120
	50	50	70
D7r	50	50	330
	25	75	200
	-	100	50
D7s	-	100	250

Fraction D7l (20.4 mg) was subjected to reversed-phase HPLC to yield four fractions (Table 30).

Table 30. Experimental details for the separation of fraction D7l.

Chromatographic conditions	
Column	Kromasil 100 C_{18} (250 mm × 8 mm i.d.)
Mobile phase	MeOH/H_2O 50:50, 1.5 mL/min

Fraction	Retention time (min)	Weight (mg)
D7l1	6.9	2.8
D7l2	7.2	9.1
D7l3	7.8	0.7
D7l4	8.2	1.3

Fraction D7n (42.0 mg) was subjected to reversed-phase HPLC to yield three fractions (Table 31).

Table 31. Experimental details for the separation of fraction D7n.

Chromatographic conditions	
Column	Kromasil 100 C_{18} (250 mm × 8 mm i.d.)
Mobile phase	MeOH/H_2O 50:50, 1.5 mL/min

Fraction	Retention time (min)	Weight (mg)
D7n1	7.0	12.3
D7n2	7.3	10.2
D7n3	7.6	3.7

Fraction D7n2 (10.2 mg) was subjected to reversed-phase HPLC to yield four fractions (Table 32).

Table 32. Experimental details for the separation of fraction D7n2.

Chromatographic conditions	
Column	Kromasil 100 C_{18} (250 mm × 8 mm i.d.)
Mobile phase	MeCN /H_2O 40:60, 1.5 mL/min

Fraction	Retention time (min)	Weight (mg)
D7n2a	5.8	0.2
D7n2b	6.0	7.4
D7n2c	7.4	0.5
D7n2d	7.8	0.2

Fraction D7n2b (7.4 mg) was subjected to reversed-phase HPLC to yield four fractions (Table 33).

Table 33. Experimental details for the separation of fraction D7n2b.

Chromatographic conditions	
Column	Kromasil 100 C_{18} (250 mm × 8 mm i.d.)
Mobile phase	MeCN /H_2O 40:60, 1.5 mL/min

Fraction	Retention time (min)	Weight (mg)
D7n2b1	5.7	0.1
D7n2b2	6.0	6.0
D7n2b3	7.3	0.2
D7n2b4	7.6	0.1

Fraction D7n3 (3.7 mg) was subjected to reversed-phase HPLC to yield three fractions (Table 34).

Table 34. Experimental details for the separation of fraction D7n3.

Chromatographic conditions	
Column	Kromasil 100 C_{18} (250 mm × 8 mm i.d.)
Mobile phase	MeCN /H_2O 35:65, 1.5 mL/min

Fraction	Retention time (min)	Weight (mg)
D7n3a	6.2	0.9
D7n3b	6.4	2.0
D7n3c	8.7	0.2

Fraction D7o (90.0 mg) was subjected to reversed-phase HPLC to yield five fractions (Table 35).

Table 35. Experimental details for the separation of fraction D7o.

Chromatographic conditions	
Column	Kromasil 100 C_{18} (250 mm × 8 mm i.d.)
Mobile phase	MeCN /H_2O 40:60, 1.5 mL/min

Fraction	Retention time (min)	Weight (mg)
D7o1	6.0	29.2
D7o2	6.2	40.2
D7o3	6.4-6.6	15.2
D7o4	6.7-8.0	1.7
D7o5	8.5	0.4

Fraction D7o2 (40.2 mg) was subjected to reversed-phase HPLC to yield four fractions (Table 36).

Table 36. Experimental details for the separation of fraction D7o2.

Chromatographic conditions	
Column	Kromasil 100 C_{18} (250 mm × 8 mm i.d.)
Mobile phase	MeCN /H_2O 40:60, 1.5 mL/min

Fraction	Retention time (min)	Weight (mg)
D7o2a	5.9	16.6
D7o2b	6.1	21.0
D7o2c	7.4	0.1
D7o2d	7.8	0.3

Fraction D7o2b (21.0 mg) was subjected to reversed-phase HPLC to yield four fractions (Table 37).

Table 37. Experimental details for the separation of fraction D7o2b.

Chromatographic conditions	
Column	Kromasil 100 C_{18} (250 mm × 8 mm i.d.)
Mobile phase	MeOH /H_2O 40:60, 1.5 mL/min

Fraction	Retention time (min)	Weight (mg)
D7o2b1	7.2	3.8
D7o2b2	7.6	12.5
D7o2b3	8.0	0.5
D7o2b4	8.5	1.6

Fraction D7o2b4 (1.6 mg) was subjected to reversed-phase HPLC to yield one fraction (Table 38).

Table 38. Experimental details for the separation of fraction D7o2b4.

Chromatographic conditions	
Column	Kromasil 100 C_{18} (250 mm × 8 mm i.d.)
Mobile phase	MeOH /H_2O 35:65, 1.5 mL/min

Fraction	Retention time (min)	Weight (mg)
D7o2b4a	8.3	1.3

Fraction D7o3 (15.2 mg) was subjected to reversed-phase HPLC to yield three fractions (Table 39).

Table 39. Experimental details for the separation of fraction D7o3.

Chromatographic conditions	
Column	Kromasil 100 C_{18} (250 mm × 8 mm i.d.)
Mobile phase	MeCN /H_2O 40:60, 1.5 mL/min

Fraction	Retention time (min)	Weight (mg)
D7o3a	5.7	2.4
D7o3b	6.1	9.4
D7o3c	7.7	1.3

Fraction D7o3b (9.4 mg) was subjected to reversed-phase HPLC to yield four fractions (Table 40).

Table 40. Experimental details for the separation of fraction D7o3b.

Chromatographic conditions	
Column	Kromasil 100 C_{18} (250 mm × 8 mm i.d.)
Mobile phase	MeOH/H_2O 50:50, 1.5 mL/min

Fraction	Retention time (min)	Weight (mg)
D7o3b1	6.4	0.5
D7o3b2	6.8	1.5
D7o3b3	7.3	4.3
D7o3b4	7.5-8.3	2.6

Fraction D7o3b3 (4.3 mg) was subjected to reversed-phase HPLC to yield three fractions (Table 41).

Table 41. Experimental details for the separation of fraction D7o3b3.

Chromatographic conditions	
Column	Kromasil 100 C_{18} (250 mm × 8 mm i.d.)
Mobile phase	MeCN /H_2O 35:65, 1.5 mL/min

Fraction	Retention time (min)	Weight (mg)
D7o3b3a	7.0	1.5
D7o3b3b	7.4	1.0
D7o3b3c	9.5	0.2

Fraction D7r (18.4 mg) was subjected to reversed-phase HPLC to yield five fractions (Table 42).

Table 42. Experimental details for the separation of fraction D7r.

Chromatographic conditions	
Column	Kromasil 100 C_{18} (250 mm × 8 mm i.d.)
Mobile phase	MeOH/H_2O 50:50, 1.5 mL/min

Fraction	Retention time (min)	Weight (mg)
D7r1	6.2-6.7	0.8
D7r2	7.1	4.2

D7r3	7.5	2.3
D7r4	7.8	1.5
D7r5	8.2	2.5

Fraction D7r2 (4.2 mg) was subjected to reversed-phase HPLC to yield one fraction (Table 43).

Table 43. Experimental details for the separation of fraction D7r2.

Chromatographic conditions	
Column	Kromasil 100 C_{18} (250 mm × 8 mm i.d.)
Mobile phase	MeCN/H_2O 40:60, 1.5 mL/min

Fraction	**Retention time (min)**	**Weight (mg)**
D7r2a	6.0	1.2

Fraction D7r3 (2.3 mg) was subjected to reversed-phase HPLC to yield two fractions (Table 44).

Table 44. Experimental details for the separation of fraction D7r3.

Chromatographic conditions	
Column	Kromasil 100 C_{18} (250 mm × 8 mm i.d.)
Mobile phase	MeCN /H_2O 35:65, 1.5 mL/min

Fraction	**Retention time (min)**	**Weight (mg)**
D7r3a	6.3	1.7
D7r3b	8.6	0.2

Fraction D7r5 (2.5 mg) was subjected to reversed-phase HPLC to yield one fraction (Table 45).

Table 45. Experimental details for the separation of fraction D7r5.

Chromatographic conditions	
Column	Kromasil 100 C_{18} (250 mm × 8 mm i.d.)
Mobile phase	MeCN /H_2O 40:60, 1.5 mL/min

Fraction	**Retention time (min)**	**Weight (mg)**
D7r5a	6.2	1.0

Fraction D8 (697.0 mg) was further fractionated by reversed-phase vacuum column chromatography, using H_2O with increasing amounts of MeOH as the mobile phase, to afford 14 fractions, which after an initial screening with TLC were combined

into eight fractions (Table 46).

Table 46. Experimental details for the separation of fraction D8.

Fraction	Mobile phase		Volume (mL)
	H_2O %	MeOH %	
D8a	80	20	25
D8b	80	20	25
D8c	70	30	25
	70	30	25
D8d	60	40	25
D8e	60	40	25
	50	50	25
D8f	50	50	25
	40	60	25
D8g	40	60	25
	30	70	25
	30	70	25
D8h	-	100	25
	-	100	25

Part of fraction D8a (240.0 mg out of 651.0 mg) was subjected to reversed-phase HPLC to yield five fractions (Table 47).

Table 47. Experimental details for the separation of fraction D8a.

Chromatographic conditions	
Column	Kromasil 100 C_{18} (250 mm × 8 mm i.d.)
Mobile phase	MeOH/H_2O 30:70, 1.5 mL/min

Fraction	Retention time (min)	Weight (mg)
D8a1	6.8	106.8
D8a2	7.2	87.0
D8a3	8.0	4.3
D8a4	8.4-14.4	13.2
D8a5	14.5-19.2	14.4

Fraction D8a3 (4.3 mg) was subjected to reversed-phase HPLC to yield four fractions (Table 48).

Table 48. Experimental details for the separation of fraction D8a3.

Chromatographic conditions	
Column	Kromasil 100 C_{18} (250 mm × 8 mm i.d.)
Mobile phase	MeOH/H_2O 30:70, 1.5 mL/min

Fraction	Retention time (min)	Weight (mg)
D8a3a	7.0	0.3
D8a3b	7.2	0.2
D8a3c	8.0	1.0
D8a3d	8.3	0.1

Fraction D8a5 (14.4 mg) was subjected to reversed-phase HPLC to yield six fractions (Table 49).

Table 49. Experimental details for the separation of fraction D8a5.

Chromatographic conditions	
Column	Kromasil 100 C_{18} (250 mm × 8 mm i.d.)
Mobile phase	MeOH/H_2O 30:70, 1.5 mL/min

Fraction	Retention time (min)	Weight (mg)
D8a5a	7.0	7.6
D8a5b	8.0	0.2
D8a5c	15.9	0.3
D8a5d	16.6	0.6
D8a5e	17.7	0.5
D8a5f	18.9	0.7

The remaining amount of fraction D8a, thereafter designated as D8/2 (411.0 mg out of 651.0 mg), was further fractionated by reversed-phase vacuum column chromatography, using H_2O with increasing amounts of MeOH as the mobile phase, to afford 19 fractions, which after an initial screening with TLC were combined into five fractions (Table 50).

Table 50. Experimental details for the separation of fraction D8/2.

Fraction	Mobile phase		Volume (mL)
	H_2O %	MeOH %	
D8/2a	100	-	25
D8/2b	100	-	25
D8/2c	100	-	50
	95	5	100
	90	10	100
D8/2d	80	20	100
	40	60	100
D8/2e	-	100	50

Fraction D8/2a (371.6 mg) was subjected to reversed-phase HPLC to yield five fractions (Table 51).

Table 51. Experimental details for the separation of fraction D8/2a.

Chromatographic conditions	
Column	Kromasil 100 C_{18} (250 mm × 8 mm i.d.)
Mobile phase	MeOH /H_2O 30:70, 1.5 mL/min

Fraction	Retention time (min)	Weight (mg)
D8/2a1	7.3	156.6
D8/2a2	7.5	108.2
D8/2a3	8.2	7.6
D8/2a4	8.5-13.2	13.9
D8/2a5	13.2-19.4	8.5

Fraction D8/2a4 (13.9 mg) was subjected to reversed-phase HPLC to yield six fractions (Table 52).

Table 52. Experimental details for the separation of fraction D8/2a4.

Chromatographic conditions	
Column	Kromasil 100 C_{18} (250 mm × 8 mm i.d.)
Mobile phase	MeOH /H_2O 30:70, 1.5 mL/min

Fraction	Retention time (min)	Weight (mg)
D8/2a4a	8.2	1.6
D8/2a4b	8.9	2.0
D8/2a4c	9.9	2.4
D8/2a4d	10.6	3.6
D8/2a4e	11.0	2.4
D8/2a4f	11.4	2.5

Fraction D8/2a4d (3.6 mg) was subjected to reversed-phase HPLC to yield four fractions (Table 53).

Table 53. Experimental details for the separation of fraction D8/2a4d.

Chromatographic conditions	
Column	Kromasil 100 C_{18} (250 mm × 8 mm i.d.)
Mobile phase	MeCN /H_2O 20:80, 1.5 mL/min

Fraction	Retention time (min)	Weight (mg)
D8/2a4d1	7.4	0.8
D8/2a4d2	7.8	0.3
D8/2a4d3	8.0	0.7
D8/2a4d4	8.6	0.8

Fraction D8/2a4e (2.4 mg) was subjected to reversed-phase HPLC to yield three fractions (Table 54).

Table 54. Experimental details for the separation of fraction D8/2a4e.

Chromatographic conditions	
Column	Kromasil 100 C_{18} (250 mm × 8 mm i.d.)
Mobile phase	MeCN /H_2O 20:80, 1.5 mL/min

Fraction	Retention time (min)	Weight (mg)
D8/2a4e1	7.4	0.2
D8/2a4e2	8.3	0.3
D8/2a4e3	8.5	1.4

Fractions D8/2a4d4 and D8/2a4e3, pooled together in one fraction thereafter designated as D8/2a4e3 (2.2 mg), were subjected to reversed-phase HPLC to yield one fraction (Table 55).

Table 55. Experimental details for the separation of fraction D8/2a4e3.

Chromatographic conditions	
Column	Kromasil 100 C_{18} (250 mm × 8 mm i.d.)
Mobile phase	MeCN /H_2O 20:80, 1.5 mL/min

Fraction	Retention time (min)	Weight (mg)
D8/2a4e3a	5.3	0.9

Fraction D8/2a5 (8.5 mg) was subjected to reversed-phase HPLC to yield four fractions (Table 56).

Table 56. Experimental details for the separation of fraction D8/2a5.

Chromatographic conditions	
Column	Kromasil 100 C_{18} (250 mm × 8 mm i.d.)
Mobile phase	MeOH /H_2O 30:70, 1.5 mL/min

Fraction	Retention time (min)	Weight (mg)
D8/2a5a	12.0	0.9
D8/2a5b	14.0	1.2
D8/2a5c	16.4	2.0
D8/2a5d	19.1	2.3

Fraction D8/2a5d (2.3 mg) was subjected to reversed-phase HPLC to yield five fractions (Table 57).

Table 57. Experimental details for the separation of fraction D8/2a5d.

Chromatographic conditions	
Column	Kromasil 100 C_{18} (250 mm × 8 mm i.d.)
Mobile phase	MeCN /H_2O 20:80, 1.5 mL/min

Fraction	**Retention time (min)**	**Weight (mg)**
D8/2a5d1	6.2	0.2
D8/2a5d2	7.7	0.2
D8/2a5d3	10.8	0.3
D8/2a5d4	11.2	0.1
D8/2a5d5	11.6	0.2

Fractions E, F and G, pooled together in one fraction thereafter designated as E (931.0 mg), were further fractionated by normal-phase gravity column chromatography, using CH_2Cl_2 with increasing amounts of MeOH, followed by MeOH with increasing amounts of H_2O as the mobile phase, to afford 205 fractions of approx. 25 mL each, which after an initial screening with TLC were combined into 25 fractions (Table 58).

Table 58. Experimental details for the separation of fraction E.

Fraction	**Mobile phase**			**Volume (mL)**
	CH_2Cl_2 %	**MeOH %**	**H_2O %**	
E1	95	5	-	260
E2	95	5	-	100
E3	95	5	-	80
E4	95	5	-	220
E5	95	5	-	160
E6	95	5	-	80
E7	95	5	-	160
E8	95	5	-	310
E9	95	5	-	230
E10	95	5	-	50
	93	7	-	150
E11	93	7	-	50
	90	10	-	70
E12	90	10	-	330
E13	87	13	-	200
	85	15	-	20
E14	85	15	-	380
E15	80	20	-	200
	75	25	-	90
E16	75	25	-	140
E17	75	25	-	70
	60	30	-	130
E18	60	30	-	70
	50	50	-	20

E19	50	50	-	170
E20	50	50	-	110
	40	60	-	120
E21	40	60	-	80
	20	80	-	200
	-	100	-	90
E22	-	100	-	310
E23	-	95	5	100
E24	-	90	10	100
E25	-	50	50	300

Fraction E4 (122 mg) was further fractionated by normal-phase vacuum column chromatography, using c-Hex with increasing amounts of EtOAc as the mobile phase, to afford 28 fractions, which after an initial screening with TLC were combined into 12 fractions (Table 59).

Table 59. Experimental details for the separation of fraction E4.

Fraction	**Mobile phase**		**Volume (mL)**
	c-Hex %	**EtOAc %**	
E4a	80	20	50
	80	20	50
E4b	75	25	50
	75	25	50
E4c	70	30	50
	30	30	50
E4d	65	35	50
	65	35	50
	60	40	50
E4e	60	40	50
	55	45	50
	55	45	50
	50	50	50
E4f	50	50	50
	45	55	50
E4g	45	55	50
	40	60	50
	40	60	50
E4h	35	65	50
	35	65	50
	30	70	50
E4i	30	70	50
	25	75	50
E4j	20	80	50
	15	85	50
E4k	10	90	50
	5	95	50

E4l	-	100	50

Fraction E4d (23.1 mg) was subjected to reversed-phase HPLC to yield three fractions (Table 60).

Table 60. Experimental details for the separation of fraction E4d.

Chromatographic conditions	
Column	Kromasil 100 C_{18} (250 mm × 8 mm i.d.)
Mobile phase	MeOH 100%, 1.5 mL/min

Fraction	**Retention time (min)**	**Weight (mg)**
E4d1	11.7	8.2
E4d2	12.9	8.1
E4d3	13.3-17.7	4.6

Fraction E4d1 (8.2 mg) was subjected to reversed-phase HPLC to yield three fractions (Table 61), among which fractions E4d1a and E4d1c were identified as metabolites **6** and **23**, respectively.

Table 61. Experimental details for the separation of fraction E4d1.

Chromatographic conditions	
Column	Kromasil 100 C_{18} (250 mm × 8 mm i.d.)
Mobile phase	MeOH/H_2O 80:20, 1.5 mL/min

Fraction	**Retention time (min)**	**Weight (mg)**
E4d1a	8.9	1.6
E4d1b	9.4	0.7
E4d1c	9.6	1.6

Fraction E4d2 (8.1 mg) was subjected to reversed-phase HPLC to yield two fractions (Table 62), among which fraction E4d2a was identified as metabolite **8**.

Table 62. Experimental details for the separation of fraction E4d2.

Chromatographic conditions	
Column	Kromasil 100 C_{18} (250 mm × 8 mm i.d.)
Mobile phase	MeOH/H_2O 90:10, 1.5 mL/min

Fraction	**Retention time (min)**	**Weight (mg)**
E4d2a	7.0	3.8
E4d2b	7.4	3.9

Fraction E4d3 (4.6 mg) was subjected to reversed-phase HPLC to yield two

fractions (Table 63), among which fraction E4d3a was identified as metabolite **7**.

Table 63. Experimental details for the separation of fraction E4d3.

Chromatographic conditions	
Column	Kromasil 100 C_{18} (250 mm × 8 mm i.d.)
Mobile phase	MeOH /H_2O 95:5, 1.5 mL/min

Fraction	**Retention time (min)**	**Weight (mg)**
E4d3a	6.7	1.2
E4d3b	9.2	0.4

Fraction E4e (17.0 mg) was subjected to reversed-phase HPLC to yield three fractions (Table 64), among which fraction E4e2 was identified as metabolite **6**.

Table 64. Experimental details for the separation of fraction E4e.

Chromatographic conditions	
Column	Kromasil 100 C_{18} (250 mm × 8 mm i.d.)
Mobile phase	MeOH /H_2O 75:25, 1.5 mL/min

Fraction	**Retention time (min)**	**Weight (mg)**
E4e1	9.3	2.1
E4e2	9.6	5.0
E4e3	10.4	3.9

Fraction E4e3 (3.9 mg) was subjected to reversed-phase HPLC to yield three fractions (Table 65), among which fractions E4e3a and E4e3c were identified as metabolites **23** and **5**, respectively.

Table 65. Experimental details for the separation of fraction E4e3.

Chromatographic conditions	
Column	Kromasil 100 C_{18} (250 mm × 8 mm i.d.)
Mobile phase	MeCN /H_2O 70:30, 1.5 mL/min

Fraction	**Retention time (min)**	**Weight (mg)**
E4e3a	8.8	1.4
E4e3b	9.2	1.2
E4e3c	9.7	1.2

Fractions E4f, E4g and E4h, pooled together in one fraction thereafter designated as E4f (21.1 mg), were subjected to reversed-phase solid phase extraction with MeOH /H_2O 80:20 and subsequently the resulting subfraction (12.5 mg) was subjected to reversed-phase HPLC to yield four fractions (Table 66).

Table 66. Experimental details for the separation of fraction E4f.

Chromatographic conditions	
Column	Kromasil 100 C_{18} (250 mm × 8 mm i.d.)
Mobile phase	MeOH /H_2O 75:25, 1.5 mL/min

Fraction	Retention time (min)	Weight (mg)
E4f1	9.6	5.2
E4f2	10.2	1.3
E4f3	11	1.4
E4f4	15.8	0.9

Fraction E4f1 (5.2 mg) was subjected to reversed-phase HPLC to yield three fractions (Table 67).

Table 67. Experimental details for the separation of fraction E4f1.

Chromatographic conditions	
Column	Kromasil 100 C_{18} (250 mm × 8 mm i.d.)
Mobile phase	MeCN /H_2O 65:35, 1.5 mL/min

Fraction	Retention time (min)	Weight (mg)
E4f1a	8.0	3.5
E4f1b	8.5	1.0
E4f1c	9.7	0.1

Fraction E4f1a (3.5 mg) was subjected to reversed-phase HPLC to yield three fractions (Table 68), among which fractions E4f1a2 and E4f1a3 were identified as metabolites **18** and **17**, respectively.

Table 68. Experimental details for the separation of fraction E4f1a.

Chromatographic conditions	
Column	Kromasil 100 C_{18} (250 mm × 8 mm i.d.)
Mobile phase	MeCN /H_2O 45:55, 1.5 mL/min

Fraction	Retention time (min)	Weight (mg)
E4f1a1	7.0	0.1
E4f1a2	9.1	0.4
E4f1a3	9.6	2.3

Fraction E4i (44.0 mg) was subjected to reversed-phase solid phase extraction with MeOH /H_2O 70:30 and subsequently the resulting subfraction (36.0 mg) was subjected to reversed-phase HPLC to yield two fractions (Table 69).

Table 69. Experimental details for the separation of fraction E4i.

Chromatographic conditions	
Column	Kromasil 100 C_{18} (250 mm × 8 mm i.d.)
Mobile phase	MeOH /H_2O 75:25, 1.5 mL/min

Fraction	Retention time (min)	Weight (mg)
E4i1	8.7	5.0
E4i2	9.6	20.1

Fraction E4i1 (5.0 mg) was subjected to reversed-phase HPLC to yield three fractions (Table 70), among which fractions E4i1b and E4i1c were identified as metabolites **16** and **2**, respectively.

Table 70. Experimental details for the separation of fraction E4i1.

Chromatographic conditions	
Column	Kromasil 100 C_{18} (250 mm × 8 mm i.d.)
Mobile phase	MeCN /H_2O 45:55, 1.5 mL/min

Fraction	Retention time (min)	Weight (mg)
E4i1a	7.0	0.2
E4i1b	8.0	1.9
E4i1c	10.8	0.3

Fraction E4i2 (20.1 mg) was subjected to reversed-phase HPLC to yield two fractions (Table 71).

Table 71. Experimental details for the separation of fraction E4i2.

Chromatographic conditions	
Column	Kromasil 100 C_{18} (250 mm × 8 mm i.d.)
Mobile phase	MeCN /H_2O 65:35, 1.5 mL/min

Fraction	Retention time (min)	Weight (mg)
E4i2a	8.0	17.4
E4i2b	18.3	0.3

Fraction E4i2a (17.4mg) was subjected to reversed-phase HPLC to yield three fractions (Table 72), among which fraction E4i2a2 was identified as metabolite **18**.

Table 72. Experimental details for the separation of fraction E4i2a.

Chromatographic conditions	
Column	Kromasil 100 C_{18} (250 mm × 8 mm i.d.)
Mobile phase	MeCN /H_2O 50:50, 1.5 mL/min

Fraction	Retention time (min)	Weight (mg)
E4i2a1	6.4	0.3
E4i2a2	8.5	7.2
E4i2a3	8.9	8.2

Fraction E4i2a3 (8.2 mg) was subjected to reversed-phase HPLC to yield two fractions (Table 73), among which fraction E4i2a3a was identified as metabolite **18**.

Table 73. Experimental details for the separation of fraction E4i2a3.

Chromatographic conditions	
Column	Kromasil 100 C_{18} (250 mm × 8 mm i.d.)
Mobile phase	MeCN /H_2O 45:55, 1.5 mL/min

Fraction	Retention time (min)	Weight (mg)
E4i2a3a	9.2	1.4
E4i2a3b	9.6	6.1

Fraction E4i2a3b (6.1 mg) was subjected to reversed-phase HPLC to yield three fractions (Table 74), among which fractions E4i2a3b2 and E4i2a3b3 were identified as metabolites **17** and **19**, respectively.

Table 74. Experimental details for the separation of fraction E4i2a3b.

Chromatographic conditions	
Column	Kromasil 100 C_{18} (250 mm × 8 mm i.d.)
Mobile phase	MeCN /H_2O 35:65, 1.5 mL/min

Fraction	Retention time (min)	Weight (mg)
E4i2a3b1	8.1	0.2
E4i2a3b2	11.6	2.6
E4i2a3b3	12.5	2.6

Fraction E5 (134.0 mg) was further fractionated by reversed-phase vacuum column chromatography, using H_2O with increasing amounts of MeOH as the mobile phase, to afford nine fractions, which after an initial screening with TLC were combined into eight fractions (Table 75).

Table 75. Experimental details for the separation of fraction E5.

Fraction	Mobile phase		Volume (mL)
	H_2O%	MeOH %	
E5a	70	30	20
	60	40	20

E5c	50	50	20
E5d	40	60	20
E5e	30	70	20
E5f	20	80	20
E5g	10	90	20
E5h	-	100	20

Fraction E5a (54.6 mg) was subjected to reversed-phase HPLC to yield eight fractions (Table 76).

Table 76. Experimental details for the separation of fraction E5a.

Chromatographic conditions	
Column	Kromasil 100 C_{18} (250 mm × 8 mm i.d.)
Mobile phase	MeOH /H_2O 50:50, 1.5 mL/min

Fraction	**Retention time (min)**	**Weight (mg)**
E5a1	6.4	3.0
E5a2	7.2-9.2	2.9
E5a3	9.7	7.1
E5a4	10.2-11.2	3.2
E5a5	11.5	10.6
E5a6	12-16	6.6
E5a7	16.5	3.7
E5a8	20.0	2.7

Fraction E5a3 (7.1 mg) was subjected to reversed-phase HPLC to yield three fractions (Table 77), among which fraction E5a3c was identified as metabolite **21**.

Table 77. Experimental details for the separation of fraction E5a3.

Chromatographic conditions	
Column	Kromasil 100 C_{18} (250 mm × 8 mm i.d.)
Mobile phase	MeCN /H_2O 30:70, 1.5 mL/min

Fraction	**Retention time (min)**	**Weight (mg)**
E5a3a	5.7	0.3
E5a3b	6.4	0.5
E5a3c	6.7	3.1

Fraction E5a7 (3.7 mg) was subjected to reversed-phase HPLC to yield three fractions (Table 78).

Table 78. Experimental details for the separation of fraction E5a7.

Chromatographic conditions	
Column	Kromasil 100 C_{18} (250 mm × 8 mm i.d.)
Mobile phase	MeCN /H_2O 30:70, 1.5 mL/min

Fraction	Retention time (min)	Weight (mg)
E5a7a	6.6	0.1
E5a7b	9.8	1.2
E5a7c	11.8	0.4

Fraction E5c (18.9 mg) was subjected to reversed-phase HPLC to yield five fractions (Table 79).

Table 79. Experimental details for the separation of fraction E5c.

Chromatographic conditions	
Column	Kromasil 100 C_{18} (250 mm × 8 mm i.d.)
Mobile phase	MeOH /H_2O 60:40, 1.5 mL/min

Fraction	Retention time (min)	Weight (mg)
E5c1	9.5	1.3
E5c2	12.2	1.9
E5c3	13.5	0.7
E5c4	14.3	0.9
E5c5	24.3	6.9

Fractions E5a5 and E5c1, pooled together in one fraction thereafter designated as E5a5 (11.9 mg), were subjected to reversed-phase HPLC to yield two fractions (Table 80), among which both fractions E5a5a and E5a5b were identified as metabolite **1**.

Table 80. Experimental details for the separation of fraction E5a5.

Chromatographic conditions	
Column	Kromasil 100 C_{18} (250 mm × 8 mm i.d.)
Mobile phase	MeCN /H_2O 30:70, 1.5 mL/min

Fraction	Retention time (min)	Weight (mg)
E5a5a	7.5	5.1
E5a5b	1.9	5.4

Fraction E5c2 (1.9 mg) was subjected to reversed-phase HPLC to yield three fractions (Table 81).

Table 81. Experimental details for the separation of fraction E5c2.

Chromatographic conditions	
Column	Kromasil 100 C_{18} (250 mm × 8 mm i.d.)
Mobile phase	MeCN /H_2O 30:70, 1.5 mL/min

Fraction	Retention time (min)	Weight (mg)
E5c2a	6.5	0.3
E5c2b	9.3	0.8
E5c2c	11.2	0.6

Fraction E5c4 (0.9 mg) was subjected to reversed-phase HPLC to yield two fractions (Table 82).

Table 82. Experimental details for the separation of fraction E5c4.

Chromatographic conditions	
Column	Kromasil 100 C_{18} (250 mm × 8 mm i.d.)
Mobile phase	MeCN /H_2O 30:70, 1.5 mL/min

Fraction	Retention time (min)	Weight (mg)
E5c4a	5.5	0.3
E5c4b	13.0	0.1

Fraction E5c5 (6.9 mg) was subjected to reversed-phase HPLC to yield two fractions (Table 83).

Table 83. Experimental details for the separation of fraction E5c5.

Chromatographic conditions	
Column	Kromasil 100 C_{18} (250 mm × 8 mm i.d.)
Mobile phase	MeCN /H_2O 50:50, 1.5 mL/min

Fraction	Retention time (min)	Weight (mg)
E5c5a	6.6	0.3
E5c2b	15.7	5.3

Fraction E5d (22.7 mg) was subjected to reversed-phase HPLC to yield four fractions (Table 84).

Table 84. Experimental details for the separation of fraction E5d.

Chromatographic conditions	
Column	Kromasil 100 C_{18} (250 mm × 8 mm i.d.)
Mobile phase	MeOH /H_2O 65:35, 1.5 mL/min

Fraction	Retention time (min)	Weight (mg)
E5d1	7.2-10.5	2.0
E5d2	10.5-13.2	2.3
E5d3	13.2-18.9	4.2
E5d4	19.3	9.7

Fraction E5d4 (9.7 mg) was subjected to reversed-phase HPLC to yield two fractions (Table 85).

Table 85. Experimental details for the separation of fraction E5d4.

Chromatographic conditions	
Column	Kromasil 100 C_{18} (250 mm × 8 mm i.d.)
Mobile phase	MeCN /H_2O 50:50, 1.5 mL/min

Fraction	Retention time (min)	Weight (mg)
E5d4a	6.2	0.4
E5d4b	16.0	6.3

Fractions E13 and E14, pooled together in one fraction thereafter designated as E13 (66.0 mg), were further fractionated by reversed-phase vacuum column chromatography, using H_2O with increasing amounts of MeOH as the mobile phase, to afford four fractions (Table 86).

Table 86. Experimental details for the separation of fraction E13.

Fraction	Mobile phase		Volume (mL)
	H_2O %	MeOH %	
E13a	100	-	20
E13b	80	20	20
E13c	60	40	20
E13d	-	100	20

Fraction E13b (9.8 mg) was subjected to reversed-phase HPLC to yield seven fractions (Table 87), among which fraction E13b7 was identified as metabolite **3**.

Table 87. Experimental details for the separation of fraction E13b.

Chromatographic conditions	
Column	Kromasil 100 C_{18} (250 mm × 8 mm i.d.)
Mobile phase	MeOH /H_2O 40:60, 1.5 mL/min

Fraction	Retention time (min)	Weight (mg)
E13b1	6.7	0.5
E13b2	7.2	0.8

E13b3	8.1	0.7
E13b4	8.7	0.4
E13b5	9.2-13.3	2.1
E13b6	13.3-21.5	3.3
E13b7	44.0-46.0	2.2

Fraction E13d (51.7 mg) was further fractionated by reversed-phase vacuum column chromatography, using H_2O with increasing amounts of MeOH as the mobile phase, to afford three fractions (Table 88).

Table 88. Experimental details for the separation of fraction E13d.

Fraction	**Mobile phase**		**Volume (mL)**
	H_2O %	**MeOH %**	
E13d1	40	60	20
E13d2	20	80	20
E13d3	-	100	20

Fraction E13d1 (11.0 mg) was subjected to reversed-phase HPLC to yield four fractions (Table 89), among which both fractions E13d1c and E13d1d were identified as metabolite **3**.

Table 89. Experimental details for the separation of fraction E13d1.

Chromatographic conditions	
Column	Kromasil 100 C_{18} (250 mm × 8 mm i.d.)
Mobile phase	MeOH /H_2O 60:40, 1.5 mL/min

Fraction	**Retention time (min)**	**Weight (mg)**
E13d1a	6.4-7.3	1.8
E13d1b	8.8-9.8	1.0
E13d1c	23.2	0.8
E13d1d	24.0	4.4

Fraction E13d2 (31.2 mg) was subjected to reversed-phase HPLC to yield three fractions (Table 90), among which fraction E13d2b was identified as metabolite **3**.

Table 90. Experimental details for the separation of fraction E13d2.

Chromatographic conditions	
Column	Kromasil 100 C_{18} (250 mm × 8 mm i.d.)
Mobile phase	MeOH /H_2O 80:20, 1.5 mL/min

Fraction	**Retention time (min)**	**Weight (mg)**
E13d2a	7.6	4.8

E13d2b	10.4	11.1
E13d2c	12.5	3.6

In total, 23 metabolites, which are summarized in Table 91, were isolated from the crude organic extract of the actinobacterial strain BI0048.

Table 91. Metabolites isolated in pure form from the organic extract of the strain BI0048.

Metabolite	Fractions	Weight (mg)
1	D1l2, D1l3, D1m3, D3b2, D5a3b, E5a5a, E5a5b	28.4
2	D1i2, D1j5, E4i1c	1.9
3	D1n2, D3d, D4f, E13b7, E13d1c, E13d1d, E13d2b	39.3
4	D1m5	1.3
5	E4e3c	1.2
6	E4d1a, E4e2	6.6
7	E4d3a	1.2
8	E4d2a	3.8
9	D1e4, D1f5	4.6
10	D1e2, D1f1, D1g4	5.1
11	D1g1	0.7
12	D1e3, D1f3, D3e	13.1
13	D1f4, D1g6, D4g1	26.4
14	D1i1, D1j4	1.3
15	D4b1	1.5
16	E4i1b	1.9
17	E4f1a3, E4i2a3b2	4.9
18	E4f1a2, E4i2a2, E4i2a3a	9.0
19	E4i2a3b3	2.6
20	D4d1	16.8
21	D4b2, D5a6b, D5a6c, E5a3c	35.5
22	D5a4a1	1.1
23	E4d1c, E4e3a	3.0

2.6. Assays for the evaluation of biological activity

2.6.1. Assay for the evaluation of cytotoxic activity

The cytotoxic activity was evaluated against the MCF7 (breast adenocarcinoma) and A549 (lung carcinoma) cancer cell lines as previously described (Mavrogonatou et al., 2010).

2.6.2. Assay for the evaluation of antibacterial activity

The antibacterial activity was evaluated against the epidemic methicillin-resistant *S. aureus* strain EMRSA-15, the *S. aureus* strain SA1199B that possesses the

gene encoding the NorA quinolone efflux protein and the *E. coli* strain NCTC-10418 as previously described (Dimou et al., 2016).

3. RESULTS AND DISCUSSION

3.1. Structure elucidation of the isolated metabolites

On the basis of preliminary screening of the chemical profiles of extracts obtained from small-scale liquid cultures of a number of marine-derived bacterial strains with HPLC, strain BI0048, isolated from the inner tissues of the red alga *Laurencia glandulifera*, was selected for further chemical investigation due to its interesting chemical profile (Fig. 15).

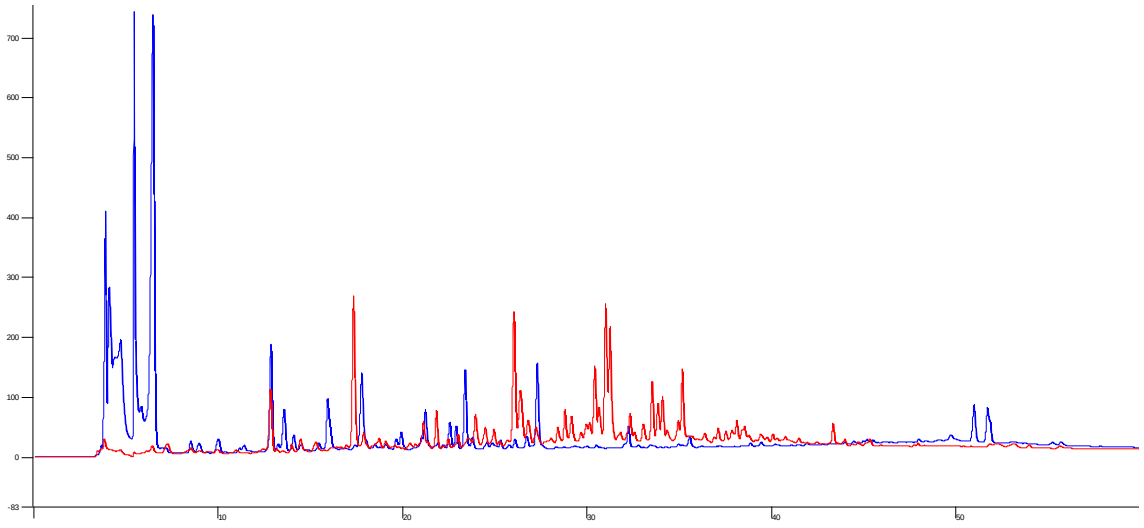

Figure 15. HPLC chromatogram (detection at 254 nm) of the organic extract of the small-scale liquid culture of strain BI0048 (red) and the organic extract of the cultivation medium (blue).

The algicolous endophytic strain, which was identified as *Streptomyces ambofaciens*, was cultured in large-scale in flasks containing a seawater-based liquid medium and the resulting organic residue derived from its extraction was subjected to repetitive chromatographic fractionations and HPLC purifications that led to the isolation of 23 metabolites (**1-23**). The structure elucidation of the isolated metabolites **1-23** was based on analysis of their spectroscopic data (NMR, MS, IR, UV) and comparison of their spectroscopic and physical characteristics with those reported in the literature.

3.1.1. Metabolite 1

Metabolite **1** was isolated after a series of chromatographic separations as a yellowish oil (28.4 mg).

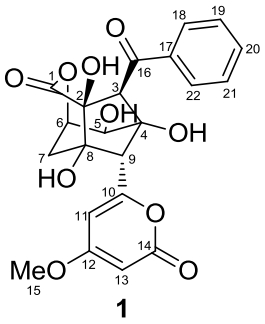

The mass spectrum of metabolite **1** (Fig. 16) exhibited a pseudomolecular ion peak $[M+H]^+$ at *m/z* 445.

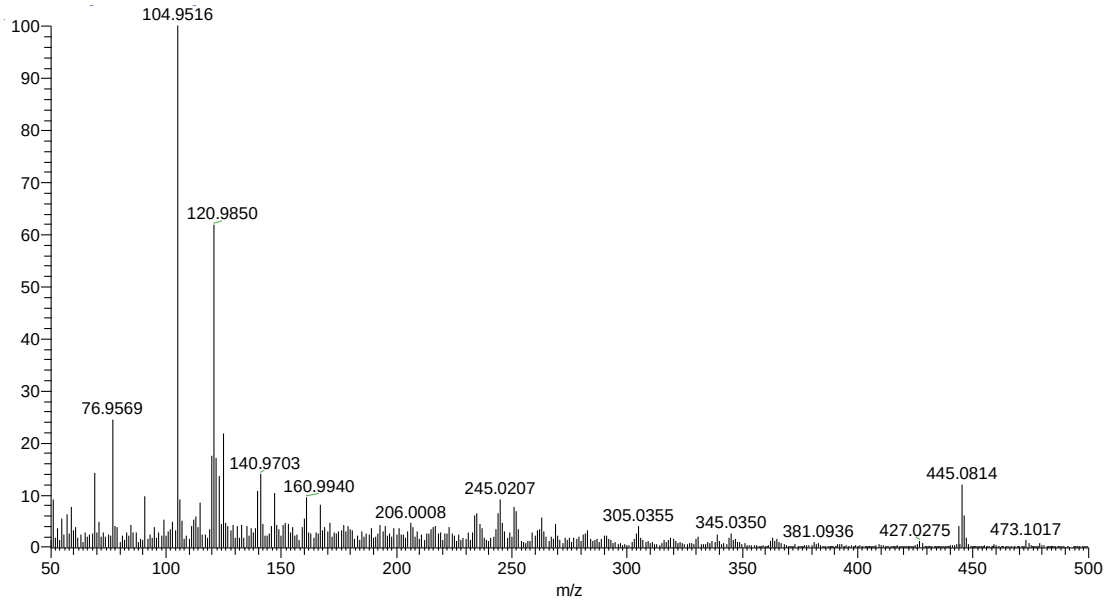

Figure 16. Mass spectrum (CIMS in positive mode) of metabolite **1**.

In the ^{13}C NMR spectrum of metabolite **1** (Fig. 17) 22 carbon signals were observed. Among them, evident were:

- one oxygenated methyl carbon at δ_C 56.1,
- two oxymethine carbons at δ_C 69.2 and 75.7,
- three oxygenated quaternary carbon signals at δ_C 76.0, 77.5 and 79.0,
- 10 carbon signals in the olefinic / aromatic region at δ_C 88.3-160.3, and

- three carbonyl carbons at δ_C 165.2, 173.6 and 197.6.

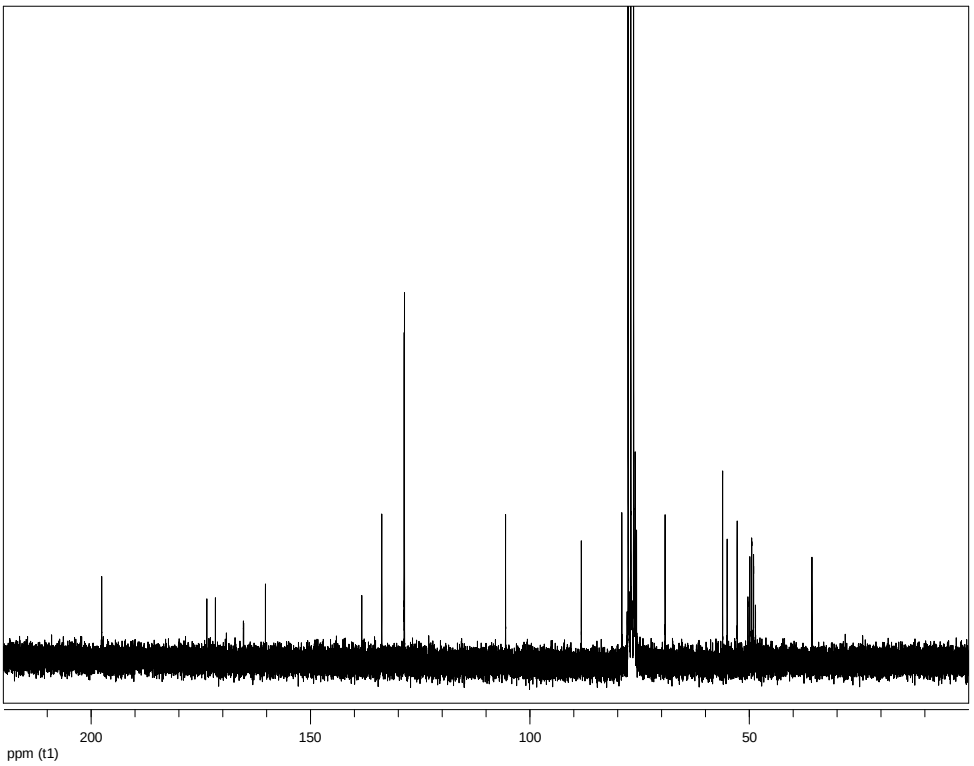

Figure 17. ^{13}C NMR spectrum of metabolite **1**.

In the ^{1}H NMR spectrum of metabolite **1** (Fig. 18) obvious were:

- one methoxy group at δ_H 3.80,
- two oxygenated methines at δ_H 4.57 and 4.79,
- two olefinic methines at δ_H 5.47 and 6.33 exhibiting a long-range coupling, and
- signals at δ_H 7.43-7.88 integrating for five protons in total with coupling constants characteristic for a mono-substituted aromatic ring.

Analysis of the NMR and MS data of **1** led to the molecular formula $C_{22}H_{20}O_{10}$. Taking into account the five carbon-carbon double bonds and the three carbonyl moieties as eight of the 13 degrees of unsaturation, the molecular structure of **1** was determined to contain five rings.

The planar structure of metabolite **1** was determined on the basis of the homonuclear and heteronuclear correlations observed in the HSQC-DEPT (Fig. 19), HMBC (Fig. 20) and COSY (Fig. 21) spectra.

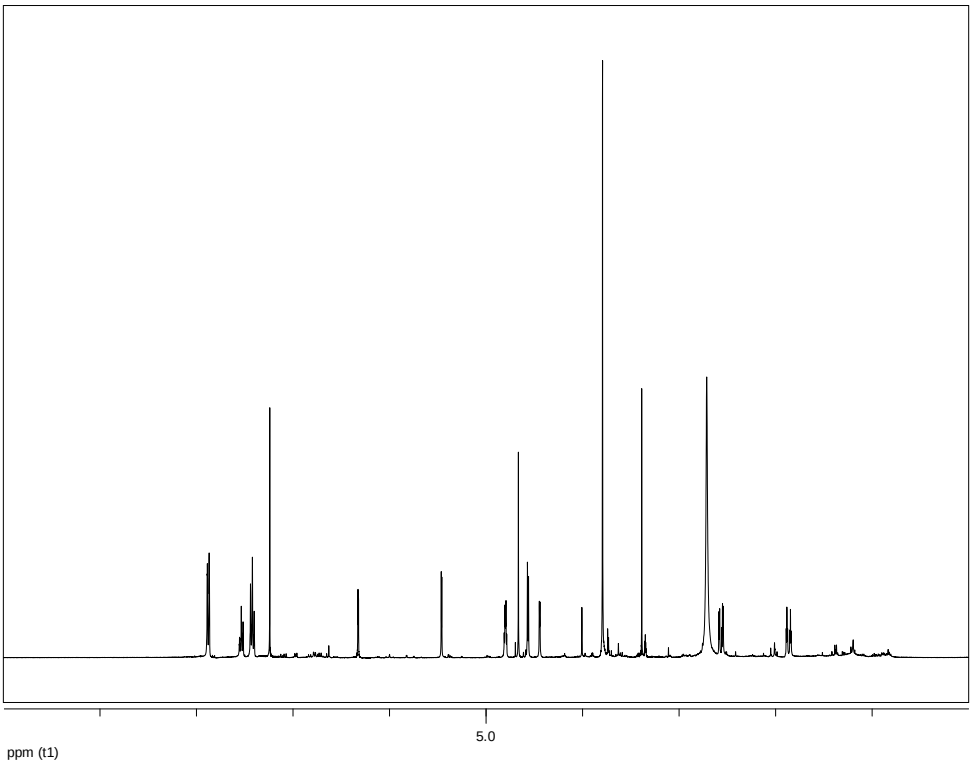

Figure 18. ^{1}H NMR spectrum of metabolite **1**.

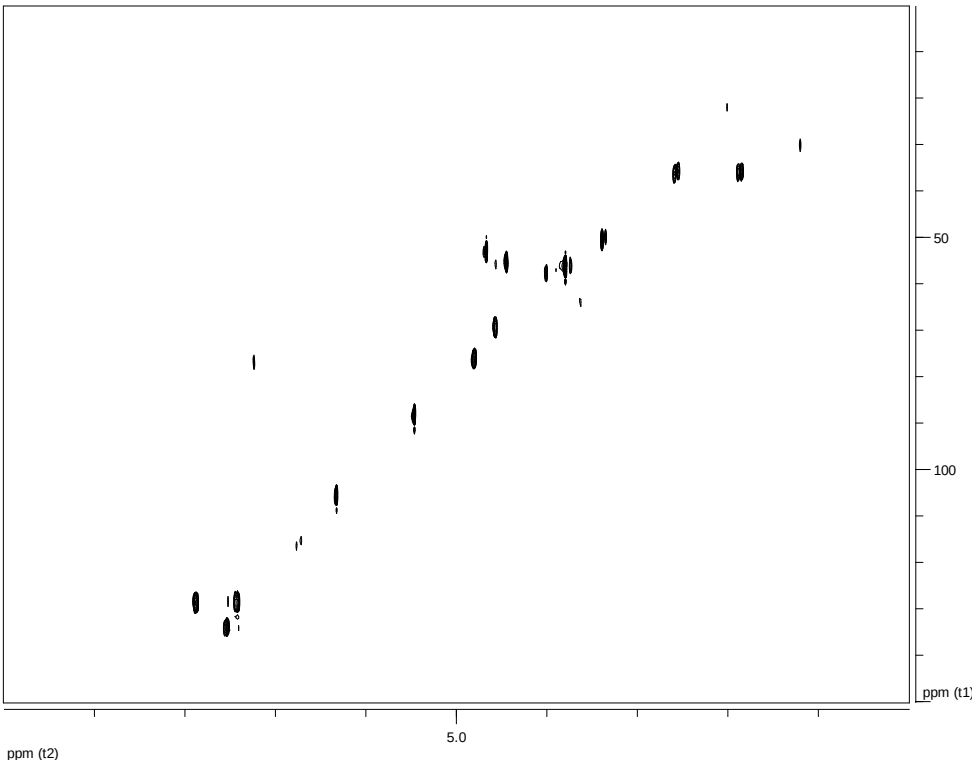

Figure 19. HSQC-DEPT spectrum of metabolite **1**.

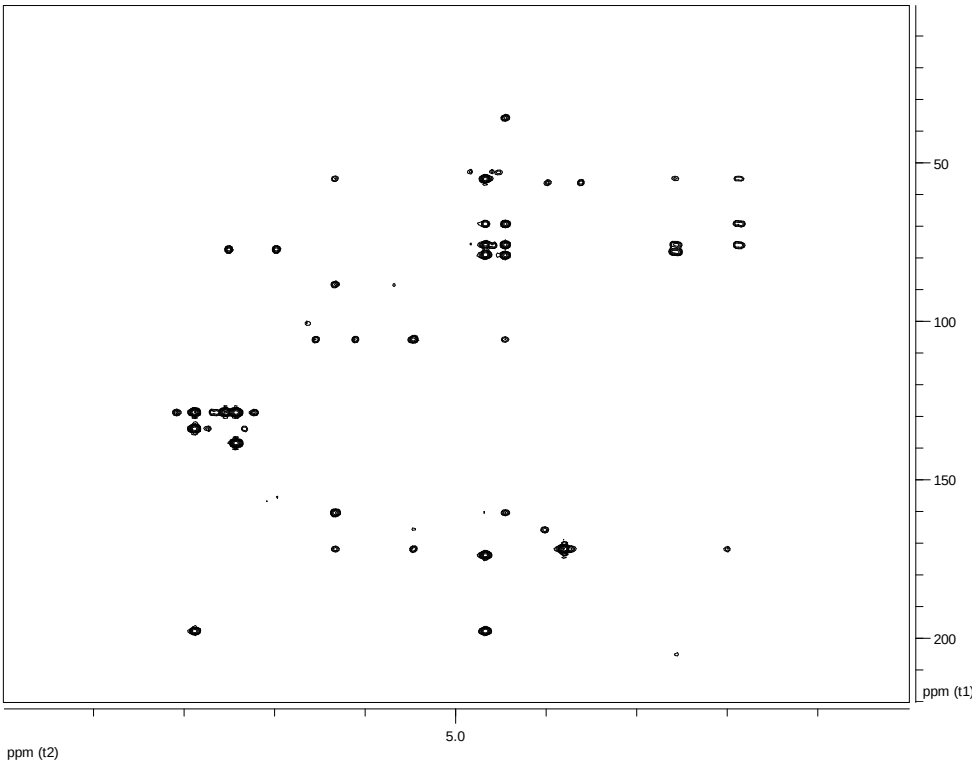

Figure 20. HMBC spectrum of metabolite **1**.

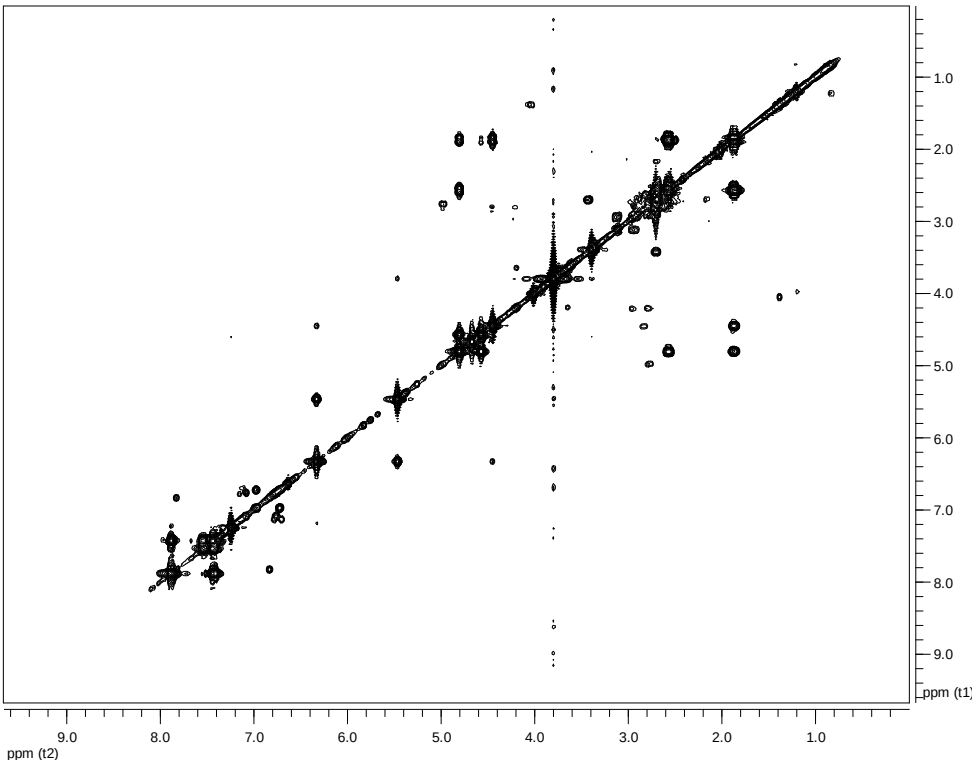

Figure 21. COSY spectrum of metabolite **1**.

Comparison of the spectroscopic and physical characteristics of metabolite **1** with those reported in the literature led to its identification as enterocin, also known as vulgamycin, previously isolated from several strains of *Streptomyces*, both of terrestrial and marine origin (Miyairi et al., 1976; Seto et al., 1976; Sitachitta et al., 1996). The ^{1}H and ^{13}C NMR data of metabolite **1** are reported in Table 92.

Table 92. ^{1}H and ^{13}C NMR data of metabolite **1** in $CDCl_3/CD_3OD$ (δ in ppm, J in Hz).

Position	δ_C	δ_H
1	173.6	
2	77.5	
3	52.8	4.67, brs
4	79.0	
5	69.2	4.57, d (4.4)
6	75.7	4.79, ddd (4.4, 2.9, 2.9)
7	35.7	2.56, dd (14.7, 2.9), 1.86, ddd (14.7, 2.9, 2.7)
8	76.0	
9	55.0	4.44, d (2.7)
10	160.3	
11	105.5	6.33, d (2.0)
12	171.7	
13	88.3	5.47, d (2.0)
14	165.2	
15	56.1	3.80, s
16	197.6	
17	138.3	
18	128.9	7.88, dd (8.3, 1.0)
19	128.6	7.43, dd (8.3, 7.3)
20	134.1	7.54, dd (7.3, 7.3)
21	128.6	7.43, dd (8.3, 7.3)
22	128.9	7.88, dd (8.3, 1.0)

In 1976, when initially isolated and characterized, enterocin (**1**) was reported to be bacteriostatic in a disk-diffusion assay at a concentration of 4 mg/mL against Gram-positive and Gram-negative bacteria, including strains of *Escherichia coli*, *Proteus vulgaris*, *Sarcina lutea*, *Staphylococcus aureus* and *Corynebacterium xerosis*, but showed no activity against strains of *Bacillus subtilis*, *Bacillus megaterium*, *Pseudomonas aeruginosa*, *Candida albicans* and *Penicillium chrysogenum* (Miyairi et al., 1976). In a subsequent study, enterocin (**1**) did not exhibit any activity against strains of *S. aureus*, *B. subtilis*, *P. aeruginosa*, *Salmonella typhimurium*, *E. coli*, *Saccharomyces cerevisiae*, *C. albicans*, *P. chrysogenum* and *Trichophyton mentagrophytes* and displayed weak activity only against a strain of *Micrococcus luteus*

(Kawashima et al., 1985). In addition, enterocin (**1**) exhibited herbicidal activity when applied post-emergence, controlling dicotyledonous weeds and grasses at dosages between 125 and 500 g ha^{-1}, being safe for application on cotton, maize and barley (Babczinski et al., 1991).

3.1.2. Metabolite 2

Metabolite **2** was isolated after a series of chromatographic separations as a colourless oil (1.9 mg).

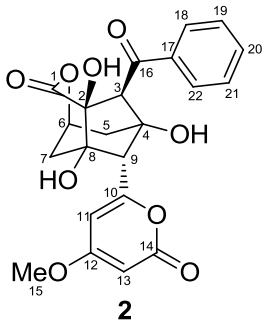

2

The mass spectrum of metabolite **2** (Fig. 22) exhibited a molecular ion peak $[M]^+$ at *m/z* 428.

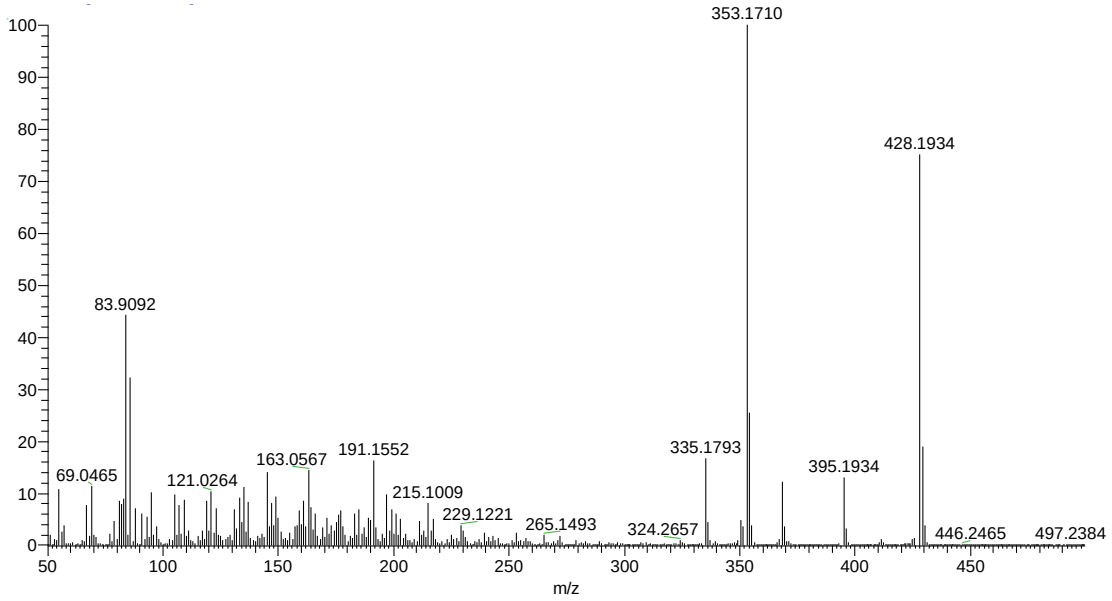

Figure 22. Mass spectrum (EIMS) of metabolite **2**.

In the ^{1}H NMR spectrum of metabolite **2** (Fig. 23) obvious were:

- one methoxy group at δ_H 3.84,
- one oxygenated methine at δ_H 4.99,
- two olefinic methines at δ_H 5.49 and 6.31 exhibiting a long-range coupling, and
- signals at δ_H 7.16-7.87 integrating for five protons in total with coupling constants characteristic for a mono-substituted aromatic ring.

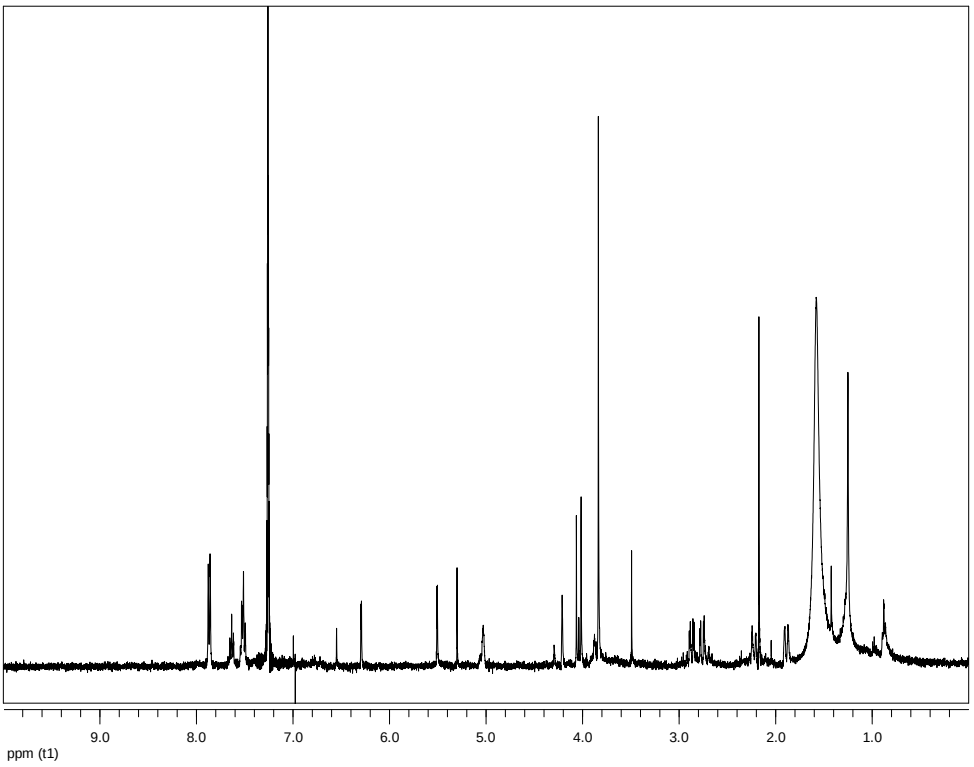

Figure 23. ^{1}H NMR spectrum of metabolite **2**.

Analysis of the NMR and MS data of **2** led to the molecular formula $C_{22}H_{20}O_9$. The ^{1}H NMR spectroscopic data of metabolite **2** closely resembled those of enterocin (**1**), with the most prominent difference between **1** and **2** being the absence of the second oxymethine which in the case of **2** is replaced by an aliphatic methylene resonating at δ_H 2.19 and 2.86. In agreement with the molecular formula, it was evident that metabolite **2** was a deoxy analogue of enterocin (**1**).

Comparison of the spectroscopic and physical characteristics of metabolite **2** with those reported in the literature led to its identification as 5-deoxy-enterocin, which was reported to inhibit strains of *S. lutea*, *S. aureus*, *Klebsiella pneumoniae* and *Vibrio percolans* at a concentration of 0.5 mg/mL (Sitachitta et al., 1996). The ^{1}H NMR data of metabolite **2** are reported in Table 93.

Table 93. ^{1}H NMR data of metabolite **2** in $CDCl_3$ (δ in ppm, J in Hz).

Position	δ_H
3	4.01 s
5	2.86 dd (15.5, 4.4), 2.19 dd (15.5, 1.9)
6	4.99 m
7	2.73 dd (14.7, 2.9), 1.86 dd (14.7, 2.4)
9	4.24 brs
11	6.31 d (1.9)
13	5.49 d (1.9)
15	3.84 s
18	7.87 d (7.5)
19	7.16 t (7.5)
20	7.49 t (7.5)
21	7.16 t (7.5)
22	7.87 d (7.5)

3.1.3. Metabolite 3

Metabolite **3** was isolated after a series of chromatographic separations as a yellowish oil (39.3 mg).

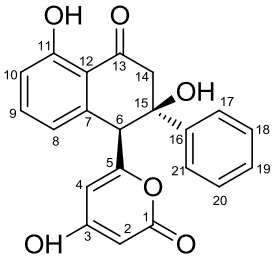

3

The mass spectrum of metabolite **3** (Fig. 24) exhibited a pseudomolecular ion peak $[M+H]^+$ at *m/z* 365, as well as fragment ion peak at *m/z* 346 corresponding to $[M-H_2O]^+$.

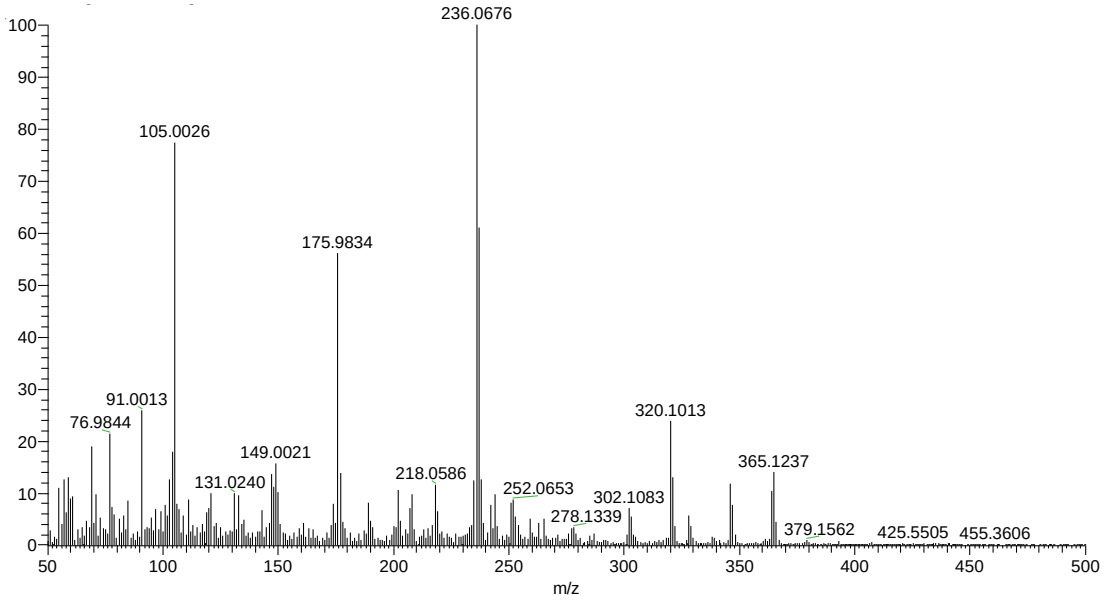

Figure 24. Mass spectrum (CIMS in positive mode) of metabolite **3**.

In the ^{13}C NMR spectrum of metabolite **3** (Fig. 25) 20 carbon signals were observed. Among them, evident were:

- one aliphatic methylene at δ_C 51.8 and one aliphatic methine at δ_C 56.5,
- one oxygenated quaternary carbon signal at δ_C 76.8,
- 15 carbon signals in the olefinic / aromatic region at δ_C 106.2-172.7, and
- two carbonyl carbons at δ_C 167.7 and 204.4.

In the ^{1}H NMR spectrum of metabolite **3** (Fig. 26) obvious were:

- one isolated aliphatic methylene at δ_H 3.20 and 3.55 and one isolated aliphatic methine at δ_H 4.74,
- one olefinic methine at δ_H 6.20,
- three signals at δ_H 6.64, 6.88 and 7.45 with coupling constants characteristic for a 1,2,3-tri-substituted aromatic ring, and
- signals at δ_H 7.26-7.52 integrating for five protons in total with coupling constants characteristic for a mono-substituted aromatic ring.

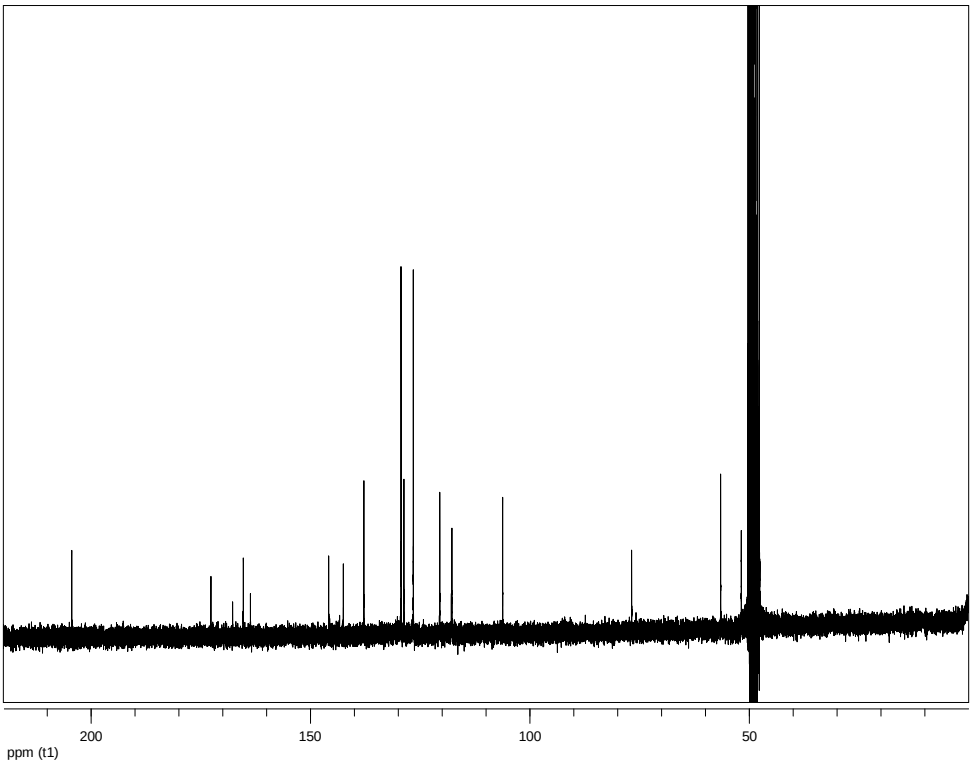

Figure 25. ^{13}C NMR spectrum of metabolite **3**.

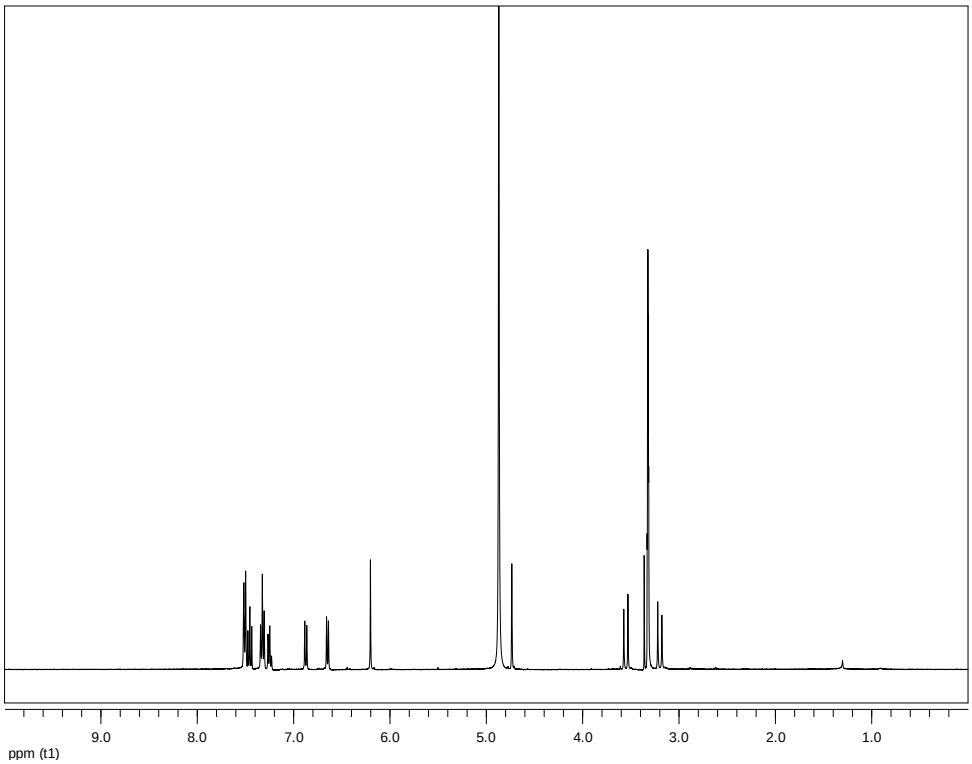

Figure 26. ^{1}H NMR spectrum of metabolite **3**.

Analysis of the NMR and MS data of **3** led to the molecular formula $C_{21}H_{16}O_6$. Taking into account the eight carbon-carbon double bonds and the two carbonyl moieties as 10 of the 14 degrees of unsaturation, the molecular structure of **3** was determined to contain four rings.

The planar structure of metabolite **3** was determined on the basis of the homonuclear and heteronuclear correlations observed in the HSQC-DEPT (Fig. 27), HMBC (Fig. 28) and COSY (Fig. 29) spectra.

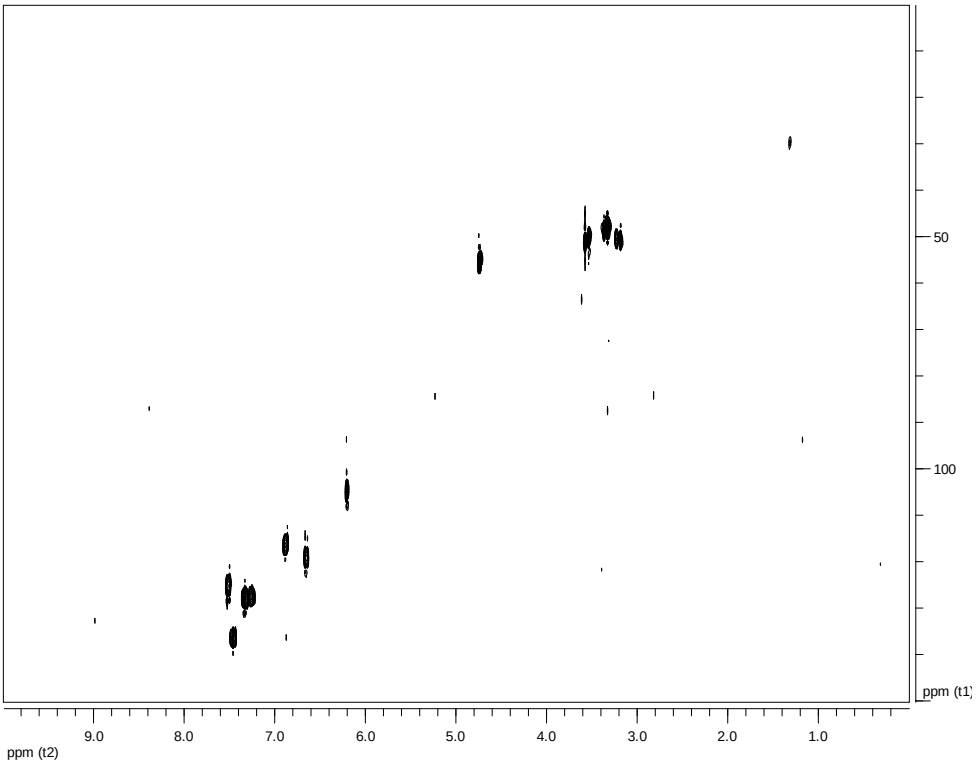

Figure 27. HSQC-DEPT spectrum of metabolite **3**.

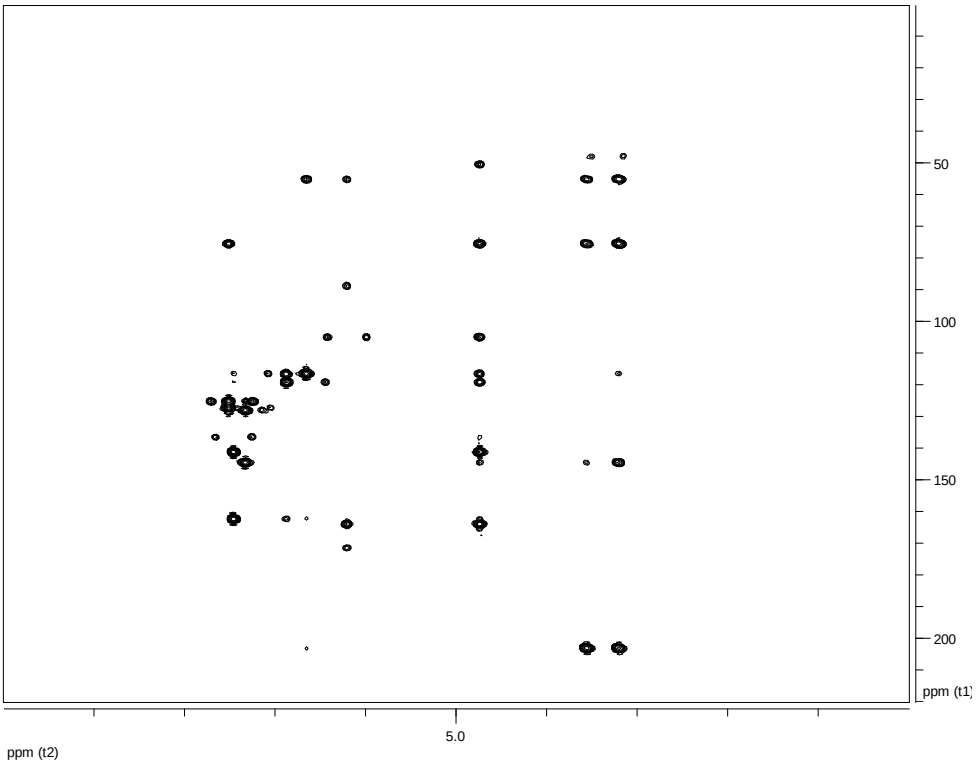

Figure 28. HMBC spectrum of metabolite **3**.

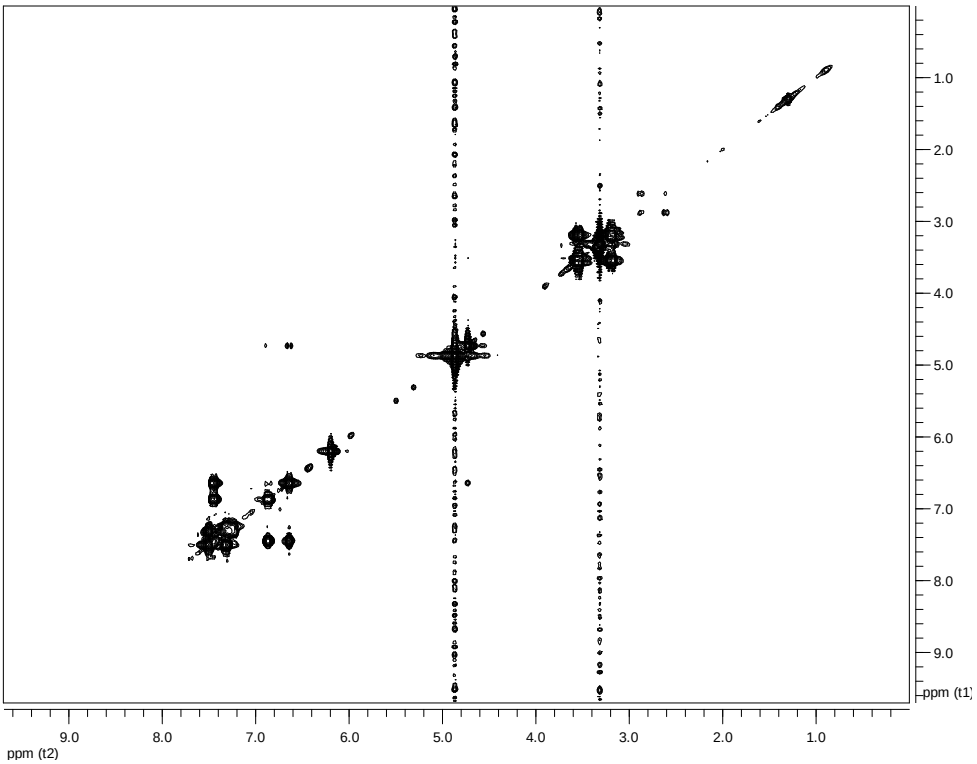

Figure 29. COSY spectrum of metabolite **3**.

Comparison of the spectroscopic and physical characteristics of metabolite **3** with those reported in the literature led to its identification as wailupemycin D (Piel et

al., 2000). The ^{1}H and ^{13}C NMR data of metabolite **3** are reported in Table 94.

It is worth noting that when the ^{1}H NMR spectrum of **3** was measured in CD_3OD, H-2 was not observed (Djinni et al., 2013). Nonetheless, when the ^{1}H NMR spectrum was measured in $(CD_3)_2SO$ it was evident, resonating at δ_H 5.01 (brs).

Table 94. ^{1}H and ^{13}C NMR data of metabolite **3** in CD_3OD (δ in ppm, J in Hz).

Position	δ_C	δ_H
1	167.7	
2	n.d.	n.d.
3	172.7	
4	106.2	6.20, s
5	165.3	
6	56.5	4.74, s
7	142.5	
8	120.5	6.64, d (8.0)
9	137.8	7.45, dd (8.0, 8.0)
10	117.8	6.88, d (8.0)
11	163.7	
12	117.9	
13	204.4	
14	51.8	3.55, d (17.2), 3.20, d (17.2)
15	76.8	
16	145.9	
17	126.6	7.52, dd (7.3, 1.6)
18	129.4	7.32, dd (7.3, 7.3)
19	128.7	7.26, dd (7.3, 7.3)
20	129.4	7.32, dd (7.3, 7.3)
21	126.6	7.52, dd (7.3, 1.6)

n.d.: not detected

3.1.4. Metabolite 4

Metabolite **4** was isolated after a series of chromatographic separations as a colourless oil (1.3 mg).

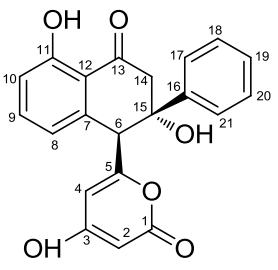

4

The mass spectrum of metabolite **4** (Fig. 30) exhibited a pseudomolecular ion peak $[M+H]^+$ at *m/z* 365, as well as fragment ion peak at *m/z* 346 corresponding to $[M-H_2O]^+$.

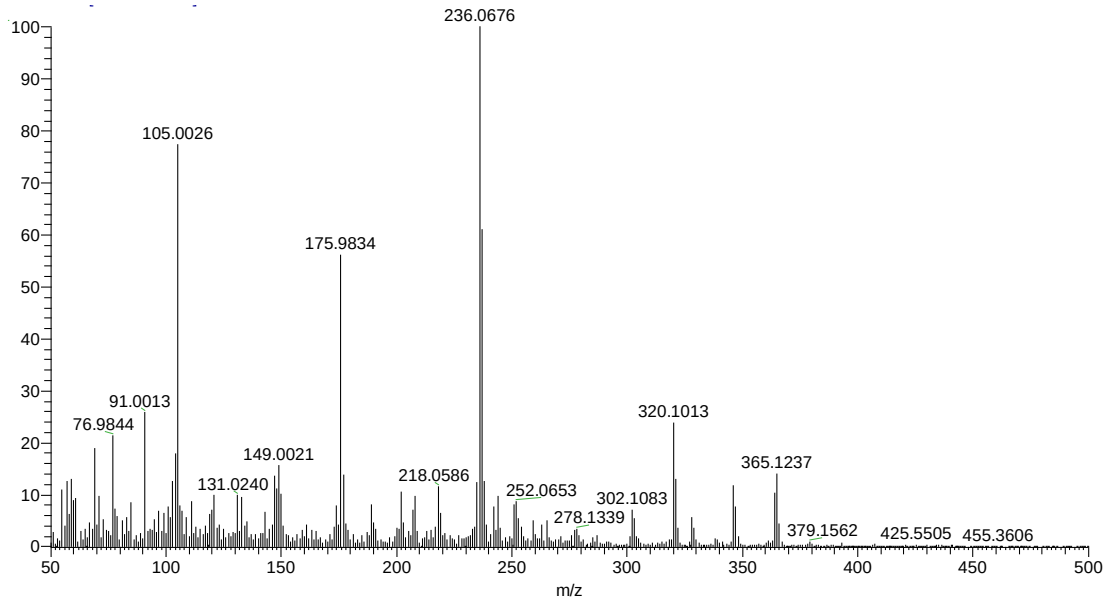

Figure 30. Mass spectrum (CIMS in positive mode) of metabolite **4**.

In the ^{13}C NMR spectrum of metabolite **4** (Fig. 31) 20 carbon signals were observed. Among them, evident were:

- one aliphatic methylene at δ_C 47.2 and one aliphatic methine at δ_C 57.9,
- one oxygenated quaternary carbon signal at δ_C 76.5,
- 15 carbon signals in the olefinic / aromatic region at δ_C 105.1-173.4, and
- two carbonyl carbons at δ_C 168.1 and 205.1.

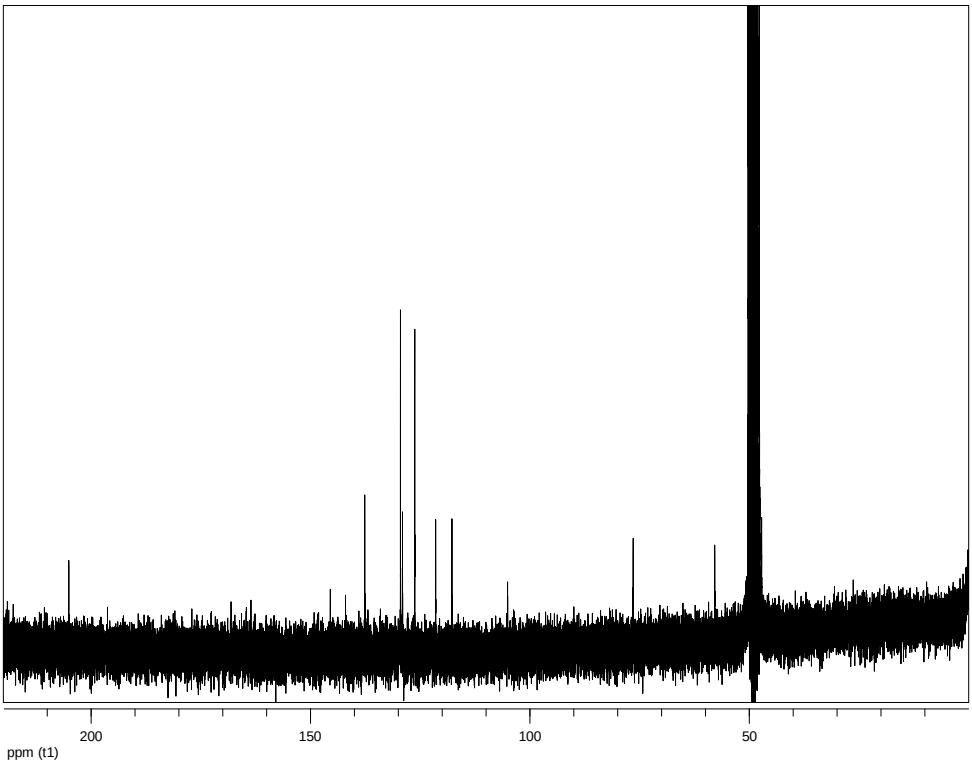

Figure 31. ^{13}C NMR spectrum of metabolite **4**.

In the ^{1}H NMR spectrum of metabolite **4** (Fig. 32) obvious were:

- one isolated aliphatic methylene at δ_H 2.96 and 4.12 and one isolated aliphatic methine at δ_H 4.26,
- one olefinic methine at δ_H 5.65,
- three signals at δ_H 6.81, 6.86 and 7.46 with coupling constants characteristic for a 1,2,3-tri-substituted aromatic ring, and
- signals at δ_H 7.26-7.42 integrating for five protons in total with coupling constants characteristic for a mono-substituted aromatic ring.

Analysis of the NMR and MS data of **4** led to the molecular formula $C_{21}H_{16}O_6$. The ^{1}H NMR spectroscopic data of metabolite **4** closely resembled those of wailupemycin D (**3**). In agreement with the molecular formula, it was evident that metabolite **4** was a stereoisomer of wailupemycin D (**3**), as also verified from the homonuclear and heteronuclear correlations observed in the HSQC-DEPT (Fig. 33), HMBC (Fig. 34) and COSY (Fig. 35) spectra.

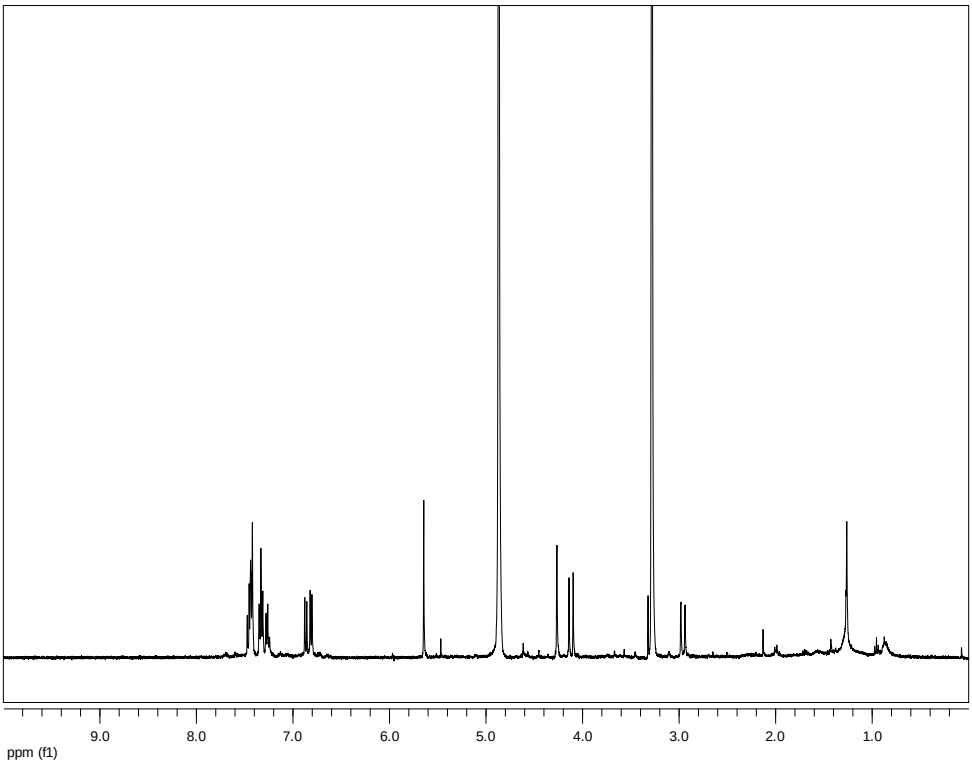

Figure 32. ^{1}H NMR spectrum of metabolite **4**.

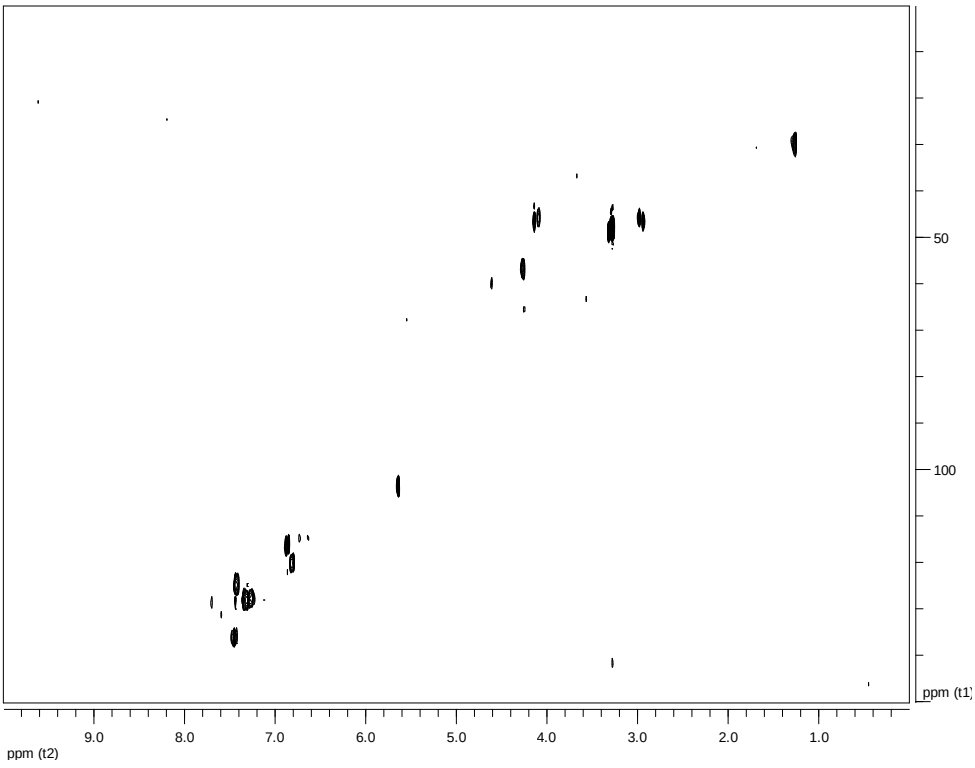

Figure 33. HSQC-DEPT spectrum of metabolite **4**.

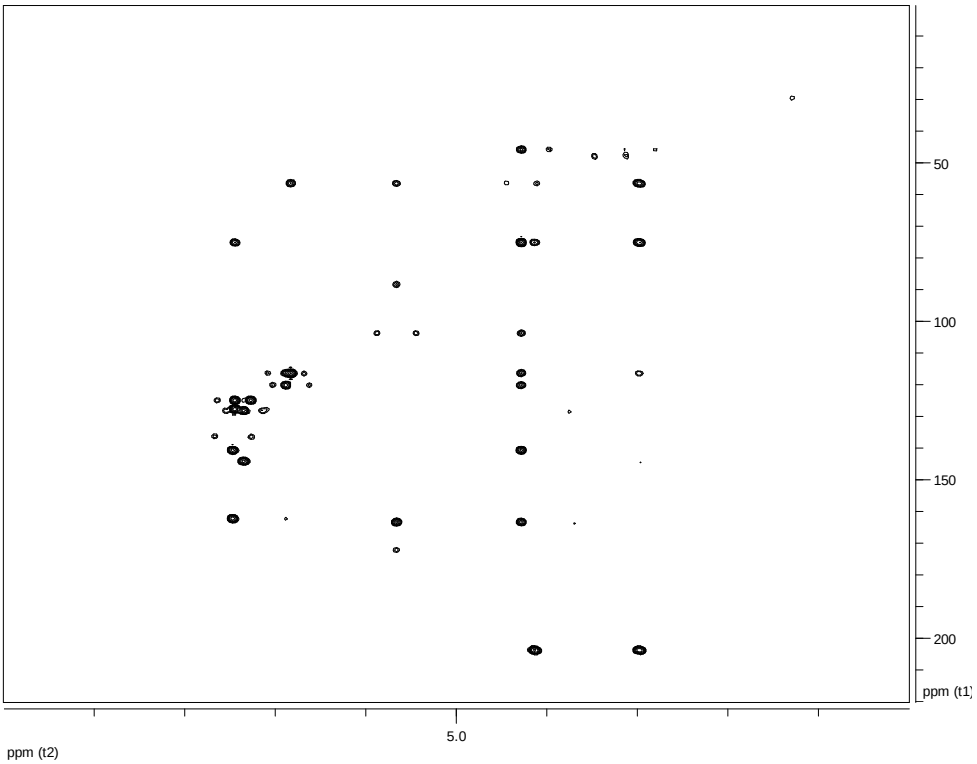

Figure 34. HMBC spectrum of metabolite **4**.

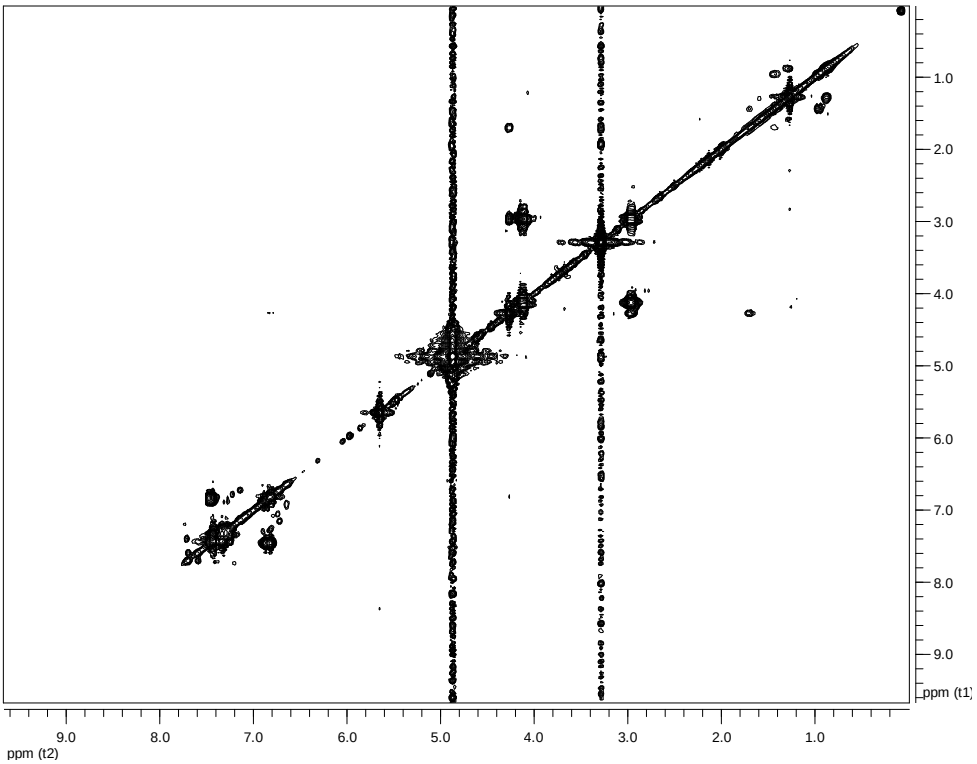

Figure 35. COSY spectrum of metabolite **4**.

Comparison of the spectroscopic and physical characteristics of metabolite **4** with those reported in the literature led to its identification as wailupemycin E (Xiang et

al., 2002). The ^{1}H and ^{13}C NMR data of metabolite **4** are reported in Table 95.

It is worth noting that, as in the case of **3**, when the ^{1}H NMR spectrum of **4** was measured in CD_3OD, H-2 was not observed (Djinni et al., 2013). Nonetheless, when the ^{1}H NMR spectrum was measured in $(CD_3)_2SO$ it was evident, resonating at δ_H 4.98 (brs).

Table 95. ^{1}H and ^{13}C NMR data of metabolite **4** in CD_3OD (δ in ppm, J in Hz).

Position	$\boldsymbol{\delta_C}$	$\boldsymbol{\delta_H}$
1	168.1	
2	n.d.	n.d.
3	173.4	
4	105.1	5.65 s
5	164.0	
6	57.9	4.26 s
7	142.0	
8	121.5	6.81 d (8.0)
9	137.6	7.46 dd (8.0, 8.0)
10	117.8	6.86 d (8.0)
11	163.6	
12	117.9	
13	205.1	
14	47.2	4.12 d (17.2), 2.96 d (17.2)
15	76.5	
16	145.5	
17	126.2	7.42 dd (7.3, 1.6)
18	129.5	7.34 dd (7.3, 7.3)
19	129.0	7.26 dd (7.3, 7.3)
20	129.5	7.34 dd (7.3, 7.3)
21	126.2	7.42 dd (7.3, 1.6)

n.d.: not detected

3.1.5. Metabolite 5

Metabolite **5** was isolated after a series of chromatographic separations as a colourless oil (1.2 mg).

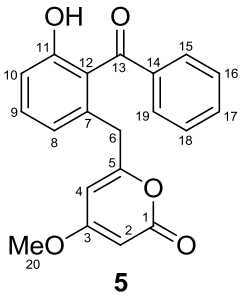

5

The mass spectrum of metabolite **5** (Fig. 36) exhibited a molecular ion peak $[M]^+$ at *m/z* 336. Furthermore, in the HRESIMS it displayed an ion peak at *m/z* 335.0928, corresponding to $C_{20}H_{15}O_5$ and consistent with $[M - H]^-$.

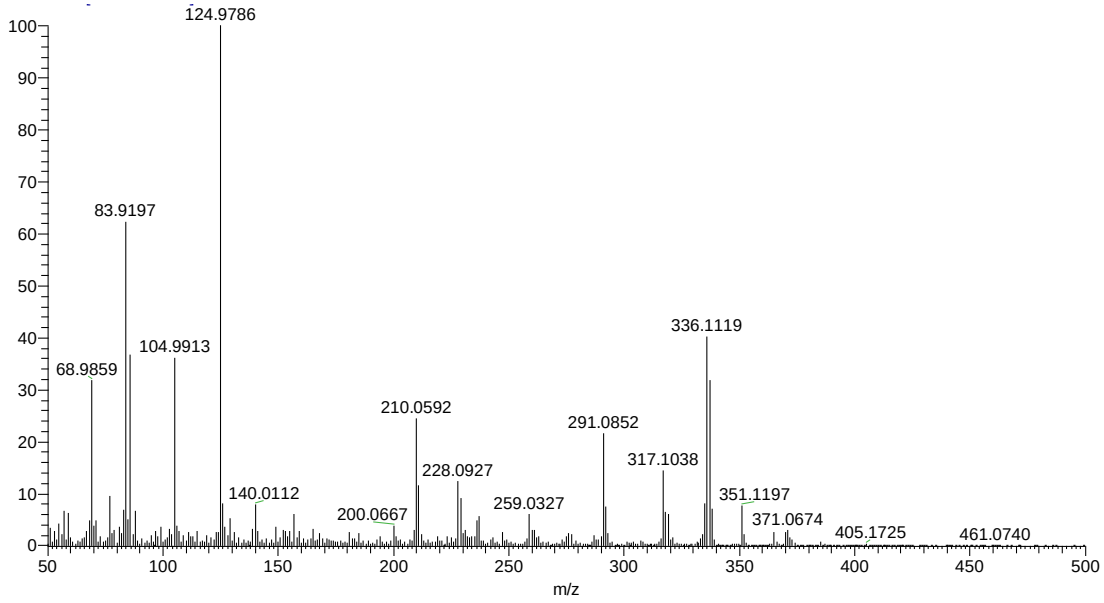

Figure 36. Mass spectrum (EIMS) of metabolite **5**.

The ^{13}C NMR spectrum of metabolite **5** (Fig. 37) revealed 20 carbon signals, which corresponded to eight non-protonated carbon atoms, among which two carbonyls at δ_C 165.2 and 199.2, ten methines, one methylene and one methyl, as determined from the HSQC-DEPT experiment.

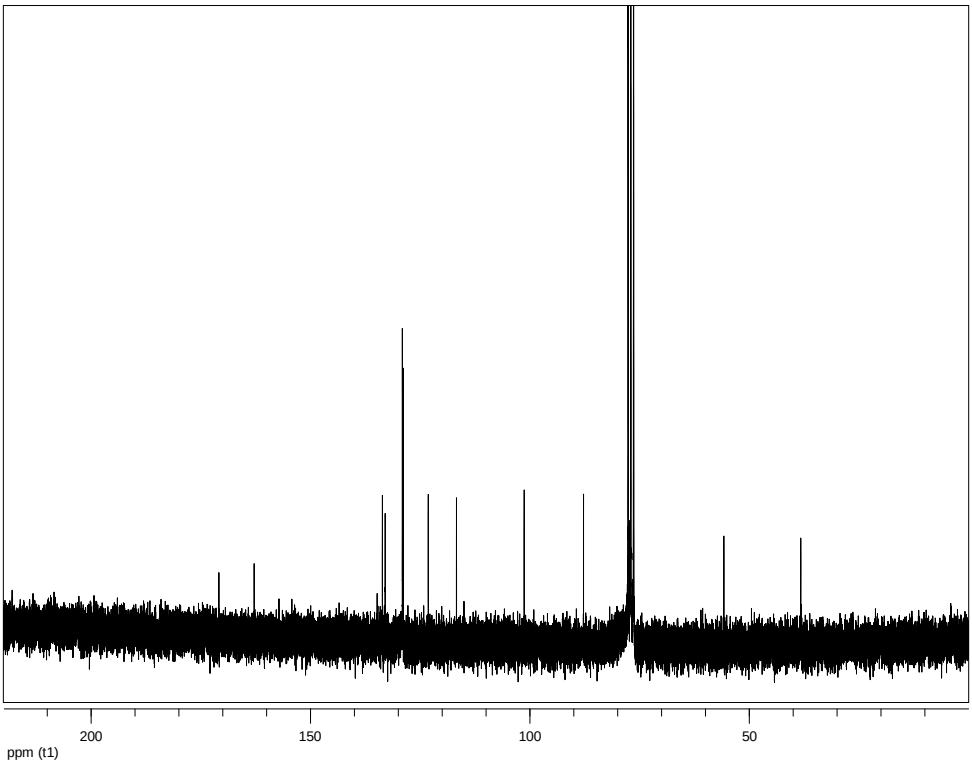

Figure 37. ^{13}C NMR spectrum of metabolite **5**.

The ^{1}H NMR spectrum of metabolite **5** (Fig. 38) included signals at δ_H 6.87 (1H, d, 7.5 Hz), 7.36 (1H, dd, 8.2, 7.5 Hz) and 6.95 (1H, d, 8.2 Hz) indicative of a 1,2,3-trisubstituted aromatic ring, as well as at δ_H 7.67 (2H, d, 8.3 Hz), 7.43 (2H, dd, 8.3, 7.4 Hz) and 7.57 (1H, t, 7.4 Hz) pointing to the presence of a monosubstituted aromatic ring. Furthermore, the ^{1}H NMR spectrum of **5** exhibited signals for a deshielded methylene at δ_H 3.52, a methoxy group at δ_H 3.69, and two methines at δ_H 5.27 and 5.43. In agreement with the literature (Seto et al., 1976; Sitachitta et al., 1996; Cutignano et al., 2003), the latter three signals, in conjunction with the ^{13}C NMR resonances of C-1 (δ_C 165.2), C-2 (δ_C 87.8), C-3 (δ_C 170.9), C-4 (δ_C 101.3) and C-5 (δ_C 162.8), were characteristic for a 4,6-disubstituted 4-methoxy-α-pyrone ring, present also in the co-occurring enterocin (**1**) and 5-deoxy-enterocin (**2**).

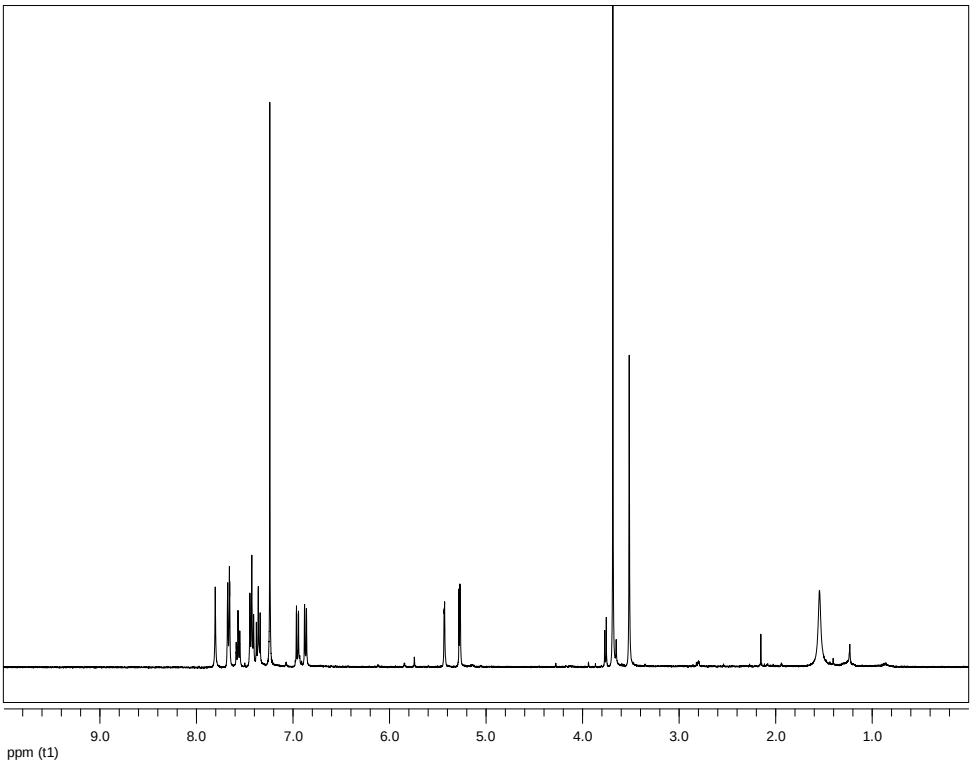

Figure 38. ^{1}H NMR spectrum of metabolite **5**.

The absorption band at 1687 cm^{-1} and the maximum absorbance at 282 nm observed in the IR and UV spectra of **5**, respectively, further supported the presence of the α-pyrone ring in the molecule.

The structure of metabolite **5** was determined on the basis of the homonuclear and heteronuclear correlations (Fig. 39) observed in the HSQC-DEPT (Fig. 40), HMBC (Fig. 41) and COSY (Fig. 42) spectra. In particular, the HMBC correlations of H_2-6 to C-4, C-5, C-7, C-8 and C-12 suggested the linkage of the α-pyrone ring to the 1,2,3-trisubstituted aromatic ring through C-6, while the monosubstituted aromatic ring was linked to the latter through C-13. This hypothesis was further supported by the fragment ions at *m*/*z* 105 and 259 observed in the EIMS of **5**, corresponding to the phenylketone moiety ($[C_7H_5O]^+$) and $[C_{14}H_{11}O_5]^+$ resulting from the cleavage of the phenyl group.

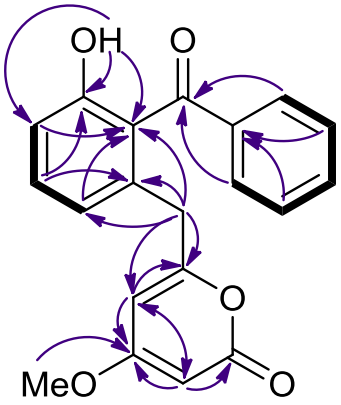

Figure 39. COSY (bold bonds) and important HMBC (arrows) correlations observed for metabolite **5**.

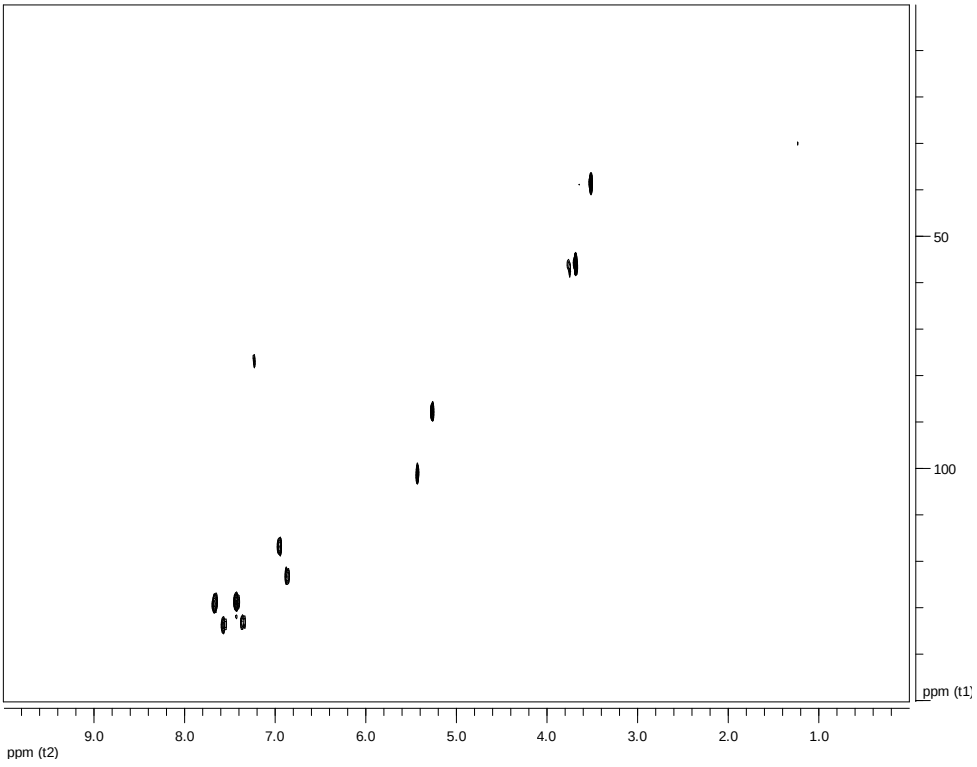

Figure 40. HSQC-DEPT spectrum of metabolite **5**.

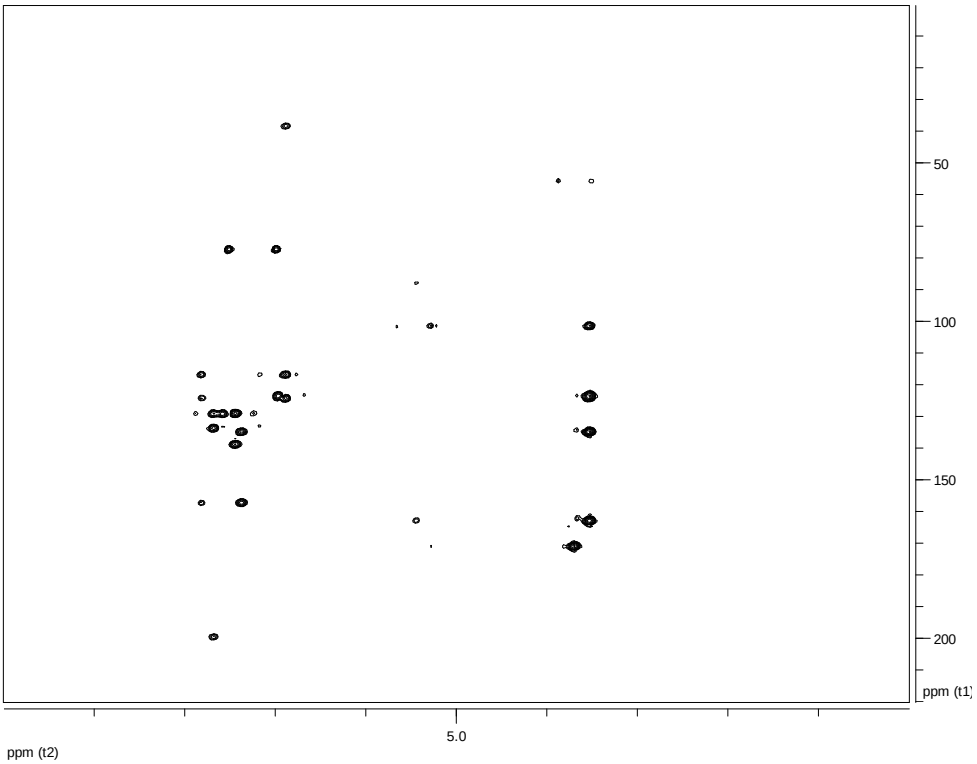

Figure 41. HMBC spectrum of metabolite **5**.

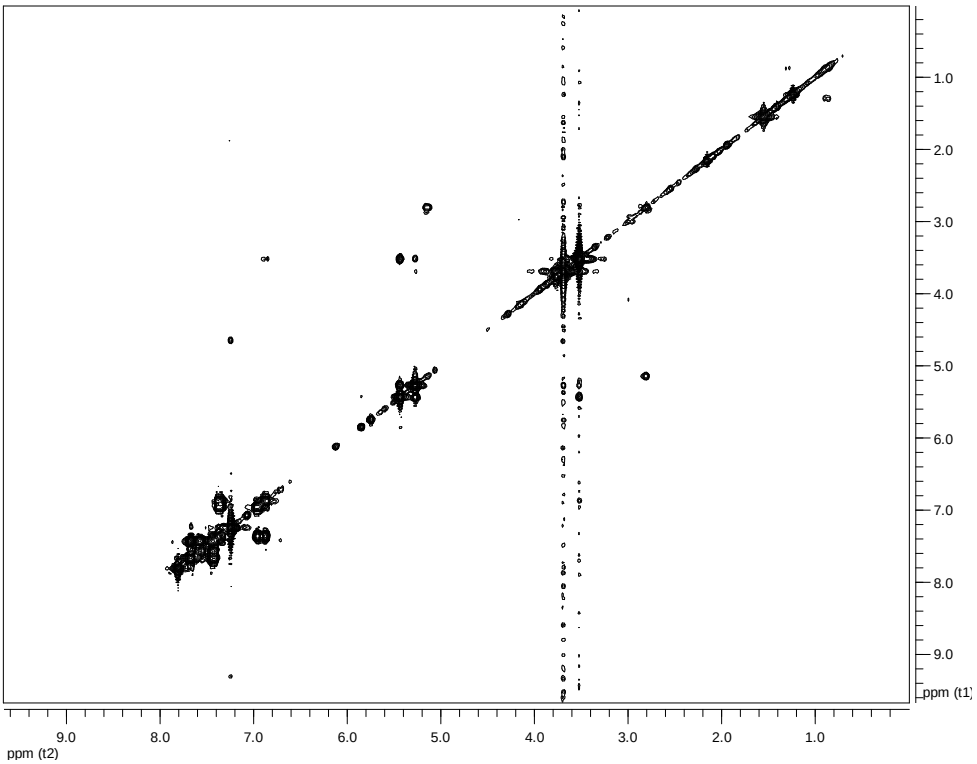

Figure 42. COSY spectrum of metabolite **5**.

Comparison of the spectroscopic and physical characteristics of metabolite **5** with those reported in the literature led to its identification as a new natural product,

which was designated as zoumbericin A (**5**) (Rab et al., 2017). The ^{1}H and ^{13}C NMR data of metabolite **5** are reported in Table 96.

Table 96. ^{1}H and ^{13}C NMR data of metabolite **5** in $CDCl_3$ (δ in ppm, J in Hz).

Position	δ_C	δ_H
1	165.2	
2	87.8	5.27, d (2.2)
3	170.9	
4	101.3	5.43, d (2.2)
5	162.8	
6	38.3	3.52, s
7	134.4	
8	123.2	6.87, d (7.5)
9	133.0	7.36, dd (8.2, 7.5)
10	116.7	6.95, d (8.2)
11	157.0	
12	123.7	
13	199.2	
14	138.2	
15	129.1	7.67, d (8.3)
16	128.9	7.43, dd (8.3, 7.4)
17	133.6	7.57, t (7.4)
18	128.9	7.43, dd (8.3, 7.4)
19	129.1	7.67, d (8.3)
20	55.8	3.69, s
OH		7.80, brs

3.1.6. Metabolite 6

Metabolite **6** was isolated after a series of chromatographic separations as a colourless oil (6.6 mg).

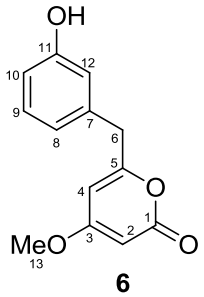

6

The mass spectrum of metabolite **6** (Fig. 43) exhibited a pseudomolecular ion peak $[M+H]^+$ at *m/z* 233. Furthermore, in the HRESIMS it displayed an ion peak at *m/z*

231.0660, corresponding to $C_{13}H_{11}O_4$ and consistent with $[M - H]^-$.

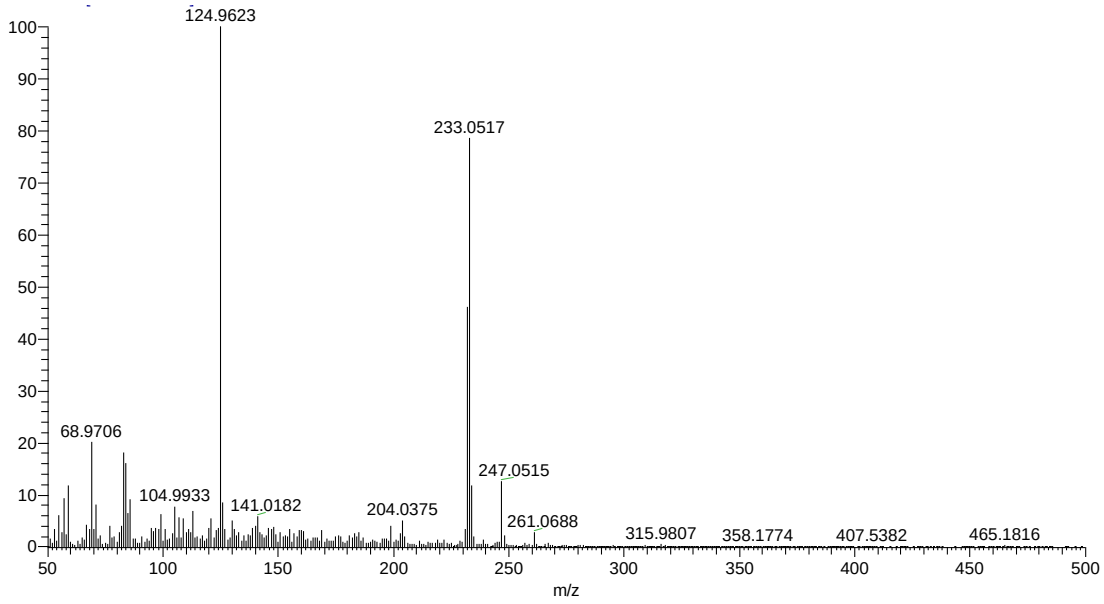

Figure 43. Mass spectrum (CIMS in positive mode) of metabolite **6**.

The spectroscopic characteristics of **6** were similar to those of metabolite **5**. Specifically, as in the case of **5**, the ^{1}H and ^{13}C NMR spectroscopic data of compound **6** (Fig. 44 and Fig. 45) included signals for a 4,6-disubstituted 4-methoxy-α-pyrone moiety and a deshielded methylene resonating at δ_H 3.67 as a singlet. However, in contrast to **5**, the only other signals present in the NMR spectra of **6** were those attributed to a 1,3-disubstituted aromatic ring.

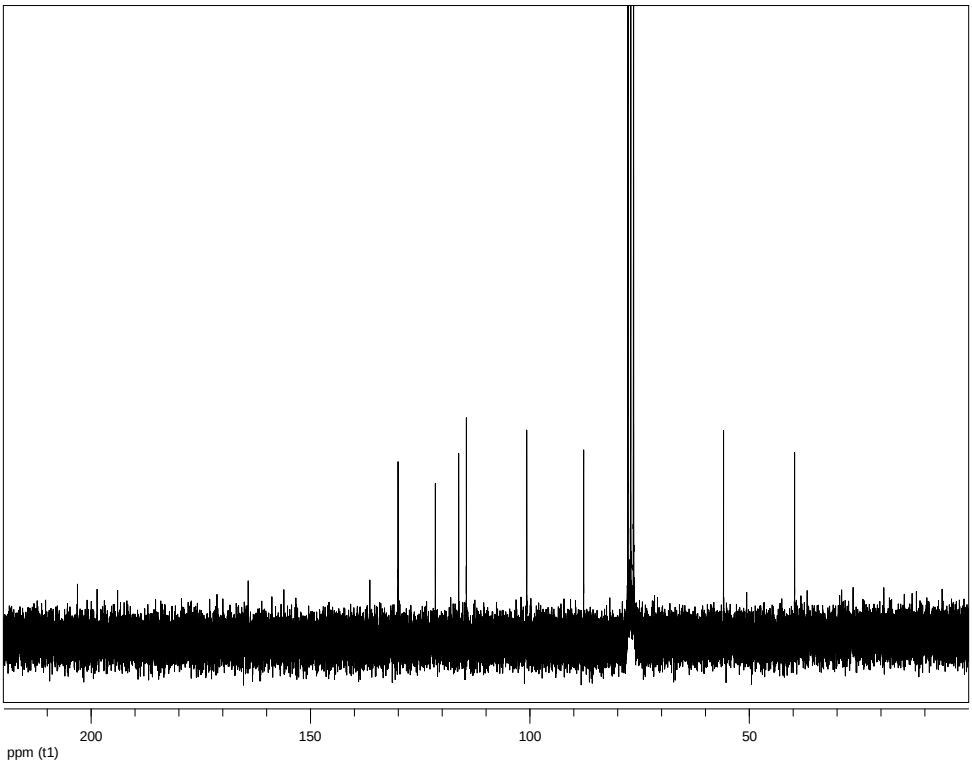

Figure 44. ^{13}C NMR spectrum of metabolite **6**.

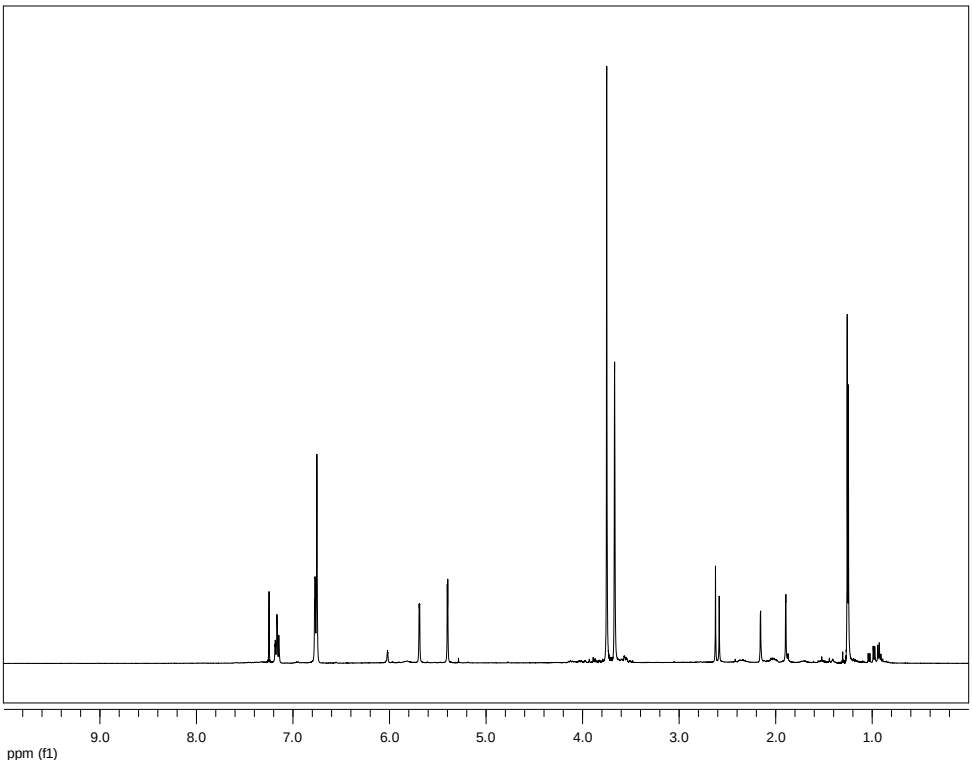

Figure 45. ^{1}H NMR spectrum of metabolite **6**.

The structure of metabolite **6** was determined on the basis of the homonuclear and heteronuclear correlations (Fig. 46) observed in the HSQC-DEPT (Fig. 47), HMBC

(Fig. 48) and COSY (Εικ. 49) spectra. Specifically, the COSY and HMBC correlations observed for **6** allowed for the unambiguous identification of the 4-methoxy-α-pyrone and the aromatic ring which were connected through C-6.

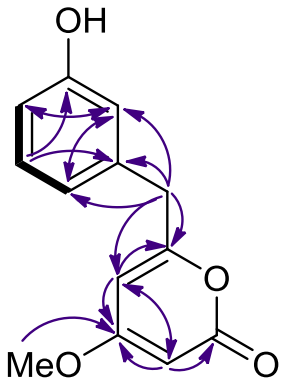

Figure 46. COSY (bold bonds) and important HMBC (arrows) correlations observed for metabolite **6**.

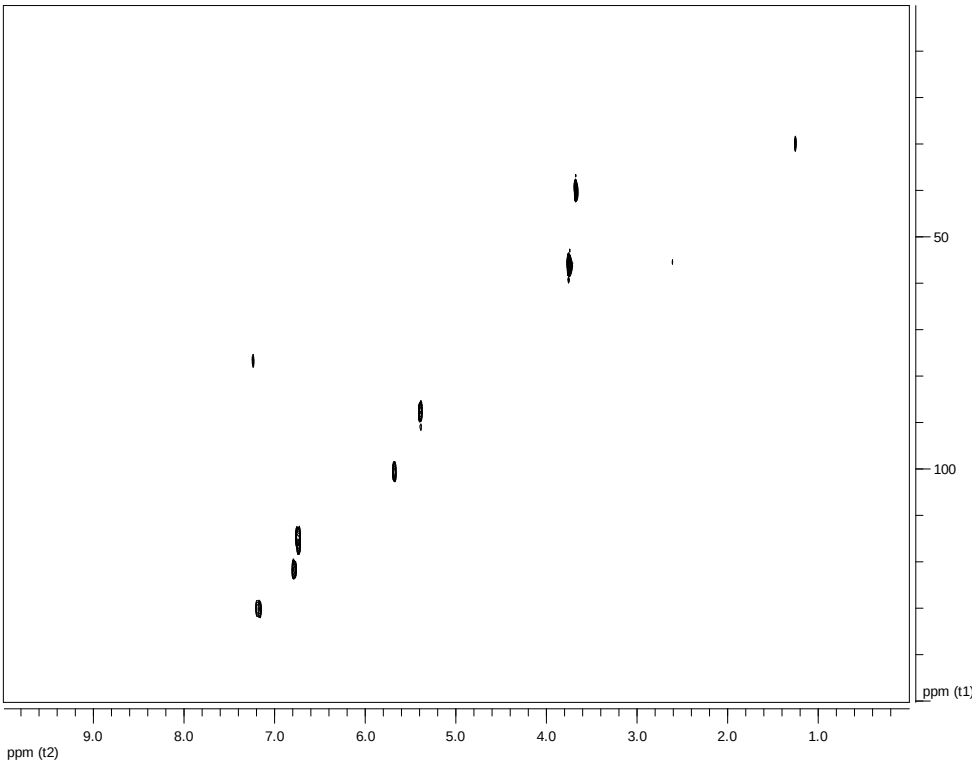

Figure 47. HSQC-DEPT spectrum of metabolite **6**.

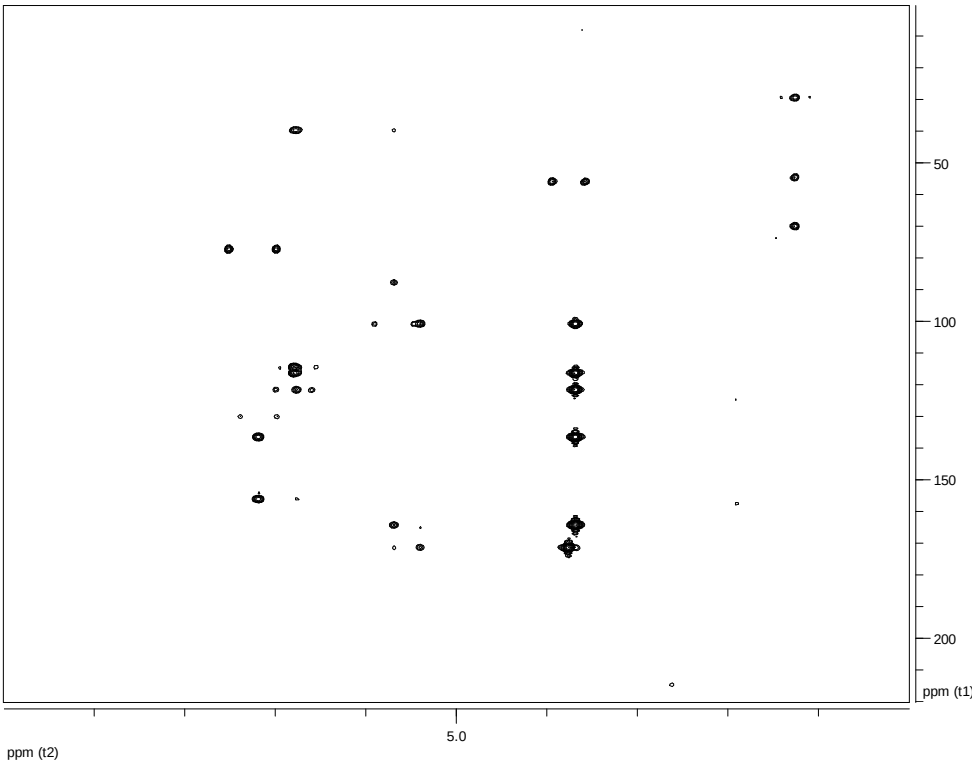

Figure 48. HMBC spectrum of metabolite **6**.

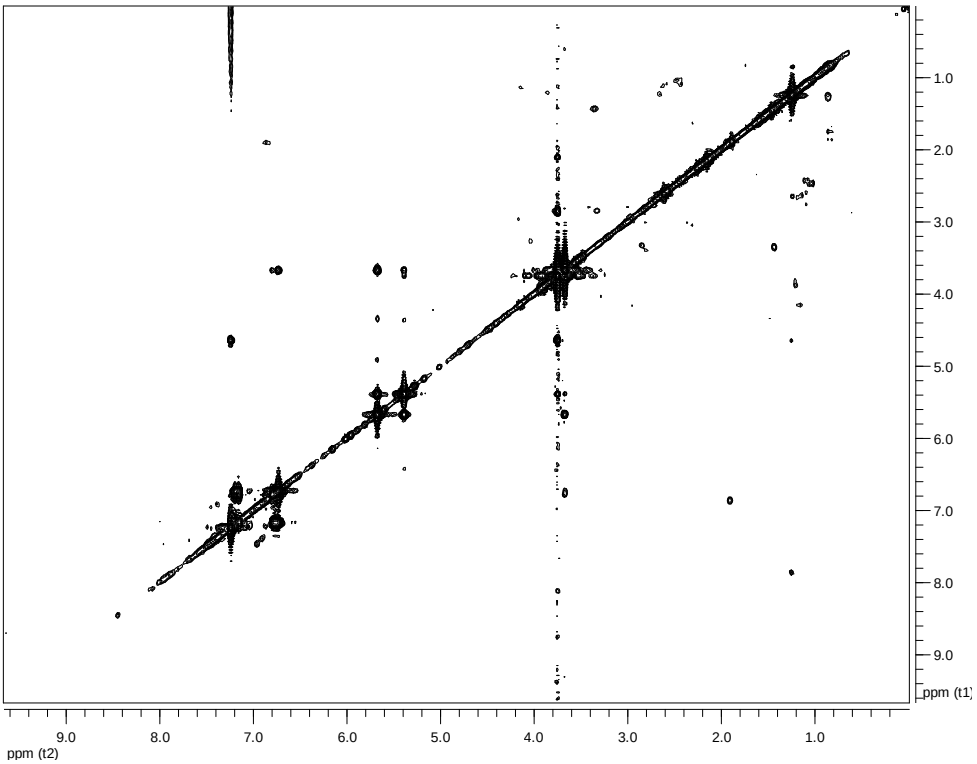

Figure 49. COSY spectrum of metabolite **6**.

Comparison of the spectroscopic and physical characteristics of metabolite **6** with those reported in the literature led to its identification as a new natural product,

which was designated as zoumbericin B (**6**) (Rab et al., 2017). The ^{1}H and ^{13}C NMR data of metabolite **6** are reported in Table 97.

Table 97. ^{1}H and ^{13}C NMR data of metabolite **6** in $CDCl_3$ (δ in ppm, J in Hz).

Position	δ_C	δ_H
1	165.0	
2	87.7	5.39, d (2.2)
3	171.3	
4	100.7	5.68, d (2.2)
5	164.2	
6	39.7	3.67, s
7	136.5	
8	121.5	6.78, brd (7.5)
9	130.0	7.17, t (7.5)
10	114.5	6.74, m
11	156.0	
12	116.2	6.73, d (1.0)
13	55.9	3.75, s

3.1.7. Metabolite 7

Metabolite **7** was isolated after a series of chromatographic separations as a colourless oil (1.2 mg).

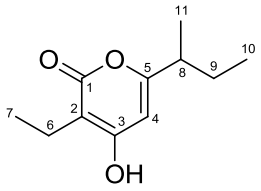

7

The mass spectrum of metabolite **7** (Fig. 50) exhibited a molecular ion peak $[M]^+$ at *m/z* 196.

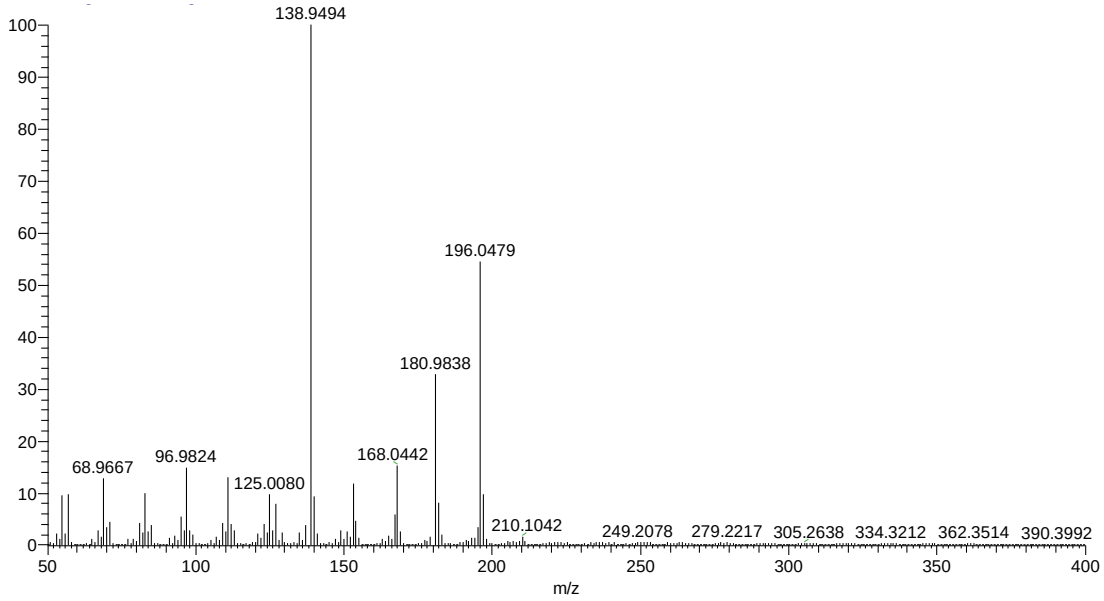

Figure 50. Mass spectrum (EIMS) of metabolite **7**.

In the ^{1}H NMR spectrum of metabolite **7** (Fig. 51) obvious were:

- one doublet methyl at δ_H 1.19 and two triplet methyls at δ_H 0.87 and 1.11, and
- one olefinic methine at δ_H 5.89.

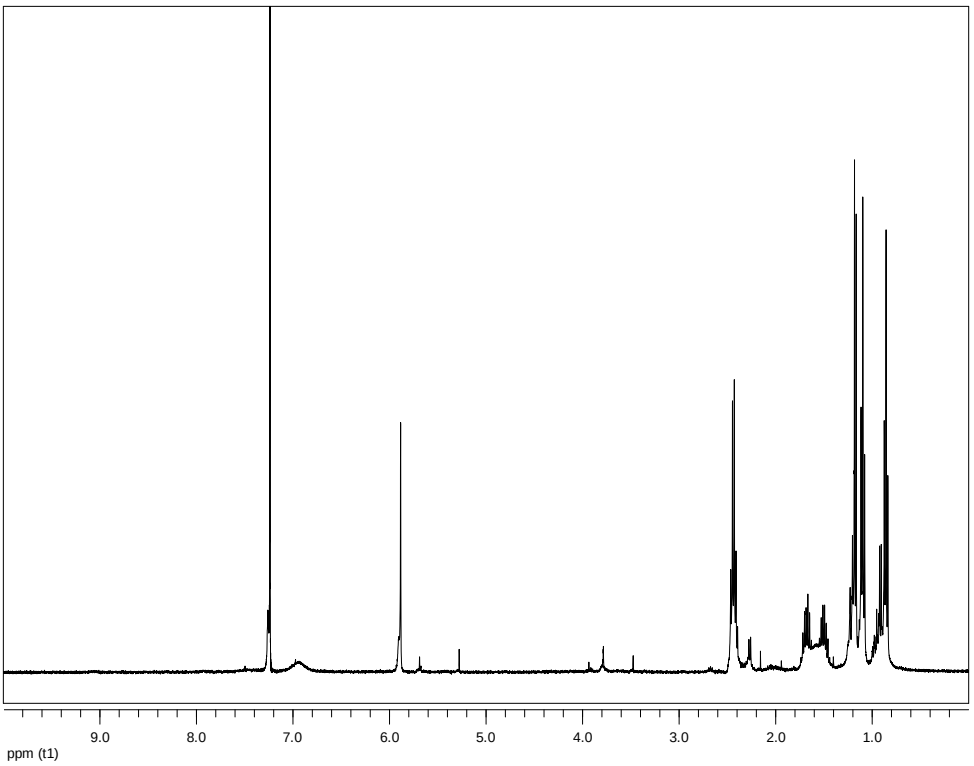

Figure 51. ^{1}H NMR spectrum of metabolite **7**.

In the HSQC-DEPT and HMBC spectra of metabolite **7** (Fig. 52 and Fig. 53) 11 carbon signals were observed. Among them, evident were:

- four olefinic carbons atoms at δ_C 98.3, 104.5, 163.5 and 167.8, and
- one ester carbonyl at δ_C 166.4.

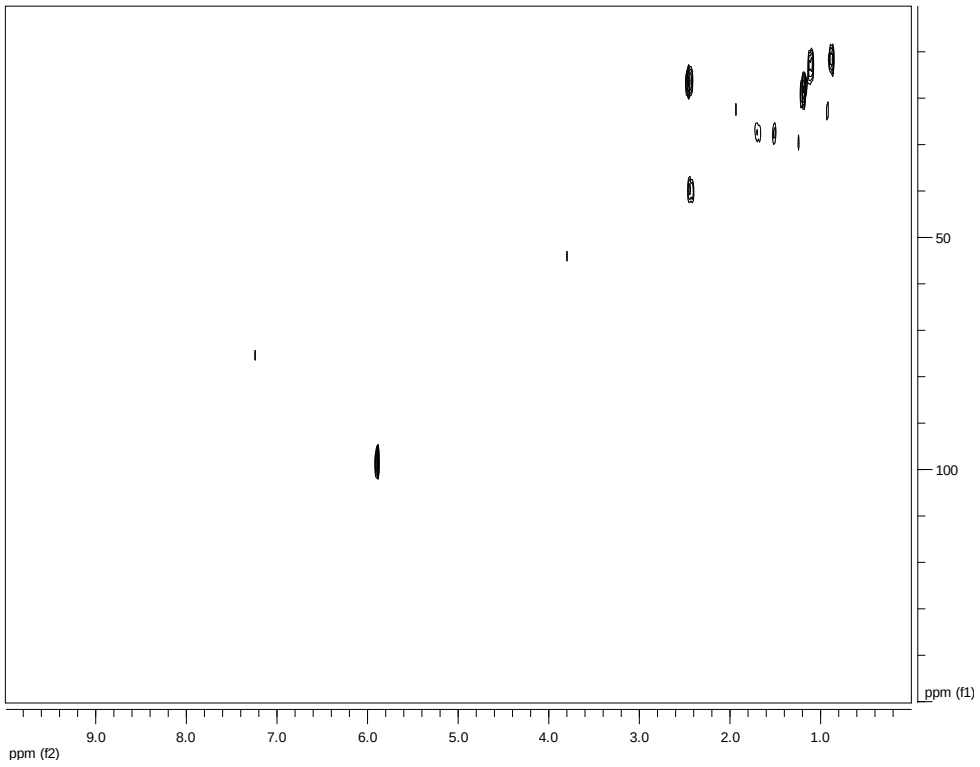

Figure 52. HSQC-DEPT spectrum of metabolite **7**.

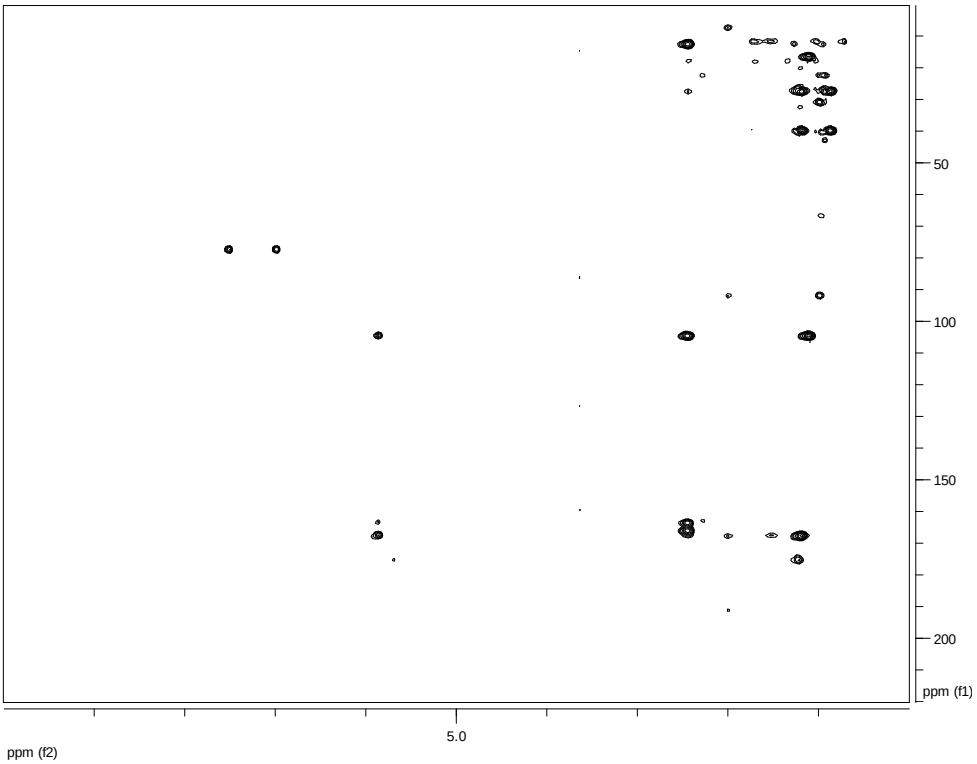

Figure 53. HMBC spectrum of metabolite **7**.

Analysis of the NMR and MS data of **7** led to the molecular formula $C_{11}H_{16}O_3$. Taking into account the two carbon-carbon double bonds and the carbonyl moiety as three of the four degrees of unsaturation, the molecular structure of **7** was determined as monocyclic.

The structure of metabolite **7** was determined on the basis of the homonuclear and heteronuclear correlations observed in the HSQC-DEPT, HMBC and COSY (Fig. 54) spectra.

Comparison of the spectroscopic and physical characteristics of metabolite **7** with those reported in the literature led to its identification as germicidin A (Petersen et al., 1993). The ^{1}H and ^{13}C NMR data of metabolite **7** are reported in Table 98.

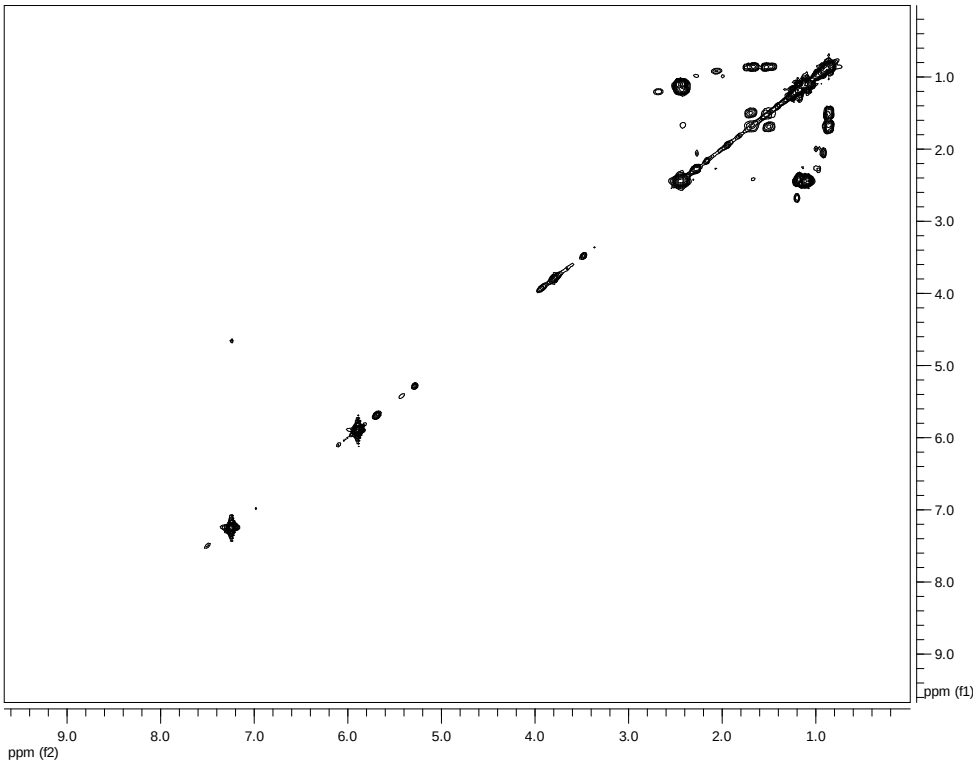

Figure 54. COSY spectrum of metabolite **7**.

Table 98. ^{1}H and ^{13}C NMR data of metabolite **7** in $CDCl_3$ (δ in ppm, J in Hz).

Position	δ_C	δ_H
1	166.4	
2	104.5	
3	163.5	
4	98.3	5.89, brs
5	167.8	
6	16.7	2.45, q (7.4)
7	13.4	1.11, t (7.4)
8	40.3	2.43, m
9	27.7	1.69, m, 1.52, m
10	11.8	0.87, t (7.4)
11	19.2	1.19, d (7.0)

Germicidin A (**7**), the first known autoregulative inhibitor of spore germination in the genus *Streptomyces*, has been shown to have an inhibitory effect on the germination of *Streptomyces* arthrospores at concentrations as low as 40 pg/mL, while at higher concentrations it inhibited porcine Na^+/K^+-activated ATPase and retarded the germination of the cress *Lepidium sativum* (Petersen et al., 1993). Moreover, germicidin A (**7**) exhibited weak activity against strains of *Streptomyces viridochromogenes* and *Streptomyces griseus*, but did not inhibit the growth of other Gram-positive and Gram-negative bacteria and several fungi and showed no effect on the mobility of the

nematode *Caenorabditis elegans* (Petersen et al., 1993). Furthermore, germicidin A (**7**) was proven inactive in a disk-diffusion assay against strains of *B. subtilis*, *Mycobacterium vaccae*, *P. aeruginosa*, methicillin-resistant *S. aureus*, vancomycin-resistant *Enterococcus faecalis* and *Sporobolomyces salmonicolor* (Xu et al., 2011).

3.1.8. Metabolite 8

Metabolite **8** was isolated after a series of chromatographic separations as a colourless oil (3.8 mg).

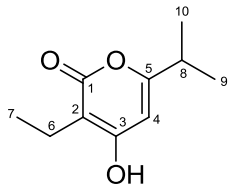

8

The mass spectrum of metabolite **8** (Fig. 55) exhibited a molecular ion peak $[M]^+$ at *m/z* 182.

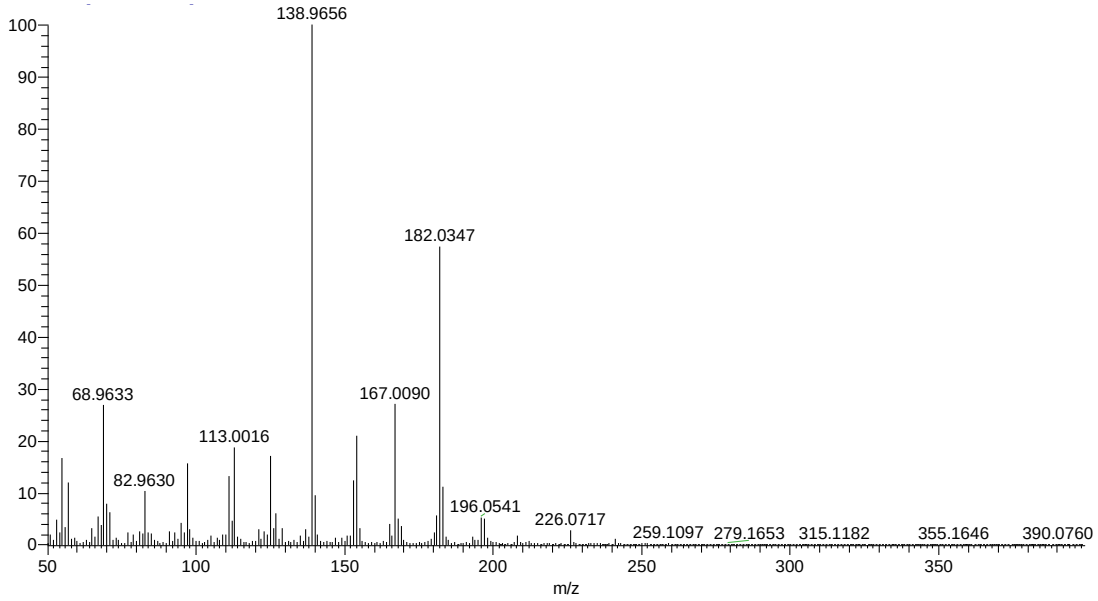

Figure 55. Mass spectrum (EIMS) of metabolite **8**.

In the ^{1}H NMR spectrum of metabolite **8** (Fig. 56) obvious were:

- two doublet methyls both resonating at δ_H 1.19 and one triplet methyl at δ_H 1.08, and
- one olefinic methine at δ_H 6.13.

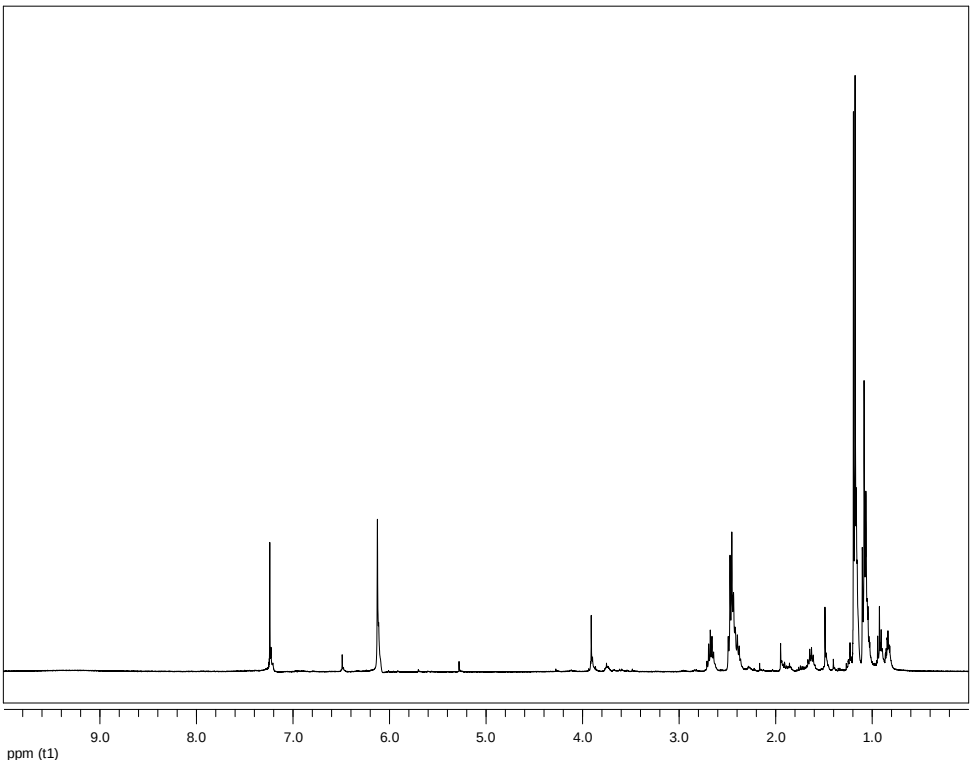

Figure 56. ^{1}H NMR spectrum of metabolite **8**.

In the ^{13}C NMR spectrum of metabolite **8** (Fig. 57) 10 carbon signals were observed. Among them, evident were:

- four olefinic carbons atoms at δ_C 98.4, 104.7, 167.5 and 168.3, and
- one ester carbonyl at δ_C 166.2.

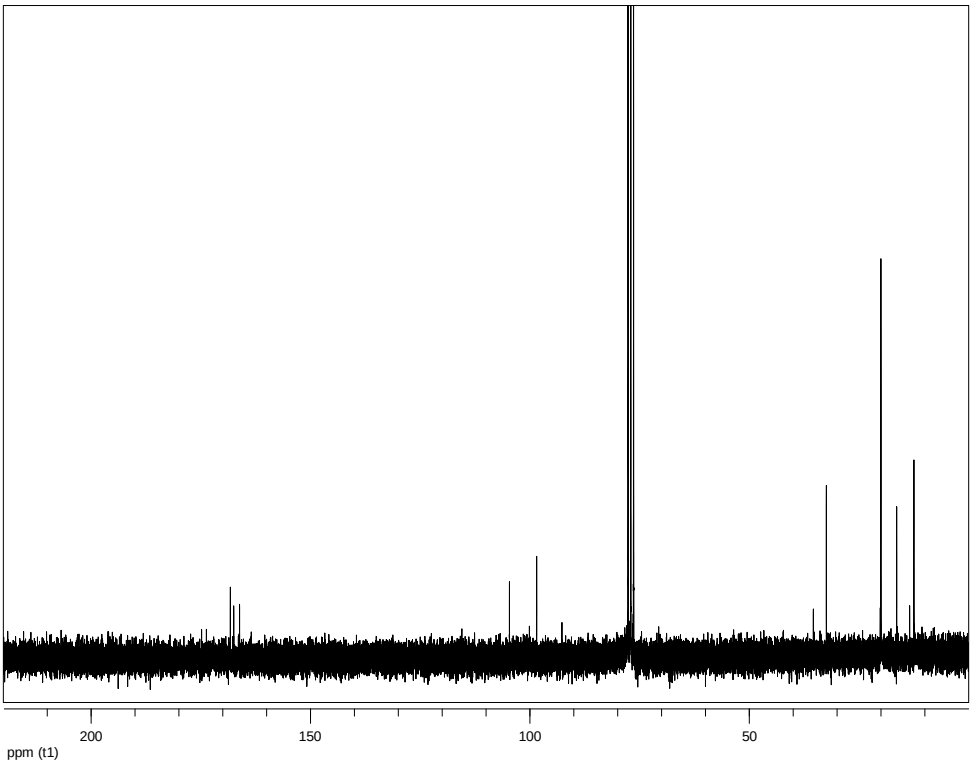

Figure 57. ^{13}C NMR spectrum of metabolite **8**.

Analysis of the NMR and MS data of **8** led to the molecular formula $C_{10}H_{14}O_3$. The ^1H NMR spectroscopic data of metabolite **8** closely resembled those of gramicidin A (**7**), with the most prominent difference between **7** and **8** being the replacement of the isobutyl side chain at C-5 by an isopropyl side chain. The structure of metabolite **8** was verified on the basis of the homonuclear and heteronuclear correlations observed in the HSQC-DEPT (Fig. 58), HMBC (Fig. 59) and COSY (Εικ. 60) spectra.

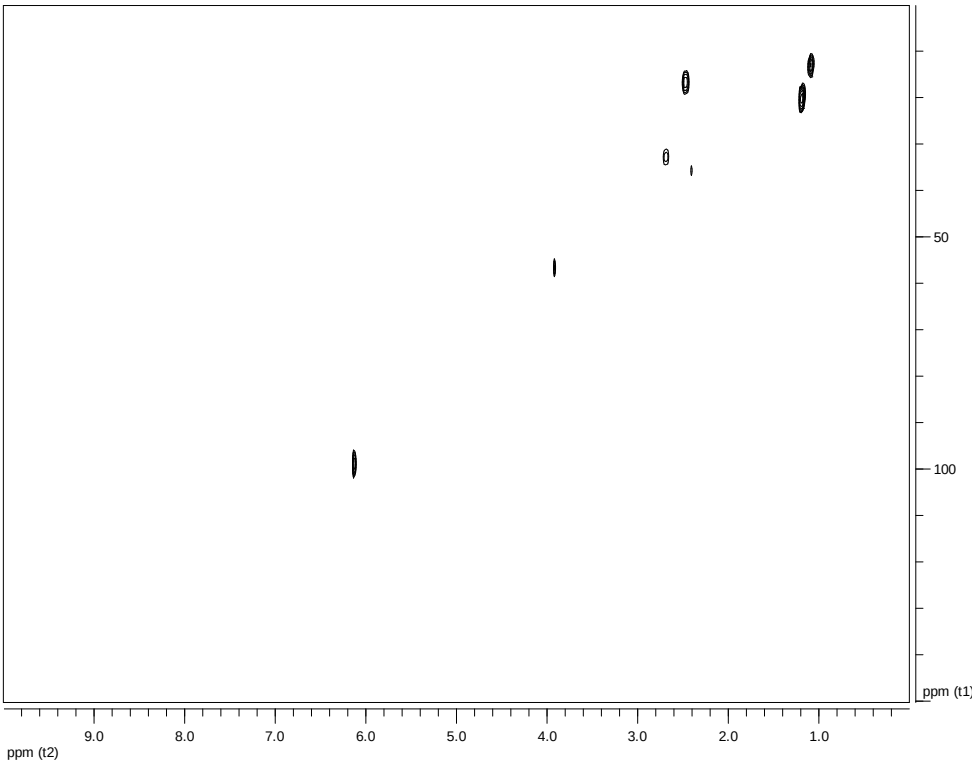

Figure 58. HSQC-DEPT spectrum of metabolite **8**.

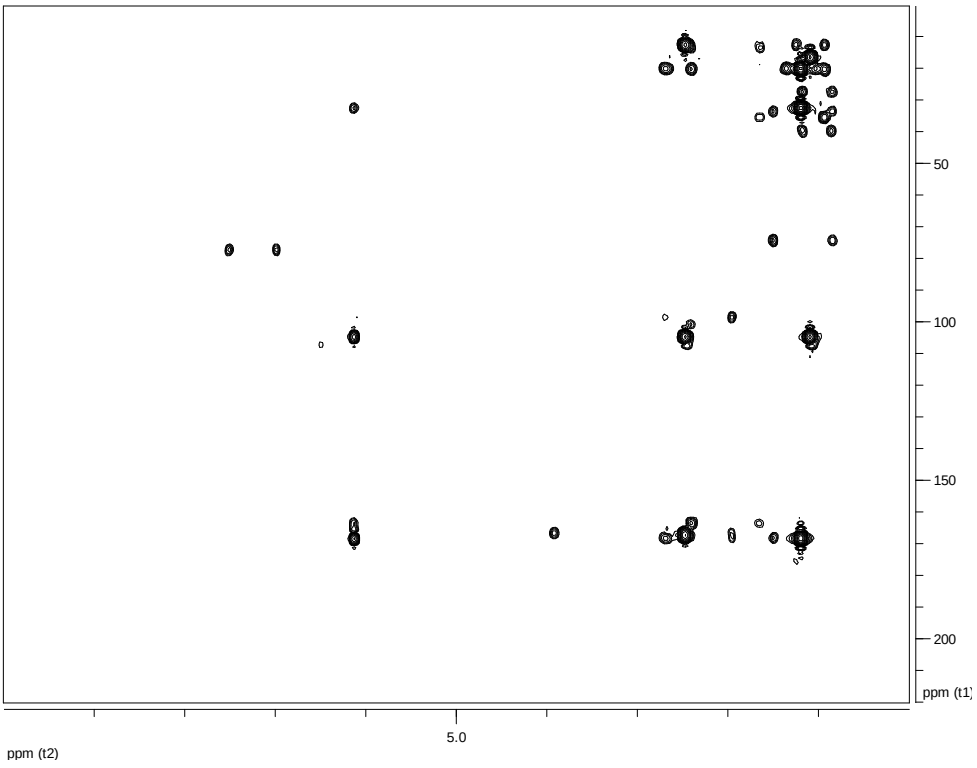

Figure 59. HMBC spectrum of metabolite **8**.

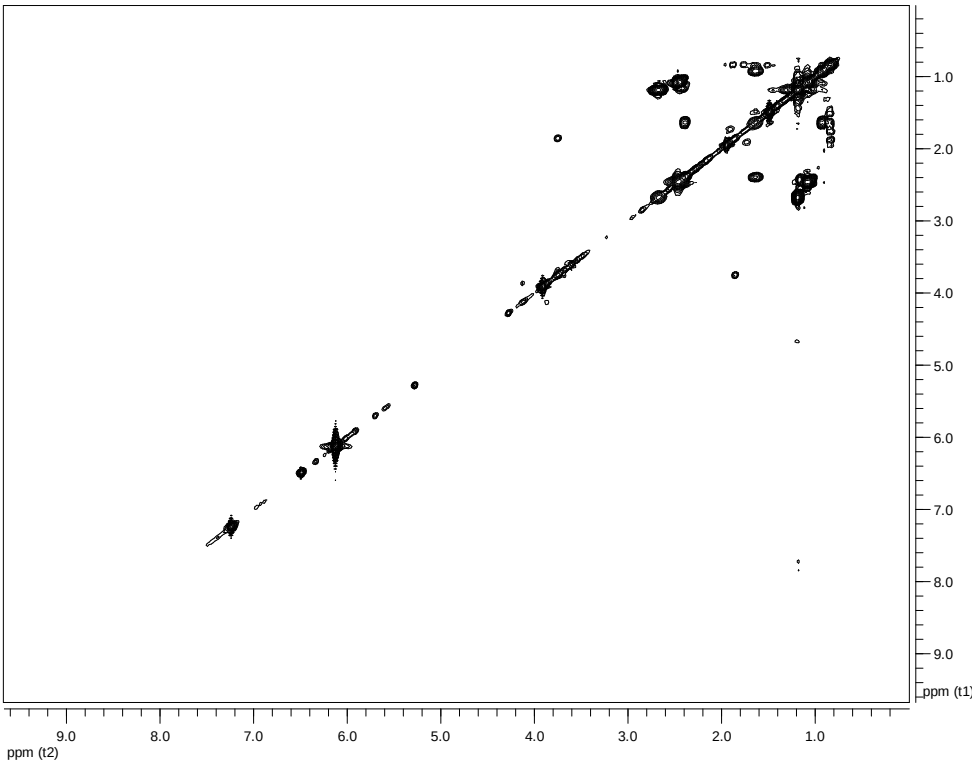

Figure 60. COSY spectrum of metabolite **8**.

Comparison of the spectroscopic and physical characteristics of metabolite **8** with those reported in the literature led to its identification as germicidin B (Petersen et al., 1993). Germicidin B (**8**) was proven inactive in a disk-diffusion assay against strains of *B. subtilis*, *M. vaccae*, *P. aeruginosa*, methicillin-resistant *S. aureus*, vancomycin-resistant *E. faecalis* and *S. salmonicolor* (Xu et al., 2011). The ^{1}H and ^{13}C NMR data of metabolite **8** are reported in Table 99.

Table 99. ^{1}H and ^{13}C NMR data of metabolite **8** in $CDCl_3$ (δ in ppm, J in Hz).

Position	δ_C	δ_H
1	166.2	
2	104.7	
3	167.5	
4	98.4	6.13, brs
5	168.3	
6	16.4	2.47, q (7.4)
7	12.5	1.08, t (7.4)
8	32.4	2.69, m
9	20.0	1.19, d (6.9)
10	20.0	1.19, d (6.9)

3.1.9. Metabolite 9

Metabolite **9** was isolated after a series of chromatographic separations as a colourless oil (4.6 mg).

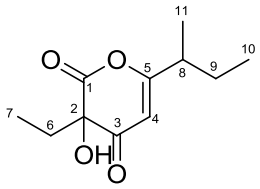

9

The mass spectrum of metabolite **9** (Fig. 61) exhibited a molecular ion peak $[M]^+$ at *m/z* 212. Metabolite **9** possessed the molecular formula $C_{11}H_{16}O_4$, as deduced from the HRESIMS measurements where an ion peak consistent with $[M - H]^-$ was observed at *m*/*z* 211.0975.

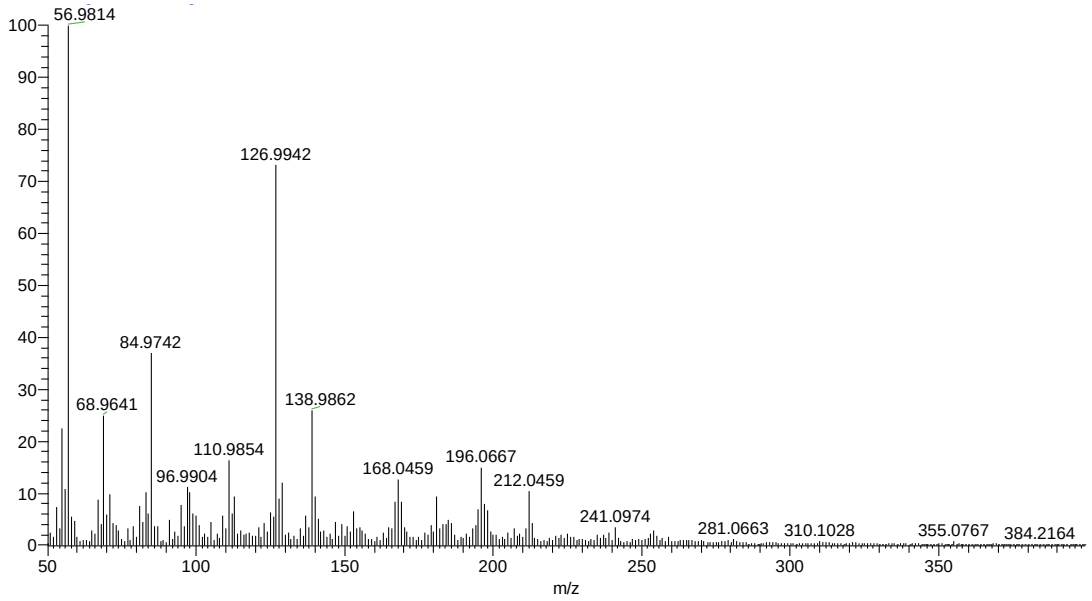

Figure 61. Mass spectrum (EIMS) of metabolite **9**.

The ^{1}H NMR spectrum of **9** (Fig. 62), including signals for two aliphatic methyls on secondary carbons (δ_H 0.92 and 0.97), one aliphatic methyl on a tertiary carbon (δ_H 1.20), two methylenes (δ_H 1.54/1.68 and 1.98), one relatively deshielded methine (δ_H 2.41) and one olefinic methine (δ_H 5.68), was rather similar to that of the co-occurring germicidin A (**7**).

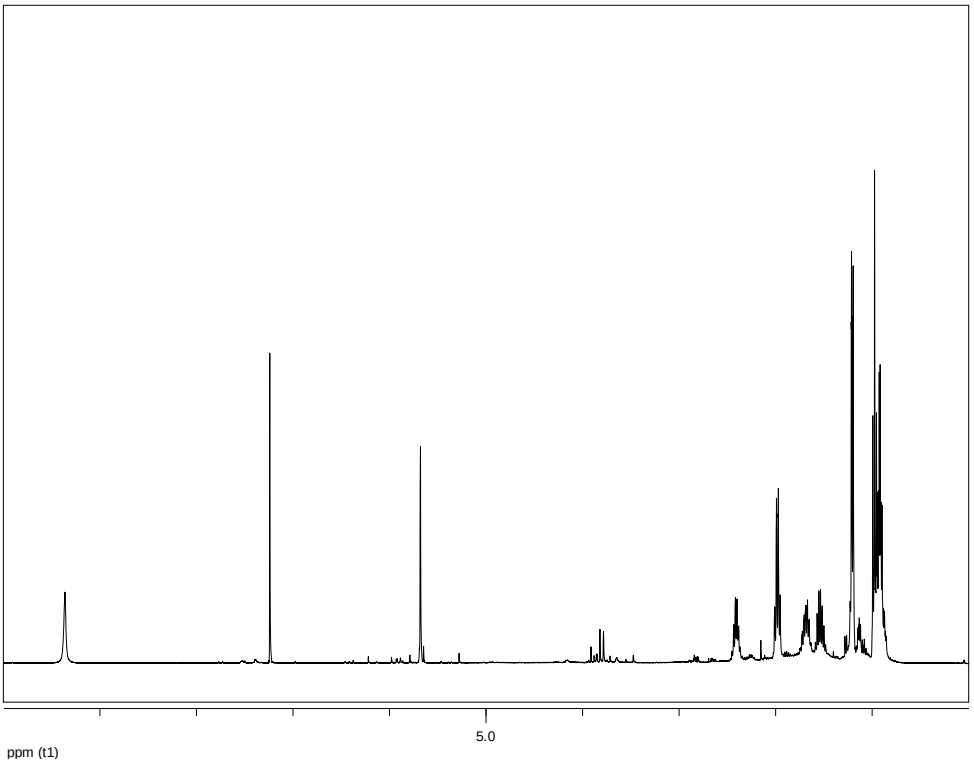

Figure 62. ^{1}H NMR spectrum of metabolite **9**.

The ^{13}C NMR spectrum of **9** (Fig. 63) exhibited 11 carbon signals, which, according to the HSQC-DEPT experiment, were attributed to three methyls, two methylenes, two methines, and four quaternary carbon atoms. However, in contrast to germicidin A (**7**), which exhibited signals for one carbonyl and four olefinic carbons, resonances for two carbonyls (δ_C 167.2 and 191.2), two olefinic carbons (δ_C 104.6 and 175.3) and one oxygenated quaternary carbon (δ_C 91.7) were evident for compound **9**.

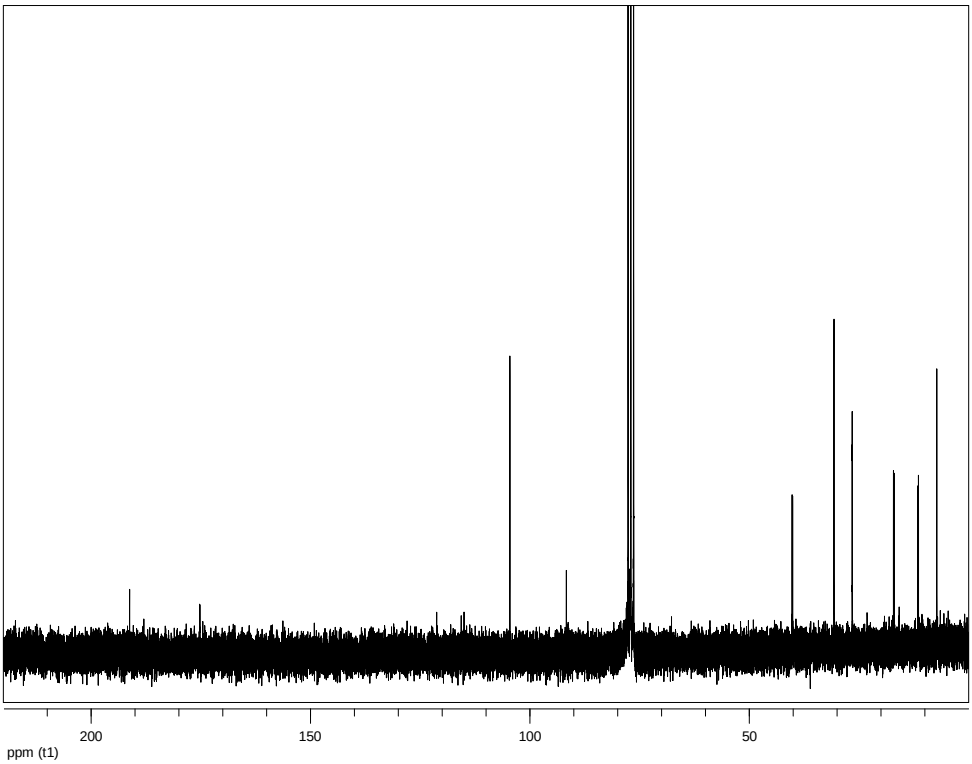

Figure 63. ^{13}C NMR spectrum of metabolite **9**.

The structure of metabolite **9** was proposed on the basis of the homonuclear and heteronuclear correlations (Fig. 64) observed in the HSQC-DEPT (Fig. 65), HMBC (Fig. 66) and COSY (Fig. 67) spectra. Due to the limited amount in which **9** was isolated, it was not possible to determine the absolute configuration at C-2 and C-8.

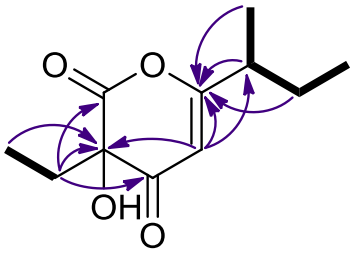

Figure 64. COSY (bold bonds) and important HMBC (arrows) correlations observed for metabolite **9**.

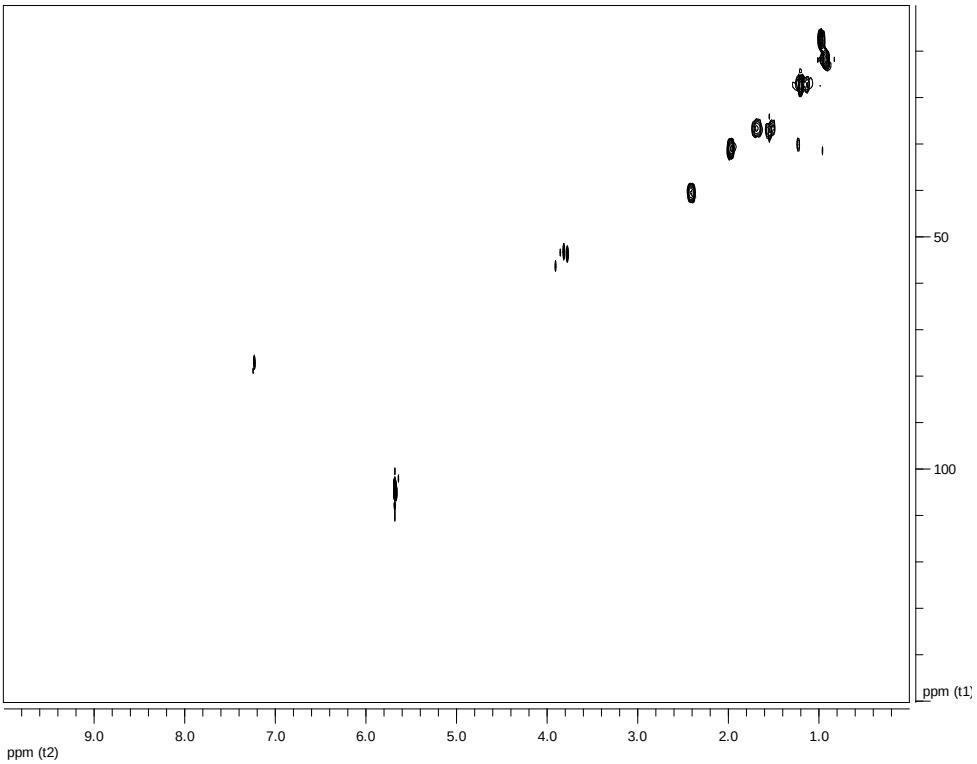

Figure 65. HSQC-DEPT spectrum of metabolite **9**.

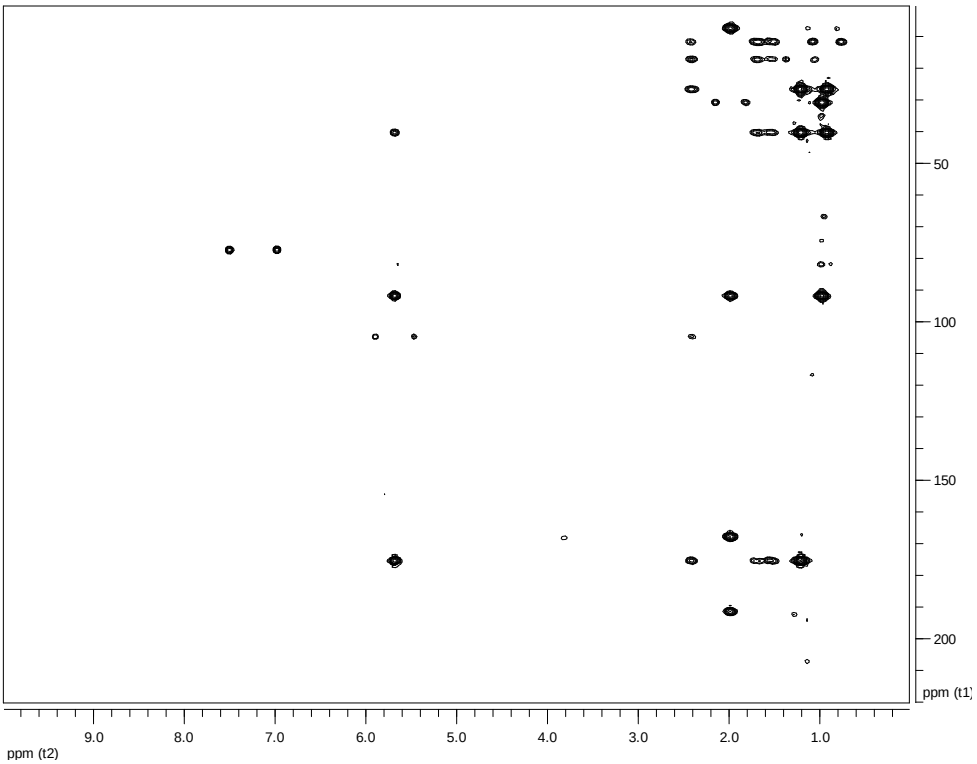

Figure 66. HMBC spectrum of metabolite **9**.

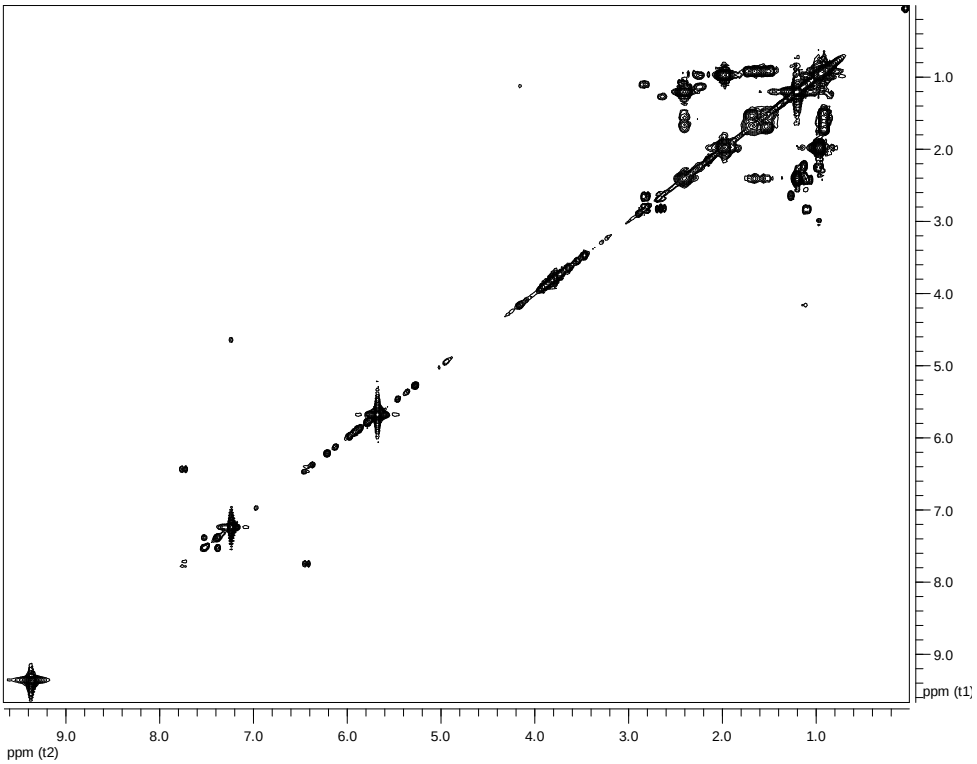

Figure 67. COSY spectrum of metabolite **9**.

Comparison of the spectroscopic and physical characteristics of metabolite **9** with those reported in the literature led to its identification as a new natural product, which was designated as germicidin K (Rab et al., 2017). The ^{1}H and ^{13}C NMR data of metabolite **9** are reported in Table 100.

Table 100. ^{1}H and ^{13}C NMR data of metabolite **9** in $CDCl_3$ (δ in ppm, J in Hz).

Position	δ_C	δ_H
1	167.2	
2	91.7	
3	191.2	
4	104.6	5.68, s
5	175.3	
6	30.7	1.98, q (7.6)
7	7.3	0.97, t (7.6)
8	40.2	2.41, m
9	26.5	1.68, m, 1.54, m
10	11.4	0.92, t (7.4)
11	17.1	1.20, d (6.9)
OH		9.36, brs

3.1.10. Metabolite 10

Metabolite **10** was isolated after a series of chromatographic separations as a colourless oil (5.1 mg).

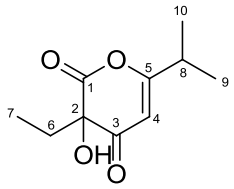

10

The mass spectrum of metabolite **10** (Fig. 68) exhibited a molecular ion peak $[M]^+$ at *m/z* 198. Metabolite **10** possessed the molecular formula $C_{10}H_{14}O_4$, as deduced from the HRESIMS measurements where an ion peak consistent with $[M - H]^-$ was observed at *m*/*z* 197.0818.

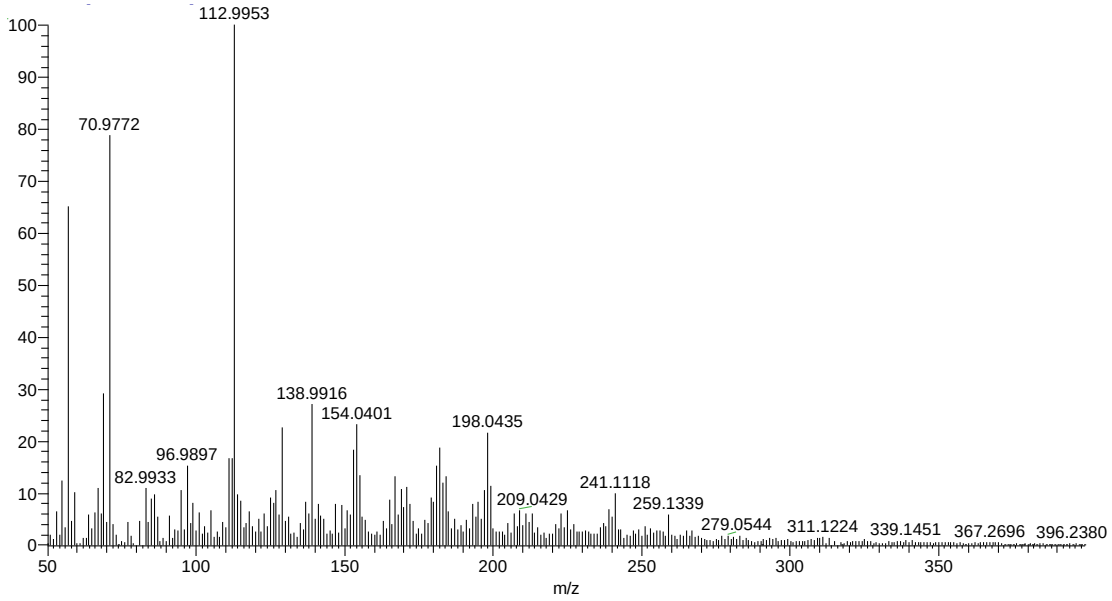

Figure 68. Mass spectrum (EIMS) of metabolite **10**.

The ^1H and ^{13}C NMR spectroscopic data of metabolite **10** closely resembled those of **9** and the co-occurring germicidin B (**8**). The most prominent differences in the ^1H NMR spectrum of **10** (Fig. 69), in comparison to **9**, were the presence of a second aliphatic methyl on a tertiary carbon and the simultaneous absence of an aliphatic methyl on a secondary carbon and a methylene.

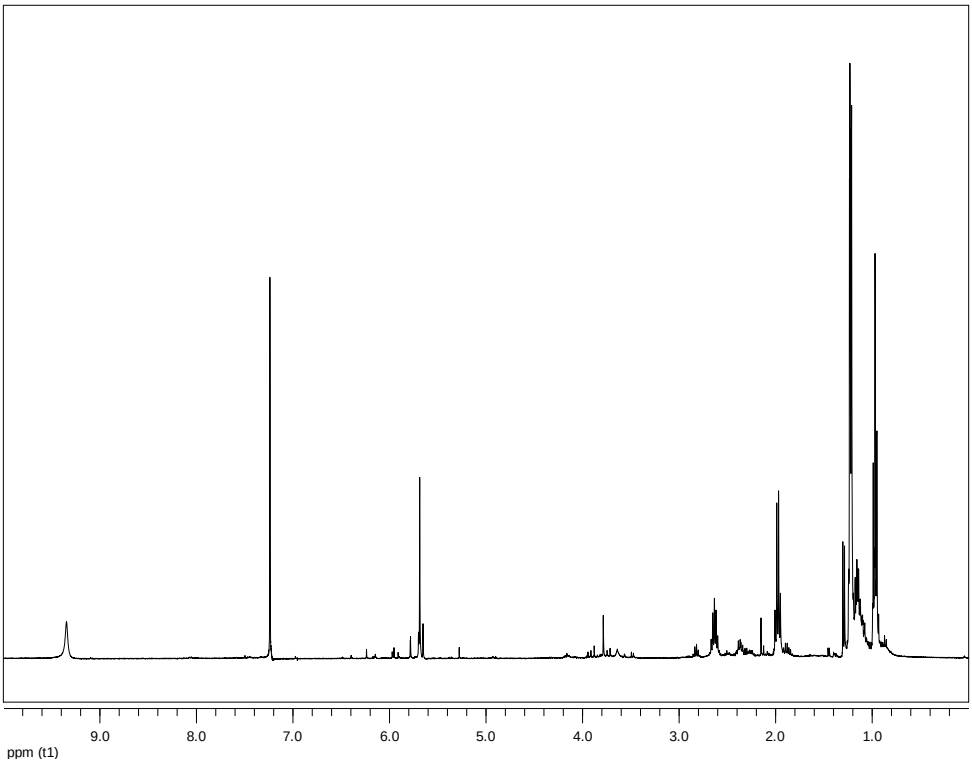

Figure 69. ^{1}H NMR spectrum of metabolite **10**.

As in the case of **9**, the ^{13}C NMR spectrum of **10** (Fig. 70) included signals for two carbonyls (δ_C 167.6 and 191.3), two olefinic carbons (δ_C 103.3 and 176.2) and one oxygenated quaternary carbon (δ_C 91.7), instead of one carbonyl and four olefinic carbons, as observed for germicidin B (**8**).

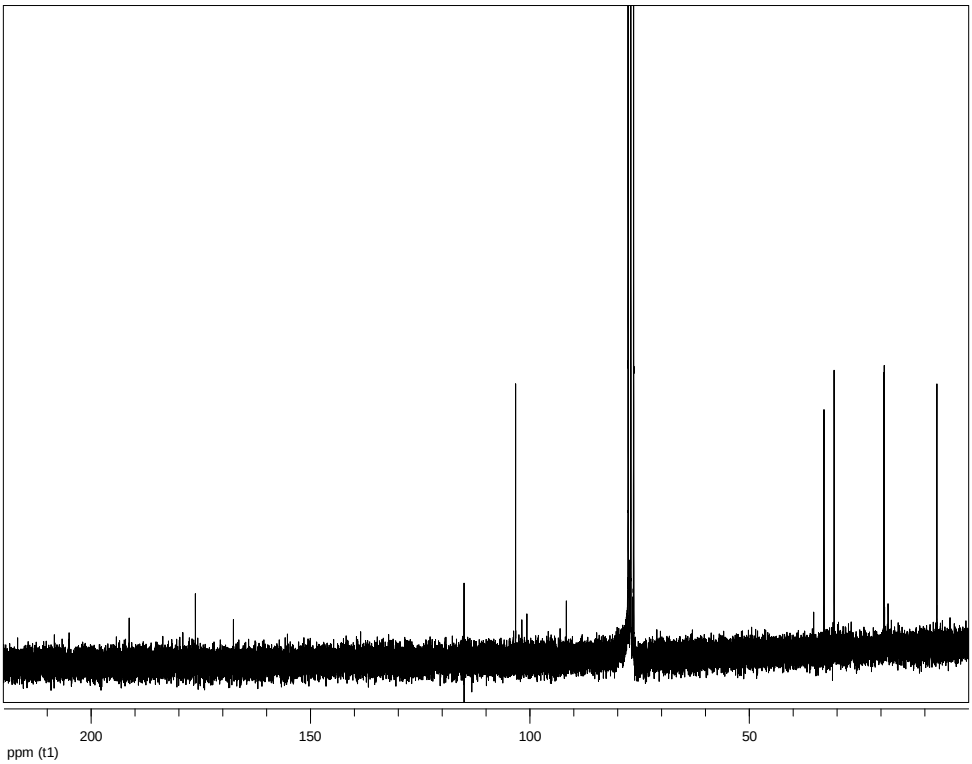

Figure 70. ^{13}C NMR spectrum of metabolite **10**.

The homonuclear and heteronuclear correlations (Fig. 71), as observed in the HSQC-DEPT (Fig. 72), HMBC (Fig. 73) and COSY (Εικ. 74) spectra, supported the proposed structure of metabolite **10**. Since **10** was isolated in limited amount, the absolute configuration at C-2 could not be established.

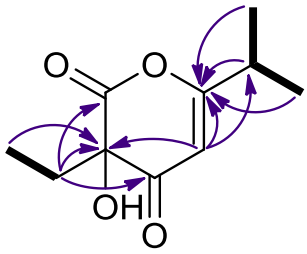

Figure 71. COSY (bold bonds) and important HMBC (arrows) correlations observed for metabolite **10**.

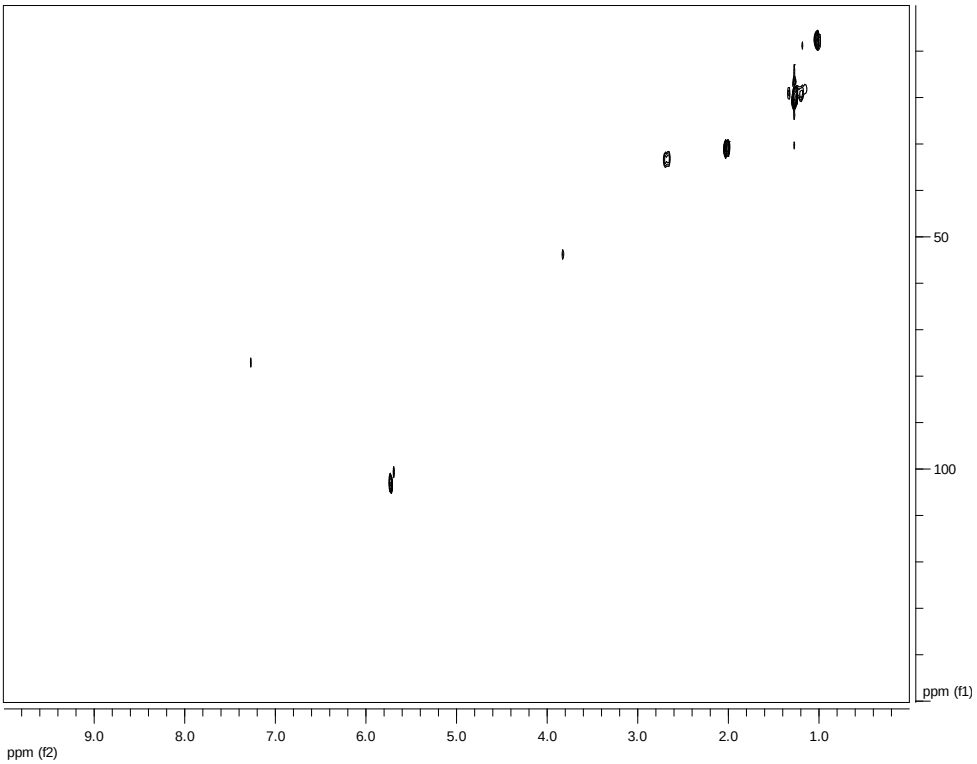

Figure 72. HSQC-DEPT spectrum of metabolite **10**.

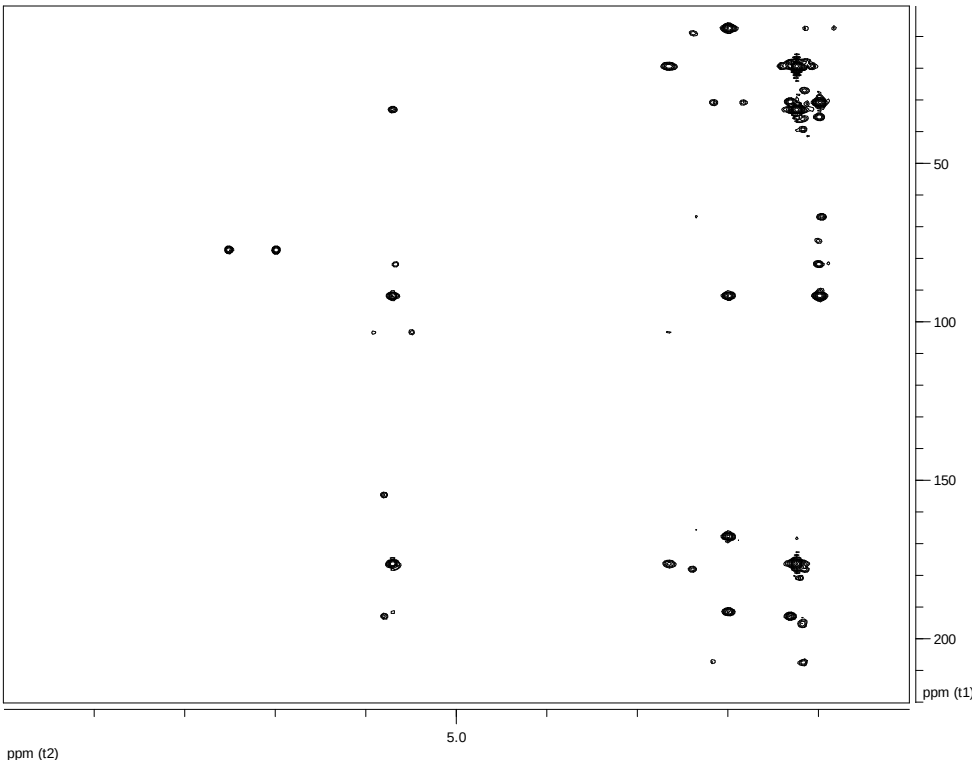

Figure 73. HMBC spectrum of metabolite **10**.

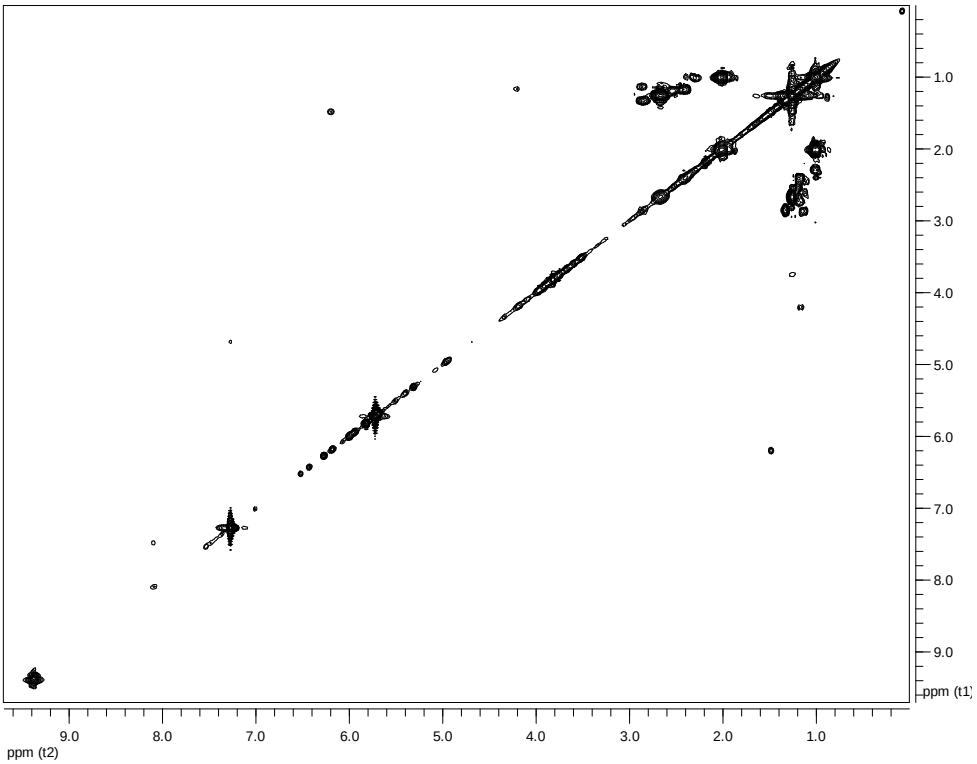

Figure 74. COSY spectrum of metabolite **10**.

Comparison of the spectroscopic and physical characteristics of metabolite **10** with those reported in the literature led to its identification as a new natural product, which was designated as germicidin L (Rab et al., 2017). The ^{1}H and ^{13}C NMR data of metabolite **10** are reported in Table 101.

Table 101. ^{1}H and ^{13}C NMR data of metabolite **10** in $CDCl_3$ (δ in ppm, J in Hz).

Position	δ_C	δ_H
1	167.6	
2	91.7	
3	191.3	
4	103.3	5.69, s
5	176.2, C	
6	30.7	1.98, q (7.6)
7	7.3	0.96, t (7.6)
8	33.0	2.64, septet (6.8)
9	19.2	1.22, d (6.8)
10	19.3	1.23, d (6.8)
OH		9.35, brs

3.1.11. Metabolite 11

Metabolite **11** was isolated after a series of chromatographic separations as a colourless oil (0.7 mg).

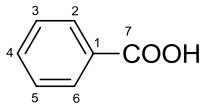

11

The mass spectrum of metabolite **11** (Fig. 75) exhibited a molecular ion peak $[M]^+$ at *m/z* 122.

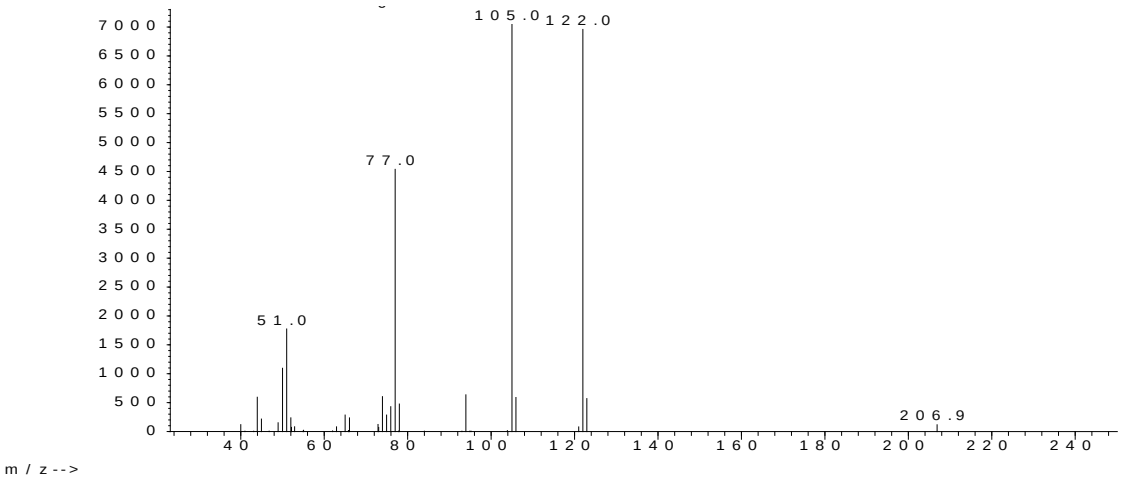

Figure 75. Mass spectrum (EIMS) of metabolite **11**.

In the ^{1}H NMR spectrum of metabolite **11** (Fig. 76) the only signals present were three at δ_H 7.35-7.75 integrating for five protons in total with coupling constants characteristic for a mono-substituted aromatic ring.

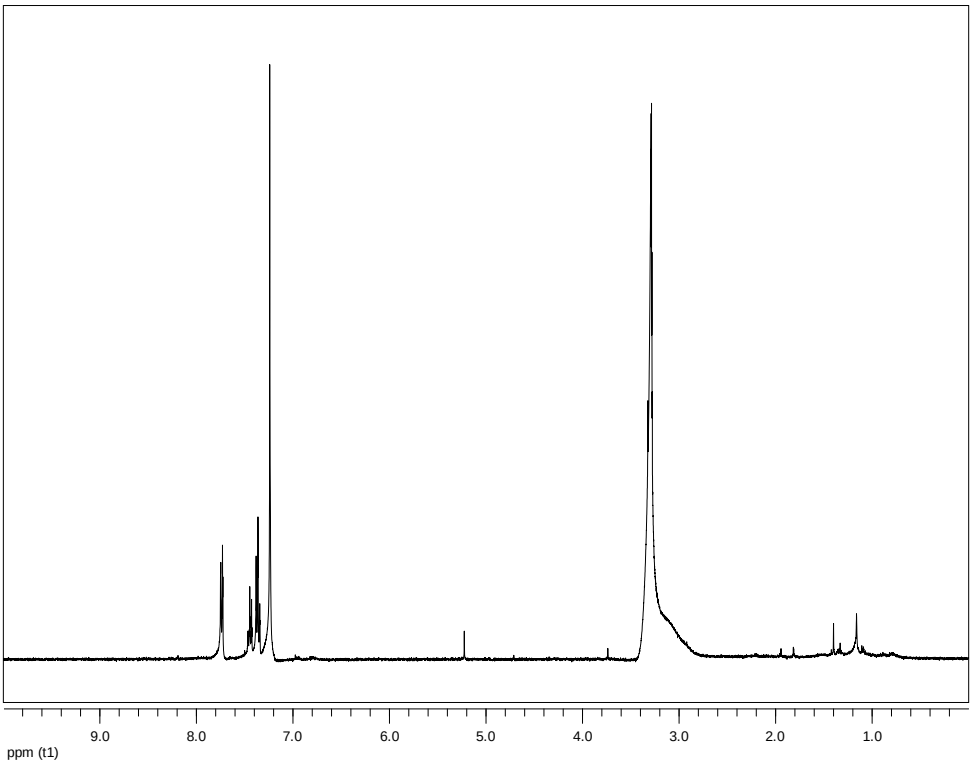

Figure 76. ^{1}H NMR spectrum of metabolite **11**.

Analysis of the NMR and MS data of **11** led to the molecular formula $C_7H_6O_2$. Comparison of the spectroscopic and physical characteristics of metabolite **11** with those reported in the literature led to its identification as benzoic acid (Pouchert & Behnke, 1993).

3.1.12. Metabolite 12

Metabolite **12** was isolated after a series of chromatographic separations as a colourless oil (13.1 mg).

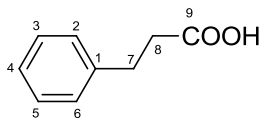

12

The mass spectrum of metabolite **12** (Fig. 77) exhibited a molecular ion peak $[M]^+$ at *m/z* 150.

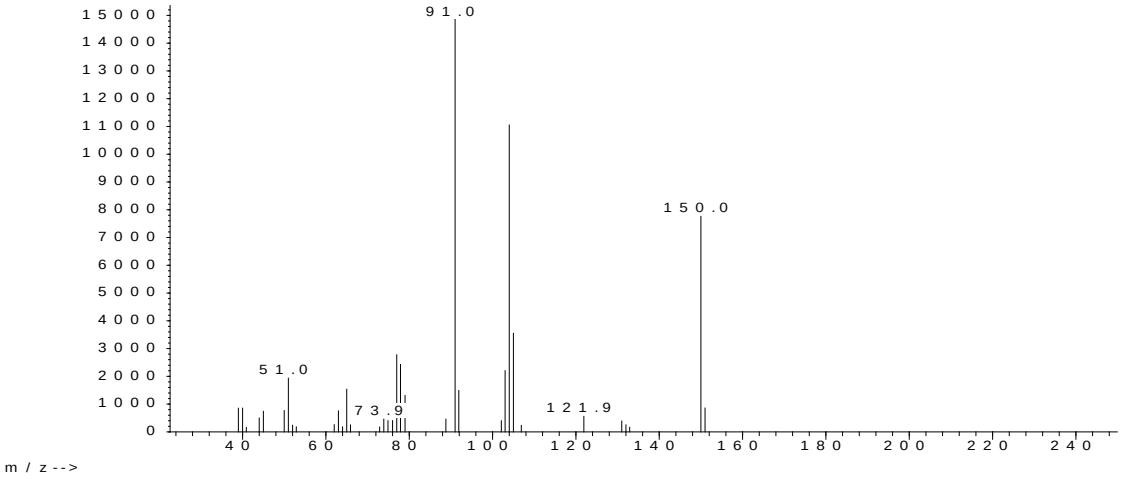

Figure 77. Mass spectrum (EIMS) of metabolite **12**.

In the ^{1}H NMR spectrum of metabolite **12** (Fig. 78) obvious were:

- two triplet signals at δ_H 2.67 and 2.95 integrating for two protons each, and
- signals at δ_H 7.18-7.33 integrating for five protons in total with coupling constants characteristic for a mono-substituted aromatic ring.

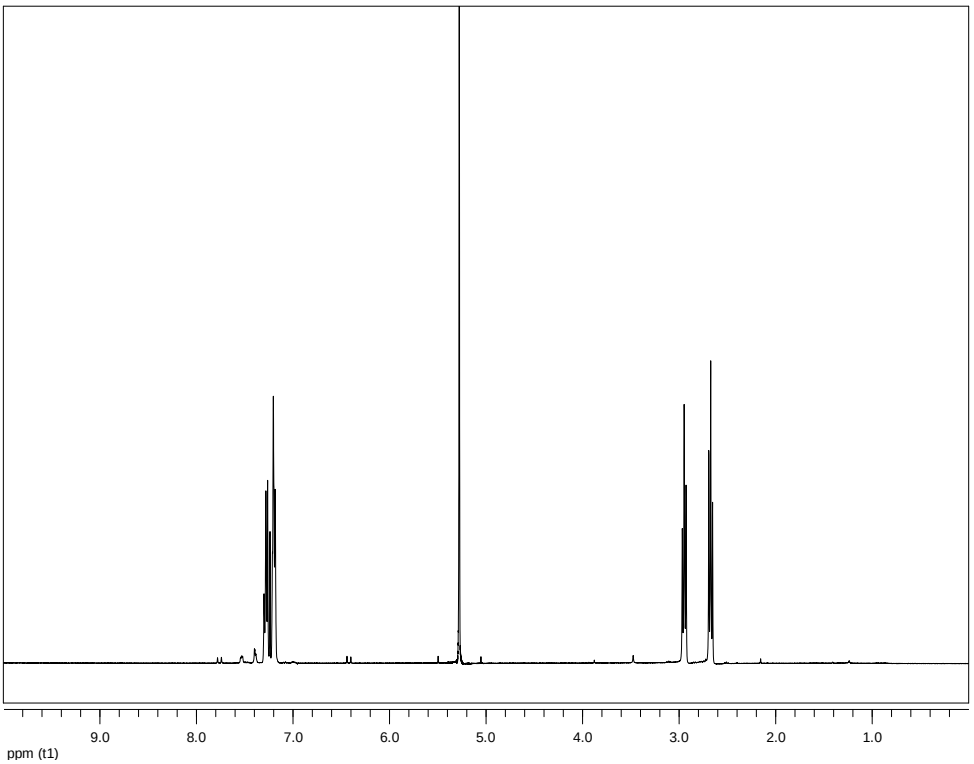

Figure 78. ^{1}H NMR spectrum of metabolite **12**.

Analysis of the NMR and MS data of **12** led to the molecular formula $C_9H_{10}O_2$. Comparison of the spectroscopic and physical characteristics of metabolite **12** with

those reported in the literature led to its identification as hydrocinnamic acid (Pouchert & Behnke, 1993).

3.1.13. Metabolite 13

Metabolite **13** was isolated after a series of chromatographic separations as a yellowish oil (26.4 mg).

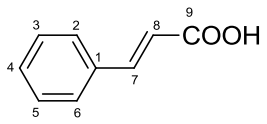

13

The mass spectrum of metabolite **13** (Fig. 79) exhibited a molecular ion peak $[M]^+$ at *m/z* 148.

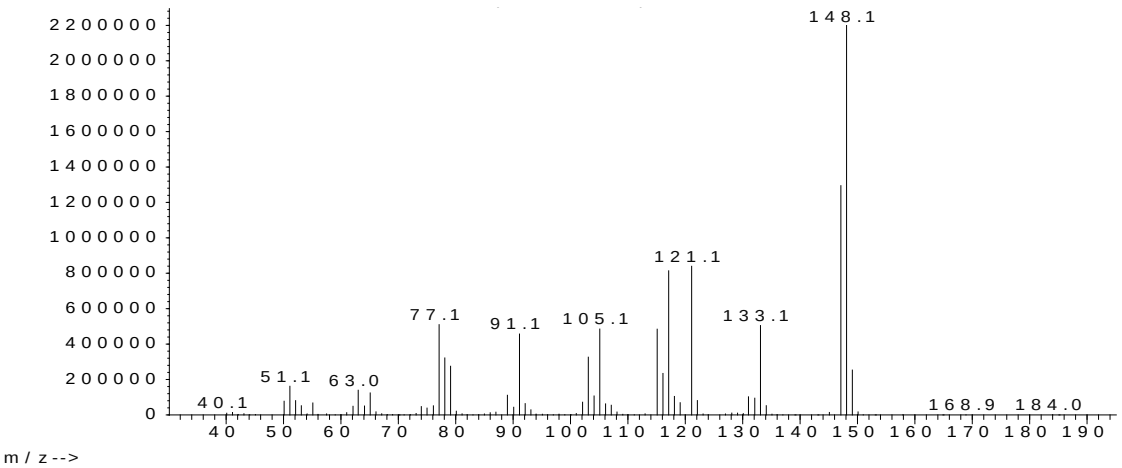

Figure 79. Mass spectrum (EIMS) of metabolite **13**.

In the ^{1}H NMR spectrum of metabolite **13** (Fig. 80) obvious were:

- two doublet olefinic methines at δ_H 6.38 and 7.66 with a coupling constant value of 15.6 Hz, indicative of an isolated 1,2-*trans*-di-substituted double bond, and
- signals at δ_H 7.32-7.52 integrating for five protons in total with coupling constants characteristic for a mono-substituted aromatic ring.

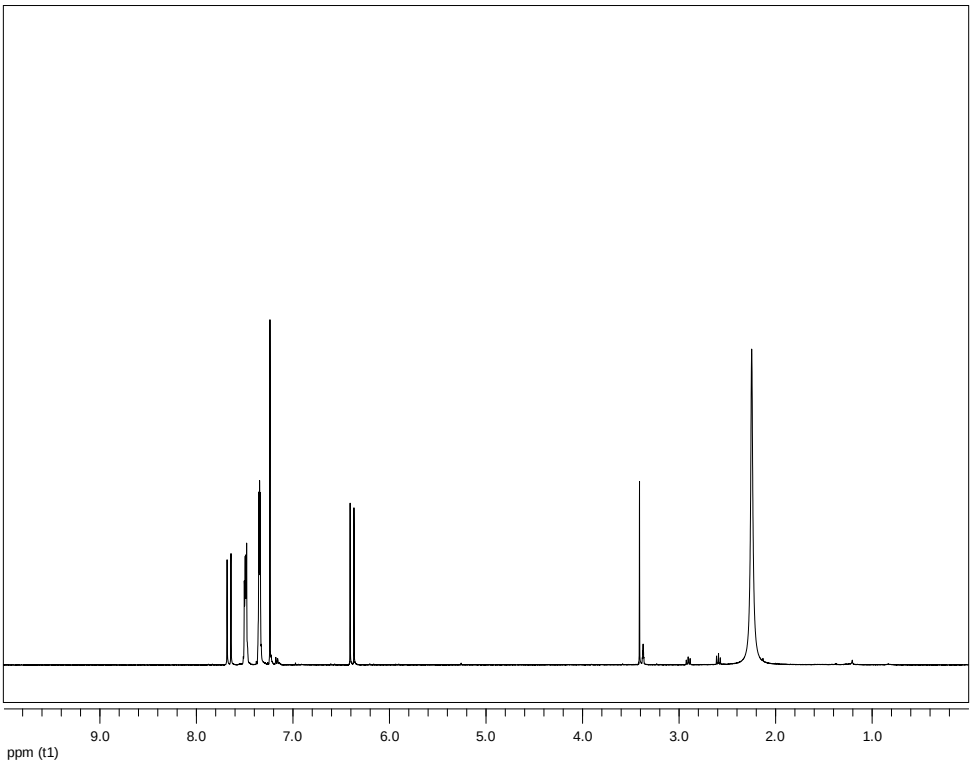

Figure 80. ^{1}H NMR spectrum of metabolite **13**.

Analysis of the NMR and MS data of **13** led to the molecular formula $C_9H_8O_2$. Comparison of the spectroscopic and physical characteristics of metabolite **13** with those reported in the literature led to its identification as (*E*)-cinnamic acid (Pouchert & Behnke, 1993).

3.1.14. Metabolite 14

Metabolite **14** was isolated after a series of chromatographic separations as a colourless oil (1.3 mg).

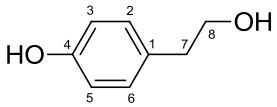

14

The mass spectrum of metabolite **14** (Fig. 81) exhibited a molecular ion peak $[M]^+$ at *m/z* 138.

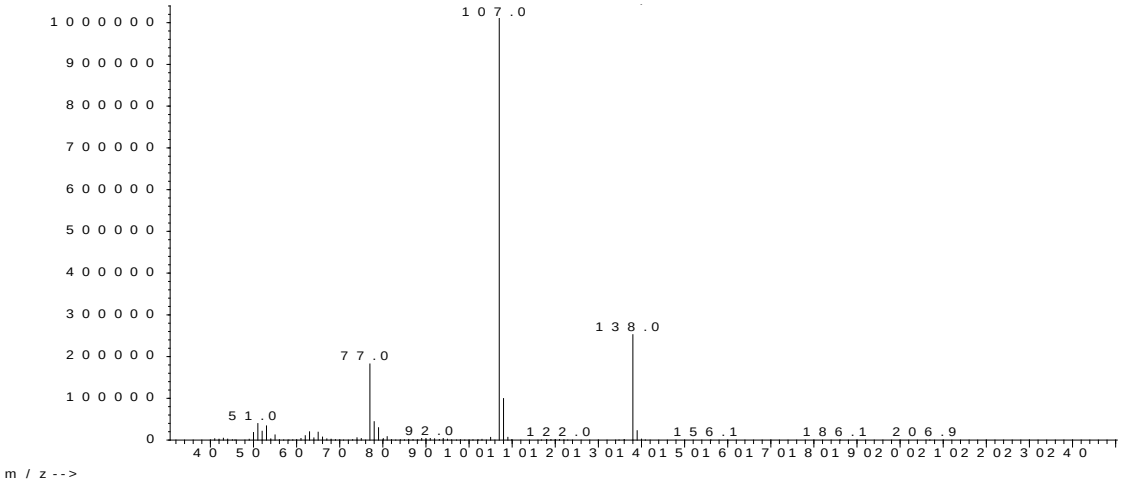

Figure 81. Mass spectrum (EIMS) of metabolite **14**.

In the ^{1}H NMR spectrum of metabolite **14** (Fig. 82) obvious were:

- two triplet signals at δ_H 2.68 and 3.68 integrating for two protons each, and
- two doublet signals at δ_H 6.69 and 6.97 integrating for two protons each and corresponding to the protons of a *para*-substituted aromatic ring.

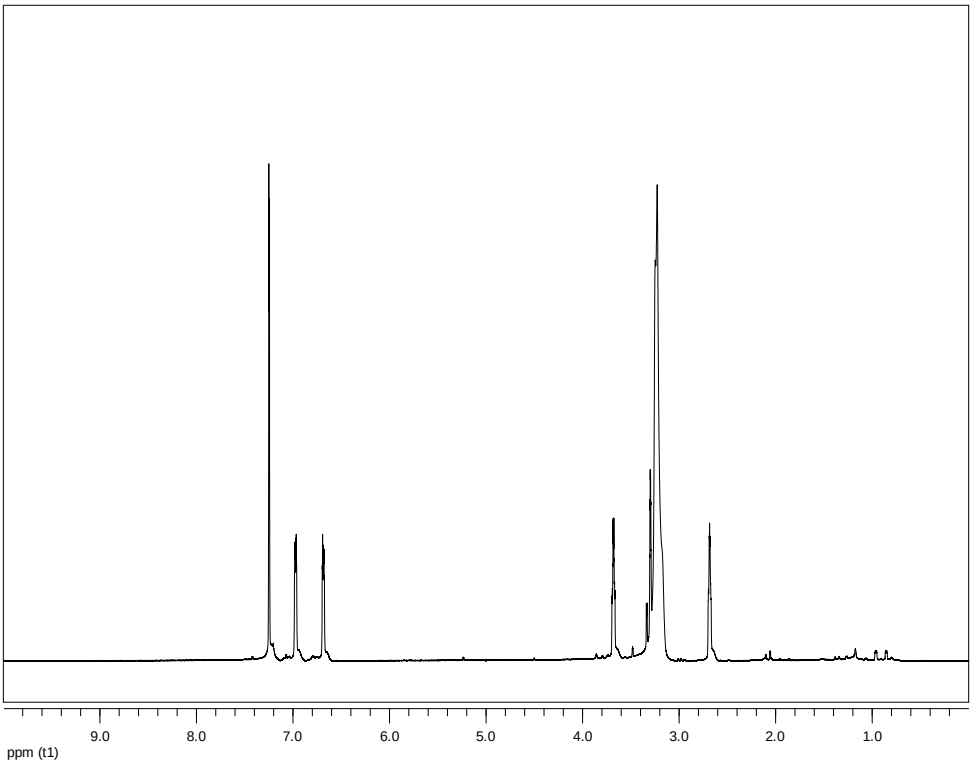

Figure 82. ^{1}H NMR spectrum of metabolite **14**.

Analysis of the NMR and MS data of **14** led to the molecular formula $C_8H_{10}O_2$. Comparison of the spectroscopic and physical characteristics of metabolite **14** with

those reported in the literature led to its identification as tyrosol, also known as *p*-hydroxy-phenethyl alcohol (Liu et al., 2010).

3.1.15. Metabolite 15

Metabolite **15** was isolated after a series of chromatographic separations as a colourless oil (1.5 mg).

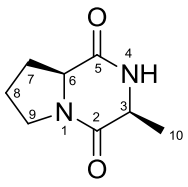

15

The mass spectrum of metabolite **15** (Fig. 83) exhibited a molecular ion peak $[M]^+$ at *m/z* 168.

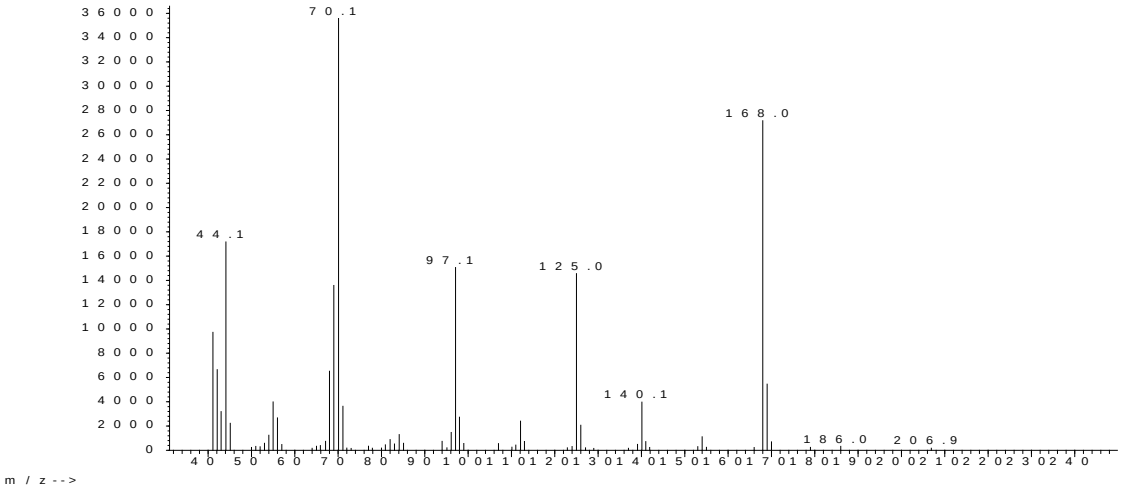

Figure 83. Mass spectrum (EIMS) of metabolite **15**.

In the ^{1}H NMR spectrum of metabolite **15** (Fig. 84) obvious were:

- one doublet signal at δ_H 1.45, integrating for three protons and attributed to a methyl group on a tertiary carbon atom,
- one signal at δ_H 4.10, integrating for two protons and attributed to two H_α methines of two aminoacids, and
- one signal at δ_H 5.66, attributed to one exchangeable proton of an amine.

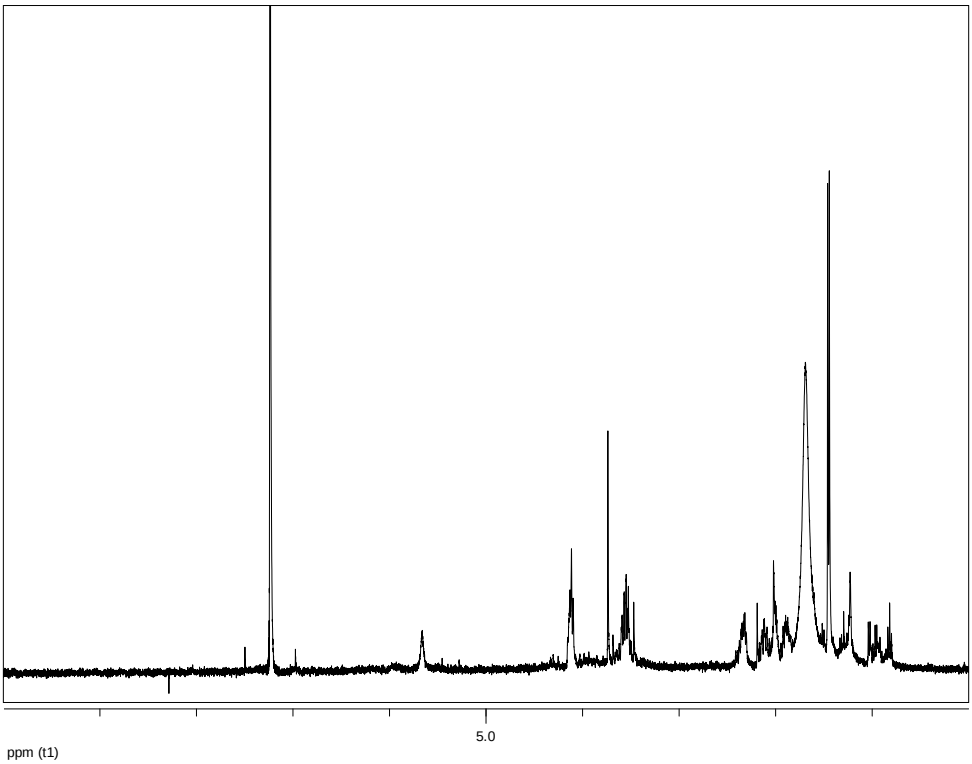

Figure 84. ^{1}H NMR spectrum of metabolite **15**.

Analysis of the NMR and MS data of **15** led to the molecular formula $C_8H_{12}N_2O_2$, corresponding to four degrees of unsaturation. The spectroscopic data of metabolite **15** were indicative of a 2,5-diketopiperazine skeleton.

The planar structure of metabolite **15** was determined on the basis of the homonuclear correlations observed in the COSY (Fig. 85) spectrum. In particular, the cross-peaks of H-3 / H_3-10 and H-3 / NH-4, as well as of H-6 / H_2-7, H_2-7 / H_2-8 and H_2-8 / H_2-9 suggested two distinct spin systems, indicative of an alanine and a proline residue, respectively.

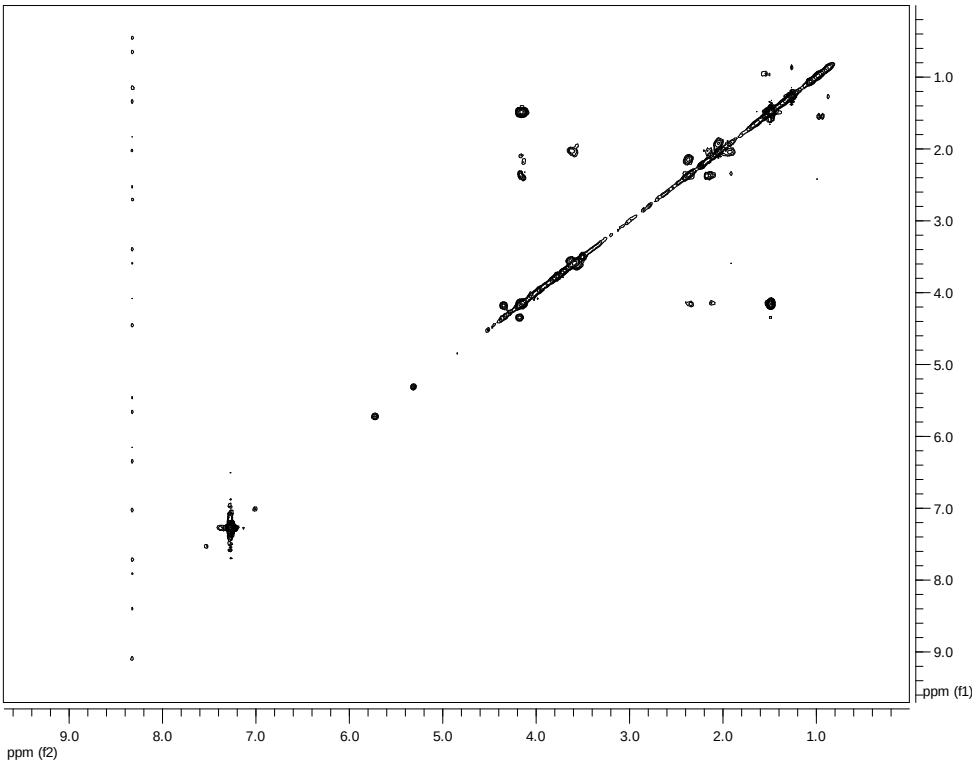

Figure 85. COSY spectrum of metabolite **15**.

Comparison of the spectroscopic and physical characteristics of metabolite **15** with those reported in the literature led to its identification as *cis-cyclo*(L-Pro-L-Ala) (Chen et al., 2012; Huang et al., 2014). The ^{1}H NMR data of metabolite **15** are reported in Table 102.

Table 102. ^{1}H NMR data of metabolite **15** in $CDCl_3$ (δ in ppm, J in Hz).

Position	$\boldsymbol{\delta_H}$
3	4.10, m
4	5.66, brs
6	4.10, m
7	2.36, m, 2.13, m
8	2.01, m, 1.89, m
9	3.56, m
10	1.45, d (7.0)

3.1.16. Metabolite 16

Metabolite **16** was isolated after a series of chromatographic separations as a colourless oil (1.9 mg).

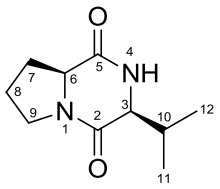

16

The mass spectrum of metabolite **16** (Fig. 86) exhibited a molecular ion peak $[M]^+$ at *m/z* 196.

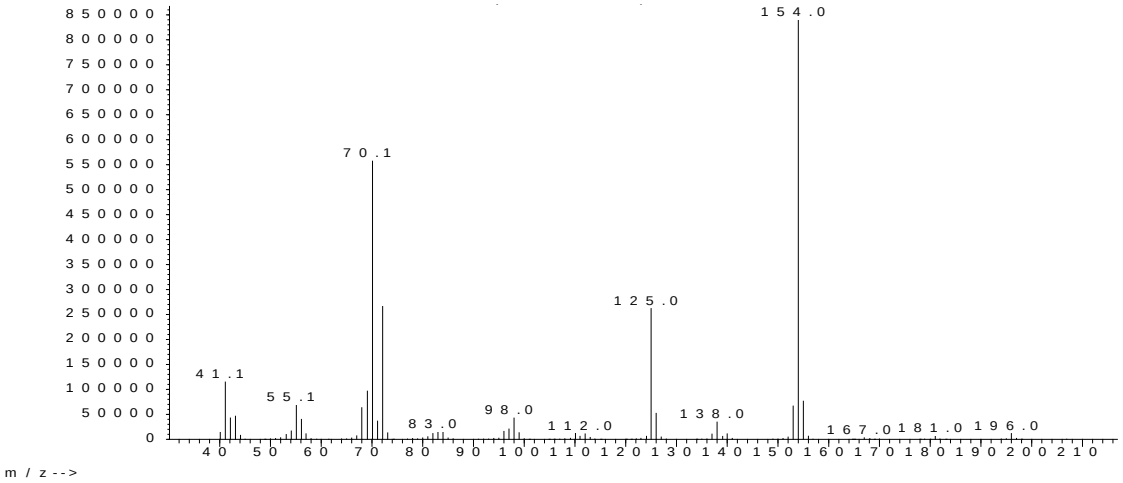

Figure 86. Mass spectrum (EIMS) of metabolite **16**.

In the ^{1}H NMR spectrum of metabolite **16** (Fig. 87) obvious were:

- two doublet signals at δ_H 0.89 and 1.04, integrating for three protons each and attributed to two methyl groups on tertiary carbon atoms,
- two signals at δ_H 3.92 and 4.07, integrating for one proton each and attributed to two H_α methines of two aminoacids, and
- one signal at δ_H 5.67, attributed to one exchangeable proton of an amine.

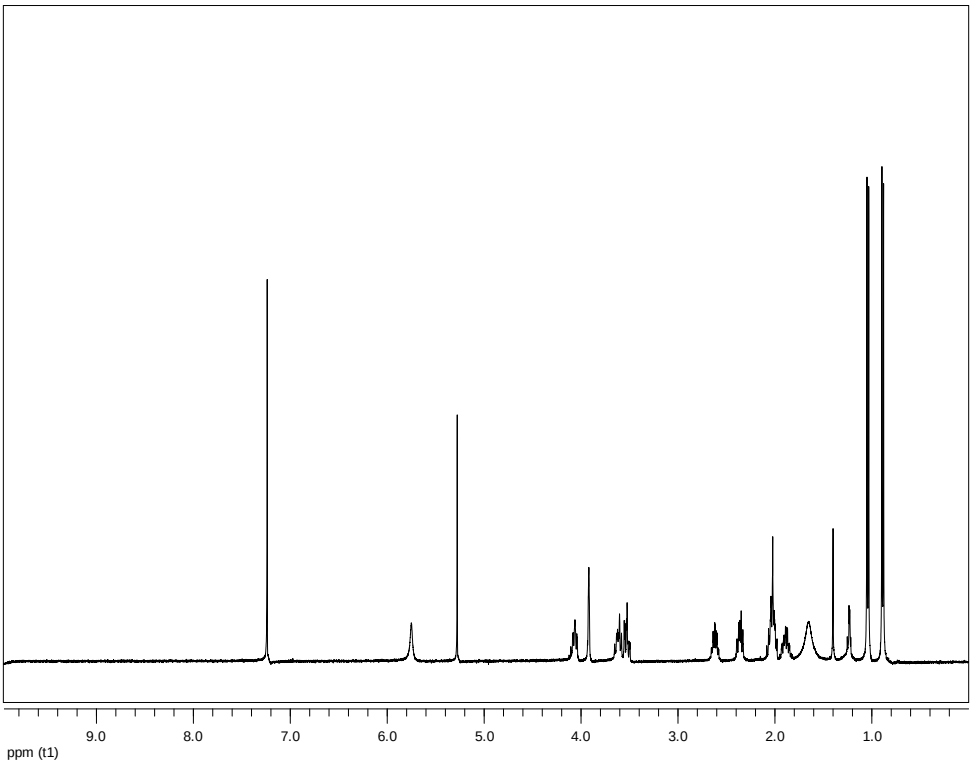

Figure 87. ^{1}H NMR spectrum of metabolite **16**.

Analysis of the NMR and MS data of **16** led to the molecular formula $C_{10}H_{16}N_2O_2$, corresponding to four degrees of unsaturation. The spectroscopic data of metabolite **16** were indicative of a 2,5-diketopiperazine skeleton.

The planar structure of metabolite **16** was determined on the basis of the homonuclear correlations observed in the COSY (Fig. 88) spectrum. In particular, the cross-peaks of H-3 / H-10, H-10 / H_3-11, H-10 / H_3-12, and H-3 / NH-4, as well as of H-6 / H_2-7, H_2-7 / H_2-8 and H_2-8 / H_2-9 suggested two distinct spin systems, indicative of a valine and a proline residue, respectively.

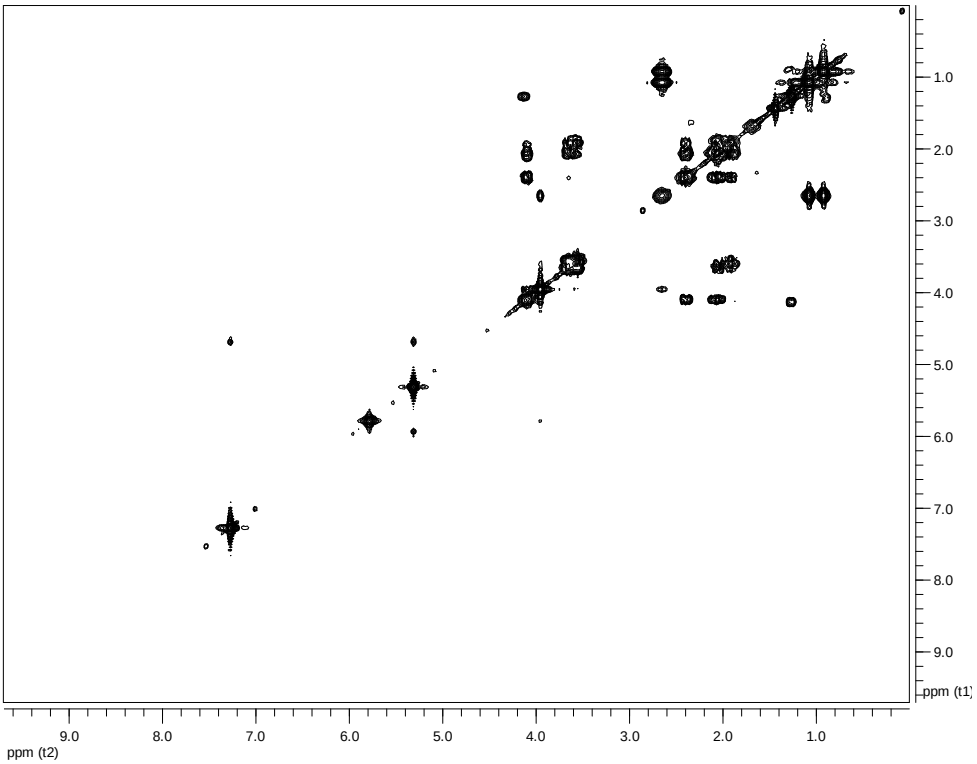

Figure 88. COSY spectrum of metabolite **16**.

Comparison of the spectroscopic and physical characteristics of metabolite **16** with those reported in the literature led to its identification as *cis-cyclo*(L-Pro-L-Val) (Tezuka et al., 1994). The ^{1}H NMR data of metabolite **16** are reported in Table 103.

Table 103. ^{1}H NMR data of metabolite **16** in $CDCl_3$ (δ in ppm, J in Hz).

Position	δ_H
3	3.92, brs
4	5.67, brs
6	4.07, t (8.1)
7	2.37, m, 2.02, m
8	2.02, m, 1.89, m
9	3.62, m, 3.53, m
10	2.62, m
11	0.89, d (6.8)
12	1.04, d (7.3)

3.1.17. Metabolite 17

Metabolite **17** was isolated after a series of chromatographic separations as a colourless oil (4.9 mg).

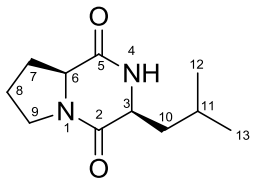

17

The mass spectrum of metabolite **17** (Fig. 89) exhibited a molecular ion peak $[M]^+$ at *m/z* 210.

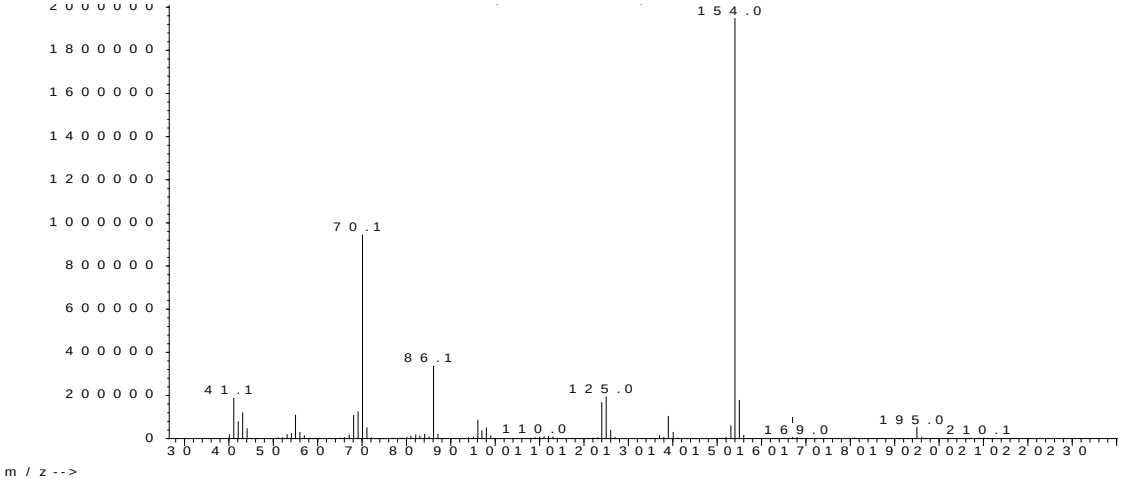

Figure 89. Mass spectrum (EIMS) of metabolite **17**.

In the ^{1}H NMR spectrum of metabolite **17** (Fig. 90) obvious were:

- two doublet signals at δ_H 0.94 and 0.98, integrating for three protons each and attributed to two methyl groups on tertiary carbon atoms,
- two signals at δ_H 4.00 and 4.10, integrating for one proton each and attributed to two H_α methines of two aminoacids, and
- one signal at δ_H 5.78, attributed to one exchangeable proton of an amine.

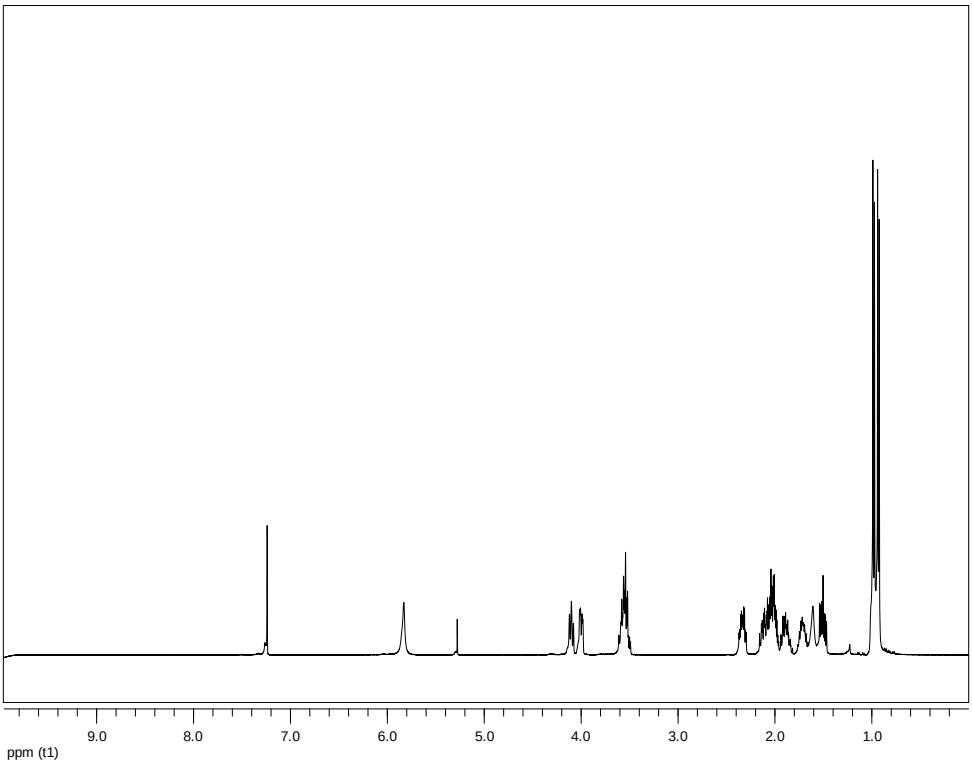

Figure 90. ^{1}H NMR spectrum of metabolite **17**.

Analysis of the NMR and MS data of **17** led to the molecular formula $C_{11}H_{18}N_2O_2$, corresponding to four degrees of unsaturation. The spectroscopic data of metabolite **17** were indicative of a 2,5-diketopiperazine skeleton.

The planar structure of metabolite **17** was determined on the basis of the homonuclear correlations observed in the COSY (Fig. 91) spectrum. In particular, the cross-peaks of H-3 / H_2-10, H_2-10 / H-11, H-11 / H_3-12, H-11 / H_3-13, and H-3 / NH-4, as well as of H-6 / H_2-7, H_2-7 / H_2-8 and H_2-8 / H_2-9 suggested two distinct spin systems, indicative of a leucine and a proline residue, respectively.

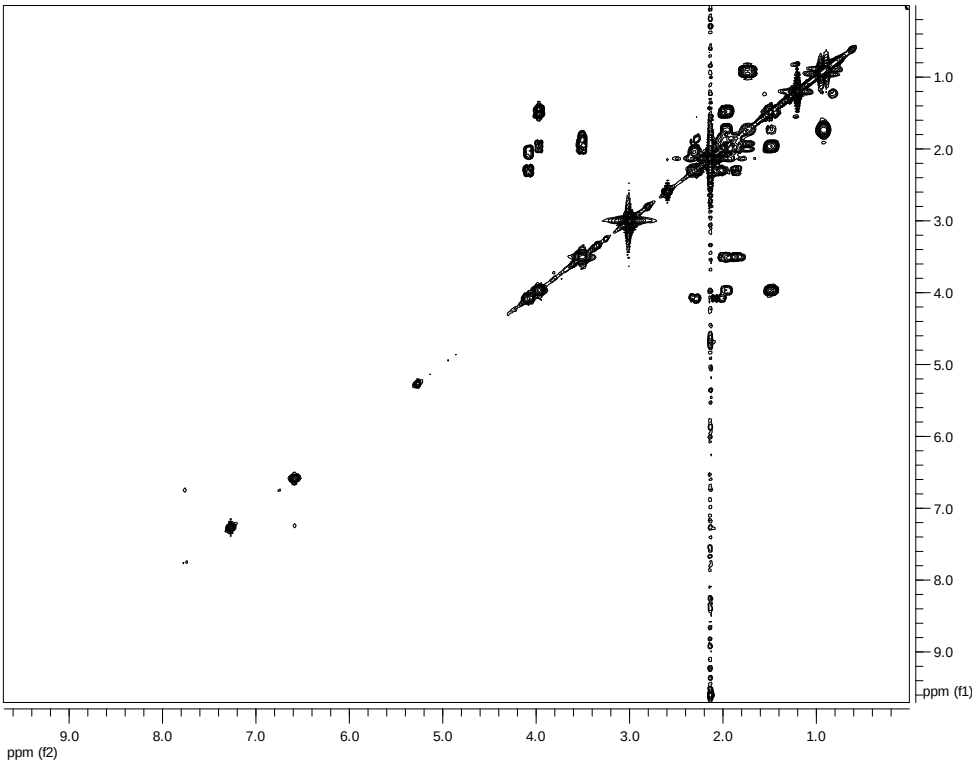

Figure 91. COSY spectrum of metabolite **17**.

Comparison of the spectroscopic and physical characteristics of metabolite **17** with those reported in the literature led to its identification as *cis-cyclo*(L-Pro-L-Leu) (Adamczeski et al., 1995). The ^{1}H NMR data of metabolite **17** are reported in Table 104.

Table 104. ^{1}H NMR data of metabolite **17** in $CDCl_3$ (δ in ppm, J in Hz).

Position	δ_H
3	4.00, dd (9.7, 3.6)
4	5.78, brs
6	4.10, t (8.2)
7	2.33, m, 2.12, m
8	2.01, m, 1.89, m
9	3.55, m
10	2.05, m, 1.51, ddd (14.5, 9.7, 5.0)
11	1.71, m
12	0.94, d (6.6)
13	0.98, d (6.5)

3.1.18. Metabolite 18

Metabolite **18** was isolated after a series of chromatographic separations as a colourless oil (9.0 mg).

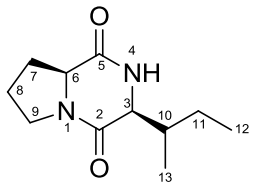

18

The mass spectrum of metabolite **18** (Fig. 92) exhibited a molecular ion peak $[M]^+$ at *m/z* 210.

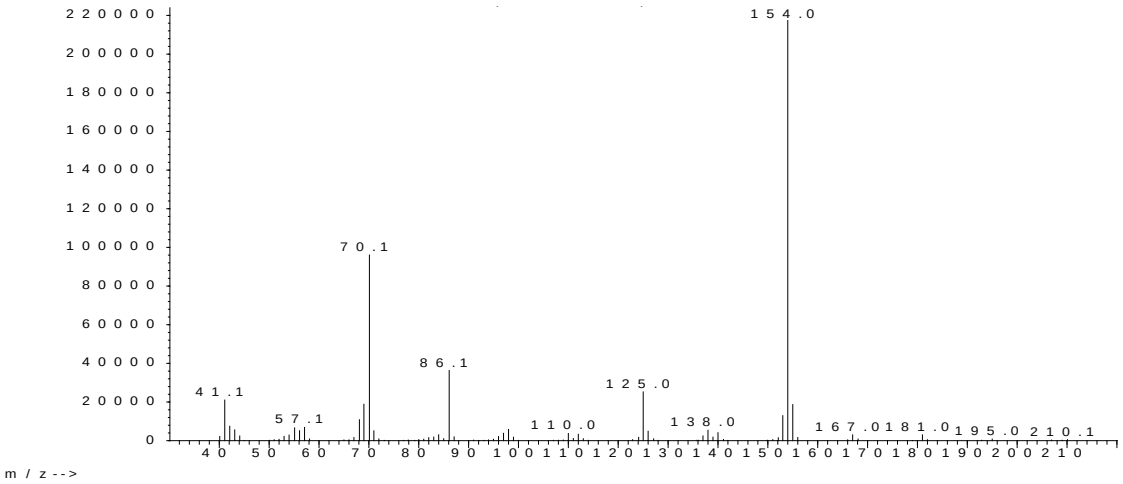

Figure 92. Mass spectrum (EIMS) of metabolite **18**.

In the ^{1}H NMR spectrum of metabolite **18** (Fig. 93) obvious were:

- one doublet signal at δ_H 1.03 and one triplet signal at δ_H 0.91, integrating for three protons each and attributed to a methyl group on a tertiary carbon atom and a methyl group on a secondary carbon atom, respectively,
- two signals at δ_H 3.95 and 4.05, integrating for one proton each and attributed to two H_α methines of two aminoacids, and
- one signal at δ_H 5.74, attributed to one exchangeable proton of an amine.

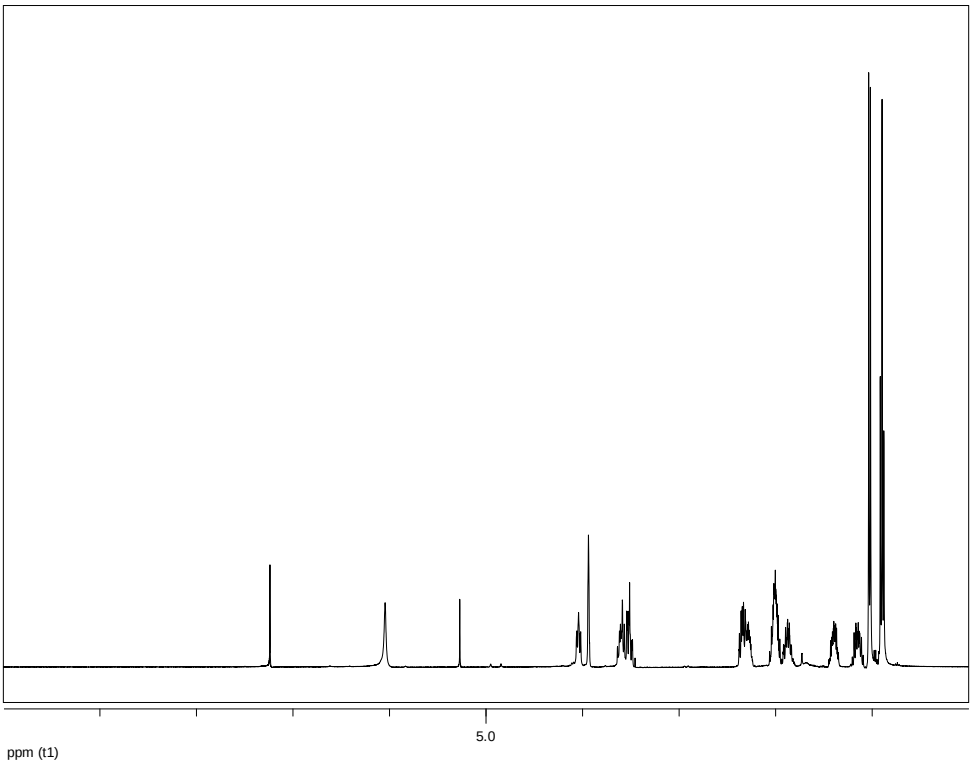

Figure 93. ^{1}H NMR spectrum of metabolite **18**.

Analysis of the NMR and MS data of **18** led to the molecular formula $C_{11}H_{18}N_2O_2$, corresponding to four degrees of unsaturation. The spectroscopic data of metabolite **18** were indicative of a 2,5-diketopiperazine skeleton.

The planar structure of metabolite **18** was determined on the basis of the homonuclear correlations observed in the COSY (Fig. 94) spectrum. In particular, the cross-peaks of H-3 / H-10, H-10 / H_3-13, H-10 / H_2-11, H_2-11 / H_3-12 and H-3 / NH-4, as well as of H-6 / H_2-7, H_2-7 / H_2-8 and H_2-8 / H_2-9 suggested two distinct spin systems, indicative of an isoleucine and a proline residue, respectively.

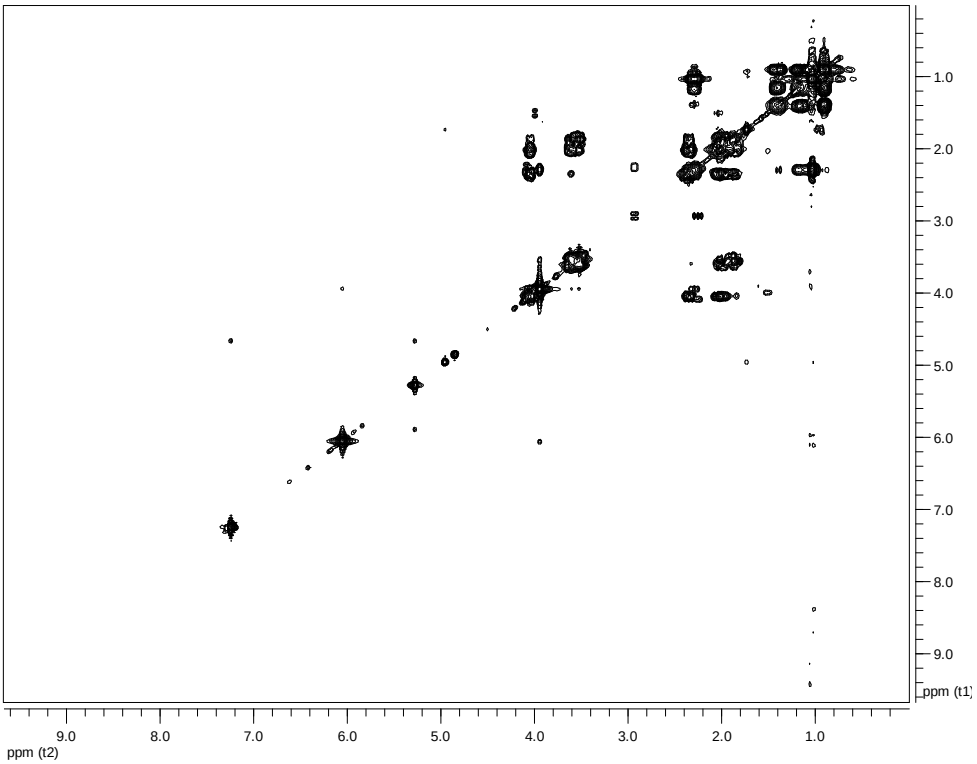

Figure 94. COSY spectrum of metabolite **18**.

Comparison of the spectroscopic and physical characteristics of metabolite **18** with those reported in the literature led to its identification as *cis-cyclo*(L-Pro-L-Ile) (Adamczeski et al., 1995). The ^{1}H NMR data of metabolite **18** are reported in Table 105.

Table 105. ^{1}H NMR data of metabolite **18** in $CDCl_3$ (δ in ppm, J in Hz).

Position	δ_H
3	3.95, brs
4	5.74, brs
6	4.05, brt (8.2)
7	2.36, m, 2.02, m
8	2.02, m, 1.89, m
9	3.61, m, 3.53, m
10	2.30, m
11	1.41, m, 1.14, m
12	0.91, t (7.4)
13	1.03, d (7.2)

3.1.19. Metabolite 19

Metabolite **19** was isolated after a series of chromatographic separations as a colourless oil (2.6 mg).

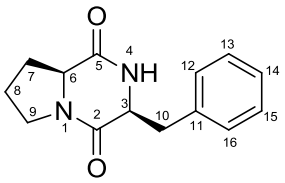

19

The mass spectrum of metabolite **19** (Fig. 95) exhibited a molecular ion peak $[M]^+$ at *m/z* 244.

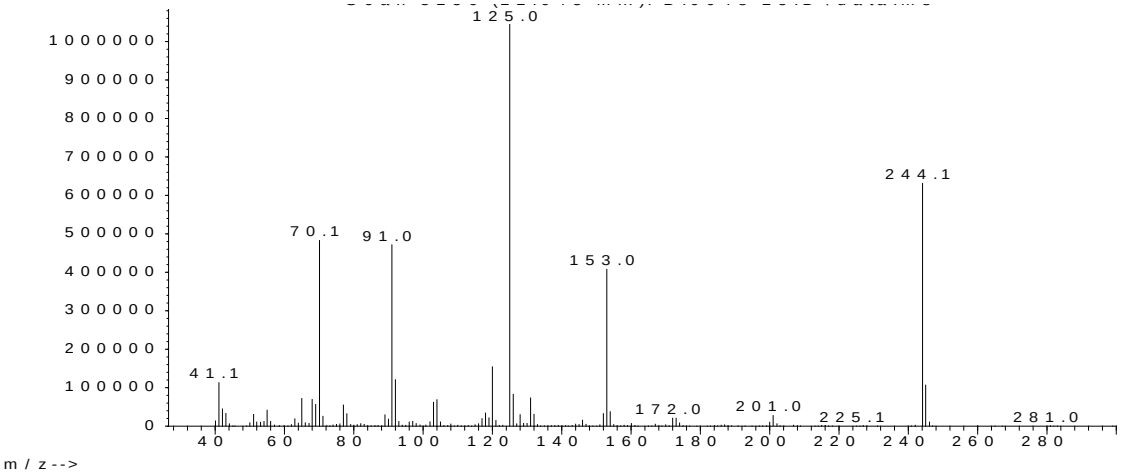

Figure 95. Mass spectrum (EIMS) of metabolite **19**.

In the ^{1}H NMR spectrum of metabolite **19** (Fig. 96) obvious were:

- two signals at δ_H 4.05 and 4.25, integrating for one proton each and attributed to two H_α methines of two aminoacids,
- one signal at δ_H 5.69, attributed to one exchangeable proton of an amine, and
- signals at δ_H 7.20-7.33 integrating for five protons in total with coupling constants characteristic for a mono-substituted aromatic ring.

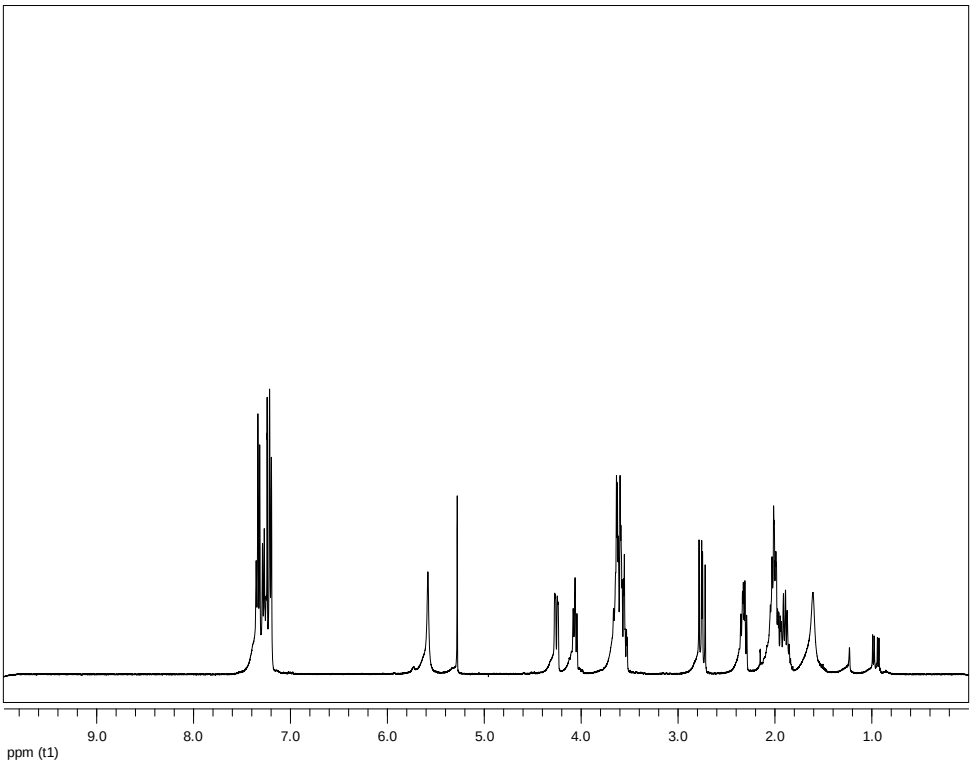

Figure 96. ^{1}H NMR spectrum of metabolite **19**.

Analysis of the NMR and MS data of **19** led to the molecular formula $C_{14}H_{16}N_2O_2$, corresponding to eight degrees of unsaturation. The spectroscopic data of metabolite **19** were indicative of a 2,5-diketopiperazine skeleton.

The planar structure of metabolite **19** was determined on the basis of the homonuclear correlations observed in the COSY (Fig. 97) spectrum. In particular, the cross-peaks of H-3 / H_2-10 and H-3 / NH-4, in combination with the presence of a mono-substituted aromatic ring indicated a phenylalanine residue, while the correlations of H-6 / H_2-7, H_2-7 / H_2-8 and H_2-8 / H_2-9 suggested a proline residue.

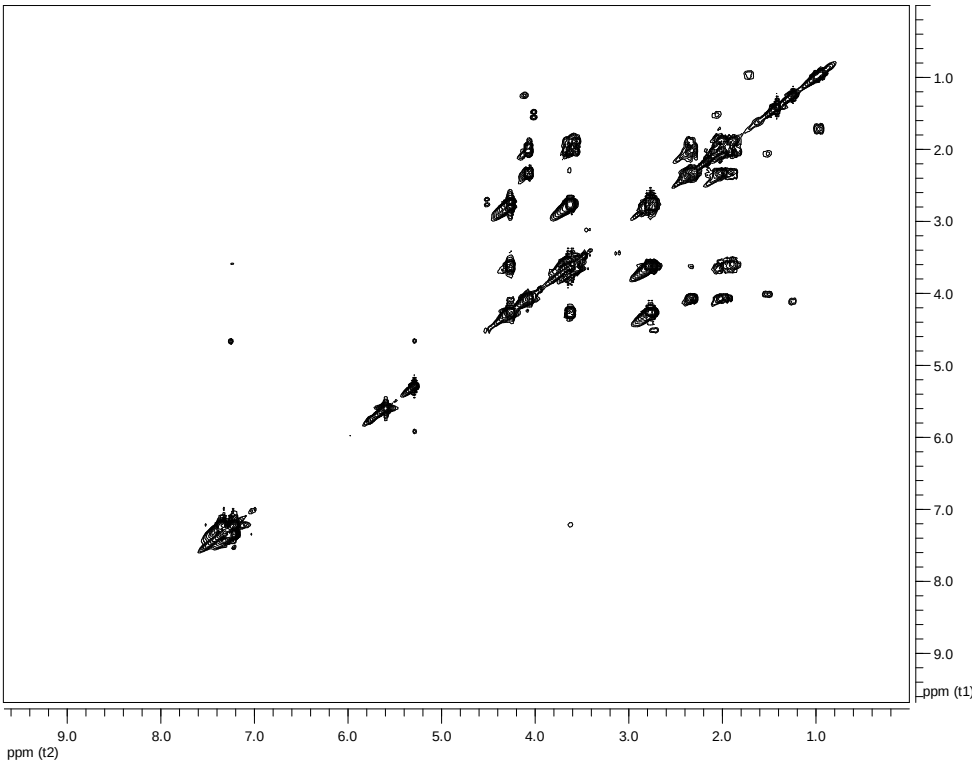

Figure 97. COSY spectrum of metabolite **19**.

Comparison of the spectroscopic and physical characteristics of metabolite **19** with those reported in the literature led to its identification as *cis-cyclo*(L-Pro-L-Phe) (Adamczeski et al., 1995). The ^{1}H NMR data of metabolite **19** are reported in Table 106.

Table 106. ^{1}H NMR data of metabolite **19** in $CDCl_3$ (δ in ppm, J in Hz).

Position	δ_H
3	4.25, dd (10.5, 3.5)
4	5.69, brs
6	4.05, t (8.0)
7	2.31, m, 2.02, m
8	2.02, m, 1.88, m
9	3.62, m, 3.60, m
10	3.62, m, 2.76, dd (14.5, 10.6)
12	7.20, d (7.2)
13	7.33, t (7.2)
14	7.28, t (7.2)
15	7.33, t (7.2)
16	7.20, d (7.2)

3.1.20. Metabolite 20

Metabolite **20** was isolated after a series of chromatographic separations as a colourless oil (16.8 mg).

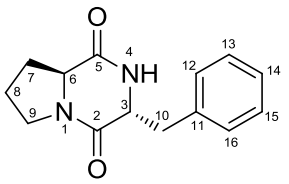

20

The mass spectrum of metabolite **20** (Fig. 98) exhibited a molecular ion peak $[M]^+$ at *m/z* 244.

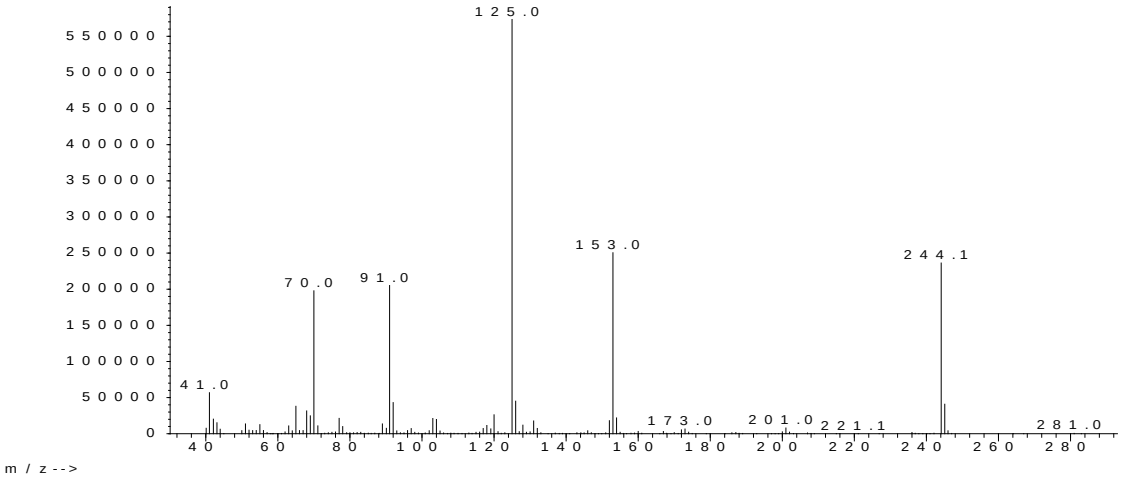

Figure 98. Mass spectrum (EIMS) of metabolite **20**.

In the ^{1}H NMR spectrum of metabolite **20** (Fig. 99) obvious were:

- two signals at δ_H 3.04 and 4.19, integrating for one proton each and attributed to two H_α methines of two aminoacids,
- one signal at δ_H 5.76, attributed to one exchangeable proton of an amine, and
- signals at δ_H 7.19-7.30 integrating for five protons in total with coupling constants characteristic for a mono-substituted aromatic ring.

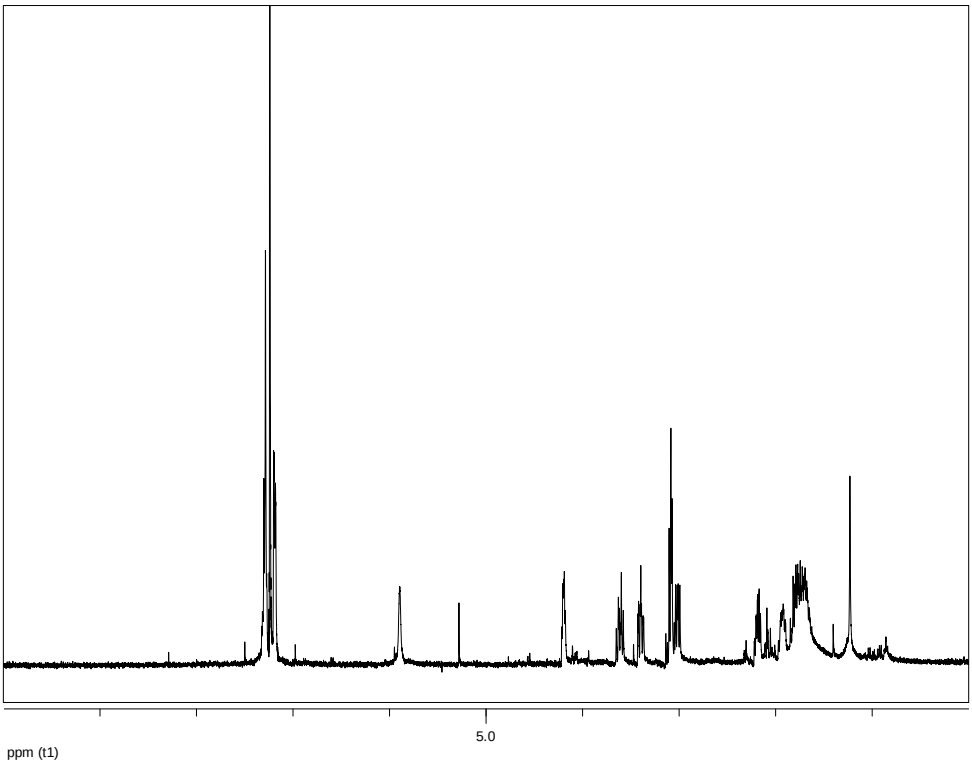

Figure 99. ^{1}H NMR spectrum of metabolite **20**.

Analysis of the NMR and MS data of **20** led to the molecular formula $C_{14}H_{16}N_2O_2$, corresponding to eight degrees of unsaturation. The spectroscopic data of metabolite **20** were indicative of a 2,5-diketopiperazine skeleton.

The planar structure of metabolite **20** was determined on the basis of the homonuclear correlations observed in the COSY (Fig. 100) spectrum. In particular, the cross-peaks of H-3 / H_2-10 and H-3 / NH-4, in combination with the presence of a mono-substituted aromatic ring indicated a phenylalanine residue, while the correlations of H-6 / H_2-7, H_2-7 / H_2-8 and H_2-8 / H_2-9 suggested a proline residue.

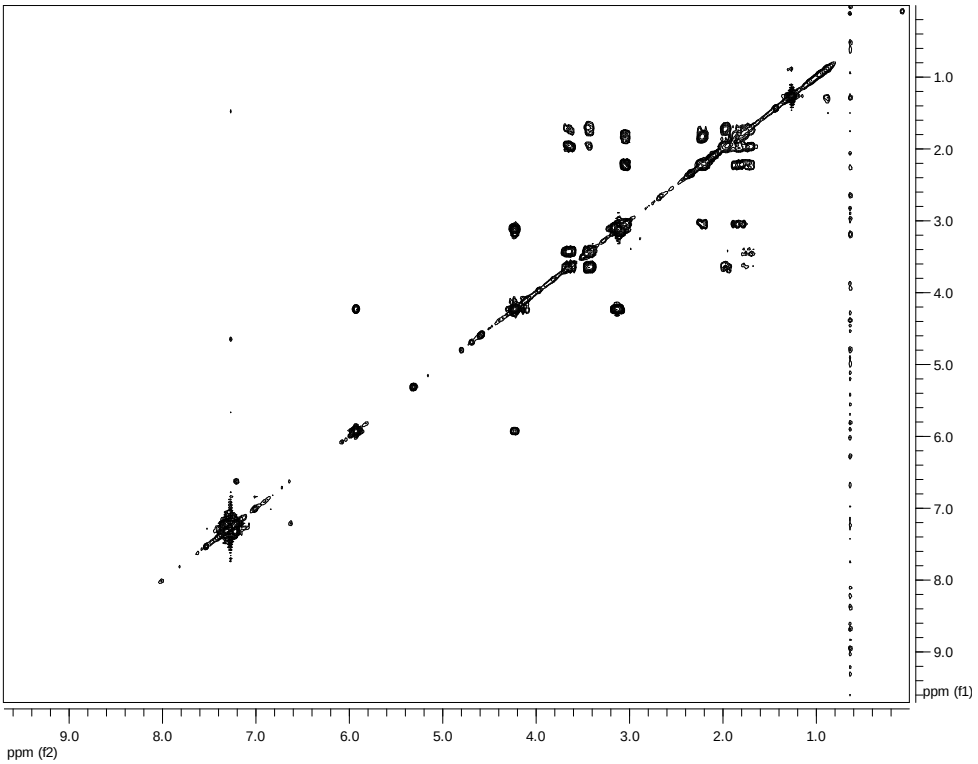

Figure 100. COSY spectrum of metabolite **20**.

Comparison of the spectroscopic and physical characteristics of metabolite **20** with those reported in the literature led to its identification as *trans-cyclo*(L-Pro-L-Phe), a stereoisomer of metabolite **19** (Wang et al., 2010). The ^{1}H NMR data of metabolite **20** are reported in Table 107.

Table 107. ^{1}H NMR data of metabolite **20** in $CDCl_3$ (δ in ppm, J in Hz).

Position	δ_H
3	4.19, ddd (6.7, 4.3, 4.3)
4	5.76, brs
6	3.04, dd (10.4, 6.6)
7	2.19, m, 1.79, m
8	1.94, m, 1.69, m
9	3.62, ddd (11.9, 9.4, 8.4), 3.40, ddd (12.0, 8.4, 3.0)
10	3.08, m
12	7.19, d (7.3)
13	7.29, t (7.3)
14	7.30, t (7.3)
15	7.29, t (7.3)
16	7.19, d (7.3)

3.1.21. Metabolite 21

Metabolite **21** was isolated after a series of chromatographic separations as a yellowish oil (35.5 mg).

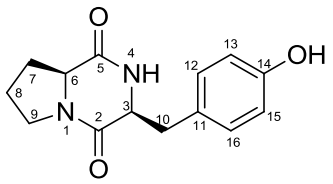

21

The mass spectrum of metabolite **21** (Fig. 101) exhibited a molecular ion peak $[M]^+$ at *m/z* 260.

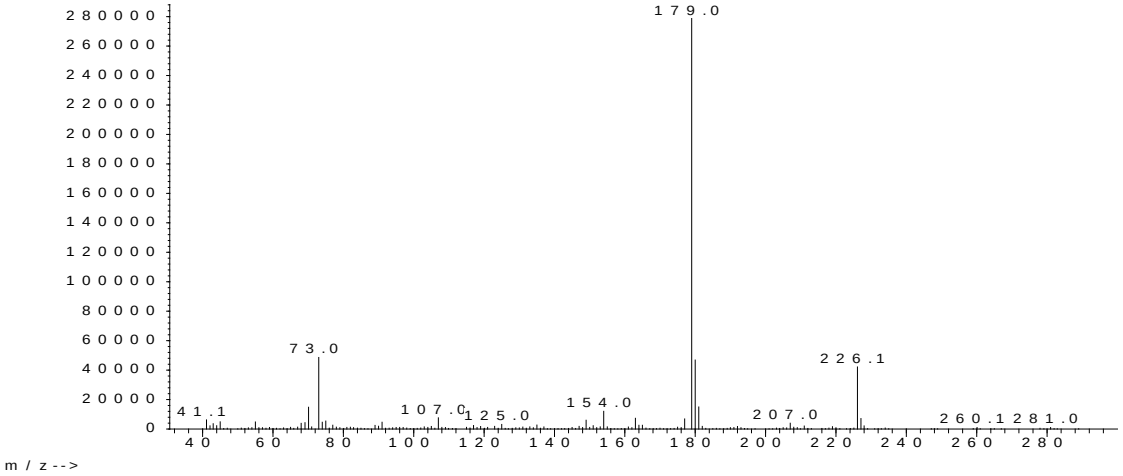

Figure 101. Mass spectrum (EIMS) of metabolite **21**.

In the ^{1}H NMR spectrum of metabolite **21** (Fig. 102) obvious were:

- two signals at δ_H 4.07 and 4.20, integrating for one proton each and attributed to two H_α methines of two aminoacids,
- one signal at δ_H 5.85, attributed to one exchangeable proton of an amine, and
- two doublet signals at δ_H 6.76 and 7.03, integrating for two protons each and corresponding to the protons of a *para*-substituted aromatic ring.

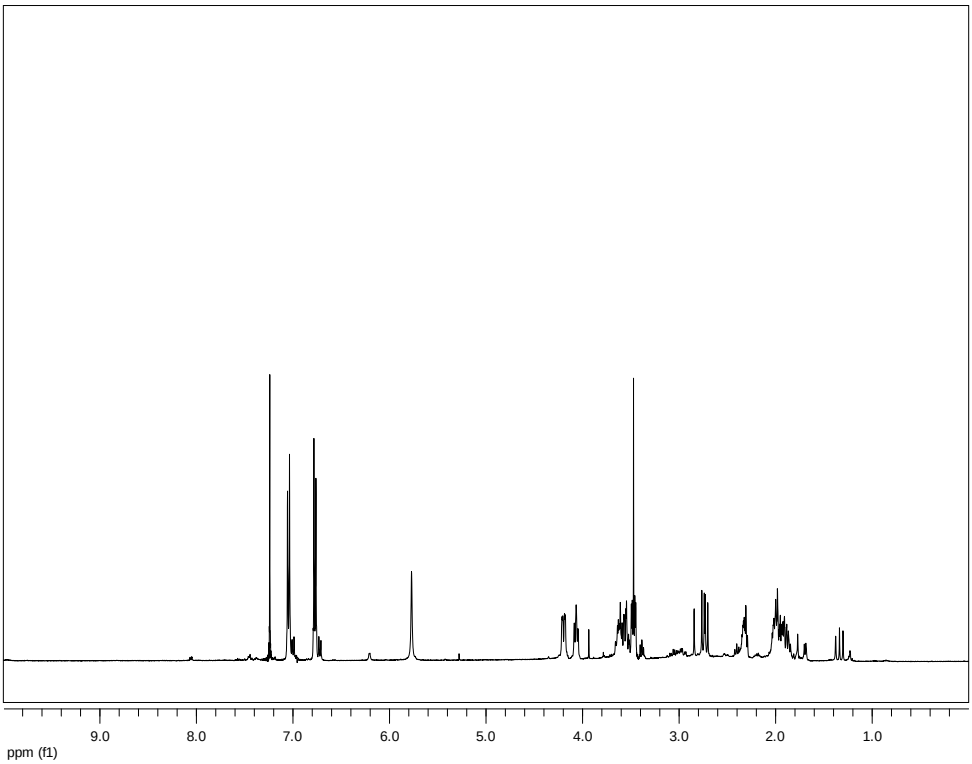

Figure 102. ^{1}H NMR spectrum of metabolite **21**.

Analysis of the NMR and MS data of **21** led to the molecular formula $C_{14}H_{16}N_2O_3$, corresponding to four degrees of unsaturation. The spectroscopic data of metabolite **21** were indicative of a 2,5-diketopiperazine skeleton.

The planar structure of metabolite **21** was determined on the basis of the homonuclear correlations observed in the COSY (Fig. 103) spectrum. In particular, the cross-peaks of H-3 / H_2-10 and H-3 / NH-4, in combination with the presence of a *para*-substituted aromatic ring indicated a tyrosine residue, while the correlations of H-6 / H_2-7, H_2-7 / H_2-8 and H_2-8 / H_2-9 suggested a proline residue.

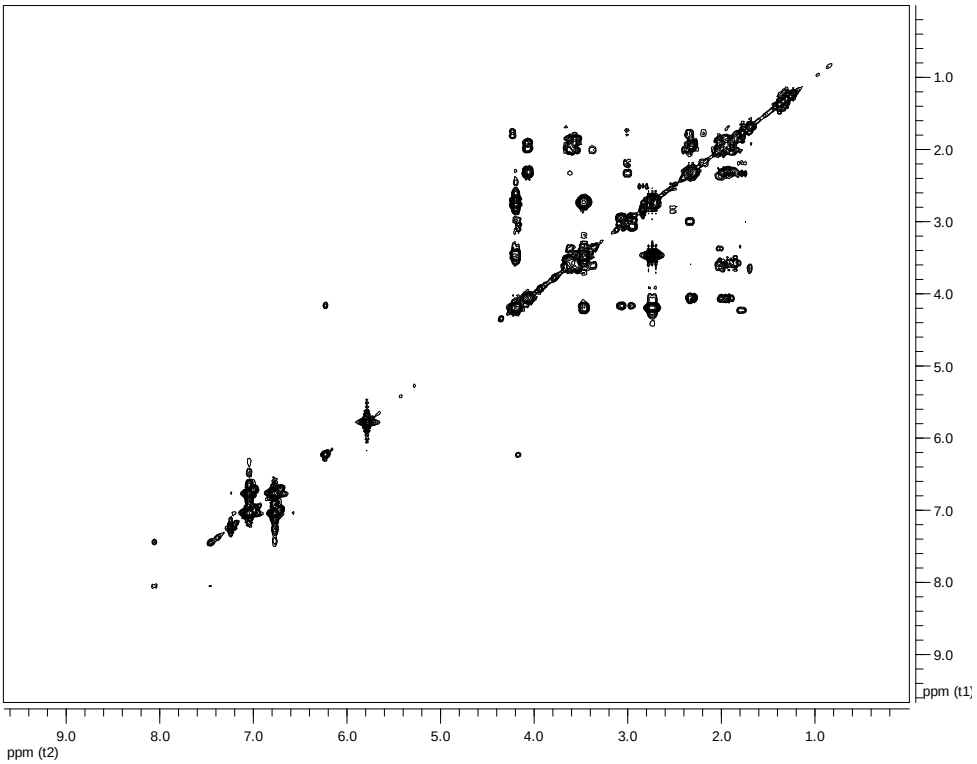

Figure 103. COSY spectrum of metabolite **21**.

Comparison of the spectroscopic and physical characteristics of metabolite **21** with those reported in the literature led to its identification as *cis-cyclo*(L-Pro-L-Tyr) (Kumar et al., 2014). The ^{1}H NMR data of metabolite **21** are reported in Table 108.

Table 108. ^{1}H NMR data of metabolite **21** in $CDCl_3$ (δ in ppm, J in Hz).

Position	$\boldsymbol{\delta_H}$
3	4.20, dd (10.1, 3.4)
4	5.85, brs
6	4.07, d (7.9)
7	2.32, m, 1.94, m
8	2.07, m, 1.87, m
9	3.63, m, 3.55, m
10	3.46, dd (14.7, 3.6), 2.74, dd (14.5, 10.1)
12	7.03, d (8.6)
13	6.76, d (8.6)
15	6.76, d (8.6)
16	7.03, d (8.6)

3.1.22. Metabolite 22

Metabolite **22** was isolated after a series of chromatographic separations as a colourless oil (1.1 mg).

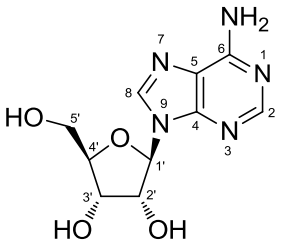

22

The mass spectrum of metabolite **22** (Fig. 104) exhibited a pseudomolecular ion peak $[M+H]^+$ at *m/z* 268.

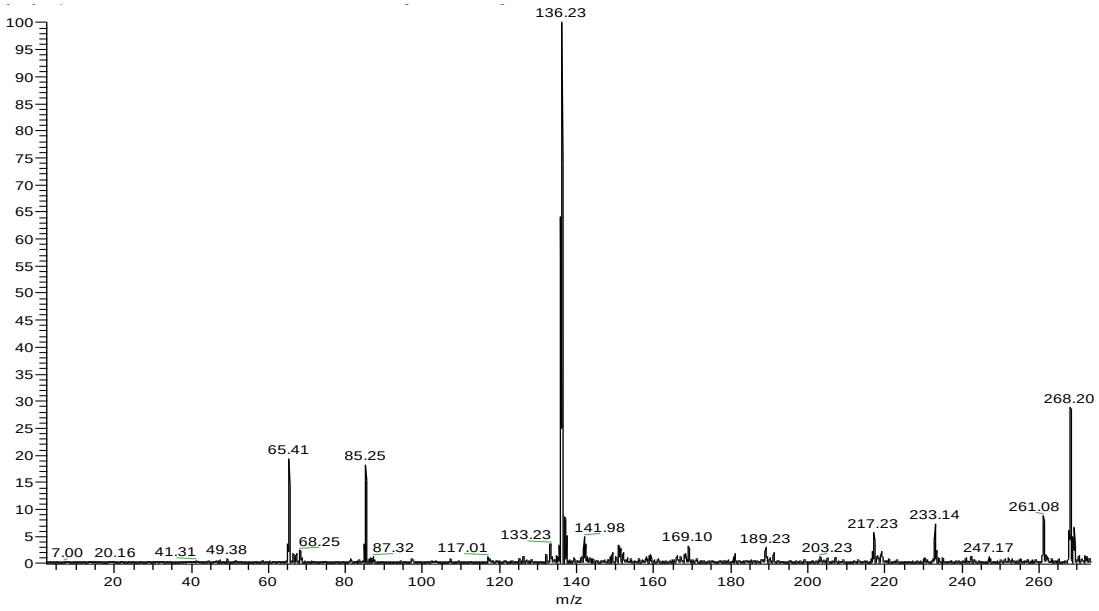

Figure 104. Mass spectrum (CIMS in positive mode) of metabolite **22**.

In the ^{1}H NMR spectrum of metabolite **22** (Fig. 105) five signals at δ_H 3.53, 3.66, 3.95, 4.10 and 4.59, integrating for one proton each and attributed to protons on oxygenated carbon atoms, as well as a signal at δ_H 5.86, attributed to an anomeric proton, suggested the presence of a pentose in the molecule. Additionally, two singlets at δ_H 8.12 and 8.32, integrating for one proton each and corresponding to two deshielded aromatic protons, indicated the presence of a heterocyclic aromatic system.

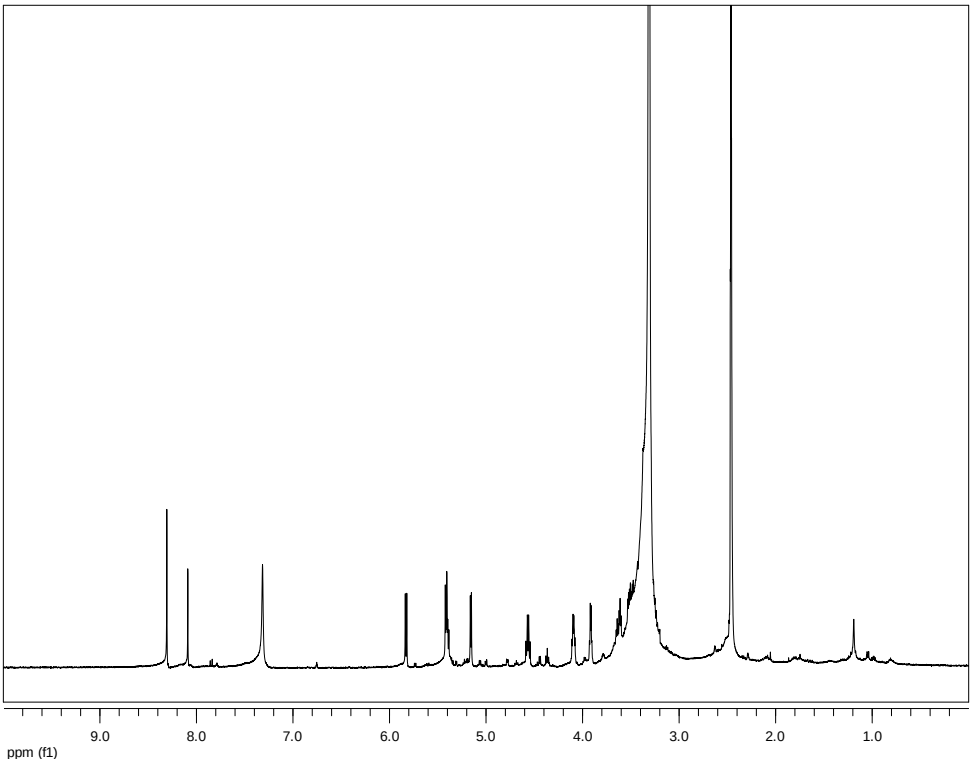

Figure 105. ^{1}H NMR spectrum of metabolite **22**.

Analysis of the NMR and MS data of **22** led to the molecular formula $C_{10}H_{13}N_5O_4$, corresponding to seven degrees of unsaturation. Comparison of the spectroscopic and physical characteristics of metabolite **22** with those reported in the literature led to its identification as adenosine (Jardetzky & Jardetzky, 1959; Jones et al., 1970), a naturally occurring endogenous purine nucleoside which is a fundamental component in biochemical processes, from providing the backbone for basic energy transfer through its adenosine triphosphate (ATP) and adenosine diphosphate (ADP) interactions to its role in signal transduction as cyclic adenosine monophosphate (cAMP) (Layland et al., 2014). The ^{1}H NMR data of metabolite **22** are reported in Table 109.

Table 109. ^{1}H NMR data of metabolite **22** in $(CD_3)_2SO$ (δ in ppm, J in Hz).

Position	δ_H
2	8.12, s
8	8.32, s
1’	5.86, d (6.2)
2’	4.59, m
3’	4.10, m
4’	3.95, m
5’	3.66, ddd (12.0, 4.1, 3.7), 3.53, ddd (12.0, 7.5, 3.7)
6-NH_2	7.31, brs

3.1.23. Metabolite 23

Metabolite **23** was isolated after a series of chromatographic separations as a colourless oil (3.0 mg).

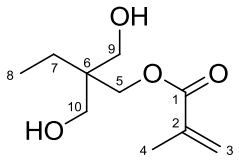

23

The mass spectrum of metabolite **23** (Fig. 106) exhibited a molecular ion peak $[M]^+$ at *m/z* 202.

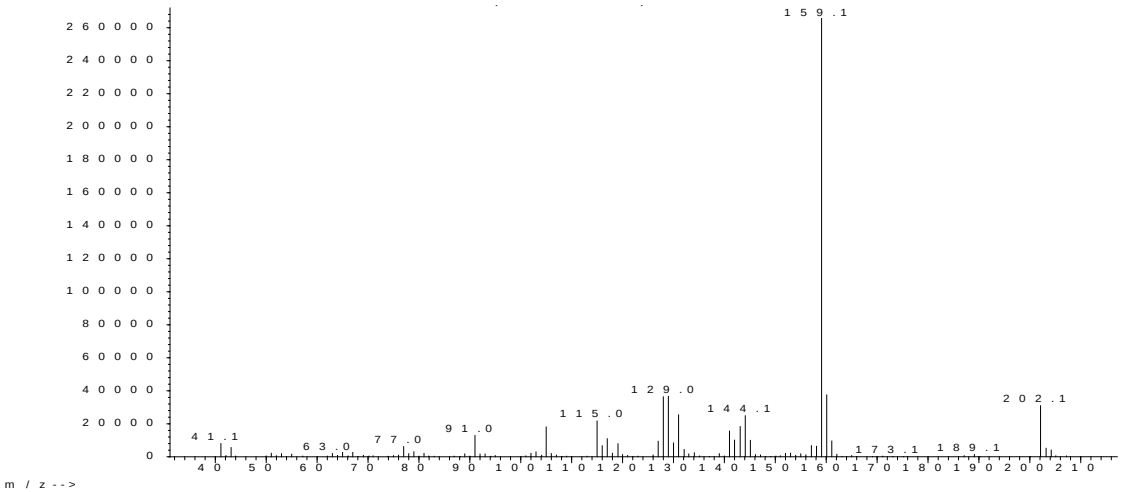

Figure 106. Mass spectrum (EIMS) of metabolite **23**.

In the ^{13}C NMR spectrum of metabolite **23** (Fig. 107) 9 signals were observed, corresponding to 10 carbon atoms. Among them, evident were:

- two signals at δ_C 64.5 and 66.1 corresponding to three oxygenated methylenes,
- two olefinic carbon atoms at δ_C 126.3 and 136.0, and
- one ester carbonyl at δ_C 168.2.

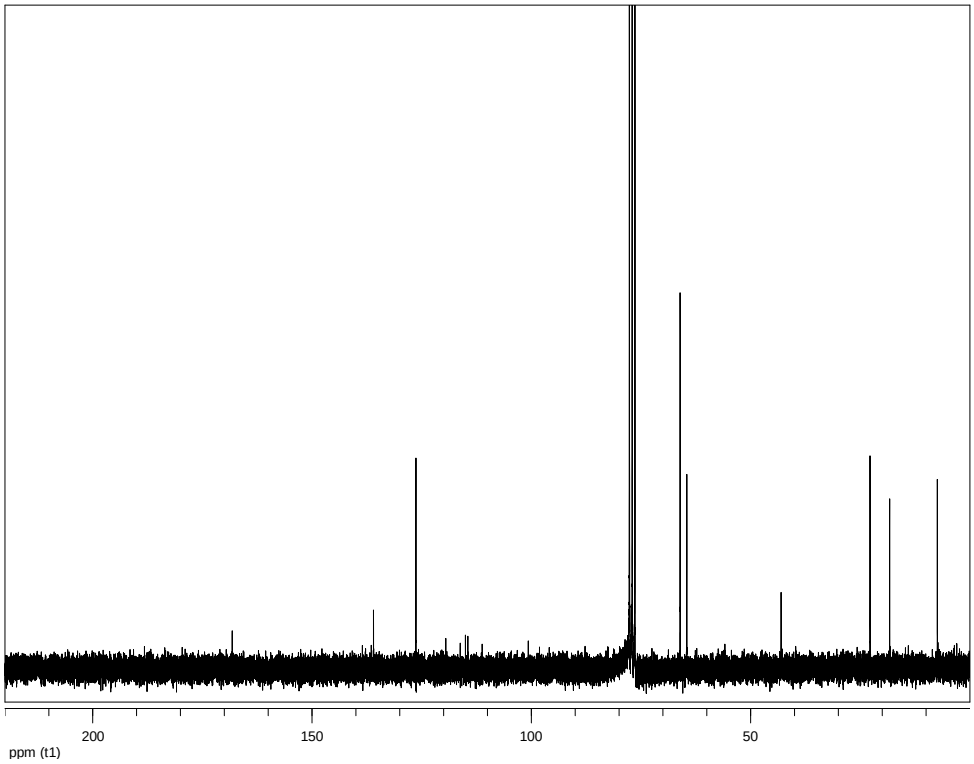

Figure 107. ^{13}C NMR spectrum of metabolite **23**.

In the ^{1}H NMR spectrum of metabolite **23** (Fig. 108) obvious were:

- one triplet at δ_H 0.86, integrating for three protons and attributed to an aliphatic methyl on a secondary carbon atom,
- one singlet at δ_H 1.94, integrating for three protons and attributed to a vinyl methyl,
- two doublets at δ_H 3.55 and 3.60, corresponding to two equivalent oxygenated methylenes,
- one singlet at δ_H 4.27, integrating for two protons and corresponding to an isolated oxygenated methylene, and
- two singlets at δ_H 5.60 and 6.12, corresponding to two olefinic protons of a 1,1-di-substituted double bond.

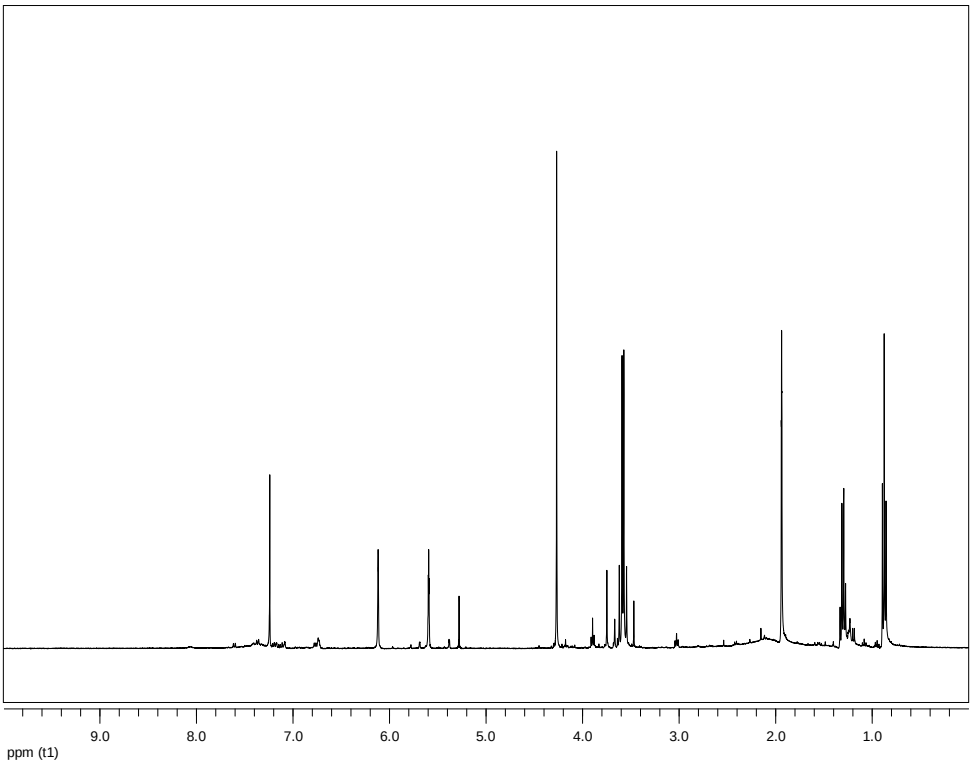

Figure 108. ^{1}H NMR spectrum of metabolite **23**.

Analysis of the NMR and MS data of **23** led to the molecular formula $C_{10}H_{18}O_4$. Taking into account the carbon-carbon double bonds and the carbonyl moiety as the two degrees of unsaturation, compound **23** was determined as acyclic.

The structure of metabolite **23** was determined on the basis of the homonuclear and heteronuclear correlations observed in the HSQC-DEPT (Fig. 109), HMBC (Fig. 110) and COSY (Fig. 111) spectra.

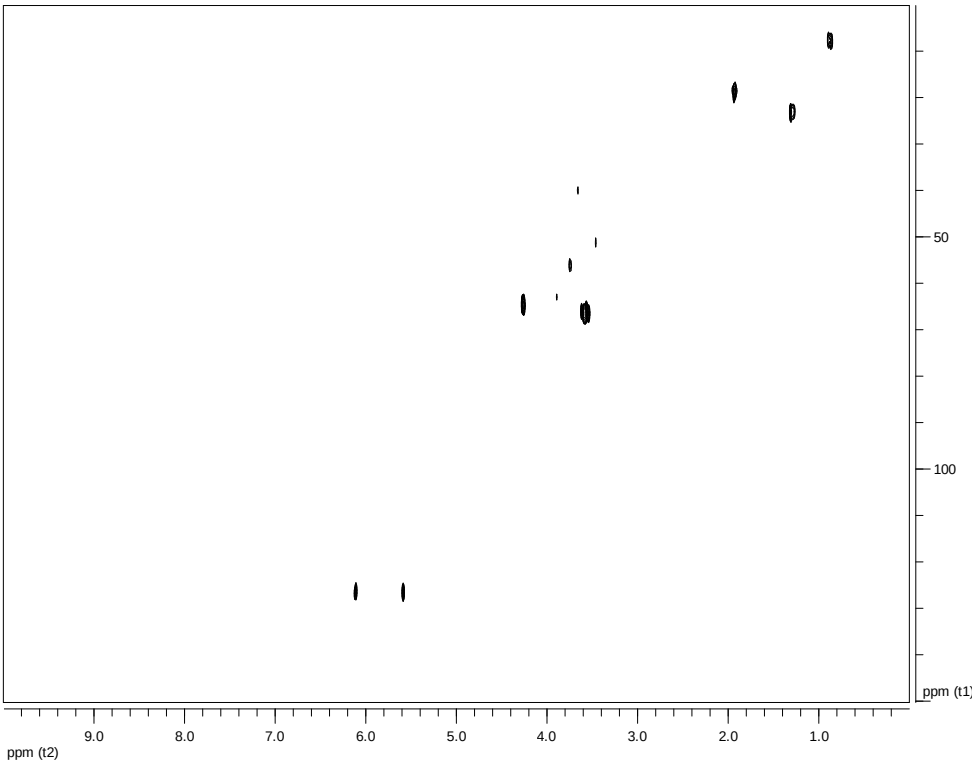

Figure 109. HSQC-DEPT spectrum of metabolite **23**.

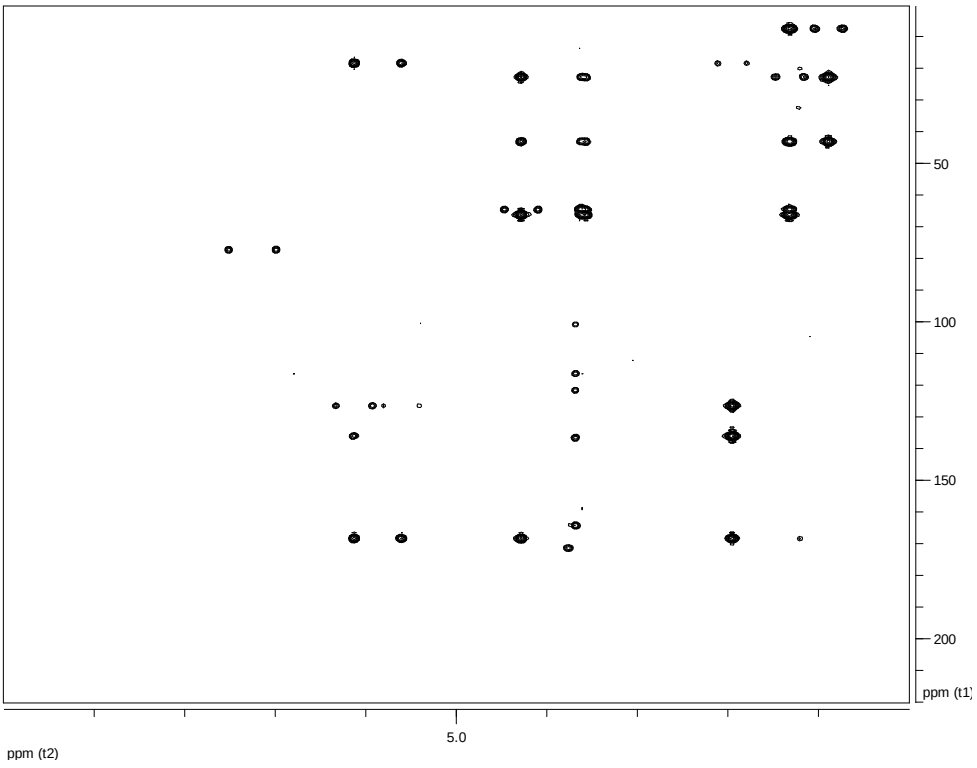

Figure 110. HMBC spectrum of metabolite **23**.

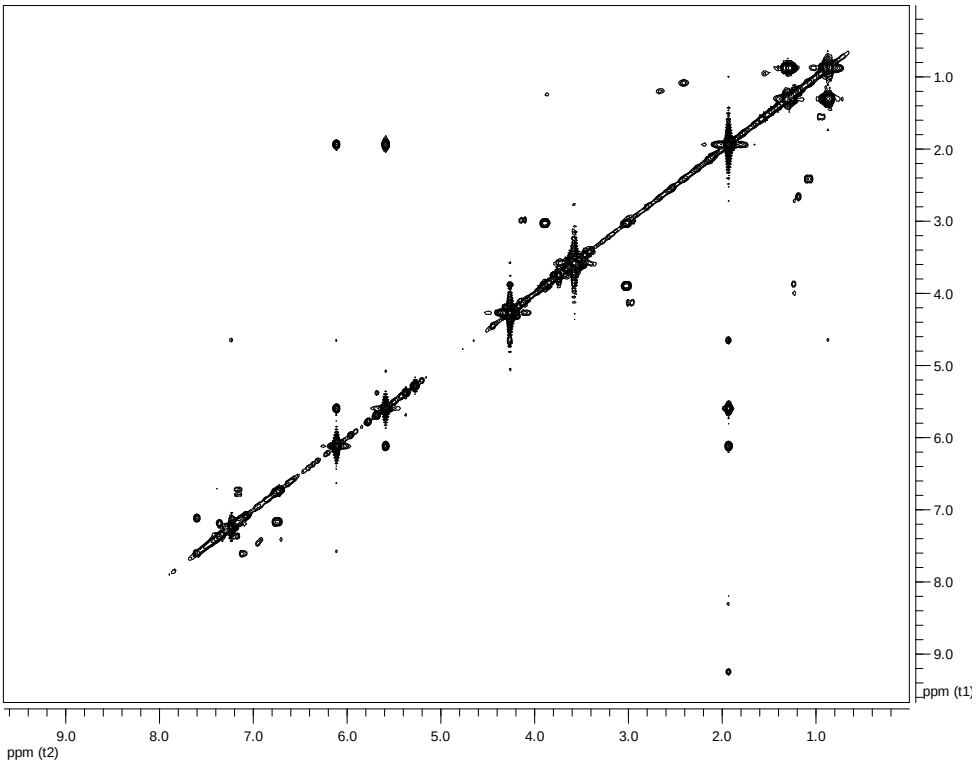

Figure 111. COSY spectrum of metabolite **23**.

Comparison of the spectroscopic and physical characteristics of metabolite **23** with those reported in the literature led to its identification as a compound bearing a rare methacrylate residue, reported for the first time as a natural product. The ^{1}H and ^{13}C NMR data of metabolite **23** are reported in Table 110.

Table 110. ^{1}H NMR data of metabolite **23** in $CDCl_3$ (δ in ppm, J in Hz).

Position	δ_C	δ_H
1	168.2	
2	136.0	
3	126.3	6.12, s, 5.60, s
4	18.3	1.94, s
5	64.5	4.27, s
6	43.0	
7	22.8	1.30, q (7.6)
8	7.4	0.86, t (7.6)
9	66.1	3.60, d (11.2), 3.55, d (11.2)
10	66.1	

3.2. Evaluation of the biological activity of the isolated metabolites

Until now, compounds **1**–**10** have been evaluated for their antibacterial activities against the epidemic methicillin-resistant strain EMRSA-15 and the multidrug-resistant effluxing strain SA1199B of *S. aureus*, as well as the *E. coli* strain NCTC-10418. Furthermore, the cytotoxic activities of **1**–**10** have been tested against the MCF7 (breast adenocarcinoma) and A549 (lung carcinoma) human cancer cell lines. However, metabolites **1**–**10** were proven inactive in both bioactivity assays.

CONCLUSIONS

Within the framework of the present PhD thesis, a number of marine-derived bacterial strains deposited at the strain collection/microbank of the Section of Pharmacognosy and Chemistry of Natural Products, Department of Pharmacy, National and Kapodistrian University of Athens, were cultivated in small-scale liquid cultures and the obtained organic extracts were screened for their chemical profiles using high pressure liquid chromatography (HPLC). Among them, strain BI0048, isolated from the inner tissues of the red alga *Laurencia glandulifera*, exhibited an interesting chemical profile and was thus selected for further chemical investigation.

The algicolous endophytic strain, which was identified as *Streptomyces ambofaciens*, was cultured in large-scale in flasks containing a seawater-based liquid medium that were incubated at 37 °C for 8 days while shaking at 130 rpm in an orbit shaker. At the end of the fermentation period, Amberlite XAD-7HP resin was added to each flask to adsorb extracellular metabolites. The culture and resin were shaken overnight at low speed. The resin and cell mass were collected by filtration through cheesecloth and washed with deionized water to remove salts. Subsequently, the resin, cell mass and cheesecloth were extracted for with acetone. Filtration of the extract and removal of the solvent under vacuum at 40 °C afforded a solid residue that was subjected to a multi-step fractionation scheme using normal and reversed-phase vacuum column chromatography, gravity column chromatography and HPLC to allow for the isolation of a number of metabolites. The structural characterization of the isolated metabolites was based on thorough analyses of their spectroscopic data, employing mainly nuclear magnetic resonance (NMR) spectroscopy and mass (MS) spectrometry, as well as infrared (IR) and ultraviolet-visible (UV-Vis) spectroscopy, and comparison of their spectroscopic and physical characteristics with those of relevant compounds previously reported in the literature.

In total, 23 metabolites were isolated and identified from the organic extract of the actinobacterial strain BI0048, including ten polyketides (**1**-**10**), four simple aromatic compounds (**11**-**14**), seven diketopiperazines (**15**-**21**), one nucleoside (**22**) and compound **23** bearing a methacrylate residue.

In particular, the isolated polyketides were identified as enterocin (**1**), also known as vulgamycin, 5-deoxy-enterocin (**2**), wailupemycin D (**3**), wailupemycin E (**4**),

zoumbericin A (**5**), zoumbericin B (**6**), germicidin A (**7**), germicidin B (**8**), germicidin K (**9**) and germicidin L (**10**). Among them, 4 metabolites (**5**, **6**, **9** and **10**) are new natural products. All the isolated polyketides feature an α-pyrone moiety, which constitutes an essential pharmacophore in many naturally occurring and synthetic bioactive compounds. Natural products featuring a α-pyrone ring are often involved in defense processes, while frequently they possess antibacterial, antifungal, antiviral, cytotoxic, phytotoxic and neurotoxic properties.

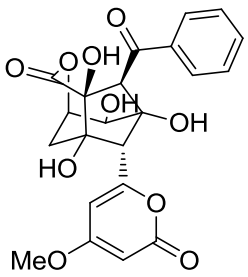

1

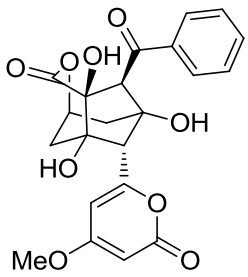

2

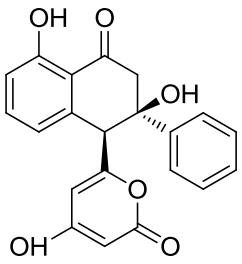

3

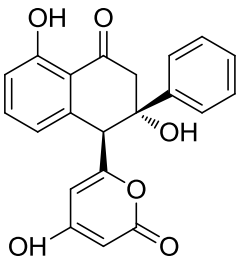

4

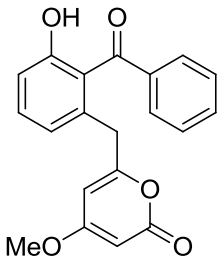

5

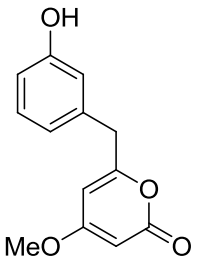

6

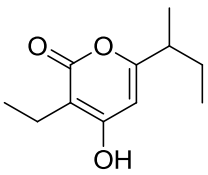

7

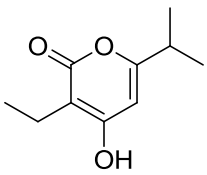

8

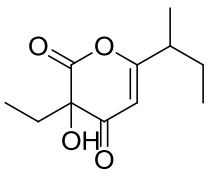

9

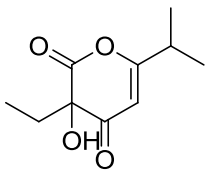

10

Furthermore, four simple aromatic compounds were isolated and identified as benzoic acid (**11**), hydrocinnamic acid (**12**), (*E*)-cinnamic acid (**13**) and tyrosol (**14**), also known as *p*-hydroxy-phenethyl alcohol.

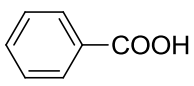

11

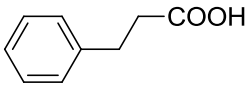

12

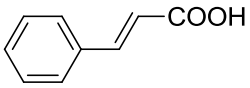

13

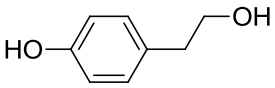

14

The isolated diketopiperazines were identified as *cis-cyclo*(L-Pro-L-Ala) (**15**), *cis-cyclo*(L-Pro-L-Val) (**16**), *cis-cyclo*(L-Pro-L-Leu) (**17**), *cis-cyclo*(L-Pro-L-Ile) (**18**), *cis-cyclo*(L-Pro-L-Phe) (**19**), *trans-cyclo*(L-Pro-L-Phe) (**20**) and *cis-cyclo*(L-Pro-L-Tyr) (**21**).

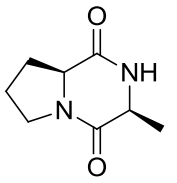

15

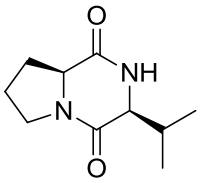

16

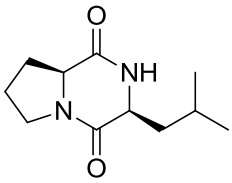

17

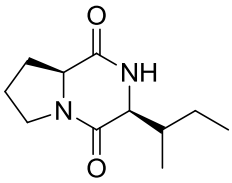

18

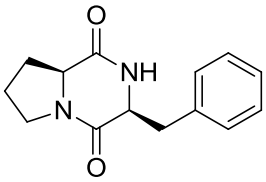

19

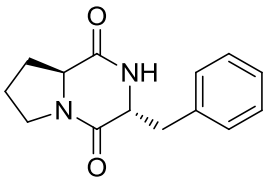

20

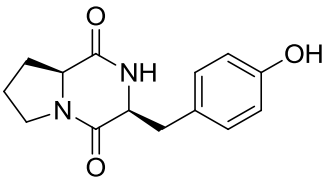

21

Additionally, one nucleoside was isolated and identified as adenosine (**22**), as well as compound **23** bearing a rare methacrylate residue.

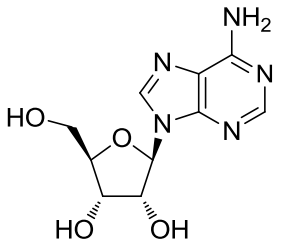

22

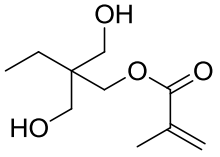

23

Compounds **1**–**10** were evaluated for their antibacterial activities against the epidemic methicillin-resistant strain EMRSA-15 and the multidrug-resistant effluxing strain SA1199B of *S. aureus*, as well as the *E. coli* strain NCTC-10418. Furthermore, the cytotoxic activities of **1**–**10** were tested against the MCF7 (breast adenocarcinoma) and A549 (lung carcinoma) human cancer cell lines. However, metabolites **1**–**10** were proven inactive in both bioactivity assays.

REFERENCES

Adamczeski M., Reed A.R., Crews P. *J. Nat. Prod.* **1995**, 58, 201-208.

Adegboye M.F., Babalola O.O. **2013**. *Actinomycetes: A yet inexhaustive source of bioactive secondary metabolites.* In: Mendez-Vilas A. (ed) Microbial Pathogens and Strategies for Combating Them: Science, Technology and Education. Formatex: Badajoz, Spain.

Ananthanarayan R., Paniker C.K.J. **2005**. Ananthanarayan and Paniker's Textbook of Microbiology. Orient Longman: Hyderabad, India.

Anderson R.J., Groundwater P.W., Todd A., Worsley A. **2012**. Antibacterial Agents: Chemistry, Mode of Action, Mechanisms of Resistance and Clinical Applications. Wiley: Chichester, West Sussex, UK.

Andréo M.A., Jimenez P.C., Siebra J.B.C.N., Costa-Lotufo L.V., Vessecchi R., Niehues M., Lopes J.L.C., Lopes N.P. *J. Braz. Chem. Soc.* **2012**, 23, 335-343.

Aoyagi T., Hatsu M., Kojima F., Hayashi C., Hamada M., Takeuchi T. *J. Antibiot*. **1992**, 45, 1079–1083.

Asolkar R.N., Jensen P.R., Kauffman C.A., Fenical W. *J. Nat. Prod.* **2006**, 69, 1756-1759.

Atlas R. **1997**. Principles of Microbiology. WCB McGraw-Hill: New York, NY, USA.

Babczinski P., Dorgerloh M., Löbberding A., Santel H.-J., Schmidt R.R., Schmitt P., Wünsche C. *Pestic. Sci.* **1991**, 33, 439-446.

Barka E.A., Vatsa P., Sanchez L., Gaveau-Vaillant N., Jacquard C., Klenk H.-P., Clément C., Ouhdouch Y., van Wezel G.P. *Microbiol. Mol. Biol. Rev.* **2016**, 80, 1-43.

Barrios-González J., Mejýa A. **2008**. *Production of antibiotics and other commercially valuable secondary metabolites*. In: Pandey A., Soccol C.R., Larroche C. (eds) Current Developments in Solid-State Fermentation. Springer: New York, NY, USA.

Bentley S.D., Chater K.F., Cerdeño-Tárraga A.M., Challis G.L., Thomson N.R., James K.D., et al. *Nature* **2002**, 417, 141-147.

Bérdy J. *J. Antibiot.* **2005**, 58, 1-26.

Berthelot M., Andre G. *Compt. Rend.* **1891**, 112, 598-599.

Bhat S.A., Nazir R., Malik T.A., Shah F.A. *Stem. Cell.* **2013**, 4, 41-46.

Birnbaum J., Kahan F.M., Kropp H., MacDonald J.S. *Am. J. Med.* **1985**, 78, 3-21.

Bonfiglio G., Furneri P.M. *Expert Opin. Investig. Drugs* **2001**, 10, 185-198.

Boonlarppradab C., Kauffman C.A., Jensen P.R., Fenical W. *Org. Lett*. **2008**, 10, 5505-5508.

Bugni T.S., Ireland C.M. *Nat. Prod. Rep.* **2004**, 21, 143-163.

Bugni T.S., Woolery M., Kauffman C.A., Jensen P.R., Fenical W. *J. Nat. Prod.* **2006**, 69, 1626-1628.

Bull A.T., Stach J.E. *Trends Microbiol.* **2007**, 15, 491-499.

Bystrykh L.V., Fernández-Moreno M.A., Herrema J.K., Malpartida F., Hopwood D.A., Dijkhuizen L. *J. Bacteriol.* **1996**, 178, 2238-2244.

Carlson J.C., Li S., Burr D.A., Sherman D.H. *J. Nat. Prod*. **2009**, 72, 2076-2079.

Chater K.F. *Phil. Trans. R. Soc. B* **2006**, 361, 761-768.

Chavan D.V., Mulaje S.S., Mohalkar R.Y. *IJPSR* **2013**, 4, 1730-1742.

Chen J.-H., Lan X.-P., Liu Y., Jia A.Q. *Bioorg. Med. Chem. Lett.* **2012**, 22, 3177-3180.

Cutignano A., Fontana A., Renzulli L., Cimino G. *J. Nat. Prod.* **2003**, 66, 1399-1401.

De Boer D., Coolen H.K.A.C., Hesselink M.B., Iwema Bakker W.I., Kuil G.D., Van Maarseveen J.H., McCreary A.C., Van Scharrenburg G.J.M. **2003**. *PCT Int. Appl*., WO 2003084955.

Demain A.L., Sanchez S. *J. Antibiot*. **2009**, 62, 5-16.

Deng Z., Bai L. *Nat. Prod. Rep.* **2006**, 23, 811-827.

Dharmaraj S. *World J. Microbiol. Biotechnol.* **2010**, 26, 2123-2139.

Dhevendaran K., Annie K. *Indian J. Mar. Sci.* **1999**, 28, 335-337.

Dickschat J.S., Martens T., Brinkhoff T., Simon M,. Schulz S. *Chem. Biodiver.* **2005**, 2, 837-865.

Dimou M., Ioannou E., Daskalaki M.G., Tziveleka L.A., Kampranis S.C., Roussis V. *J. Nat. Prod.* **2016**, 79, 584-589.

Ding L., Pfoh R., Ruhl S., Qin S., Laatsch H. *J. Nat. Prod*. **2009**, 72, 99-101.

Djinni I., Defant A., Kecha M., Mancini I. *Mar. Drugs*, **2013**, 11, 124-135.

El-Gendy M.M.A., Shaaban M., Shaaban K.A., El-Bondkly A.M., Laatsch H. *J. Antibiot*. **2008**, 61, 149-157.

El-Tarabily K.A., Sivasithamparam K. *Soil Biol. Biochem*. **2006**, 38, 1505-1520.

Fenical W. *Chem. Rev*. **1993**, 93, 1673-1683.

Flärdh K., Findlay K.C., Chater K.F. *Microbiology* **1999**, 145, 2229-2243.

Fotso S., Wu S.J., Qin S., Laatsch H. *Nat. Prod. Commun.* **2006**, 1, 9-13.

Fowler-Goldsworthy K., Gust B., Mouz S., Chandra G., Findlay K.C., Chater K.F. *Microbiology* **2011**, 157, 1312-1328.

Fremlin L., Farrugia M., Piggott A. M., Khalil Z., Lacey E., Capon R. J. *Org. Biomol. Chem*. **2011**, 9, 1201-1211.

Fukuda T., Miller E.D., Clark B.R., Alnauman A., Murphy C.D., Jensen P.R., Fenical W. *J. Nat. Prod*. **2011**, 74, 1773-1778.

Gerber N.N. *CRC Crit. Rev. Microbiol*. **1979**, 7, 191-214.

Ghai R., Rodriguez-Valera F., McMahon K.D., Toyama D., Rinke R., de Oliveira T.C.S., Wagner Garcia J., de Miranda F.P., Henrique-Silva F. *PLoS one* **2011**, 6, e23785.

Gorajana A., Kurada B.V.V.S.N., Peela S., Jangam P., Vinjamuri S., Poluri E., Zeeck A. *J. Antibiot.* **2005**, 58, 526-529.

Gorlero M., Wieczorek R., Adamala K., Giorgi A., Schinina M.E., Stano P., Luisi P.L. *FEBS Lett.* **2009**, 583, 153-156.

Hagenmaier H., Jaschke K.H., Santo L., Scheer M., Zahner H. *Arch. Microbiol*. **1976**, 109, 65-74.

Han X.-X., Cui C.-B., Gu Q.-Q., Zhu W.-M., Liu H.-B., Gu J.-Y., Osada H. *Tetrahedron Lett.* **2005**, 46, 6137-6140.

Hawas U.W., Shaaban M., Shaaban K.A., Speitling M., Maier A., Kelter G., Fiebig H.H., Meiners M., Helmke E., Laatsch H. *J. Nat. Prod*. **2009**, 72, 2120-2124.

Hayakawa Y., Shirasaki S., Shiba S., Kawasaki T., Matsuo Y., Adachi K., Shizuri Y. *J. Antibiot.* **2007**, 60, 196-201.

Hernández I.L.C., Godinho M.J.L., Magalhães A., Schefer A.B., Ferriera A.G., Berlinck R.G.S. *J. Nat. Prod.* **2000**, 63, 664-665.

Hernández I.L.C., Macedo M.L., Berlinck R.G.S., Ferreira A.G., Godinho M.J.L. *J. Braz. Chem. Soc.* **2004**, 15, 441-444.

Hohmann C., Schneider K., Bruntner C., Brown R., Jones A.L., Goodfellow M., Krämer M., Imhoff J.F., Nicholson G., Fiedler H.-P., Süssmuth R.D. *J. Antibiot.* **2009**, 62, 75-79.

Huang R., Yan T., Peng Y., Zhou X., Yang X., Liu Y. *Chem. Nat. Comp.* **2014**, 50, 191-193.

Huang X.-L., Gao Y., Xue D.-Q., Liu H.-L., Peng C.-S., Zhang F.-L., Li Z.-Y., Gu Y.-W. *Helv. Chim. Acta* **2011**, 94, 1838-1842.

Hughes C.C., Kauffman C.A., Jensen P.R., Fenical W. *J. Org. Chem*. **2010**, 75, 3240-

3250.

Hughes C.C., MacMillan J.B., Gaudencio S.P., Fenical W., La Clair J.J. *Angew. Chem. Int Ed.* **2009**a, 48, 728-732.

Hughes C.C., MacMillan J.B., Gaudencio S.P., Jensen P.R., Fenical W. *Angew. Chem. Int. Ed.* **2009**b, 48, 725-727.

Hughes C.C., Prieto-Davo A., Jensen P.R., Fenical W. *Org. Lett.* **2008**, 10, 629-631.

Igarashi Y., Shimasaki R., Miyanaga S., Oku N., Onaka H., Sakurai H., Saiki I., Kitani S., Nihira T., Wimonsiravude W., Panbangred W. *J. Antibiot.* **2010**, 63, 563-565.

Itoh T., Kinoshita M., Aoki S., Kobayashi M. *J. Nat. Prod.* **2003**, 66, 1373-1377.

Iwata F., Sato S., Mukai T., Yamada S., Takeo J., Abe A., Okita T., Kawahara H. *J. Nat. Prod*. **2009**, 72, 2046-2048.

Izumikawa M., Khan S.T., Komaki H., Takagi M., Shin-ya K. *J. Antibiot*. **2010**b, 63, 33-36.

Izumikawa M., Khan S.T., Takagi M., Shin-ya K. *J. Nat. Prod*. **2010**a, 73, 208-212.

Jardetzky C.D., Jardetzky O. *J. Am. Chem. Soc.* **1959**, 82, 222-229.

Jeong S.-Y., Shin H.J., Kim T.S., Lee H.-S., Park S.-k., Kim H.M. *J. Antibiot.* **2006**, 59, 234-240.

Jeya M., Moon H.-J., Lee K.-M., Kim I.-W., Lee J.K. *Curr. Pharm. Biotechnol*. **2011**, 12, 1194-1204.

Jones A.J., Grant D.M., Winkley M.W., Robins R.K. *J. Am. Chem. Soc.* **1970**, 92, 4079-4087.

Kawashima A., Seto H., Kato M., Uchida K., Otake N. *J. Antibiot.* **1985**, 38, 1499-1505.

Kock I., Maskey R.P., Biabani M.A.F., Helmke E., Laatsch H. *J. Antibiot.* **2005**, 58, 530-534.

Kumar S.N., Nambisan B., Mohandas C. *J. Enzyme Inhib. Med. Chem.* **2014**, 29, 190-197.

Lam K.S. *Trends Microbiol*. **2007**, 15, 279-289.

Layland J., Carrick D., Lee M., Oldroyd K., Berry C. *JACC Cardiovasc Interv.* **2014**, 7, 581-591.

Lee H.-S., Shin H. J., Jang K.H., Kim T.S., Oh K.-B., Shin J. *J. Nat. Prod.* **2005**, 68, 623-625.

Li B., Chen G., Bai J., Jing Y.-K., Pei Y.-H. *J. Asian Nat. Prod. Res*. **2011**, 13, 1146-1150.

Li F., Maskey R.P., Qin S., Sattler I., Fiebig H.H., Maier A., Zeeck A., Laatsch H. *J. Nat. Prod.* **2005**, 68, 349-353.

Li J., Lu C.-H., Zhao B.-B., Zheng Z.-H., Shen Y.-M *Beilstein J. Org. Chem*. **2008**, 4, 46.

Li Q., Chen X., Jiang Y., Jiang C. **2016**. *Morphological identification of Actinobacteria*. In: Dhanasekaran D., Jiang Y. (eds) Actinobacteria: Basics and biotechnological applications. IntechOpen, DOI: 10.5772/61461.

Lin Z., Reilly C.A., Antemano R., Hughen R.W., Marett L., Concepcion G.P., Haygood M.G., Olivera B.M., Light A., Schmidt E.W. *J. Med. Chem*. **2011**, 54, 3746-3755.

Liu F.F., Li G.H., Yang Z.S., Zheng X., Yang Y., Zhang K.Q. *Helv. Chim. Acta* **2010**, 93, 1737-1741.

Macherla V.R., Liu J., Bellows C., Teisan S., Nicholson B., Lam K.S., Potts B.C.M. *J. Nat. Prod.* **2005**, 68, 780-783.

Manam R.R., Teisan S., White D.J., Nicholson B., Grodberg J., Neuteboom S.T.C., Lam K.S., Mosca D.A., Lloyd G.K., Potts B.C.M. *J. Nat. Prod.* **2005**, 68, 240-243.

Martin G.D.A., Tan L.T., Jensen P.R., Encarnacion Dimayuga R., Fairchild C.R., Raventos-Suarez C., Fenical W. *J. Nat. Prod.* **2007**, 70, 1406-1409.

Maskey R.P., Helmke E., Fiebig H.-H., Laatsch H. *J. Antibiot.* **2003**, 55, 1031-1035.

Maskey R. P., Helmke E., Kayser O., Fiebig H.H., Maier A., Busche A., Laatsch H. *J. Antibiot.* **2004**b, 57, 771-779.

Maskey R.P., Sevvana M., Uson I., Helmke E., Laatsch H. *J. Antibiot.* **2002**, 55, 1031-1035.

Maskey R.P., Sevvana M., Uson I., Helmke E., Laatsch H. *Angew. Chem. Int. Ed.* **2004**a, 43, 1281-1283.

Matsuo Y., Kanoh K., Jang J.-H., Adachi K., Matsuda S., Miki O., Kato T., Shizuri Y. *J. Nat. Prod*. **2011**, 74, 2371-2376.

Mavrogonatou E., Eliades T., Eliades G., Kletsas D. *Biomaterials* **2010**, 31, 8530-8538.

McGhie J.F., Ross W.A., Evans D., Tomlin J.E. *J. Chem. Soc.* **1962**, 350-355.

Mertens H., Schmidt O., Adam K. **1960**. Patents DE 1083011 and GB 875720.

Meyer C.E. *J. Antibiot.* **1971**, 24, 558-560.

Miller E.D., Kauffman C.A., Jensen P.R., Fenical W. *J. Org. Chem*. **2007**, 72, 323-330.

Mitova M.I., Lang G., Wiese J., Imhoff J.F. *J. Nat. Prod*. **2008**, 71, 824-827.

Miyadoh S., Hamada M., Hotta K., Seino A., Vobis G., Yokota A. **1997**. Atlas of Actinomycetes. Askura Publishing Co. Ltd: Tokyo, Japan.

Miyairi N., Sakai H.-I., Konomi T., Imanaka H. *J. Antibiot.* **1976**, 29, 227-235.

Motohashi K., Inaba K., Fuse S., Doi T., Izumikawa M., Khan S.T., Takagi M., Takahashi T., Shin-ya K. *J. Nat. Prod*. **2011**, 74, 1630-1635.

Motohashi K., Irie K., Toda T., Matsuo Y., Kasai H., Sue M., Furihata K., Seto H. *J. Antibiot*. **2008**, 61, 75-80.

Motohashi K., Takagi M., Shin-ya K. *J. Nat. Prod*. **2010**b, 73, 226-228.

Motohashi K., Takagi M., Shin-ya K. *J. Nat. Prod*. **2010**c, 73, 755-758.

Motohashi K., Toda T., Sue M., Furihata K., Shizuri Y., Matsuo Y., Kasai H., Shin-ya K., Takagi M., Izumikawa M., Horikawa Y., Seto H. *J. Antibiot*. **2010**a, 63, 549-552.

Muindi J.R., Sinha B.K., Gianni L., Myers C.E. *FEBS Lett*. **1984**, 172, 226-230.

Mukku V.J.R.V., Speitling M., Laatsch H., Helmke E. *J. Nat. Prod*. **2000**, 63, 1570-1572.

Na M., Meujo D.A.F., Kevin D., Hamann M.T., Anderson M., Hill R.T. *Tetrahedron Lett*. **2008**, 49, 6282-6285.

Nachtigall J., Schneider K., Bruntner C., Bull A.T., Goodfellow M., Zinecker H., Imhoff J.F., Nicholson G., Irran E., Süssmuth R.D., Fiedler H.-P. *J. Antibiot*. **2011**, 64, 453-457.

Nam S.-J., Kauffman C.A., Jensen P.R., Fenical W. *Tetrahedron* **2011**, 67, 6707-6712.

Nelson M.L., Levy S.B. *Ann. NY Acad. Sci.* **2011**, 1241, 17-32.

Ogawa Y., Mori H., Ichihashi M., Ueno T., Nakashima T., Fukami H., Nakajima R., Ida H. *Pept. Chem*. **1977**, 14, 123-126.

Paquet V., Carreira E.M. *Org. Lett*. **2006**, 8, 1807-1809.

Pérez M., Crespo C., Schleissner C., Rodríguez P., Zúñiga P., Reyes F. *J. Nat. Prod*. **2009**, 72, 2192-2194.

Petersen F., Zähner H., Metzger J.W., Freund S., Hummel R.-P. *J. Antibiot.* **1993**, 46, 1126-1138.

Piel J., Hoang K., Moore B.S. *J. Am. Chem. Soc.* **2000**, 122, 5415-5416.

Pimentel-Elardo S., Buback V., Gulder T.A.M., Bugni T.S., Reppart J., Bringmann G., Ireland C.M., Schirmeister T. *Mar. Drugs* **2011**, 9, 1682-1697.

Pimentel-Elardo S.M., Kozytska S., Bugni T.S., Ireland C.M., Moll H., Hentschel U. *Mar. Drugs* **2010**, 8, 373-380.

Pouchert C.J., Behnke J. **1993**. The Aldrich library of ^{13}C and ^{1}H FT NMR spectra, 1st ed.; Aldrich Chemical Company, Inc.: Milwaukee, WI, USA; Volume 2, pp. 985, 1043, 1063.

Poumale H.M.P., Ngadjui B.T., Helmke E., Laatsch H. *Z. Naturforsch. B: Chem. Sci.* **2006,** 61, 1450-1454.

Quitschau M., Schuhmann T., Piel J., von Zezschwitz P., Grond S. *Eur. J. Org. Chem*. **2008**, 5117-5124.

Rab E., Kekos D., Roussis V., Ioannou E. *Mar. Drugs* **2017**, 15, 389.

Raja A., Prabakarana P. *Am. J. Drug Discov. Develop.* **2011**, 1, 75-84.

Raju R., Piggott A.M., Conte M., Aalbersberg W.G.L., Feussner K., Capon R.J. *Org. Lett*. **2009**, 11, 3862-3865.

Raju R., Piggott A.M., Conte M.M., Capon R.J. *Org. Biomol. Chem*. **2010**a, 8, 4682-4689.

Raju R., Piggott A.M., Diaz L.X.B., Khalil Z., Capon R.J. *Org. Lett*. **2010**b, 12, 5158-5161.

Sakula A. *Br. J. Dis. Chest.* **1988**, *82*, *23*-31.

Sanchez S., Demain A.L. *Enzyme Microb. Technol.* **2002,** 31, 895-906.

Sánchez López J.M., Martinez Insua M., Perez Baz J., Fernández Puentes J.L., Canedo Hernández L.M. *J. Nat. Prod.* **2003**, 66, 863-864.

Sato S., Iwata F., Mukai T., Yamada S., Takeo J., Abe A., Kawahara H. *J. Org. Chem*. **2009**, 74, 5502-5509.

Sato S., Iwata F., Yamada S., Kawahara H., Katayama M. *Bioorg. Med. Chem. Lett*. **2011**, 21, 7099-7101.

Schleissner C., Perez M., Losada A., Rodriguez P., Crespo C., Zuniga P., Fernandez R., Reyes F., de la Calle F. *J. Nat. Prod.* **2011**, 74, 1590-1596.

Schneemann I., Kajahn I., Ohlendorf B., Zinecker H., Erhard A., Nagel K., Wiese J., Imhoff J.F. *J. Nat. Prod*. **2010**, 73, 1309-1312.

Schumacher R.W., Talmage S.C., Miller S.A., Sarris K.E., Davidson B.S., Goldberg A. *J. Nat. Prod.* **2003**, 66, 1291-1293.

Seto H., Sato T., Urano S., Uzawa J., Yonehara H. *Tetrahedron Lett.* **1976**, 17, 4367-4370.

Shaaban K.A., Helmke E., Kelter G., Fiebig H.H., Laatsch H. *J. Antibiot*. **2011**, 64, 205-209.

Shaaban K.A., Shaaban M., Facey P., Fotso S., Frauendorf H., Helmke E., Maier A., Fiebig H. H., Laatsch H. *J. Antibiot*. **2008**, 61, 736-746.

Shirahata K., Iida T., Hirayama N. *Tennen Yuki Kagobutsu Toronkai Koen Yoshishu*, **1981**, 24, 199-206.

Singh R., Pandey B., Mathew C.Y. *Indian J. Sci. Res*. **2014**, 4, 149-154.

Sitachitta N., Gadepalli M., Davidson B.S. *Tetrahedron* **1996**, 52, 8073-8080.

Sobolevskaya M.P., Fotso S., Havash U., Denisenko V.A., Helmke E., Prokofeva N.G., Kuznetsova T.A., Laatsch H., Elyakov G.B. *Chem. Nat. Comp.* **2004**, 40, 282-285.

Solecka J., Zajko J., Postek M., Rajnisz A. *Cent. Eur. J. Biol.* **2012**, 7, 373-390.

Stackebrandt E., Goebel B.M. *Int. J. Syst. Evol. Microbiol.* **1994**, 44, 846-849.

Stackebrandt E., Rainey F.A., Ward-Raine N.L. *Int. J. Syst. Bacteriol.* **1997**b, 47, 479-491.

Stackebrandt E., Sproer C., Rainey F.A., Burghardt J., Pauker O., Hippe H. *Int. J. Syst. Bacteriol*. **1997**a, 47, 1134-1139.

Strangman W.K., Kwon H.C., Broide D., Jensen P.R., Fenical W. *J. Med. Chem*. **2009**, 52, 2317-2327.

Sun P., Maloney K.N., Nam S.-J., Haste N.M., Raju R., Aalbersberg W., Jensen P.R., Nizet V., Hensler M.E., Fenical W. *Bioorg. Med. Chem*. **2011**, 19, 6557-6562.

Takeuchi T., Hamada M., Nanagawa H., Takahashi Y., Sawa R. **1998**. *Jpn. Kokai Tokkyo Koho*, JP 96216484.

Takeuchi T., Hamada M., Osanawa H., Takahashi Y., Sawa R. **1996**. *Jpn. Kokai Tokkyo Koho*, JP 08165286.

Tamaoki T., Shirahata K., Iida T., Tomita F. *J. Antibiot.* **1981**, 34, 1525-1530.

Tang Y.-Q., Sattler I., Thiericke R., Grabley S., Feng X.-Z. *J. Antibiot.* **2000**, 53, 934-943.

Tezuka Y., Huang Q., Kikuchi T., Nishi A., Tubaki K. *Chem. Pharm. Bull.* **1994**, 42, 2612-2617.

Tietze L.F., Dietz S., Schützenmeister N., Biller S., Hierold J., Scheffer T., Baag M.M. *Eur. J. Org. Chem.* **2013**, 7305-7312.

Tomita F., Tamaoki T., Morimoto M., Fujimoto K. *J. Antibiot.* **1981**, 34, 1519-1524.

Ueda J., Khan S.T., Takagi M., Shin-ya K. *J. Antibiot*. **2010**, 63, 267-269.

Vakulenko S.B., Mobashery S. *Clin. Microbiol. Rev.* **2003**, 16, 430-450.

Ventura M., Canchaya C., Tauch A., Chandra G., Fitzgerald G.F., Chater K.F., van Sinderen D. *Microbiol. Mol. Biol. Rev.* **2007**, 71, 495-548.

Waksman S.A. **1961**. The Actinomycetes, vol. 2, Classification, Identification and Description of Genera and Species. Williams & Wilkins: Baltimore, MD, USA.

Wang G., Dai S., Chen M., Wu H., Xie L., Luo X., Li X. *Chem. Nat. Comp.* **2010**, 46, 583-585.

Williams D.E., Dalisay D.S., O'Patrick B., Matainaho T., Andrusiak K., Deshpande R., Myers C.L., Piotrowski J.S., Boone C., Yoshida M., Anderson R.J. *Org. Lett.* **2011**, 13, 3936-3939.

Wilson M.C., Nam S.-J., Gulder T.A.M., Kauffman C.A., Jensen P.R., Fenical W., Moore B.S. *J. Am. Chem. Soc*. **2011**, 133, 1971-1977.

Wu S.J., Fotso S., Li F., Qin S., Kelter G., Fiebig H.H., Laatsch H. *J. Antibiot.* **2006**, 59, 331-337.

Wu S.J., Fotso S., Li F., Qin S., Laatsch H. *J. Nat. Prod*. **2007**, 70, 304-306.

Xiang L., Kalaitzis J.A., Nilsen G., Chen L., Moore B.S. *Org. Lett.* **2002**, 4, 957-960.

Xu L.-Y., Quan X.-S., Wang C., Sheng H.-F., Zhou G.-X., Lin B.-R., Jiang R.-W., Yao X.-S. *J. Antibiot*. **2011**, 64, 661-665.

Xu Z., Ding L., Hertweck C. *Angew. Chem. Int. Ed.* **2011**, 50, 4667-4670.

Yao C.B.F., Schiebel M., Helmke E., Anke H., Laatsch H. *Z. Naturforsch. B: Chem. Sci.* **2006**, 61, 320-325.

Zhang H., Wang H., Cui H., Li Z., Xie Z., Pu Y., Li F., Qin S. *Mar. Drugs* **2011**, 9, 1502-1509.

Zuckerman J.M. *Infect. Dis. Clin. N. Am.* **2004**, 18, 621-638.